APPLICABILITY OF MAGNETIC SUSCEPTIBILITY TECHNIQUES AND NOVEL TEMPLATES FOR IMPROVED HYDROCARBON RESERVOIR CHARACTERIZATION

Salem Abdalglel Salem Abdalah

Submitted for the
Degree of Doctor of Philosophy in
Petroleum Engineering

Heriot-Watt University
Institute of Petroleum Engineering
Edinburgh
United Kingdom
2014

Abstract

The work presented in this thesis is an effort to help petrophysicists and reservoir engineers in improving reservoir characterization. Magnetic susceptibility techniques were used for prediction of important reservoir parameters in hydrocarbon sedimentary sequences.

For the first time ever I have shown that the grain lining hematite cement surrounding quartz grains has significant control on permeability in hydrocarbon bearing reservoir rock samples. This work also shows that it is not only the dispersed hematite and clay minerals in a reservoir rock matrix that control permeability, but also that the grain lining hematite has additional and dominant control on permeability. In addition, for the first time ever, magnetic susceptibility techniques have been applied on core samples from relatively tight gas sandstone reservoirs. Such techniques were previously known to have been used in only conventional clastic reservoirs. Magnetic hysteresis measurements were used to show that the permeability is dependent on hematite content and independent of hematite particle size.

Identifying and Evaluating faults and fluid contact in hydrocarbon bearing reservoir rocks are challenging tasks. The work presented in this thesis has shown for the first time that raw magnetic susceptibility measurements performed on drill cuttings can be used to detect faults and fluid contacts in sedimentary sequences. Such measurements can be performed at well site, thereby enabling companies to make important field development decisions quickly.Additionally, a series of novel crossplots have been developed between magnetic susceptibility and various wireline log data for determination of mineralogy, mixture porosity and mineral quantification. These crossplots are similar in format to standard industry charts, which provide a further tool for improved petrophysical characterization using rapid, non-destructive magnetic susceptibility measurements.

Dedication

To my parents Abdalgalel and Aisha for their unfailing love, their inspirational upbringing, the sacrifices rendered to provide me with all the facilities and comfort for completing my studies up to this end. Without their continued support, my education would not have been possible. Their patience and selflessness has shaped me into the person I am today.

Dedication

This project is dedicated to

The

ALMIGHTY ALLAH

for

His

Enabling Grace that was

Sufficient for me

Acknowledgements

I spent the last three years working on the subject of this thesis at the petrophysics laboratory. This period has been full of satisfactions, both on the professional and cultural side and on the personal and human side. A lot of people made it possible: I thank them all and I apologize for anyone missing.

I would like to give the Almighty God all the glory, honour and adoration for seeing me through this great journey of overwhelming challenges.

First and foremost, I would like to thank Dr. S. Zheng and Dr. Jingsheng Ma for taking their time to exam my thesis and providing me with a valuable feedback.

I would like to say a special thank you to my supervisor, Dr Arfan Ali, for giving me the chance to be one of your PhD students, and for all of your support and advice over the last three years. I have learned so much and grown in a number of ways both professionally and personally as a result of the PhD, and I thank you so much for your considerable part in that. This project would not have been possible without your guidance and innovative ideas. I would like to thank Dr. Arfan Ali again, for keeping me on the right track.

I am highly grateful to my secondary supervisor Prof Mehran Sohrabi who gave me the chance to be one of the PhD students at the IPE, and for his support during my study.

It gives me great pleasure in acknowledging the support and help of Professor David Potter from Alberta University in Canada, who was always willing to help and give his best suggestions.

Sincere appreciation is extended to Dr. Helen Lever for her kind help.

I would like to express sincere thanks to Mr. John Mills, Mr. Mohamed Ahmed, Mr. Khalid Alruwaili, Mrs. Marta Swierczek and Mrs. Mina Esentia for helping me learn how to operate the microscope.

I thank all the students and staff in the Institute of Petroleum Engineering, whose presence and fun-loving spirits made the gruelling times tolerable. I enjoyed all the lively discussions we had on various topics and had lots of fun being a member of this fantastic group.

I am also very grateful to my brothers and sisters especially, Abdulfattah and Khiri, for always being there when I needed them most, and for supporting me through all these years.

Last but not least, I would like to acknowledge four special people who made incredible sacrifices for me: my beloved wife Nabela, for her understanding, patience, and encouragement, my sons Abdalmoeen and Mohab and my daughter Maab whom give me some fun for relaxing. I am so thankful for their support through the years. This accomplishment is really for the four of them.

Table of contents

List of Figures

List of Tables

List of Abbreviations

AMS	Anisotropy of Magnetic Susceptibility
B	Magnetic Flux Density
DT	Sonic travel time
GDF	Gas de France
GR	Gamma Ray
GWC	Gas Water Contact
H	Magnetic Field Strength
Hc	Coercivity of Magnetisation (Coercive Force)
Hcr	Coercivity of Remanent Magnetisation
IRM	Isothermal Remanent Magnetisation
K	Kelvin/ Potassium
M	Magnetisation
MD	Multi-Domain
MDT	Modular Formation Dynamics Tester
Mrs	Saturation Remanent Magnetisation
Ms	Saturation Magnetisation
$^{\circ}C$	Degree Celsius
ppm	Parts Per Million
PSD	Pseudo-Single Domain
SD	Single Domain
SEM	Scanning Electron Microscope
SI	Systems International
SP	Super-Paramagnetic
Tc	Curie Temperature
TDS	Temperature Dependent Susceptibility
Th	Thorium
VFTB	Variable Field Translation Balance
XRD	X-ray Diffraction
μ_0	Permeability of Free Space

μ_r	Relative Permeability of the Specimen
μT	Micro-Tesla
χ , MS	Magnetic Susceptibility
χ_{dia}	Diamagnetic Susceptibility
χ_{ferro}	Ferromagnetic Susceptibility
$\chi_{Hfld'}$ H_{fld} MS	High Field Magnetic Susceptibility
χ_{Lfld}, L_{fld} MS	Low Field Magnetic Susceptibility
χ_{para}	Paramagnetic Susceptibility
χ_m, χ	Mass Magnetic Susceptibility
χ_o	Initial Magnetic Susceptibility
χ_v, k	Volume Magnetic Susceptibility
ϕ	Porosity

List of publications

- Ali, A., Abdalah, S. and Potter, K. D., 2012. "Quantifying the Role of Hematite Cement on Permeability in Deep Tight Gas Reservoirs", 2012 SPE International Conference, Abu Dhabi, UAE. Paper SPE 152382.

- Ali, A., Abdalah, S. and Potter, K. D., 2012 "Quantifying the Role of Grain Lining Hematite Cement in Controlling Permeability in a Relatively Tight Gas Sandstone Reservoir from the North Sea", SPE Reservoir Evaluation & Engineering Journal, 15(6):618-623.

- Abdalah, S., Ali, A. and Potter, K. D 2013. "Improved Reservoir Characterisation Using Novel Unconventional Crossplots between Magnetic Susceptibility and Downhole Wireline Log Data". 2013 International Symposium of the Society of Core Analysts, Napa Valley, California, USA. Paper SCA 2013-075

Chapter 1 Introduction

Magnetic susceptibility is known as one of the most important magnetic properties of rocks. It is a measurement of the ease of magnetization of the material. Magnetic minerals in sediments are of practical interest in the petroleum industry because they can cause anomalous readings on magnetic logs. These minerals, in many cases, can also directly affect the reservoir quality (Philip, 1993).

1.1 Magnetic Measurements

There are two types of magnetic measurements, high frequency and low frequency. The more common one is the low-frequency measurement, which measures the reduction of the magnetic field when the sample is placed in a moderate magnitude low-frequency magnetic field. The differences in the frequency measurements of the applied magnetic field can be useful to detect the presence of superparamagnetic grains. Magnetic susceptibility can be expressed as a sample mass basis (the mass specific susceptibility) with density units (m^3kg^{-1}). This can be obtained by dividing the volume magnetic susceptibility by the bulk density of the sample.

Isothermal remanent magnetisation (IRM) is a measure of the acquired of the self-sustaining magnetism imparted to the sample after this sample placed in high magnetic field which equal to about one tesla (1T). (Moskowits, 1991).

1.2 The Role of Iron Oxide Hematite Cement in Controlling Permeability

In the early days of hydrocarbon exploration and production, clays were thought to be one of the most significant key of minerals that have got the ability of destroying permeability in reservoir rocks (in particular clastic reservoirs). In the presence of the drilling muds and completion fluids clays can cause a formation damage and piratical migration during the hydrocarbon production (Worden and Morad, 2003). The illite clay is a mineral of hairy appearance which bridges the pore throats and causes a drastic reduction in permeability (Wilson and Pittman, 1977; Todd and Tweddie, 1978). Expandable minerals of the smectite group (e.g., montmorillonite) are also notorious among petrophysicists for affecting permeability (Lupini et al., 1981; Morrow et al., 1992; Saffer and Marone, 2003).

Apart from the clays, a lot of research has been carried out on various cements that impose a drastic level of control on permeability. Cementation is known as one of the chemical processes that occur within reservoir rocks. It happens when the material precipitates between the grains and within the pore network.(Pittman and Larese, 1991). Generally, cement can block the pore throat, and affects the size of the pore and reduce the pore volume. The most common cemen minerals are calcite ($CaCO_3$), silica (SiO_2), and iron oxides (hematite).Illite, chlorite and kaolinite clay minerals may also precipitate onto grains, acting as weak bond cements (Bruno and Nelson, 1991).

Cement can be divided into two groups; rim cements and occluding cements (Pittman and Larese, 1991). Rim cements exist in two ways, as a coating on the grain surfaces or as overgrowths which react unequally from the surfaces of the grain (Wilson and Stanton, 1994). Rim cement is not considered to be as a part of the connection between the two grains. As Figure 1.1 shows, rim cement is grain-coating, a characteristic of clays, such as chlorite and illite, which have large surface-to-volume ratios. Rim cements generally have a blocky habit. (Wilson and Stanton, 1994). The variation in the thicknesses of the rim cement ranges from a micrometre to tens of micrometres but commonly ranges from 2 to 20 μm. (McBride,1989).

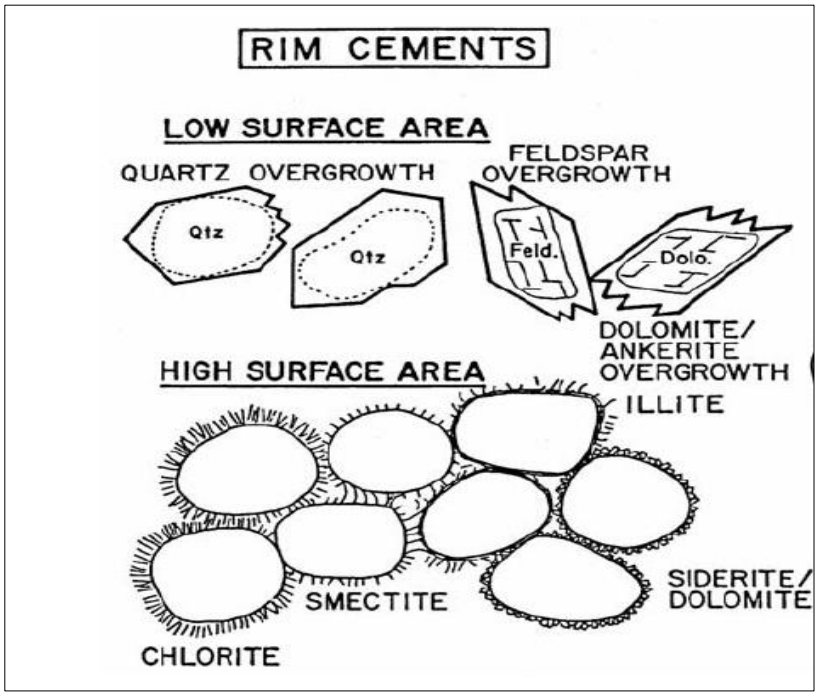

Figure 1-1: Rim cements (after Wilson, 1994).

occludin cements has a significant effect on the petrophysical parameters such as porosity and permeability , the percentage of this effect is depends on crystal size, abundance, and distribution of particular cement. (Wilson and Stanton, 1994). Figure 1.2 shows the effect of occluding cement on the porosity and the permeability.

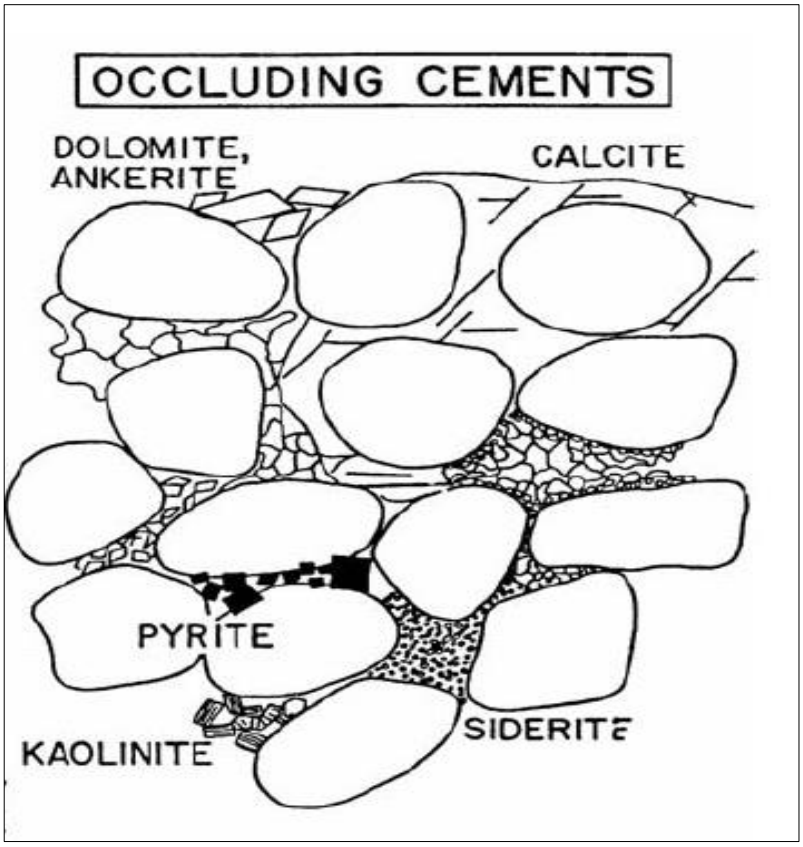

Figure 1-2: Occluding cement (after Wilson, 1994).

Permeability can be affected in different ways by different kinds of clay minerals and cements because they occupy different positions within the network. (Worden and Morad, 2003). However, the major magnetic properties of rocks are controlled by the presence of oxide minerals from the ternary system FeO (wüstite) - Fe_2O_3 (hematite, maghemite) - TiO2 (rutile). Hematite cement and its role in controlling permeability is a major part of the study in this thesis (Worden and Morad, 2003).

1.3 Magnetic Mineralogy

Magnetic minerals typically present present in the reservoir rock samples (iron-oxides) such as magnetite, and hematite were the target of this study. Others include iron oxy hydroxides and iron sulphides. The ternary diagram for iron oxides is shown in Figure 3.1.

- Iron oxides

Hematite (Fe2O3) and magnetite (Fe3O4) are well-known as the most important magnetic minerals of the iron oxides. Generally, the ternary diagram provides a better understanding of the substitution of both hematite and magnetite. If the $Ti4^{+}$ introduced in the compensation of both iron minerals (hematite and magnetite), the magnetisation will be reduced (Tauxe, 2008). Figure 3.1 shows the common iron minerals

- Iron oxyhydroxides

Goethite (αFeOOH) is one of the most well-known in this iron oxyhydroxide group. It is formed as a direct precipitate from the iron bearing solution (Tauxe, 2008). In this thesis goethite is not important as the hematite and magnetite.

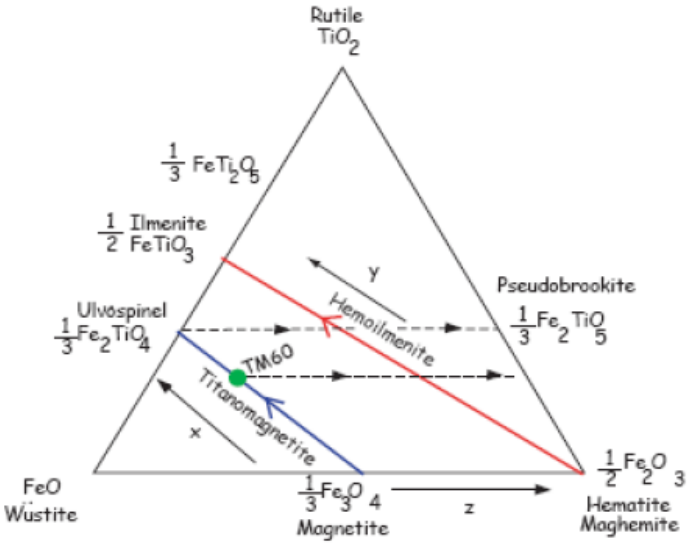

Figure 1-3: Ternary diagram for iron-oxides. The increase of the oxidation is indicated by the dashed lines and supported by the arrows. The solid lines represent a solid solution series, (after Tauxe, 2008).

1.4 Identifying Faults and Fluid Contacts

1.4.1 Recent techniques used to identify faults

Faults in a reservoir can greatly affect fluid flow (Yang, 1992). Different methods have been used to identify faults include logging tools such as Formation Micro Imager (FMI),Borehole Televiewer (BHTV), Formation Microscanner (FMS), Dipole Shear Sonic Imager (DSI) and Ultrasonic Borehole Imager (UBI). Each tool type has its resolution range optimized to observe structures appropriate for that tool's resolution. Almost of the log measurements can only be carried out when the borehole still not cased. However, rocks sometimes change their log characteristics as a result of remaining open for the drill fluids, as the mud filtrate penetrates into the borehole; as a consequence, logs should be carried out soon after the drill is finished (Spies and Frischknecht,1992).

- Formation Micro Imager (FMI)

The Formation Micro Imager (FMI) tool may give the better reliable data to detect the location of the fault in wells. However, the image quality can be affected by build-up of the mud cake on the borehole with operation (Hearts et al., 2000). The Formation Micro Imager (MFI) tool requires a consolidated open borehole and is therefore not useable with unconsolidated formations (Monier-Williams et al., 2009). Sometimes there can be a misleading interpretation of the Formation Micro Imager (FMI), so the result obtained from this tool should be compared with the core data results (Siddiqui et al., 2003). Many of the efforts to detect faults and fractures with commonly used logs are unsuccessful or, at best, marginally successful because the tools were designed for functions other than feature detection (Collier and Ridder, 1992).

- Borehole Televiewer (BHTV)

The Borehole Televiewer (BHTV) tool first proposed by Zemanek et al., in 1970 is a 360^{o} circumference acoustic imaging device that can be used to image borehole features such as faults and fractures (Williams and Johnson, 2000). It uses an ultrasound beam and scans the borehole using a rotating mirror (Ahmed and Harb. 2013).The amplitude and travel time appear as separate images on the log. Features such as faults appear as dark lines or spots on the log due to the reduction of the reflected amplitude (Chung et al., 2007). The Borehole Televiewer (BHTV) requires a liquid-filled uncased hole. It can be used in normal drilling muds, but the image will be affected by the suspended

particles in the mud (Chung et al., 2007). The tool should be run in a centralized position in the borehole (Collier and Ridder, 1992).Many features such as faults have will appear too small, which is related to the limit resolution of the Borehole Televiewer (BHTV) (Barton and Zoback,1992). Another disadvantage of the BHTV is its relatively slow logging speed and limited temperature range. The image quality of data also suffers in highly elliptic wellbores (Bear, et al., 1993). Georgi (1985) describes such geometrical problems as leading to dark stripes of poor image quality on the log.

- Dipole Shear Sonic Imager (DSI)

The Dipole Shear Sonic Imager (DSI) measures the sonic waves propagated in the formation by using a combination of monopole and dipole transducers (Schlumberger Corp., 1995). The dipole transmitters in the shear sonic imager emit waves at low frequency around the borehole, which are dispersive. The velocity of shear waves at a low frequency allow shear wave slowness to be measured in slow formation (Alford et al., 2012). The disadvantages of this kind of tool, the low resolution, and the tool; should be run in a centralized position in the borehole.

- Ultrasonic Borehole Imager (UBI)

The Ultrasonic Borehole Imager (UBI) tool sends ultrasonic waves and waves back to the tool are recorded by the receivers on the tool (Cornet, 2013). The changes in the amplitude of the waves provide the information about the formation and the changes in the borehole radius can be obtained by transit time. However, high mud weights have a large impact on signal attenuation (Cornet, 2013).

The quality of measurements acquired by the Ultrasonic Borehole Imager (UBI) may affected by the diameter of the borehole, the signal heavy mud and cycle skipping. The most affect factor on the measurement is the mud weight, because mud weight causes a major problem for slowing signal in muds equal to 15.5 ppg. (DI, 2008)

Another disadvantage is that the logging speed is somewhat slow comparing with other well tools; the speed of Ultrasonic Borehole Imager (UBI) tool is 91-152 m/hr, hence, it is highly cost-effective (Li et al., 2009).

The result of previous methods (well logs) used to identify faults are not strong enough for identify the presence of faults. For this reason, it may necessary to provide a new technique to identify faults. This may be achieved by means of mass magnetic susceptibility measurements. The value of this evaluation technique is in diagnosing the presence of faults in an accurate way, with high resolution and a short time compared with other well logging tools used to identify faults. More details for using mass magnetic susceptibility to identify faults and oil–water content will be found in Chapter Four.

1.4.2 Methods used to identify fluid contact

Most of the last generation of logging tools based on resistivity, induction and dielectric measurements have certain limitations in providing reliable information on fluid contacts in the wellbore (Loi, et al., 2011). In addition, using traditional methods it is extremely difficult to determine fluid contact in low permeability gas reservoirs (Abd_elmoula et al., 2010). The Modular Formation Dynamics Tester (MDT) is a wireline formation tester tool has the ability of collecting fluid samples from the formation and then transfer them to the surface to test and analyse them by specialists (Siswantoro, Indra, and Prasetyo, 1999).

1.5 Magnetic techniques used in the hydrocarbon industry

Historically, the magnetic studies for hydrocarbon applications were mainly focused on exploration of magnetic mineralogy (Donovan et al., 1979). Some limited work was done on petrophysical investigations (Bagin et al., 1973, Bagin and Malumyan, 1976). On the geophysics side, electromagnetic surveys were used for investigating the seismic properties of earth rocks and fluids (Eventov, 1997, 2000). Palaeomagnetism has been used for magnetostratigraphy in the petroleum industry (Gillen et al., 1999: Cioppa et al., 2001; Filippycheva et al., 2001), while environmental magnetism has been investigated for the detection of hydrocarbon seepage (Yeremin et al., 1986; Liu et al., 1996; Costanzo-Alvarez et al., 2000).

Different laboratory techniques have been used in the past to measure the magnetic properties of minerals. Some important ones include using a magnetic separator (Stradling, 1991), the magnetometer (Foner and McNiff, 1968), the resonant coil (Cooke and De Sa, 1981) and the inductance bridge (Drobace and Maronic, 1999;Tarling and Hrouda, 1993).

The first commercial equipment to measure magnetic susceptibility was proposed by the Julius Kruttschnitt Mineral Research Centre (JKMRC) (Cavanough and Holtham, 2001 and Cavanough and Holtham, 2004). The CS-2 and KLY-2 Kappabridge was used for thermomagnetic studies of weakly magnetic rocks (Hrouda, 1994).

Anisotropy of magnetic susceptibility (AMS) (Hrouda, 2002), the intensity, inclination and the declination of the natural remanent magnetisation have paved the way for high-resolution rock magnetic analyses (Hall and Evans, 1995; Liu and Liu, 1999; Robin et al., 2000).

Recently, the petrophysics research group at Heriot-Watt University has proposed a novel way of processing the magnetic susceptibility data to predict important petrophysical parameters, such as clay content and permeability, for reservoir characterization (Potter, 2004a; Potter 2004b; Potter et al., 2004; Potter, 2005 andPotter, 2007; Ivakhnenko and Potter, 2008; Potter and Ivakhnenko, 2008). None of these techniques has yet been used for characterizing the effect of natural cements on permeability and various other petrophyscial parameters. Additionally, no work has been done on the Polycrystalline Diamond Compact (PDC) drill cuttings as an application of the magnetic susceptibility technique in detecting faults and fluid contacts. The correlations between the magnetic susceptibility and other well-logging are particularly important in applying this knowledge to practical field problems. Since log-derived petrophysical parameters such as porosity and permeability are generally used for reservoir characterization, the correlations between mass magnetic susceptibility and the conventional wireline log data would prove to be very useful for various petrophysical parameter predictions.

1.6 Aims and objectives of the thesis

The first objective of the research work presented in this thesis is to investigate the effect of grain lining hematite cement on permeability in clastic reservoir rock samples. The work is essentially an extension of the early work by Potter and Ali, (2010; 2011). For the first time, the study has shown that not only the dispersed hematite but also the grain lining hematite cement surrounding the quartz grains has significant control on permeability in reservoir rock samples. It was demonstrated

how magnetic susceptibility correlated with permeability and grain lining hematite cement in a relatively tight gas sandstone reservoir.

The second objective of this thesis is to provide a method of identifying faults and reservoir fluid contacts using magnetic susceptibility measurements on drill cuttings. Currently, there is no well site or laboratory-based method used on drill cuttings to help in the determination of faults and free water level. Well site magnetic susceptibility data can potentially help in identifying faults, as well as in refining the depth uncertainty in fluid contacts, due to the rapid and high number of measurements on drill cuttings.

The third objective of this thesis is to create novel crossplots between the magnetic susceptibility of various rocks and clay minerals versus data from other key wireline logging tools. These new cross plots have their own importance and in some cases overcome the limitations from other conventional crossplots.

1.7 Thesis Organization

This thesis is organized into six different chapters.

Chapter One is a detailed literature survey that reviews previous studies and constitutes the impetus for the present study.

Chapter Two presents an introduction to the different types of magnetic minerals found in hydrocarbon-bearing reservoirs. A brief summary of the main physical laws that govern the behaviour of these minerals is given. The magnetic properties such as domain states and magnetic hysteresis are explained in terms of mineral grain size and magnetic phase. The chapter also describes the instruments used for the various magnetic measurements undertaken in the research.

Chapter Three explains the importance of hematite cement and its effect on permeability. This chapter also explains how magnetic susceptibility measurements can be used for permeability predictions in reservoirs where permeability is controlled by a thin lining of hematite cement around quartz grains.

Chapter Four describes the importance of magnetic susceptibility measurements in identification of faults and fluid contacts in hydrocarbon-bearing reservoirs.

Chapter Five explains the step by step process of creating the new template cross plots between magnetic susceptibility and other downhole wireline log data. The new crossplots help in the determination of mineralogy and mixture porosity in reservoir rock samples.

Finally**, Chapter Six** summarizes the results from work presented in this thesis along with recommendations for future work.

Chapter 2 Theoretical Background and Equipment Used for the Work Presented in the Thesis

2.1 Introduction

This chapter deals with the relevant theoretical background regarding magnetism, including the main types of magnetism which are diamagnetism, paramagnetism, ferromagnetism and antiferromagnetism. The equipment and sensors used for the experimental work are also described in full detail in this chapter, to give more understanding of the magnetic measurements presented in this thesis.

2.2 Basics of rock magnetism and magnetic susceptibility

Magnetic susceptibility is the degree of magnetisation of a substance in the presence of an external magnetic field (Blum, 1997). All the substances around us have a magnetic susceptibility, which may be positive such as paramagnetic, ferromagnetic or antiferromagnetic susceptibility or negative such as diamagnetic susceptibility. If there is a coil has length (L) and the number of turns in this coil is (n), when the current (I) passes through this coil a magnetic field will be generated in this coil (Kailas, 2008). (A/m) is the unit used for the magnetic field, given by the following equation:

$$H = \frac{nI}{L} \tag{2.1}$$

Weber (Wb) / m^2 or Tesla is the unit used for magnetic flux density (Kailas, 2008).

The magnetic induction (B) and the magnetic field (H) are related to each other by the following equation (Tauxe, 2005):

$$B = \mu_o(H+M), \tag{2.2}$$

where

$\mu_o = (4\pi \times 10^{-7}$ Henry/m) . μ_o is the permeability of free space.

Volume magnetic susceptibility χ_v and the magnetic permeability μ are related by the following formula:

$$\mu = \mu_o (1+\chi_v), \quad (2.3)$$

where

$1+\chi_v$ is the relative permeability.

To convert the volume magnetic susceptibility into mass susceptibility, one simply needs to divide volume magnetic susceptibility by the bulk density of the sample, using the following formula:

$$\chi_m = \chi_v/\rho \ , \quad (2.4)$$

m^3kg^{-1} is the unit of magnetic susceptibility in the SI system. Table 2.1 shows various magnetic terms, units and conversion factors.

Magnetic Term	**Symbol**	**SI unit** **International System of Units**	**CGS unit** **Centimetre–gram–second system**	**Conversion factor**
magnetic induction	B	A/m	Gauss (G)	1 T = 10^4 G
magnetic field	H	Tesla (T)	Oersted (Oe)	1 A/m =$4\pi/10^3$ Oe
magnetization	M	A/m	emu/cm^3	1 A/m = 10^{-3} emu/cm^3
magnetic moment	m	Am^2	emu	1 Am^2 = 10^3emu
volume susceptibility	χ_v, k	dimensionless	dimensionless	4π (SI) = 1 (cgs)
mass susceptibility	χ_m	m^3/kg	emu/ Oe·g	1 m^3/kg = $10^3/4\pi$ emu /Oe·g
permeability of free space	μ_0	H/m	dimensionless	$4\pi x10^{-7}$ H/m = 1 (cgs)

Table 2-1: Common magnetic terms, their units and conversion factors. (Moskowits, 1991).

2.3 Types of magnetic materials

Materials behave differently in their response to the magnetic field, so magnetism can be divided into five basic types which are:

- Diamagnetic
- Paramagnetic
- Ferromagnetic
- Ferrimagnetic
- Antiferromagnetic

Diamagnetic and paramagnetic materials do not have a collective magnetic interaction in the absence of the magnetic field, whereas ferromagnetic substances in the absence of magnetic field and at a certain temperature have a high interaction between their magnetic moments. (Rao, 2012). Ferromagnetic and ferrimagnetic materials are usually considered to be magnetic martial (i.e. behaving like iron).

2.3.1 Diamagnetism

The first appearance of the theory of the diamagnetism and paramagnetism was in a paper published by Paul Langevin in 1905 (Evans and Heller, 2003). In the absence of a magnetic field, diamagnetic minerals do not have orbital moments because all of the orbital shells are filled, and the magnetic moments are randomly oriented (Hinze et al., 2013). All materials contain diamagnetic, but is so weak the reason behind that the diamagnetism appears only in substances that do not exhibit another type of the magnetic behaviour (Hinze et al., 2013). The magnetic moment induced by the diamagnetism is too small against the direction of the magnetic field, causing a reduction in strength of the external applied field (Hinze et al., 2013). This is shown in Figure 2.1. The induced magnetization disappears as soon as the applied magnetic field is reduced to zero. Typical examples of diamagnetic minerals are shown in Table 2.2.

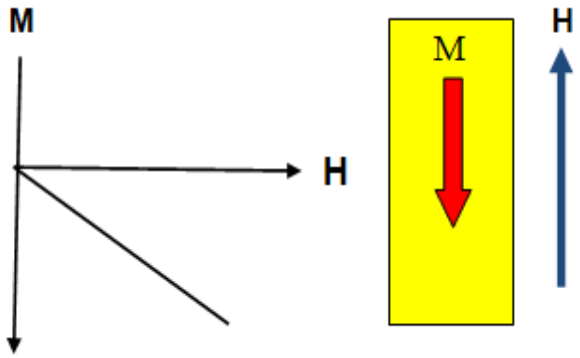

Figure 2-1: Schematic behaviour of diamagnetic material: magnetisation versus an applied magnetic field.

Diamagnets				
Anhydrite	-0.5 - -2	2.8	$CaSO_4$	bi,br,pa,to
Calcite	-0.48	1.56	$CaCO_3$	bi,br,wy
Dolomite	~-1.2	3.16	$CaMg(CO_3)_2$	to,wy
Feldspar	-0.49 - -0.67	2.65	$(K,Na)AlSi_3O_8$ and $Ca(Na)Al_2Si_2O_8$	bl,du,mu,pe
Graphite	-3.7 - -9.3	2.16	C	bi,sh,to,wa,wy
Gypsum	-0.5 - -1.3	2.6	$CaSO_4 \cdot nH_2O$	bi,sh,wa,wy
Halite Sodium Chlorite	-0.48 - -0.75 -0.64	2.08	NaCl	bi,br,sh,wa,wy
Kaolinite	-2	2.63	$Al_4[Si_4O_{10}](OH)_8$	de
Magnesite	-0.48		$MgCO_3$	co
Quartz	-0.5 - -0.6	2.6	SiO_2	bi,br,pa,to

Table 2-2:"Initial mass magnetic susceptibilities of diamagnetic minerals of petroleum-bearing sediments and compounds related to the hydrocarbon industry. All magnetic susceptibilities were measured in weak fields at room temperature and a pressure of one atmosphere. Literature values for susceptibilities were converted into SI units when necessary. And from volume to mass susceptibility, using appropriate values for densities. [bi]Biot, 1962, [bl]Bleil et al. 1982, [bo]Borradaile et al. 1990, [br]Brace. 1965, [ca]Carmichael, 1989, [co]Collinson, 1983, [de]Deer et al. 1992, [do]Dortman, 1976, [du]Dunlop and Ozdemir, 1997, [fo]Foex et al. 1957, [hi]Hill, 1963, [ma]Matteson et al., 2000. [me]Melnikov, 1975, [mu]Mullins, 1977, [pa]Parasnis, 1979, [pe]Petersen, 1985, [sh]Sharma, 1986, [ta]Tarling and Hrouda, 1993, [te]Telford et al. 1990,[th]Thompson and Oldfield, 1986, [to]Torquato, 1991, [wa]Watt, 1988, [wy]Wyllie et al. 1958". (Ali. A, 2009 Ph.D. thesis).

2.3.2 Paramagnetism

Paramagnetic minerals have a small, positive magnetisation to an applied magnetic field. As the external magnetic field increases, this will be associated with an increase in the magnetisation. Figure 2.2 shows the behaviour of the paramagnetic mineral when a magnetic field is applied. The strong magnetisation in this kind of magnetisation is due to the alignment of the magnetic moment in the same direction with the magnetic field. The magnetic moment dipoles will relax to their random motion as soon as the magnetic field is removed; this is related to losses in the net magnetic alignment (Ramanujan, 2009). Typical examples of paramagnetic minerals are illite, montmorillonite, muscovite, and pyrite, as shown in Table 2.3.

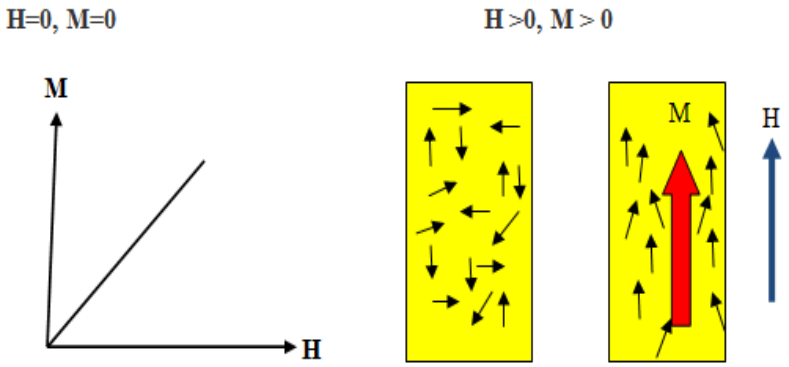

Figure 2-2: Schematic behaviour of paramagnetic material: magnetisation versus applied magnetic field.

Minerals and compounds	Mass magnetic susceptibility, χ_m (10^{-8} m^3 kg^{-1})	Density (10^3 kg m^{-3})	Composition	References
Paramagnets and Compensated Antiferromagnets				
Arsenopyrite	50	6.05	FeAsS	te,wy
Chalcopyrite	(0.55-10)	4.2	$CuFeS_2$	bi,bl,te,wy
Chamosite	~90		$(Mg,Fe)_3Fe_3[AlSi_3O_{10}](OH)_8$	co,th
Chlorite Chlorite BVS[bo]	2.5-55.4	2.8	$(Mg,Al,Fe)_{12}[(Si,Al)_8O_{20}](OH)_{16}$	ta
Chlorite CFS	52.5			
Fe-dolomite	1.1		$(Ca,Mg,Fe)CO_3$	mu
Ferrous chlorite	145		$FeCl_2$	co
Ferrous sulphite	51.7		$FeSO_4 \cdot 7H_2O$	co
Glauconite	~41.6	2.4	$(K,Na)(Al,Fe,Mg)_2[(Al,Si)_4O_{10}](OH)_2$	de
Illite	15	2.75	$(K_{1-1.5}Al_4)[(Si_{7-6.5}Al_{1-1.5}O_{20}](OH)_4$	br,ca,co,du,th
Ilmenite	100-115		$FeTiO_3$	bl,ca,co,du,fo
Lepidocrocite	40-70	4.25	γ- FeOOH	bl,fo,th
Limonite	66-74	4.24	$FeOOH \cdot nH_2O$	bl,th
Manganese sulphate	81		$MnSO_4 \cdot 4H_2O$	co
Montmorillonite	13-14	2.5	$Na_{0.7}(Mg_{0.7}Al_{3.3}Si_8O_{20})OH_4 \cdot nH_2O$	br,ca,co,du
Muscovite	1-15	1.1	$KAl_2[(AlSi3)O_{10}](OH)_2$	mu
Nontronite	65, ~90		$Na_{0.33}Fe_2[(Al_{0.33}Si_{3.67})_4O_{10}](OH)_2 \cdot nH_2O$	co,th
Pyrite	1-100	5.02	FeS_2	bi,bl,fo,hi,to,wy
Siderite	32-270	3.96	$FeCO_3$	bi,br,hi,me,te,pa
Smectite	~3.2	7.06	$(1/2Ca,NA)_{0.7}(Al,Mg,Fe)_4[(Si,Al)_8O_{20}]\ nH_2O$	ma
Troilite	13-36	4.83	FeS	bi,bl,fo,hi
Vermiculite	15.2		$(Mg,Fe,Al)_3[(Al,Si)_4O_{10}](OH)_2 \cdot 4H_2O$	mu

Table 2-3:"Initial mass magnetic susceptibilities of paramagnetic and compensated antiferromagnetic minerals of petroleum-bearing sediments and compounds related to the hydrocarbon industry. All magnetic susceptibilities were measured in weak fields at room temperature and at a pressure of one atmosphere. Literature values for susceptibilities were converted into SI units when necessary. And from volume to mass susceptibility, using appropriate values for densities. [bi]Biot, 1962, [bl]Bleil et al. 1982, [bo]Borradaile et al. 1990, [br]Brace. 1965, [ca]Carmichael, 1989, [co]Collinson, 1983, [de]Deer et al. 1992, [do]Dortman, 1976, [du]Dunlop and Ozdemir, 1997, [fo]Foex et al. 1957, [hi]Hill, 1963, [ma]Matteson et al., 2000. [me]Melnikov, 1975, [mu]Mullins, 1977, [pa]Parasnis, 1979, [pe]Petersen, 1985, [sh]Sharma, 1986, [ta]Tarling and Hrouda, 1993, [te]Telford et al. 1990, [th]Thompson and Oldfield, 1986, [to]Torquato, 1991, [wa]Watt, 1988, [wy]Wyllie et al. 1958." (Ali. A, 2009 Ph.D. thesis).

2.3.3 Ferromagnetism

Ferro is a Latin word referring to the substances which has a high interaction between its magnetic moment (high magnetic properties), for this reason the iron mineral has the symbol of the (Fe). (Kirkland, 2007).There is a reasonable number of small domains in ferromagnetic substances that are randomly magnetized. In the demagnetized state, the domains inside the substance are oriented in such way resulting in zero magnetic moments (Smith and Zrostlik, 1999). In the presence of the magnetic field, all the magnetic moment will align themselves with the magnetic field and, as a result, there is a net magnetic moment as shown in figure (Figure 2.3).

Ferromagnetic materials have unpaired electrons in their atoms. This phenomenon allows for a greater interaction to occur between the unpaired electron spins, resulting in an additive magnetizing effect of ferromagnetism. This effect can occur in the absence on an applied field (Smith and Zrostlik, 1999). Ferromagnetism is correlated with the elements of iron, such as nickel and cobalt (hence the name ferromagnetic), but it also occurs in iron oxides such as magnetite (Evans and Heller, 2003).

Ferromagnetic properties can be changed at a certain temperature called the Curie temperature. Different minerals have different Curie temperature. Table 2.4 shows the Curie temperature of certain minerals. Below that temperature, the ferromagnetic material can hold the magnetisation obtained from an external field, and while above that point (Curie temperature) thermal energy enhances alignment and the substance acts as paramagnetic material (Thompson & Oldfield. 1986).

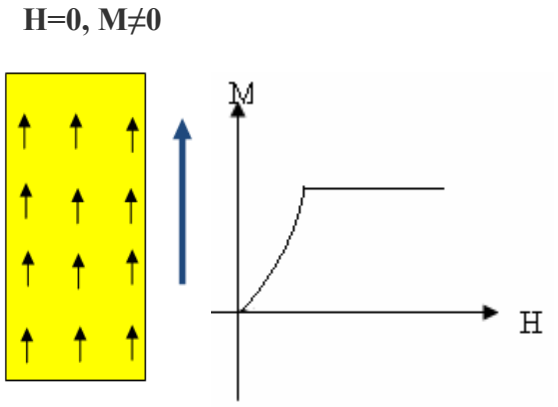

Figure 2-3: Schematic behaviour of ferromagnetic material: magnetisation versus applied magnetic field.

Mineral	Magnetic order	Curie temperature
Magnetite	Ferrimagnetic	575-600 ˚C
Hematite	Canted antiferromagnetic	675-695 ˚C
Pyrrhotite	Ferrimagnetic	300-325 ˚C
Greigite	Ferrimagnetic	330-530 ˚C
Titanomagnetite	Ferrimagnetic	90-530 ˚C

Table 2-4: Curie temperature of some minerals

2.3.4 Ferrimagnetism

Ferromagnetic materials are a mixture of both ferromagnetic and antiferromagnetic. As in antiferromagnetic materials (which we will see next), the adjacent magnetic spins align anti- magnetism parallel, so as to cancel their magnetic moments (Figure 2.4). However, the adjacent spins at the substance have a different magnitude, so this substance in the absence of an external magnetic field (demagnetized state) exhibits a net magnetic moment. Magnetite is one of the most commonly known ferrimagnetic materials but was considered as one of the ferromagnetic materials until Neel in the 1940's presented his theoretical framework for understanding the differences between the behaviour of ferromagnetic and ferrimagnetic materials (Fuller, 1987).

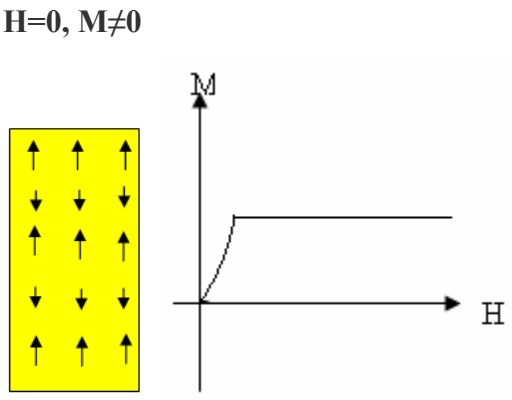

Figure 2-4: Schematic behaviour of ferrimagnetic material: magnetisation versus applied magnetic field.

2.3.5 Antiferromagnetic

In antiferromagnetic substances, the magnetic moments align themselves in opposite directions (antiparallel) and are equal in magnitude (Sattler, 2011). Thus, where is no magnetic field applied, the net magnetisation of the antiferromagnetic material is zero (Sattler, 2011) (Figure 2.5). However, a tiny of the magnetic moment will be account if magnetic moments are not completely cancelling each other. This phenomena known as a imperfect antiferromagnetism, also called canted antiferromagnetism (Sattler, 2011). Hematite and goethite are examples of canted antiferromagnetic minerals.

Table 2.5 lists the magnetic susceptibility of the most common ferromagnetic, ferrimagnetic and canted antiferromagnetic minerals of petroleum-bearing sediments and compounds.

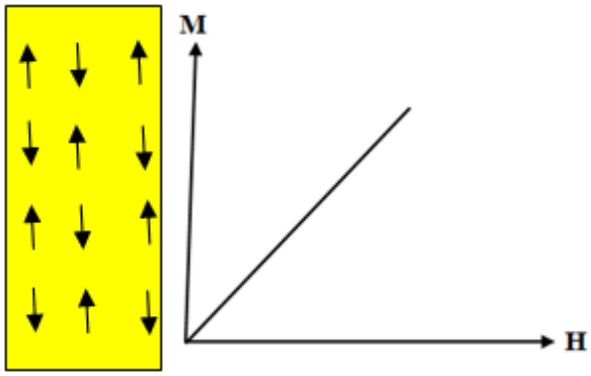

Figure 2-5: Schematic behaviour of antiferromagnetic material: magnetisation versus applied magnetic field.

Minerals	Magnetic order	Mass magnetic susceptibility, χ_m (10^{-8} m^3 kg^{-1})	Density (10^3 kg m^{-3})	Composition	Spontaneous magnetisation, Ms (10^3 A m^{-1})	References
Iron	Ferromagnetic	50000	7.87	αFe	1715	co,du,hu,th
Magnetite	Ferrimagnetic	20000-110000	5.18	$FeFe_2O_4$	480	du,hu,th
Maghemite	Ferrimagnetic	40000-50000	4.90	λFe_2O_3	380	du,hu,th
Titano magnetite	Ferrimagnetic	2500-12000	4.98	$Fe_{3-x}Ti_xO_4$, x=0.6	125	du,hu
Titano maghemite	Ferrimagnetic	57000	4.99	$Fe_{(3-x)R}Ti_{xR\cdot 3(1-R)}O_4$, R=8/[8+z(1+x)]		co,hu
Greigite	Ferrimagnetic			Fe_3S_4	~125	du
Pyrrhotite	Ferrimagnetic	10-30000	4.62	$Fe_{1-x}S$	~80	du,hu
Hematite	Canted AFM	10-760	5.26	Fe_2O_3	~2.5	du,hu,mu
Goethite	AFM, weak FM	26-280	4.27	$\alpha FeOOH$	~2, <1	du,hu,th
Hydrated iron (II) sulphate	Ferrimagnetic	0.5-100	4.13	$FeSO_4.7H_2O$		ha

Table 2-5: "Initial mass magnetic susceptibilities of ferromagnetic, ferrimagnetic and canted antiferromagnetic minerals of petroleum-bearing sediments and compounds related to the hydrocarbon industry. All magnetic susceptibilities were measured in weak fields at room temperature and at a pressure of one atmosphere. Literature values for susceptibilities were converted into SI units when necessary and from volume to mass susceptibility, using appropriate values for densities. FM: Ferromagnetic; AFM: Antiferromagnetic.[co]Collinson, 1983, [du]Dunlop, Ozdemir, 1997, [ha]Hanson and Sauchuk, 1991, [hu]Hunt et al., 1995, [mu]Mullins, 1977, [th]Thompson and Oldfield, 1986." (Ali. A, 2009 PhD thesis).

2.4 Magnetic Hysteresis

Different rock magnetic parameters can be obtained by analysing hysteresis curves using one of the types of hysteresis measurement equipment, such as The Variable Field Translation Balance (VFTB). If two a high applied magnetic fields with the same strength, but in the opposite direction applied to for a sample the parameters of hysteresis loop can be easily obtained.(Evans, 2006). Tesla (T) is the unit of measuring the magnetic field.

Figure 2.6 shows the behaviour of a ferromagnetic sample. When the magnetic field applied the magnetisation increases. By increasing the magnetic field the magnetisation will reach a point that known as saturation. At the saturation all the domains and the magnetic moments will have the same direction of the external applied field. All the domains and the magnetic moments return to their previous direction as soon as the magnetic field is reduced. The magnetic moment remains randomly distributed as the magnetic field is reduced lower and lower until it reaches zero, and there is still net magnetization in the sample, called remanent magnetization. This happens because some of the magnetic moment is still in the same direction as the magnetic field before the magnetic field was removed completely and became zero.

From the hysteresis curve, a number of hysteresis parameters are obtained, which are defined below.

- Saturation Magnetisation (Ms) is the highest possible magnetisation obtained with an externally applied field.
- Remanence Magnetisation (Mrs) is the residual magnetisation when the applied field is removed, in other words, when the applied magnetic field reaches zero after reaching the saturation magnetisation.
- Coercivity (H_c) is a field at which the magnetisation becomes zero in the hysteresis curve. The coercivity is always smaller than or equal to the coercivity of remanence.
- Coercivity of Remanence (H_{cr}): is the reverse applied field which, when removed, leaves the sample in the demagnetized state.

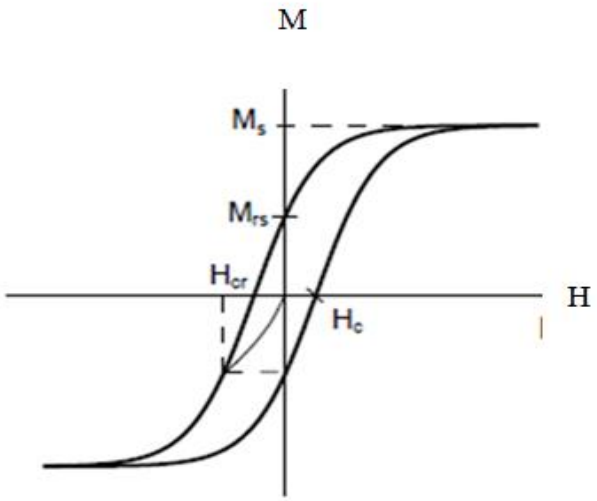

Figure 2-6: Schematic behaviour of the magnetic susceptibility of ferromagnetic material.

Figure 2.7 shows a typical hysteresis curve for the magnetic types. It's clear that that the negative high slope is for the clean diamagnetic sample, whereas the positive high field slope is related to the presence of a paramagnetic sample. The combination of antiferromagnetic and diamagnetic minerals show a large kink or loop at the low magnetic field, confirming that there is a reasonable percentage of the antiferromagnetic mineral in this sample. The combination ferromagnetic and paramagnetic at the low magnetic field shows a small kink or loop, which means that the sample contains a small amount of the ferromagnetic minerals. (Ali. A, 2009 PhD thesis).

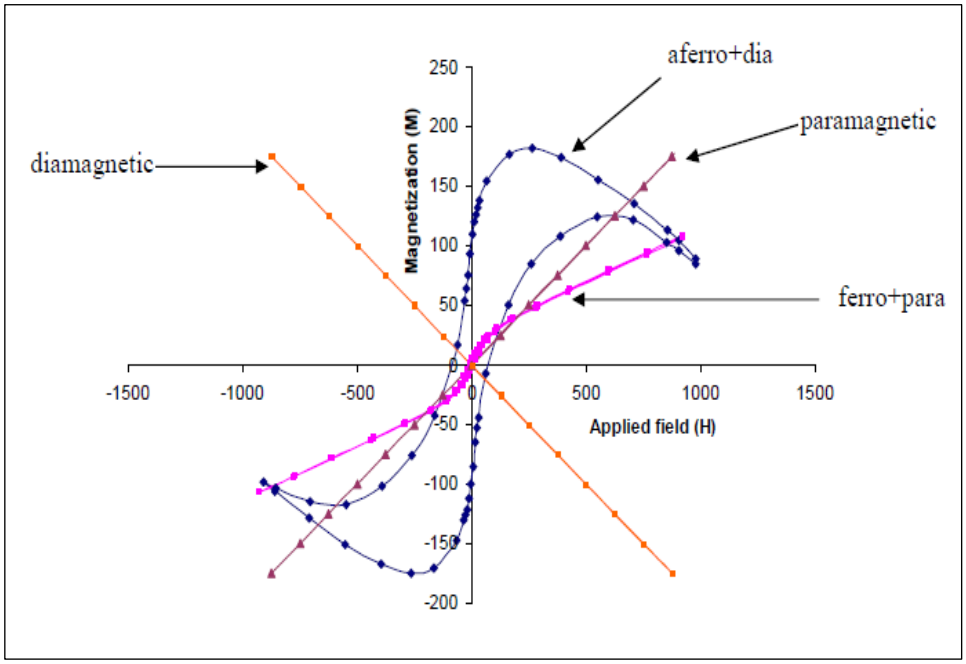

Figure 2-7: Typical hysteresis curve for samples containing combinations of different types of the magnetism. (Ali. A, 2009. PhD thesis).

2.5 Magnetic Domain Theory and Grain Size

2.5.1 Domain theory

The term magnetic domain was first introduced by Pierre-Ernest Weiss in 1926. Magnetic grain-size measurements are estimated using two hysteresis ratios, Mrs/Ms versus Hcr/Hc.

There is a difference between ferromagnetism and the other type of magnetic material such paramagnetism and diamagnetism. In the ferromagnetism each domain is separated by the domain wall from its neighbour. In the absence of the external field, all the domains in the specimen line up themselves to reduce the magnetostatic energy associated with their surface poles (Hrouda, 1993). A substance which has a single domain behaves completely different from one which contains multidomains, even if there is a similarity in the total amount the composition of the ferromagnetic materials. When an external magnetic field applied, the domains in the ferromagnetic substance align themselves with the external field, resulting in the net magnetisation of the substance. As the magnetic field increases more alignment of the domains will occurs, until all the domains rotated in the same direction with the magnetic field. The local magnetisation of each domain is saturated, but it is not necessary to be parallel (Dunlop and Ozdemir, 1997; ,Hrouda, 1993).

The number of domains is controlled by the shape and size of the grain. A domain that is too big and unstable will be divided into smaller domains. In contrast, a smaller domain can be stable and will not split. Generally, larger grains may contain more than one domain, known as multiple- domains (hence, multi-domain), whereas the small grain once has only one domain (single domain).

Figure 2.8 shows the behaviour of the domain wall in demagnetised state and in the presence of an external magnetic field.

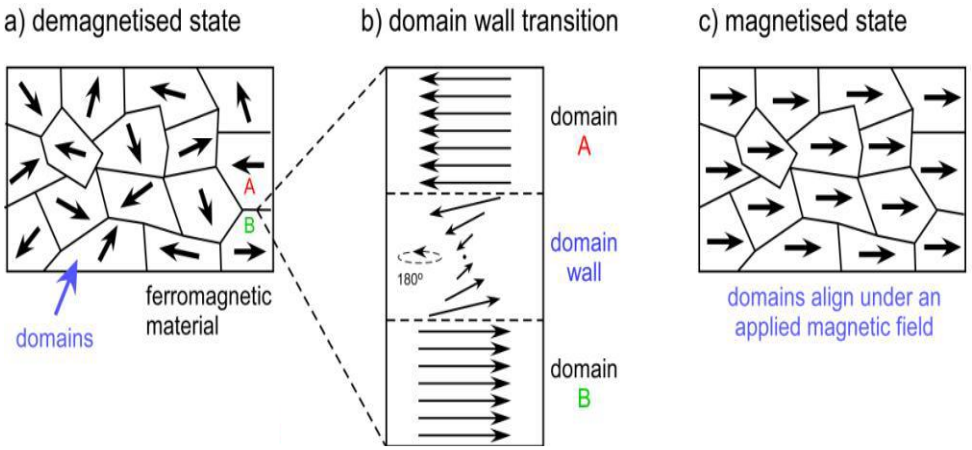

Figure 2-8: (a) Domains align randomly in the absence of the magnetic field. (b) The transition of the domain wall from one domain to another. (c) Domains point in the same direction in the presence of the magnetic field. (*Dunlop and O¨zdemir*, 1997)

2.5.2 Grain Size

Grain size subdivided in four ranges depended on the behaviour of their magnetic.

SD: single domain; PSD: Pseudo-single domain; MD: multidomain and SP: superparamagnetic (Dunlop and Ozdemir, 1997).). If the grain size is small, which may contain only domain and the magnetisation will uniform in the same direction, whereas, if the domain is large which may has more than one domain which will align in the easy axes (Hrouda, 1993).

- ***Single domain (SD):***

Small-grained particles are only able to have a single domain. This kind of grain size is unstable and can flip its magnetic axis through 180 degrees. By contrast, a particle that is single-domain has larger coercivity, because any external magnetic field should forc all the magnetic moments to align in the same direction.

- ***Multi domain (MD)***

A specimen that contains more than one domain is known as a multi-domain. MD grains have lower coercivities and lower remanences, compared with SD grains, since the direction of all the domains started to rotate in the same direction of the external magnetic field.

- ***Pseudo-single domain (PSD):***

The boundary between MD & SD is not sharp, so there is a kind of grain that contains only few numbers of domains, known as a pseudo-single domain (PSD). This is in between a single domain and-multi-domain and behaves like either a single domain (high remanence) or a multi-domain (low coercivity).

- ***Superparamagnetic (SP):***

Within a single domain (SD) range, as the particle size becomes smaller and smaller, it reaches a critical threshold. At this point, the grain is called superparamagnetic, when the coercivity and the remanence become equal to zero (Fuller, 1987). SP grains range from 20-25 nm in size.

Figure 2.9 shows that the breakup of magnetisation from one domain to multi domain (more than one domain).

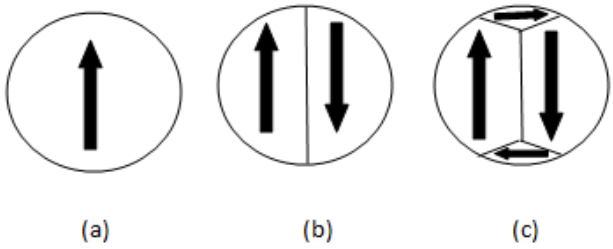

Figure 2-9: The breakup of magnetisation into domains: (a) single domain, (b) two domains, (c) closure domains.

2.6 Day Plot

The Day plot method differentiates between the mineral which has different domain states; the grain size is graphically considered to be a function of the domain state. (Dunlop, 2002). There are two ratios, Mrs/Ms and Hcr/Hc, plotted against each other in a graph known as a Day plot, as shown in Figure 2.10 (Dunlop and Carter-Stiglizt, 2006). Day et al. (1977) divided the plot into regions of a single domain (SD), pseudo single domain (PSD), and multidomain (MD) behaviour and suggested that hysteresis parameters could be used to infer magnetic grain size.

For the SD the M_{rs}/M_S ratio is great for SD particles and this ratio decreases gradually as the grain size increases into the PSD and MD states. The boundaries between regions on the Day plot are summarised in Table 2.6.

Grain type	Hc (mT)	Hcr/Hc	Mrs/Ms
MD	LOW (2.5-4)	HIGH >4	LOW (0.01-0.03)
PSD	MEDIUM	MEDIUM (1.5-4)	MEDIUM (0.03-0.5)
SD	HIGH (10-40)	LOW <2	HIGH (0.5-0.9

Table 2-6: Typical hysteresis parameter values for MD, PSD and SD grains. (Ali, 2009, PhD thesis).

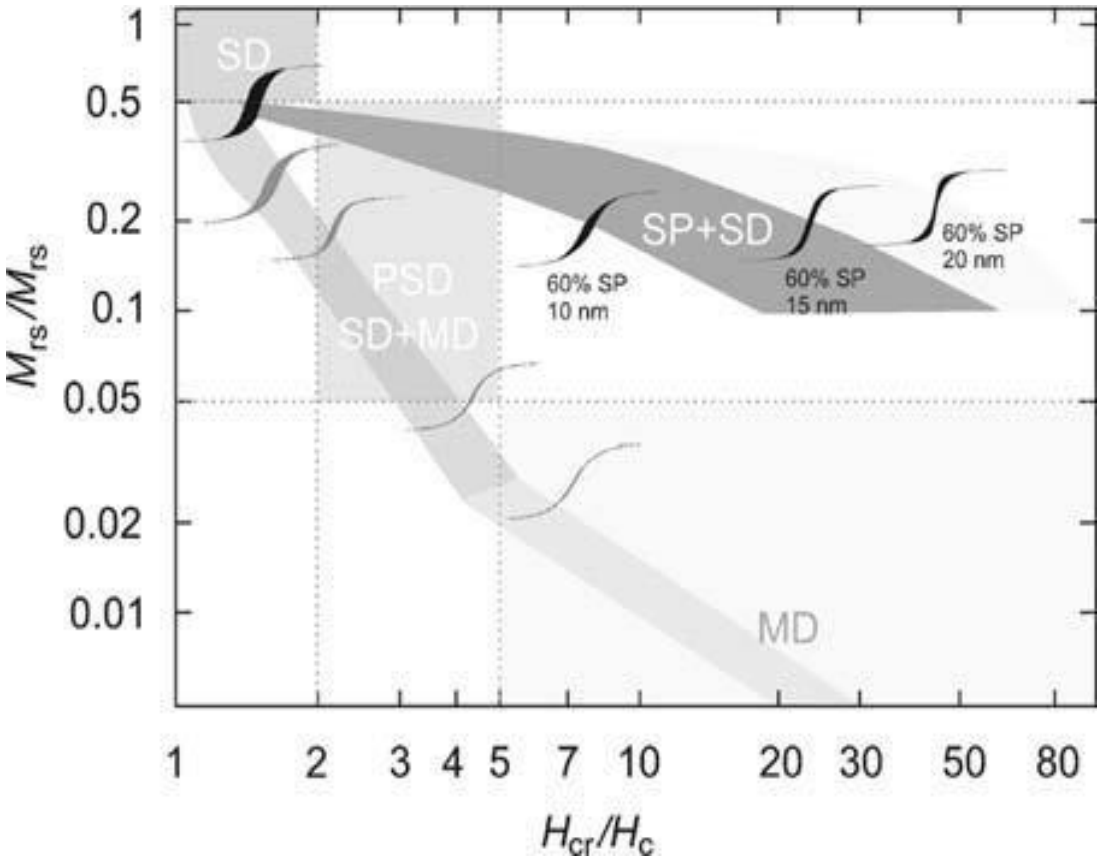

Figure 2-10: The Day plot classifies hysteresis curves in terms of the grain size sensitive quantities Mrs/Ms and Bcr/Bc (Dunlop, 2006).

2.7 Equipment Used for the Work Presented in the Thesis

2.7.1 Bartington Instruments: MS2B Sensor, MS2 and MS3 Meters

The MS2B sensor accepts 10cc plastic vials for measurements. The sensor is shown in Figure 2.11. This instrument is suitable for measuring samples with a diameter of 2.54 cm and a length of 2.5 cm. Magnetic susceptibility for powder samples or small cuttings can be measured using this sensor by putting them in 10cc plastic vials. Two different frequencies 4.65 kHz and 0.465 kHz can be used for measuring the susceptibility in the MS2B. This allows the detection of superparamagnetic minerals in reservoir rock samples, which are very fine grained ($\leq$0.03μm) and sometimes have an impact on permeabilities of the rock samples (Dearing 1999).

The two types of meters used for reading out the magnetic susceptibility data are shown in Figures 2.12 and 2.13. They are called, Bartington Instruments MS2 and Bartington Instruments MS3 meters, respectively. The meters calculate the susceptibility in the range of either 1.0 or 0.1, the latter being more precise (Dearing 1999). A calibration sample with low frequency-dependency is available with this sensor. The accuracy of this calibration is within 1%. The modern Bartington Instruments MS3 meter has the advantage of automatically doing the correction for background measurements on magnetic susceptibility readings. It also copies all of the measurement data automatically into an Excel spreadsheet. The Bartington Instruments MS2 meter, on the other hand, requires manual intervention for background corrections, as well as noting down the readings into the spreadsheet.

Figure 2-11: Bartington magnetic susceptibility balance (MS2B on the right).

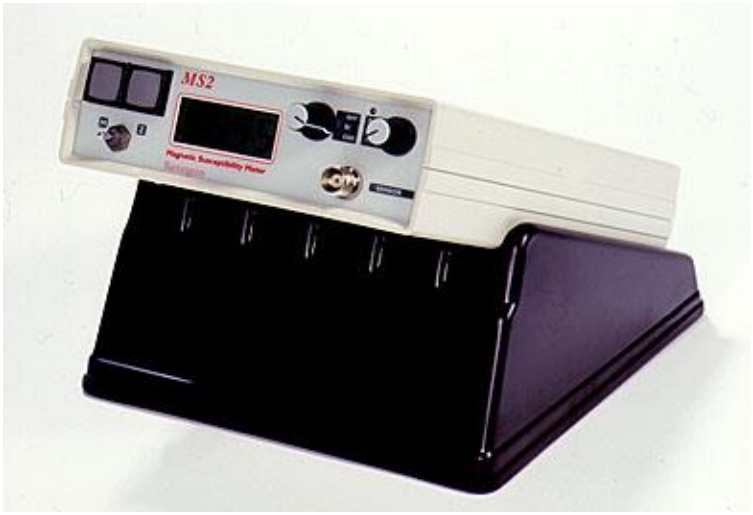

Figure 2-12: MS2 meter from Bartington Instruments

Figure 2-13: MS3 meter from Bartington Instruments.

2.7.2 Sherwood Magnetic Susceptibility Balance

The Magnetic Susceptibility Balance (MSB) is a microprocessor balance showed in Figure 2.14. It can accept solid or liquid samples as small as 50 mg. This piece of kit was used to perform magnetic susceptibility measurements on individual drill cuttings, which were of mm size. The Bartington kits take larger volume samples and are therefore not sensitive enough to measure small sized samples.

The Sherwood balance is simple, fast and highly accurate. The device provides information on volume magnetic susceptibility of the samples. To calculate the mass magnetic susceptibility the following equation can be used:

$$\chi = \frac{C*L*(R-R_o)}{10^9*m} \quad , \tag{2.5}$$

where:

C= calibration constant of the balance

L= length of the sample (cm)

m= mass of the sample (g)

R= reading on MSB of the sample in the tube

R_o= reading of the empty tube.

Figure 2-14: Sherwood Scientific magnetic susceptibility balance (MSB).

2.7.3 Variable Field Translation Balance (VFTB)

The magnetic hysteresis curves shown in **Chapters 3-5** were measured by using the Variable Field Translation Balance (VFTB) (Figure 2.15) located in the petrophysics laboratory at Heriot-Watt University. This instrument operates with high magnetic fields, up to 1.2 Tesla. It can perform a variety of magnetic measurements, including Curie temperature measurements up to 700 ^{o}C, Isothermal Remanent Magnetization (IRM) acquisition (-180 to +700 ^{o}C), back-field coercivity and hysteresis loops. The measurements of each hysteresis loop takes about fifteento be completed .Magnetic moment sensitivity of the Variable Field Translation Balance (VFTB) amounts to $5*10^{-8}Am^2$. Sample holder used in this equipment can hold a sample with diameter arrnge from 5 or 10 mm and with of 9 mm (Gubbins and Herrero-Bervera, 2007).

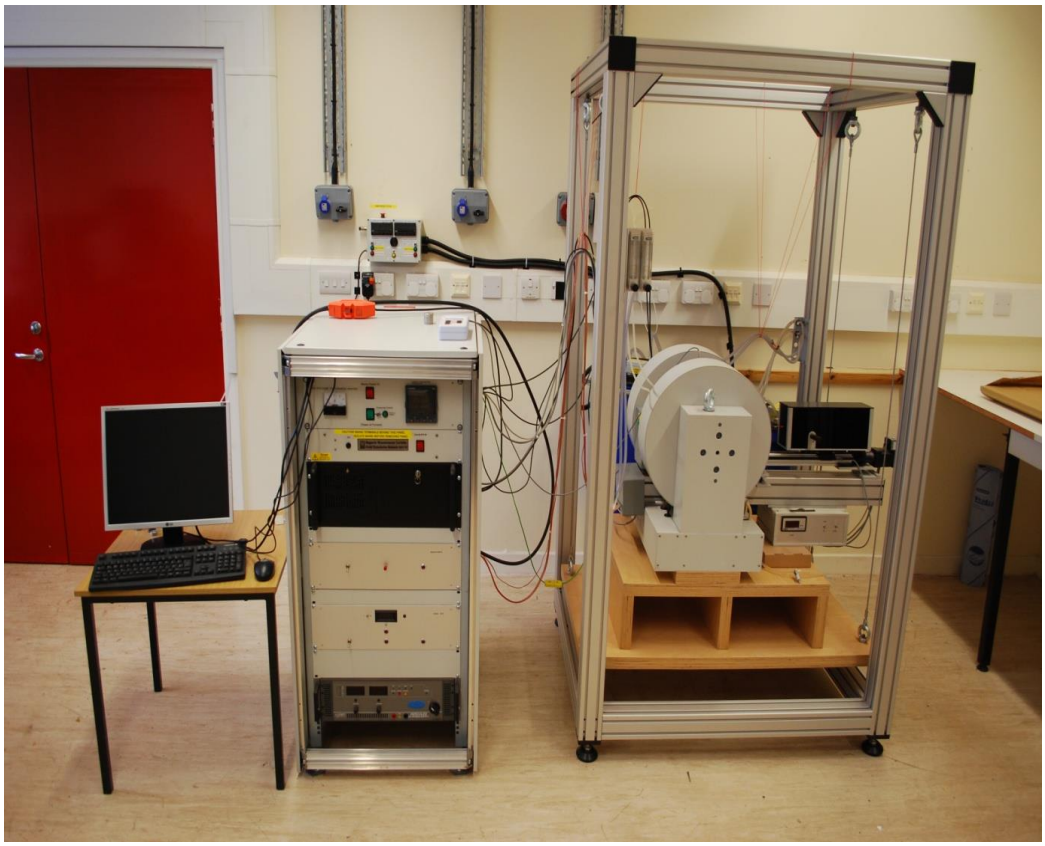

Figure 2-15: The Variable Field Translation Balance (VFTB).

2.7.4 The Olympus Microscope (BHTP)

"Polarized-light microscopy provides a non-destructive way to identify solid substances with relatively high spatial resolution while the phases can be studied within their textural framework" (Raith, 2012. ppII). The Olympus microscope (BHTP) has two states: polarizer, one that polarizes the incoming light source, and another that polarizes the light after it has passed through. The microscope is connected with a camera so that the image can be viewed and saved in the computer (Siemianowski, 2010). (Figure 2.16). A thin slice of rock under study is placed under the polarising microscope. One of the sides of this rock slice is polished and affixed to a sliding glass with adhesive. Next, the opposite side is polished to a 30 micron thickness and affixed to the cover glass with balsam. By using only one polarity, the color, size and the shape of the crystals inside the rock can be seen and detected. With these facilities, different kind of rock minerals can be identified. (Raith, 2012).

Figure 2-16: The Olympus Microscope BHT.

Chapter 3 Quantifying the Role of Hematite Cement in Controlling Permeability Using Magnetic Susceptibility Measurements

3.1 Introduction

Permeability and porosity are the key petrophysical parameters in reservoir rocks containing hydrocarbons (oil, gas) or water. Clastic reservoir rocks usually show a good correlation between permeability and porosity. The presence of clays and other iron oxide minerals, such as hematite, in reservoir rocks can have a significant impact on permeability (Moll, 2001). The reduction in permeability sometimes carries with it little or no effect on porosity and this ultimately deteriorates the correlation between porosity and permeability in reservoir rocks.

3.2 Previous studies

Recent studies have shown the potential usefulness of magnetic susceptibility and hysteresis measurements in assessing the impact of fine grained hematite on permeability (Potter et al., 2009; Ali and Potter, 2011b). In these studies, the hematite was dispersed in the matrix of relatively tight gas red sandstone samples. This phenomenon is similar to dispersed clays in sandstone matrixes. The work presented in this chapter is essentially an extension of the early work by Potter and Ali. In this chapter, for the first time, it is shown that the grain lining hematite cement surrounding quartz grains also has significant control over permeability in reservoir rock samples.

It is shown that the presence of a thin (approximately 10-15μm) rim of hematite cement blocks pore connections and reduces permeability. In other words, these results support the earlier work of Ali and Potter by finding that not only does the dispersed hematite have an impact on permeability, but also the grain lining hematite cement has a significant impact in reducing permeability in the reservoir rock samples. The samples with a higher content of hematite exhibited lower permeability values and vice versa.

The studies on clastic (Potter, 2007; Potter and Ivakhnenko, 2008) and carbonate (Potter et al., 2011b) reservoir rock samples have shown strong correlations between low field magnetic susceptibility measurements and key petrophysical parameters such as clay

content, permeability, cation exchange capacity per unit pore volume (Qv), flow-zone indicator, and the downhole gamma ray signal. Strong correlations between low field magnetic susceptibility, hematite content, and permeability have been observed by Potter et al. (2009) and Ali and Potter (2011b), where small amounts of fine-grained hematite in the matrix played an important role in controlling the permeability in relatively tight gas red sandstone reservoirs in the North Sea. In the present work, it is demonstrated how magnetic susceptibility correlates with permeability and grain lining hematite cement in a relatively tight gas sandstone reservoir in the German Sector of the North Sea.

3.3 Measurements and Results

In this study, more than 90 core plugs were taken from Well Y; this well was drilled in a relatively tight gas sandstone reservoir in the German sector of the North Sea. The core plugs, measuring 2.54 cm in diameter, and 2.5 cm in length, The core plugs were divided into three major groups: the first group exhibiting relatively low permeabilities, ranging between 1-10 mD; the second group with a permeability range of 20-40 mD, and the third group between 50-70 mD. Magnetic susceptibility measurements were performed on these plug samples, using an MS2 magnetic susceptibility meter and the dual frequency MS2B sensor from Bartington Instruments Ltd. The details of these items of equipment were covered in **Chapter 2**. For consistency, all susceptibility measurements are given in dimensionless units of volume susceptibility. The volume magnetic susceptibility of each of the plug samples was measured three times and the average of the three readings was taken, to reduce measurement errors. The volume susceptibility data were subsequently converted into mass specific susceptibility with units of m^3kg^{-1}, through division of the volume specific susceptibility by the density of each plug sample. The density of individual plugs was measured by dividing the weight by the volume of the individual plug samples. Probe permeability measurements were also performed using Core labs pressure decay (PDPK) permeameter, located at the Petrophysics laboratory at Heriot-Watt University. The probe permeability data was used to look at the correlations between magnetic susceptibility and permeability of the plugs.

Figure 3.1 shows a crossplot between mass magnetic susceptibility and probe permeability of the plug samples. The first set, with a relatively high correlation coefficient (R^2 = 0.73), contains a relatively high (1–3%) hematite content and low permeability values (0-1 mD). The second set (with R^2 = 0.54) contained lower amounts of hematite content (less than 1%) and higher permeability values (50-70 mD).The hematite content was initially derived from X-ray diffraction (XRD) measurements (Table 3.1) and also later estimated from the low field magnetic susceptibility measurements, using Equation 3.1 below (modified from Equation 4 of Potter, 2007).

$$F_H = (\chi_Q - \chi_T) / (\chi_Q - \chi_H) \quad , \tag{3.1}$$

where:

F_H is the fraction of hematite,

χ_Q and χ_H are the mass magnetic susceptibilities of quartz and hematite

χ_T is the total mass magnetic susceptibility of the sample, measured with the Bartington susceptibility bridge.

χ_Q was taken as -0.62 x 10^{-8} m^3 kg^{-1} (from Ivakhnenko, 2006) and χ_H was taken as 115 x 10^{-8} m^3 kg^{-1}, after calibration with the XRD data.

Since samples with higher hematite content exhibit lower permeability, it appears that hematite is exerting a major control on permeability, in this reservoir. Whilst the paramagnetic clays present in these plug samples (and which were confirmed by the X-ray diffraction (XRD) measurements) would undoubtedly have an influence on the absolute permeability values, the presence of hematite appears to have an additional and dominant effect on permeability in these reservoir rock samples. To confirm this, two representative samples, circled (i) and (ii) in Figure 3.1 were studied. These samples show a very similar magnetic susceptibility but different permeabilities. The objective was to show that the sample with lower permeability has higher hematite content and the other sample, with higher permeability, has lower hematite content. XRD measurements were therefore performed on the two samples to quantify the amount of hematite and other clay minerals. The X-ray diffraction (XRD) data confirmed that sample (i) has a lower hematite content compared with sample (ii), which was consistent with the apparent colour of this plug sample, that is less red than sample (ii). The hematite content was also magnetically derived for the two plug samples using Equation 3.1. The magnetically derived hematite content is in good agreement with the

X-ray diffraction (XRD) derived hematite content in sample (ii). However, the low field magnetic susceptibility measurements for sample (i) overestimate the hematite content. This is merely because Equation 3.1 assumes a simple mixture of hematite and quartz. The presence of any other minerals with a positive magnetic susceptibility, such as ferrimagnetic minerals and paramagnetic clays, will cause the hematite content to be overestimated using this equation. The presence of a ferrimagnetic mineral and low hematite content in this sample was later confirmed by magnetic hysteresis measurements (this is shown later in the chapter in Figure 3.6a).

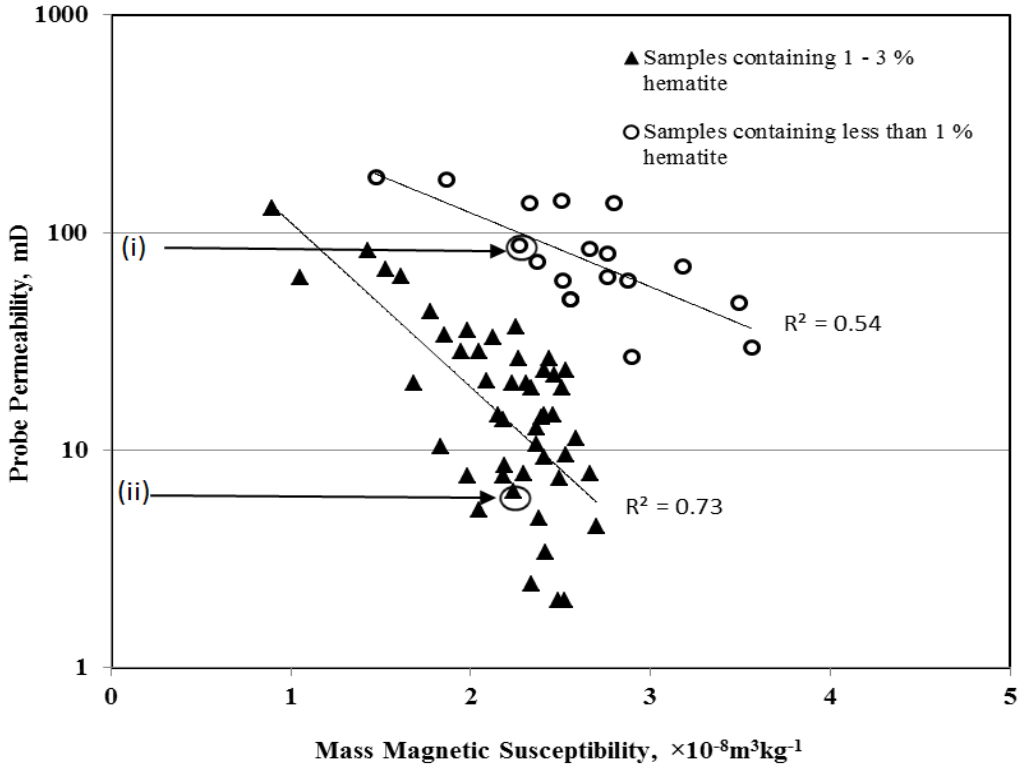

Figure 3-1: Crossplot between mass magnetic susceptibility and probe permeability on cleaned core plugs from Well Y, a relatively tight gas reservoir in the German Sector of the North Sea. Two sets of samples are apparent: one with higher hematite content and lower permeability values, the other with lower hematite content and higher permeability values. (Hematite values quoted were derived from X-ray diffraction **(**XRD).

Sample	XRD derived hematite (%)	Magnetically derived hematite (%)	Probe permeability (mD)	Measured mass magnetic susceptibility (10^{-8} m^3 kg^{-1})
Sample (i)	0.3	2.50 (overestimated)	87	2.27
Sample (ii)	2.2	2.47	6	2.24

Table 3-1: X-ray diffraction and magnetically derived (using Equation 3.1) hematite content for the two samples circled in Figure 3.1. The probe permeability and mass magnetic susceptibility values are also shown.

Thin section analysis was also carried out on the two representative samples shown in Figure 3.1. The objective was to confirm that it is in fact the hematite which is mainly controlling permeability in the low permeability sample (ii). Thin section analysis was done at the School of Geosciences at the University of Edinburgh. Figure 3.2 shows thin section analysis results for the relatively lower permeability sample (ii). The hematite rim of approximately 10-15µm can be seen surrounding the quartz grain and potentially blocking pore connections. The white colour can be seen as mostly desiccation quartz, whereas hematite cement is seen as a brownish coloured lining around the quartz grain, and porosity is indicated as a blue colour. Figure 3.3 shows the thin section analysis results for the relatively higher permeability sample (i). There is evidence of some hematite coating around some of the quartz grains, but majority of quartz grains do not have hematite around them. The results agree with the X-ray diffraction (XRD) measurements for the plug (i) consisting of a lower hematite content and therefore showing relatively higher permeability.

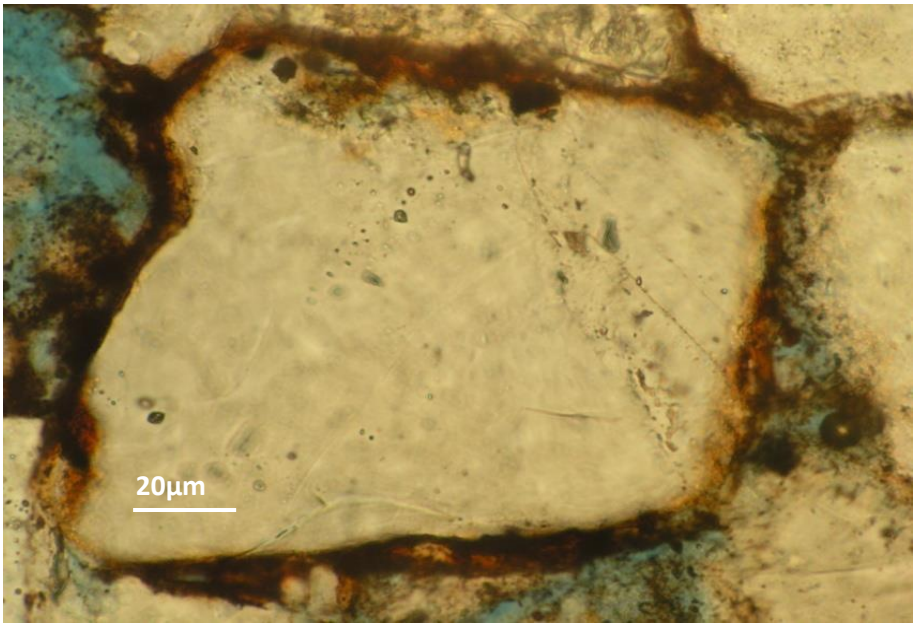

Figure 3-2: Thin section analysis of a red sandstone sample (ii) from Well Y (a low permeability sample) showing a thin hematite rim cement coating a quartz grain.

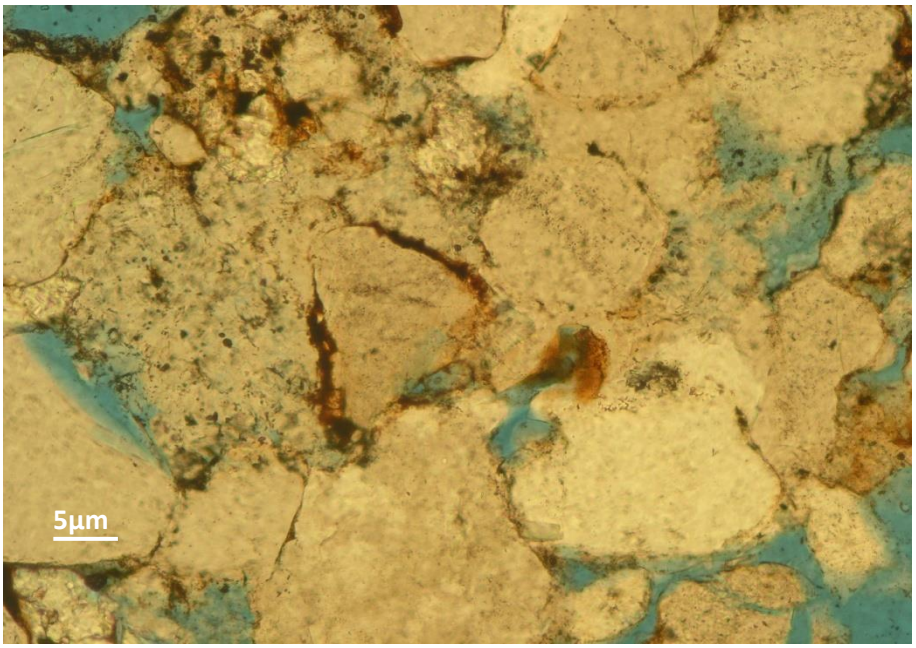

Figure 3-3: Thin section analysis of a high permeability sample (i) showing one or two areas where hematite lining around quartz grains is developing. Otherwise, the sample is mostly of high porosity and high permeability.

The high resolution probe porosity and permeability data taken on the slabbed cores for the same reservoir interval as the plugs were shown in Figure 3.1. The permeability results were derived from the PDPK permeameter and the porosity results from probe *p*-wave measurements (using the probe acoustic transducer add-on for the PDPK) in conjunction with calibration data from core plug porosity. Figure 3.4 displays the observed relationship between permeability and porosity of the samples used in this study. The data points between porosity and permeability are very scattered, reflective of a weak correlation (R^2=0.38), contrary to what might be expected. On the other hand, the mass magnetic susceptibility is strongly correlated with samples having low permeability values (closed triangles in Figure 3.1). The work by Ali and Potter (2011b) showed that samples with similar porosity but having higher hematite content always exhibited a lower permeability. It is possible that the hematite rims in this study are microporous, so that although the porosity does not vary greatly, whilst the rims can dramatically reduce permeability. Lu et al. (1994) also demonstrated for a similar reservoir that the hematite rims were microporous and comprised small acicular laths of hematite. Previously, microporous illite rims (Potter, 2007) have also been shown, which have had little effect on porosity, but caused a significant reduction in permeability.

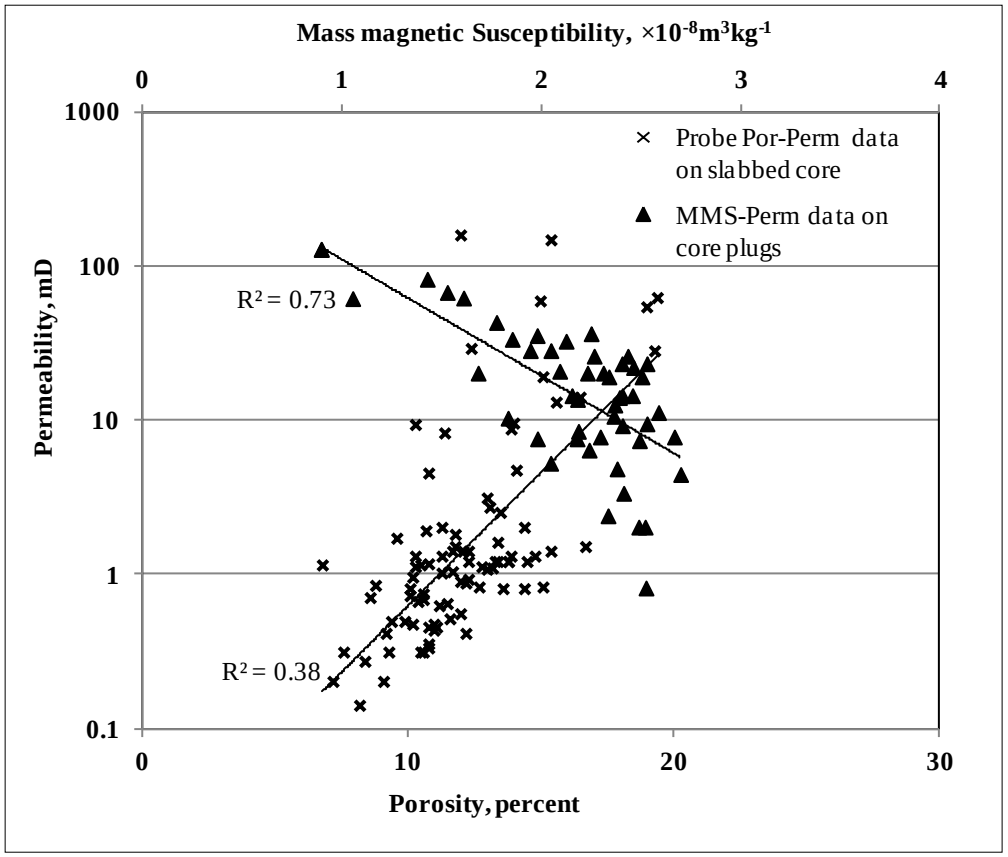

Figure 3-4: Crossplot between high resolution probe porosity and probe permeability data (crosses) undertaken on the slabbed core of Well Y. Also shown is a crossplot between mass magnetic susceptibility (MMS) and probe permeability data (closed triangles) taken on core plugs from Well Y.

Figure 3.5 shows mass magnetic susceptibility and permeability profiles versus depth for the set of plugs previously shown in closed triangles in Figure 3.1. One can see that the mass magnetic susceptibility closely follows the permeability profile, in that the lower magnetic susceptibility is related to higher permeability values and vice versa. The crossplots between magnetic susceptibility and permeability, shown previously in this section, potentially mean that if we have such correlations from the representative set of plug data, we can then make high resolution permeability predictions on the slabbed core by simply acquiring magnetic susceptibility data. This also shows the potential importance of having a downhole magnetic susceptibility tool for acquiring high resolution measurements downhole and thereafter making permeability predictions downhole from the correlations on the existing core data.

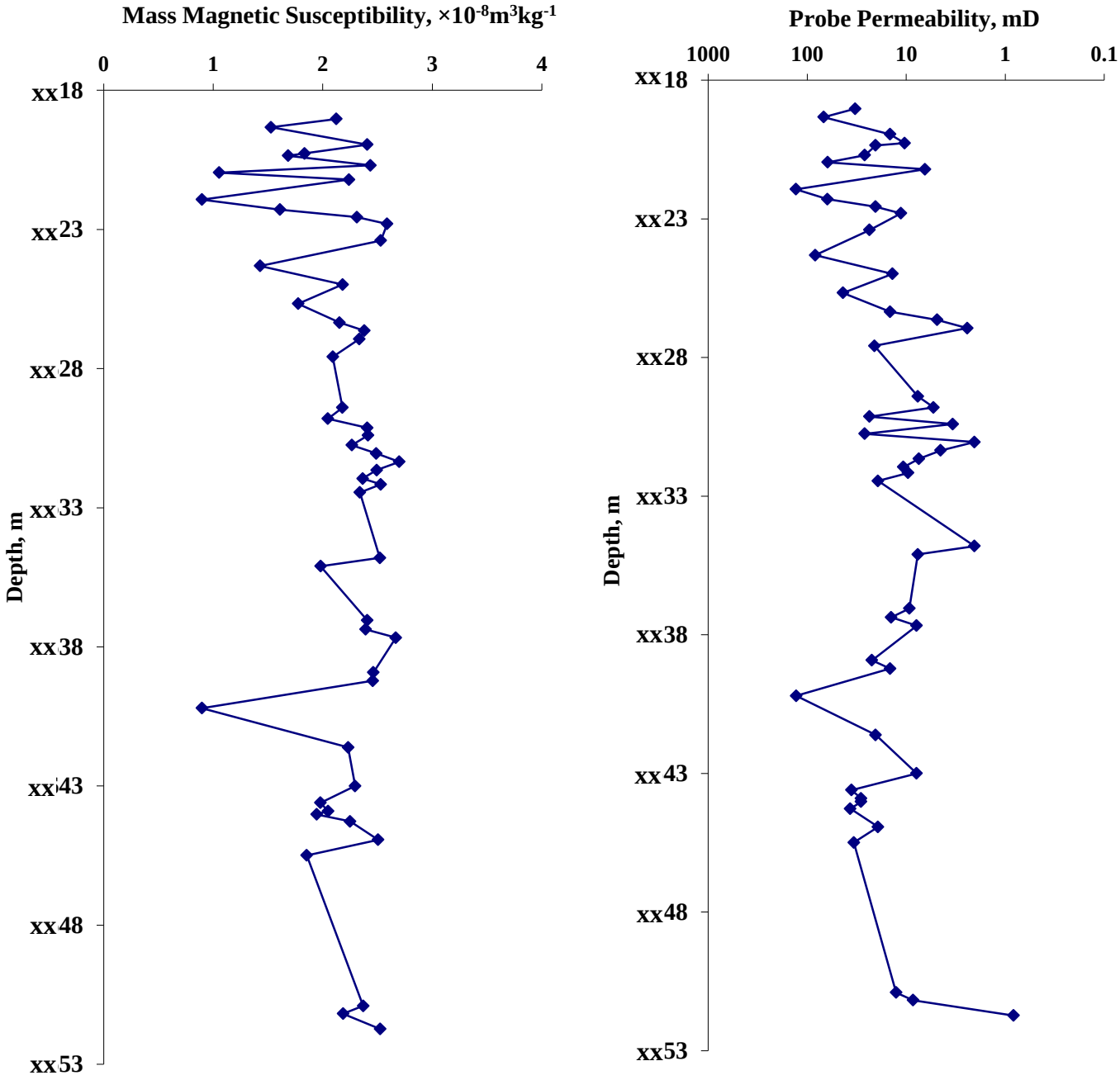

Figure 3-5: Profiles of mass magnetic susceptibility and probe permeability conducted on core plugs for the closed triangle samples with R^2 = 0.73, from Figure 3.1, which have a relatively higher hematite content.

3.3.1 Magnetic hysteresis for Mineralogy Identification in Reservoir Rock Samples

To investigate further the effect of hematite on permeability in the set of reservoir rock samples studied in this chapter, magnetic hysteresis measurements were performed on some representative sets of plug samples consisting of low, medium and high permeability values. These measurements consisted of hysteresis measurements at room temperature. Since the content of certain clays can also have a significant effect on permeability (Potter, (2007) showed how increasing illite content dramatically reduced permeability), magnetic hysteresis measurements were conducted to quantify the clay content and hematite content of these representative plug samples and their relation to permeability in these samples.

Magnetic hysteresis measurements were performed using Variable Field Translation Balance (VFTB) equipment in the petrophysics laboratory at Heriot-Watt University. The details of this equipment are covered in **Chapter 2**. Powdered samples (about 0.5 g in weight) were placed in the sample holder. Quartz wool was used to fix the sample inside the glass tube (sample holder). The magnetic hysteresis curves were obtained by varying the applied magnetic field between 0 and 1 Tesla.

The presence of clay minerals can be identified and quantified from the high field slope of the hysteresis curves. The modeled response of different quartz plus illite mixtures on the magnetic hysteresis plot results in different slopes that represent the magnetic susceptibility values (Ivakhnenko and Potter, 2008).

Figure 3.6 shows that the increase of small percentage of the paramagnetic mineral (illite) has affected the slope of the hysteresis loop. The higher the high the field slope, the higher the amount of the illite content, whereas the ferromagnetic minerals such as magnetite are indicated by the kink at a relatively low applied magnetic field. The presence of antiferromagnetic minerals such as hematite is indicated by the large loop or kink at the high magnetic field. (Ivakhnenko and Potter, 2008).Comparing the magnetic hysteresis results for different permeability samples allows us to assess the role of the different mineral components on permeability. Magnetic hysteresis parameters (Ms,Mrs,Hc and Hcr) also can be derived from the hysteresis curves; these parameters help us to determine the effect of hematite particle size on the permeability.(Ivakhnenko and Potter, 2008).

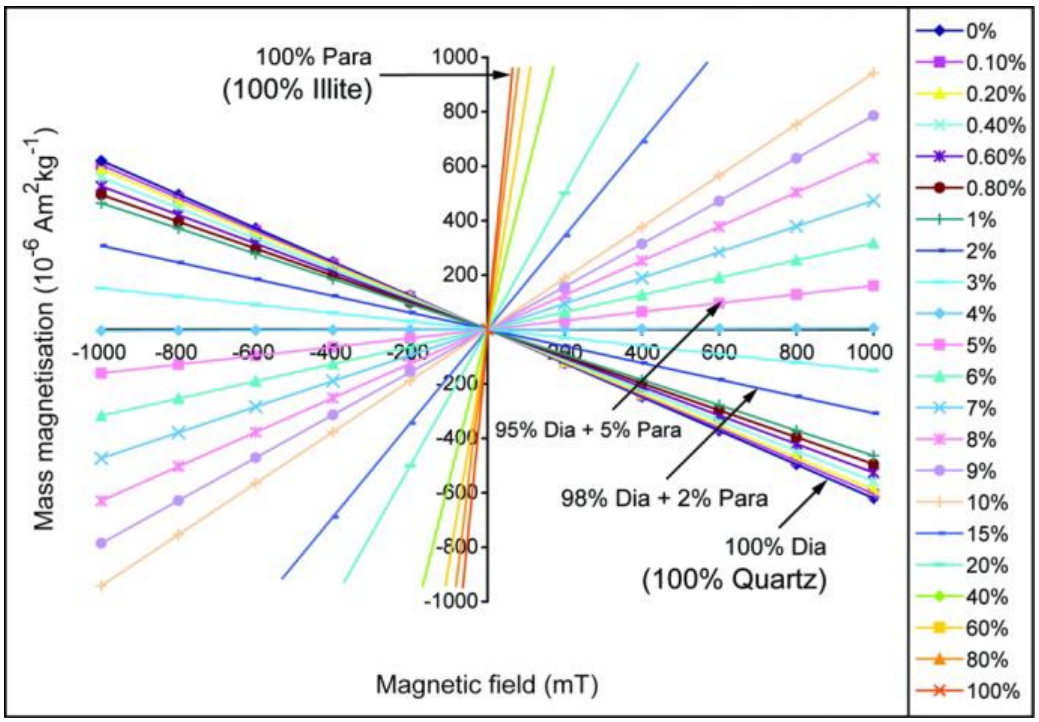

Figure 3-6: Typical template model of a magnetic hysteresis loops for various mixtures of illite (paramagnetic) and quartz (diamagnetic). The slopes of the lines represent the mass magnetic susceptibly. (Ivakhnenko and Potter, 2008).

Figure 3.7a shows the magnetic hysteresis curve of sample (i), which contains 0.3% hematite from X-ray diffraction (XRD) analysis. The hysteresis curve confirmed the presence of both a very small amount of hematite and a ferrimagnetic mineral. The latter is evident from a pinching effect towards the centre of the hysteresis loop at low applied fields, whereas the presence of hematite is shown by the relatively wide hysteresis loop which does not saturate at high fields. Curie point analysis suggested the ferrimagnetic mineral was magnetite, and also confirmed the presence of hematite. The magnetic hysteresis curve of sample (ii) (Figure 3.7b), which contains 2.2 % hematite from X-ray diffraction (XRD) analysis, revealed only the presence of hematite.

The ferrimagnetic mineral (magnetite) concentration in the sample shown in Figure 3.7 (a) and the other similar samples in Figure 1 (those with low hematite content, the open circles) is extremely small. Magnetite has a very high mass magnetic susceptibility at low fields, usually in the range of 20,000–110,000 x 10^{-8} m^3 kg^{-1} (Hunt et al. 1995),

whereas the mass magnetic susceptibility values of the open circle samples in Figure 3.1 are in the approximate range of 1.5–3.5 x 10^{-8} m^3 kg^{-1}. The presence of an extremely small fraction of magnetite in these samples is enough to shift them to the right (higher

magnetic susceptibilities) in Figure 3.1. Hematite, on the other hand, exhibits a much lower mass magnetic susceptibility, usually in the range of 10–760 x 10^{-8} m^3 kg^{-1} (Hunt et al. 1995). Thus, the samples with the higher hematite content, but negligible magnetite (Figure 3.7(b) and closed triangle samples in Figure 3.1) exhibit the lower magnetic susceptibility values. The presence of just hematite in sample (ii) explains the lower mass magnetization in Figure 3.7 (b), and the lower magnetic susceptibility values in Figure 3.1 and Table 3.1 compared to sample (i). The poorer correlation coefficient for the samples with lower hematite content in Figure 3.1 may be due to extremely small variations in magnetite concentration, which could affect the magnetic susceptibility.

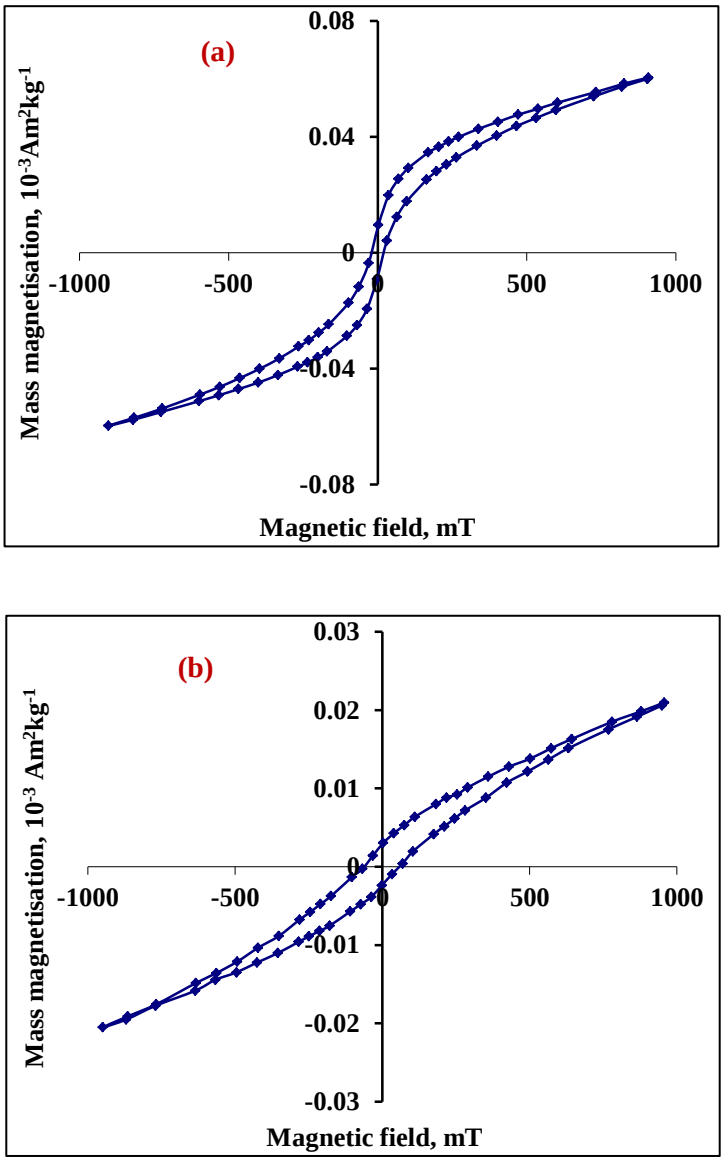

Figure 3-7: (a) Sample (i) in Figure 3.1 shows the presence of both a ferrimagnetic mineral and hematite. (b) Sample (ii) in Figure 3.1 shows the presence of hematite only.

Figure 3.8 (a, b, c) shows the hysteresis curves for the low permeability samples; Figure 3.9 (a, b, c); for medium permeability and Figure 3.10 (a, b, c) for the relatively higher permeability samples, respectively. Among the different samples, one can see that the high field slope of the hysteresis curves is very similar, indicating that the content of paramagnetic clays in these samples is quite uniform. That does mean that there is some other mineral having an additional (in this case dominant) control on permeability in these samples.

The hysteresis curves of the samples in Figure 3.8 show a relatively bigger kink at low applied fields and which reasonably extends to higher fields, thus indicating the presence of antiferrimagnetic minerals (hematite in this case) in these samples. This supports the previous analysis in this chapter that samples with relatively lower permeability values have higher hematite content and that the hematite mineral is exerting dominant control on permeability in these samples. On the other hand, the hysteresis curves of the samples in Figure 3.9 did show some presence of hematite (due to the kink) but not as significantly as in the samples shown in Figure 3.8. The same is true for the samples in Figure 3.10, and the reason is that they have relatively high permeability values.

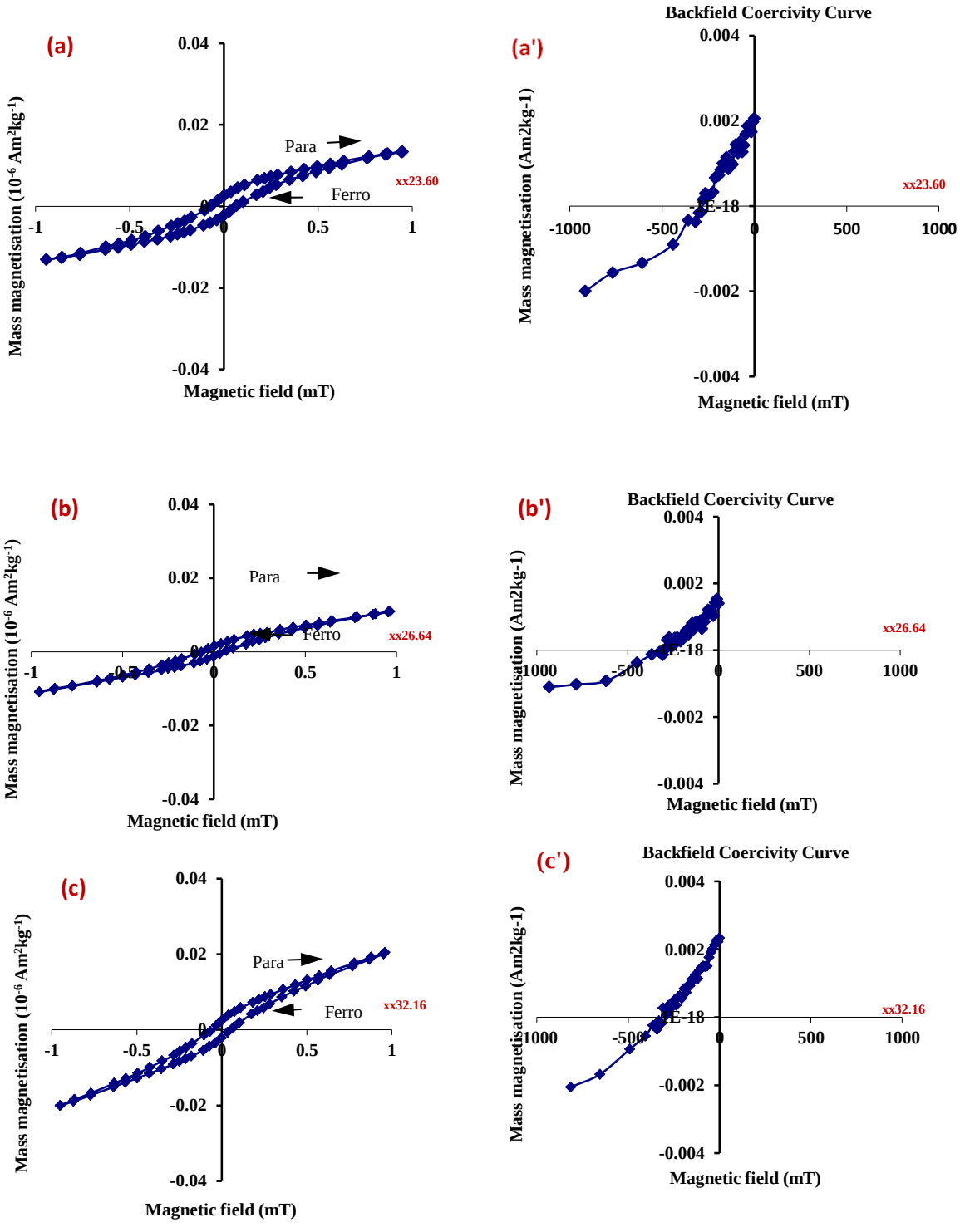

Figure 3-8: (a), (b) and (c) represent the magnetic hysteresis curves for red sandstone samples (xx 23.60, xx 26.64 and xx 32.16) containing relatively higher hematite content (low permeability samples). (a') (b') and (c') represent the (Hcr) curve of the samples.

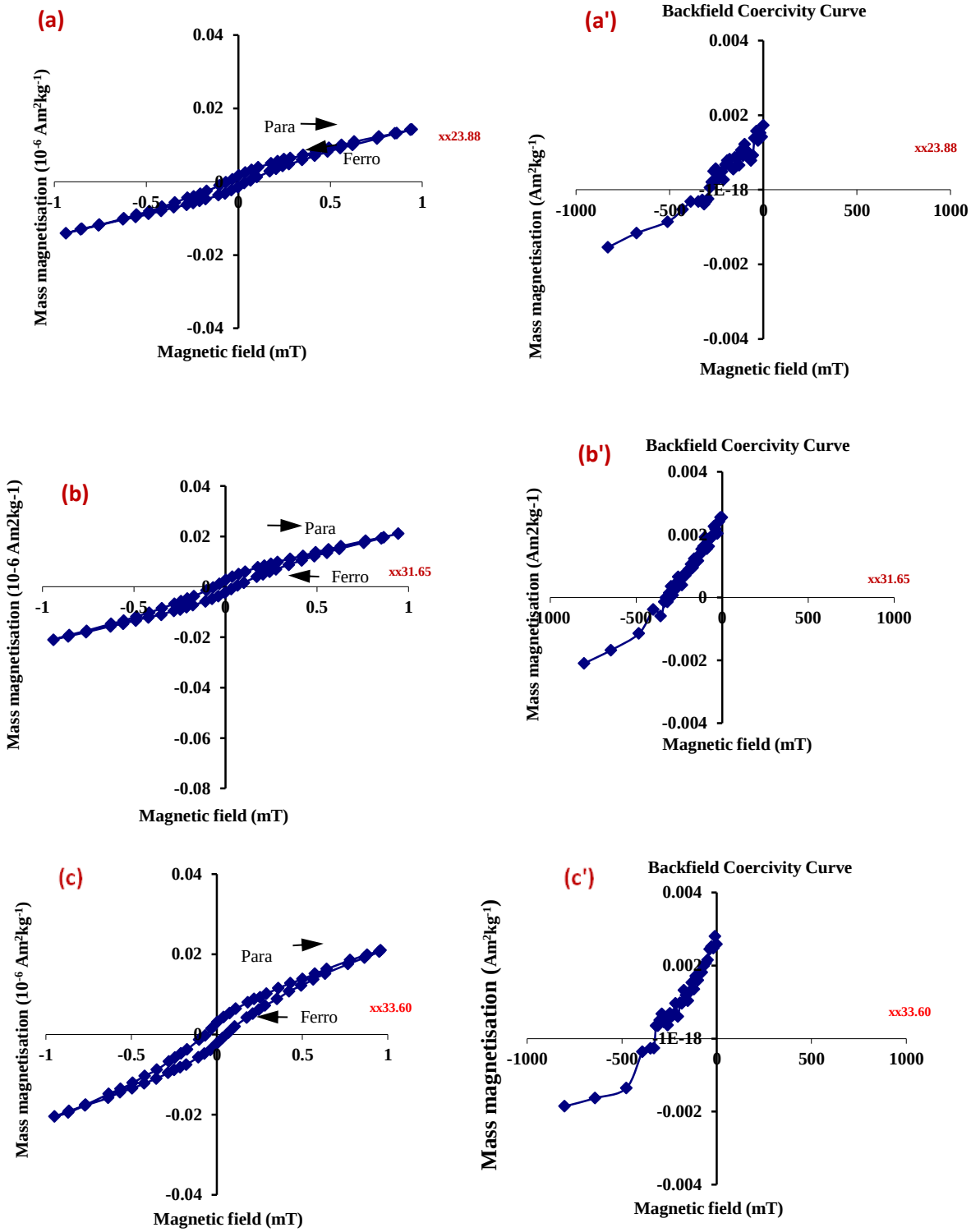

Figure 3-9: (a), (b) and (c) represent the magnetic hysteresis curves for medium permeability red sandstone samples (xx 23.88, xx 31.65 and xx 33.60). (a') (b') and (c') represent the (Hcr) curve of the three samples.

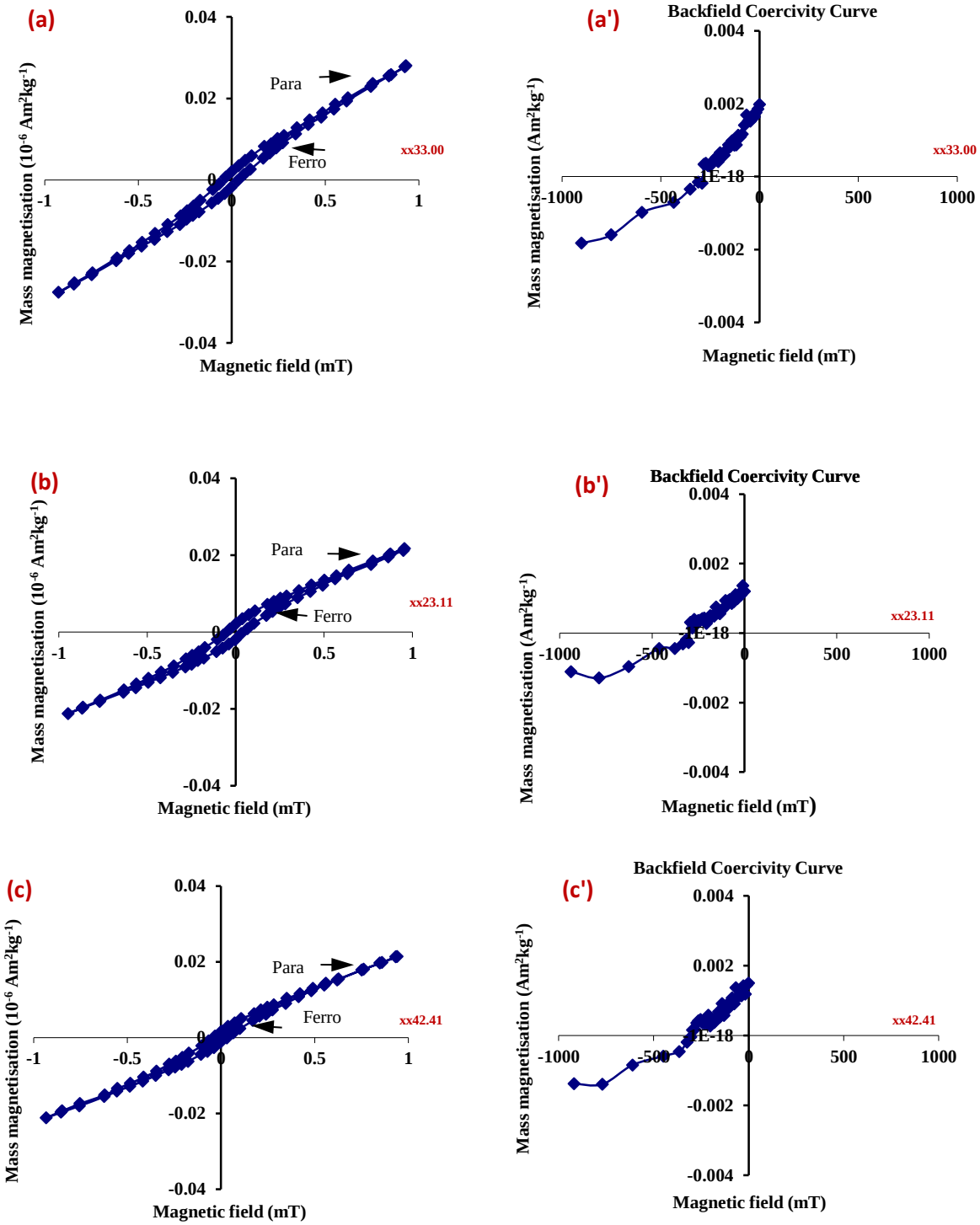

Figure 3-10: (a), (b) and (c) represent the magnetic hysteresis curves for relatively higher permeability sandstone samples (xx 33.00, xx23.11 and xx 42.41) with very low contents of hematite. (a') (b') and (c') represent (Hcr) curve of the samples.

Figure 3.11 shows the results of magnetic hysteresis measurements on all the plug samples which have been used in the laboratory. It is interesting to see that all the samples show a very similar high field slope, suggesting that all the samples, both the higher permeability (lower hematite) and the lower permeability (higher hematite) ones, contain a very similar concentration of paramagnetic clay minerals. This suggests that it is not the paramagnetic clay content that is controlling the variations in permeability in this reservoir. These clays will nonetheless have some control on the absolute values of permeability, but the variations in permeability are likely caused by variations in the hematite (and possibly magnetite) content, since the width and height of the hysteresis curves are the only differences between samples in Figure 3.11.

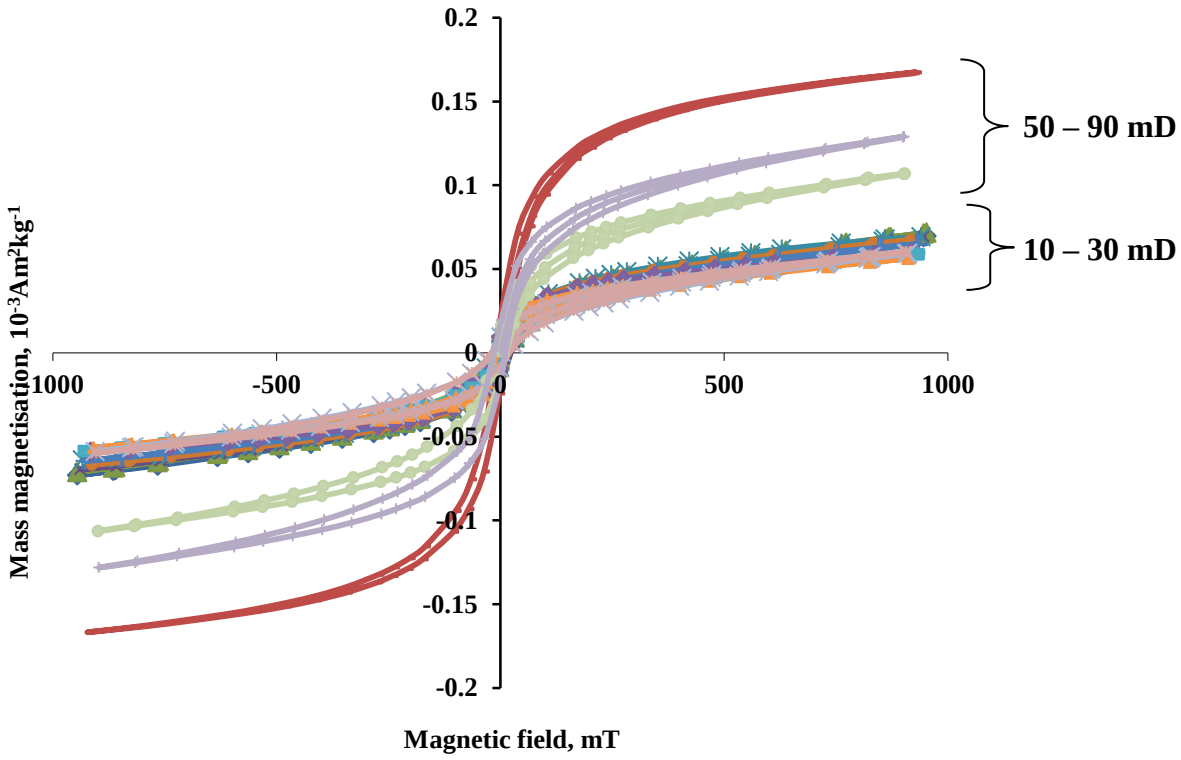

Figure 3-11: Magnetic hysteresis curves of representative Well Y samples. Samples with probe permeabilities from the core plugs in the 10–30 mD range belong to the set of samples which have higher hematite content (closed triangles in Figure 3.1). Samples with probe permeabilities from the core plugs in the 50–90 mD range belong to the set of samples which have lower hematite content (open circles in Figure 3.1). The high field slopes of the hysteresis curves are very similar, suggesting that all the samples contain a similar concentration of paramagnetic clays (if the composition is the same). Small amounts of magnetite in the 50–90 mD samples cause the mass magnetization values to be higher in these samples.

3.3.2 Effect of Hematite Particle Size on Permeability

Values of saturation magnetization (M_s), saturation remanence magnetisation (M_{rs}), coercive force (H_c) and remanent coercivity (H_{cr}) (the definitions of these various parameters are covered in **Chapter 2**) were acquired for the samples shown in Figures 3.8 through 3.10, from their hysteresis loops. The corresponding parameters are included in Tables 3.2 to 3.4 for the three sets of samples (with low, medium and high permeability). The ratios of M_{rs} / M_s and H_{cr} / H_c are commonly plotted on a so-called Day plot (Figure 3.12), to visualize the dominant state of the ferromagnetic materials (Day et al., 1977; Dunlop, 2002).

Sample at depth	H_{cr}	H_c	M_{rs}	M_s	M_{rs}/M_s	H_{cr}/H_c	Permeability (mD)
xx26.64	0.29	0.1046	0.00237	0.00405	0.585185	2.77247	4.86336
xx23.60	0.31	0.13	0.0034	0.00568	0.598592	2.38462	7.408486
xx31.95	0.325	0.1	0.00204	0.01063	0.19191	3.25	10.06965
xx32.16	0.315	0.12	0.00308	0.00712	0.432584	2.625	9.536858
xx34.51	0.352	0.15	0.004365	0.0091	0.47967	2.34667	1.674405

Table 3-2: Hysteresis parameters for the samples with permeability ranging from 1-10 mD

Sample at depth	H_{cr}	H_c	M_{rs}	M_s	M_{rs}/M_s	H_{cr}/H_c	Permeability (mD)
xx31.65	0.2975	0.0915	0.0025	0.006382	0.391727	3.25137	37.7163
xx19.03	0.323	0.105	0.0029	0.009904	0.292811	3.07619	32.7792
xx45.49	0.282	0.11	0.00275	0.01047	0.262655	2.56364	33.712
xx38.61	0.298	0.091	0.002655	0.006765	0.392461	3.27473	35.658
xx23.88	0.2865	0.131	0.002455	0.003104	0.790915	2.18702	31.8722
xx33.6	0.283	0.073	0.002749	0.00924	0.297511	3.87671	39.9334

Table 3-3: Hysteresis parameters for the samples with permeability ranging from 20-40 mD.

Sample at depth	H_{cr}	H_c	M_{rs}	M_s	M_{rs}/M_s	H_{cr}/H_c	Permeability (mD)
xx34.8	0.346	0.175	0.00369	0.00678	0.544248	1.97714	70.098
xx42.7	0.31	0.0955	0.00265	0.00618	0.428803	3.24607	68.559
xx33.00	0.2875	0.1215	0.002	0.00353	0.566572	2.36626	68.559
xx24.17	0.275	0.161	0.002	0.002538	0.788022	1.70807	57.935
xx42.41	0.3005	0.0825	0.00204	0.004352	0.46875	3.64242	70.510
xx23.11	0.27	0.07	0.00273	0.013422	0.203546	3.85714	68.93

Table 3-4: Hysteresis parameters for the samples with permeability ranging from 50-70 mD.

In Figure 3.12, the regions single-domain (SD) and multi domain (MD) refer to single-domain (SD) and multidomain (MD) regions respectively. Particle size increases going from the SD (top left) towards the MD (bottom right) regions. A domain represents a small region within a particle where all the magnetic moments are aligned in the same direction. Larger particle sizes (>15μm in hematite) contain more than one domain and are therefore called multidomain (MD). The domains are separated by domain walls. Once the particle becomes small enough so that the energy to make a domain wall is larger than the decrease in magnetostatic energy from separating the particle into two domains, then the particle will only contain one domain (a single domain, SD).

To investigate whether hematite particle size is having a major control on permeability, the hysteresis parameters for the three sets of samples (with low, medium and high permeability) were plotted on the Day plot. The permeability range of each sample (from the probe permeability data for the core plugs) is also shown on Figure 3.12. There appears to be no particle size dependence on permeability, suggesting that permeability is independent of hematite particle size in these reservoir rock samples. It may be significant that the thickness of the hematite cement rim (10-15μm) shown in Figure 3.2 is close to the critical single domain (SD) to multi domain (MD) transition size of 15μm in hematite (Banerjee, 1971; Chevallier and Mathieu, 1943), below which hematite particles are single domain (SD) and above which particles are multi-domain

multi domain (MD). Perhaps the stronger magnetic attractive forces between the fine-grained hematite particles in these samples, which are single domain or close to single domain in size, play a role in forming hematite cement rims of the observed thickness. Larger multi-domain (MD) hematite grains might not form continuous rims, since the attractive magnetic forces between multi domain (MD) particles are likely to be weaker. As we can see from Figure 3.12, the ratios of the hysteresis parameters show that grain sizes are scattered within the SD- MD for the three sets of samples, which indicates that the permeability is independent of hematite particle size for the samples in this reservoir. This is a good indicator that the presence of hematite cement plays a significant role in controlling permeability, rather than the hematite particle size.

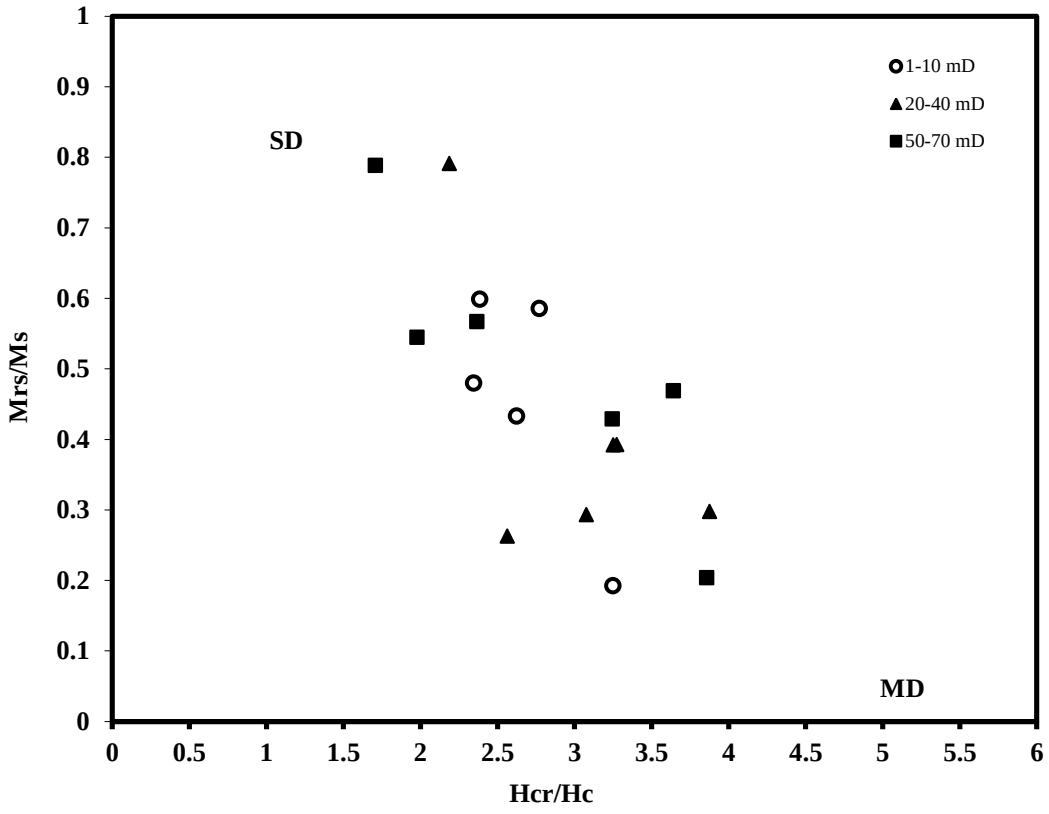

Figure 3-12: Coercivity / coercivity of remanence ratio (Hcr/Hc) versus remanent magnetization / saturation magnetization ratio (Mrs/Ms) for representative Well Y samples (containing 1-3 % hematite in Figure 3.1). The scatter of data points for different permeability samples (from the probe data on the core plugs) suggests that permeability is independent of hematite particle size in this reservoir.

3.4 Conclusions

The main conclusions from this work can be summarized as follows:

- Magnetic susceptibility measurements undertaken on core samples from Well Y, a relatively tight gas sandstone reservoir in the North Sea, correlated well with permeability.

- Samples with higher hematite content (1-3%) exhibited significantly lower permeabilities than samples with extremely low hematite content (less than 1%). In the samples with higher hematite content, thin section analysis revealed thin (approximately 10-15µm) rims of hematite cement surrounding quartz grains and blocking pore connections. This suggests that grain lining hematite cement exercises a major control on permeability in this reservoir.

- Magnetic hysteresis parameters plotted on a Day plot showed that permeability is independent of hematite particle size for the samples in this reservoir. Therefore it appears that the presence of the grain lining hematite cement rims (rather than the hematite particle size) is the main factor in reducing the permeability.

- Magnetic hysteresis measurements revealed the presence of hematite, paramagnetic clays, and a ferrimagnetic mineral (identified as magnetite from Curie temperature analysis) in the core samples. The measurements showed that all of the representative samples (both the ones with low and high hematite content) had a similar high field magnetic hysteresis slope, suggesting similar paramagnetic clay content. Samples with higher hematite content had lower permeability values. This further suggests that hematite cement is a major control on permeability in these samples.

- The results of this analysis may have important implications for the prediction of permeability in similar red samples in the North Sea. In addition, they may provide a direct link between permeability and the depositional system of hematite cement, thereby connecting to the geology.

Chapter 4 Novel Magnetic Susceptibility Techniques for Identifying Faults and Gas-Water Contact in Hydrocarbon Bearing Reservoirs

4.1 Introduction

When the well is being drilled the rocks are grained by the drill bit into cuttings, these cuttings will infiltrate into the drilling mud and will then carried out to the surface. (EPA, 2000). The size of the cuttings depends on the type of the drill bit used and the type of rocks being drilled. The size ranges from fine sand to gravel (Neff et al., 1987). Cuttings are always obtained over the total length of the well with a sampling rate from one to a few metres. As a guide, the cuttings from a Polycrystalline Diamond Compact (PDC) drill bit are shown in Figure 4.1. Drill cuttings are useful and can give rapid information about the characterization of the reservoir when the core data is not available. Drill cuttings are produced continuously at the surface on the drill floor at a rate proportionate to the advancement of the drill bit. The composition of the drill cuttings depends on the type of sediment and rock encountered.

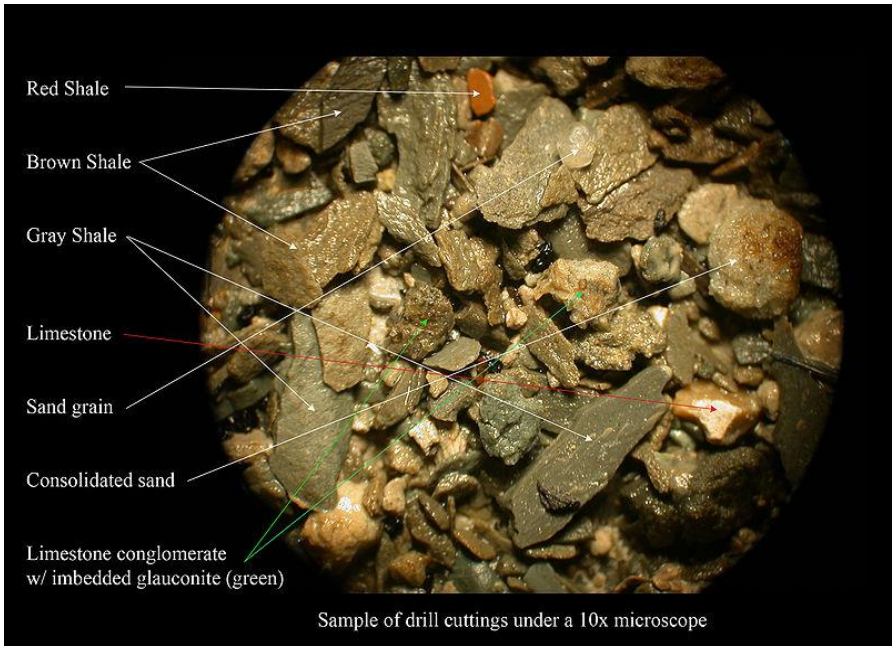

Figure 4-1: Sample of drill cuttings with different sediments shown by colour. (Leroy and Raese, 1977).

Fault is a large movement in the curst of the earth when part of the rock moves against another part (Assam and Nagar, 2004). There are four types of faults, each type differentiated from the others by its movement. They are: a normal fault**,** a reverse fault, a thrust fault, and a strike-slip fault. The definition of the individual faults is outside the scope of this thesis, however, identifying and characterizing faults and fractures are vital steps in reservoir evaluation. (Klimentos and Qleibo, 2003; Lin, et al., 2010).

Traditionally, geological descriptions of the drill cuttings and data from LWD (logging while drilling) and wireline logging tools have been used to identify faults and fluid contacts (gas-oil contact, and oil-water contact). The cuttings description and biostratigraphy usually takes some time for analysis and interpretation. The LWD and wireline logging tools also have certain limitations, for example, due to their poor vertical resolution, to about two feet (Flaun, 1990). The modern day image logs such as Dual OBMI (oil based micro imager) and FMI (formation micro imager) and the very latest NGI (next generation imaging) tools have much higher vertical resolution. These tools are able to identify faults and fractures in both water based and oil based mud systems, with very high borehole coverage. However, such tools cannot be run in every well, due to their cost, hole conditions, the hostile environment offshore and in cases where no reliable data can be obtained from these tools, for instance, due to tool failure.

4.2 Objective of this Chapter

In this chapter, a method of identifying faults using magnetic susceptibility measurements was developed on drill cuttings. Currently, there is no wellsite or laboratory-based method that can be used on drill cuttings to help in the determination of faults and free water level (in this case gas-water contact) in hydrocarbon bearing reservoirs. Often, the fluid contact determined from the resistivity logs is some distance away from the free water level, due to poor vertical resolution of the resistivity logs. Magnetic susceptibility data can potentially help in refining the depth uncertainty in fluid contacts, due to the rapid and high number of measurements on drill cuttings.

The wellsite geology and biostratigraphy can provide some of the information on different lithologies, but these data are limited due to time and cost constraints. Often, cuttings are sent onshore for detailed analysis using X-ray diffraction, scanning electron

microscope and thin section analysis measurements. There are certain limitations of each of these techniques. For instance, they usually take several weeks before the result comes back. They are also expensive and hence, only selective samples can be used for study. This poses a risk of missing the representative samples from the analysis at all. The wellsite magnetic susceptibility measurements on drill cuttings are very quick, allowing a large number of samples to be analyzed. In this chapter, it is demonstrated how the magnetic susceptibility measurements performed on drill cuttings can help in the prediction of faults and free water level at the well site. The information can be very quick compared with conventional wellsite techniques. The magnetic susceptibility measurements also take relatively larger volumes of drill cuttings compared to, for example, X-ray diffraction, which takes only a tiny sample for analysis.

4.3 Sample Descriptions

We were supplied with drill cuttings by a major operator working in the German Sector of the North Sea. The cuttings belonged to three oil producing wells, named wells A1, A2 and A3. The number of bags used in the experiments is shown in table 4.1. The drill cuttings were collected every five metres at the well site and contained in sealed bags. The cuttings were initially dried for 10 – 12 days in the Petrophysics laboratory at Heriot-Watt University. Although the magnetic susceptibility measurements would not require drying of the cuttings sample, this was done in order to avoid any contamination of the drilling mud on the cuttings by individuals handling and measuring the drill cuttings. Figure 4.2 shows one set the of drill cuttings after it has been dried. The gamma ray, sonic, density and neutron logs were provided from 3650 m to 3880 m for well A2 (Figure 4.3), from 3550 m to 3750 m for well A3 (Figure 4.4), and from 3600 m to 3900 m for well A1 (figure 4.5).

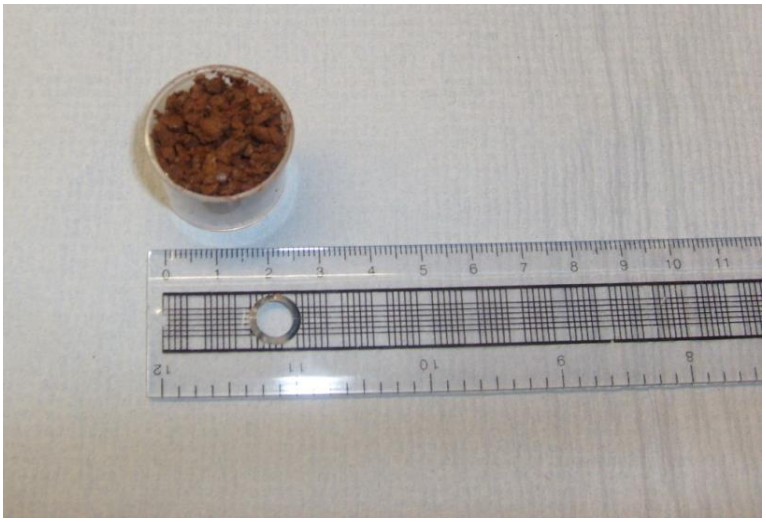

Figure 4-2: Dried drill cutting in the plastic vial ready for analysis on the magnetic susceptibility apparatus.

Well	Number of bags
A1	55
A2	42
A3	28

Table 4-1: Number of bags used in these measurements.

4.4 Measurements and Results

The cuttings were put in 10cc plastic vials. The volume magnetic susceptibility of the drill cuttings was measured from depth 3576-3753 m in well A1, 3620-3830 m in well A2, and 3595-3730 m in well A3 using the MS2B apparatus (the details of this are explained in **Chapter 2**). Because the MS2B sensor could take only 10cc vials for measurements and each bag of drill cuttings acquired every 5 metres contained a significant volume of the cuttings, 28-29 separate measurements were made to finish off the individual bags. The average of these measurements was then taken, which represented the volume magnetic susceptibility of that bag. The weight of the vial (empty and with drill cuttings) was also measured in order to calculate the bulk density of the drill cuttings. The bulk density was subsequently used to convert volume magnetic susceptibility measurements into mass magnetic susceptibility, by dividing the volume magnetic susceptibility by the bulk density of the samples.

Mass magnetic susceptibility provides information on the magnetic susceptibility of the samples which is independent of the porosity effects.

The mass magnetic measurement data acquired from drill cuttings were plotted against the wireline log data in individual wells at corresponding depths. Since the cuttings were acquired every 5 metres, there is a certain depth uncertainty in plotting the mass magnetic susceptibility data against the wireline log data. The composite logs showing the wireline and mass magnetic susceptibility data are presented in Figure 4.3 for well A2 and in Figure 4.4 for well A3.

From the geological information provided by the operator, the anticipated fault zones were at around 3750 m in well A2 and at 3675 m for well A3. From Figure 4.3, the wireline log data, including gamma ray, density, sonic transit time and neutron porosity, does not show any indication of the presence of the fault in the logged interval. However, the magnetic susceptibility measurements clearly indicate two different trends in track 6 of Figure 4.3. A clear transition at around 3750 m from relatively lower magnetic susceptibility values (at shallower depths) to much higher magnetic susceptibility values (deeper down) can be seen. The information ties very well with the prediction of the fault from geological data in the area and also from geophysical seismic data. For confidentiality reasons, the geological and geophysical information is not included in this thesis.

A similar trend of mass magnetic susceptibility was seen in Well A3, with relatively lower mass magnetic susceptibility values (above 3675 m) to much higher magnetic susceptibility values (deeper down). Again, this information was consistent with the geological and geophysical data in this well regarding the presence of a fault at this depth. The wireline log data in Well A3, including gamma ray, density, and sonic transit time (neutron porosity was not acquired in this well), once again did not show any indication of the presence of the fault in the logged interval (Figure 4.4).

Apart from wells A2 and A3, drill cuttings were also supplied for Well A1. For this well, there was uncertainty in the depth of the Free Water Level (FWL). The original gas-water contact (GWC) from the existing wells' reservoir formation tests, extracted cores and saturation height modelling, was found at 3750 m.

The gas water contact (GWC) was assumed to be flat across the field. From Figure 4.5, the wireline log data, including gamma ray, density, sonic transit time and neutron porosity, does not show any indication of the gas water contact (GWC) at the specified depth. However, the magnetic susceptibility measurements clearly indicate two different trends in track 5 of Figure 4.5. The mass magnetic susceptibility data show a clear transition at around 3750 m from relatively lower magnetic susceptibility values (at shallower depths) to much higher magnetic susceptibility values (deeper down). Unfortunately, only 3 bags of cuttings were received which came from the water leg. However considering each bag was collected every 5 metres; the 3 points on the magnetic susceptibility profile in the water leg represent a considerable distance into the water leg.

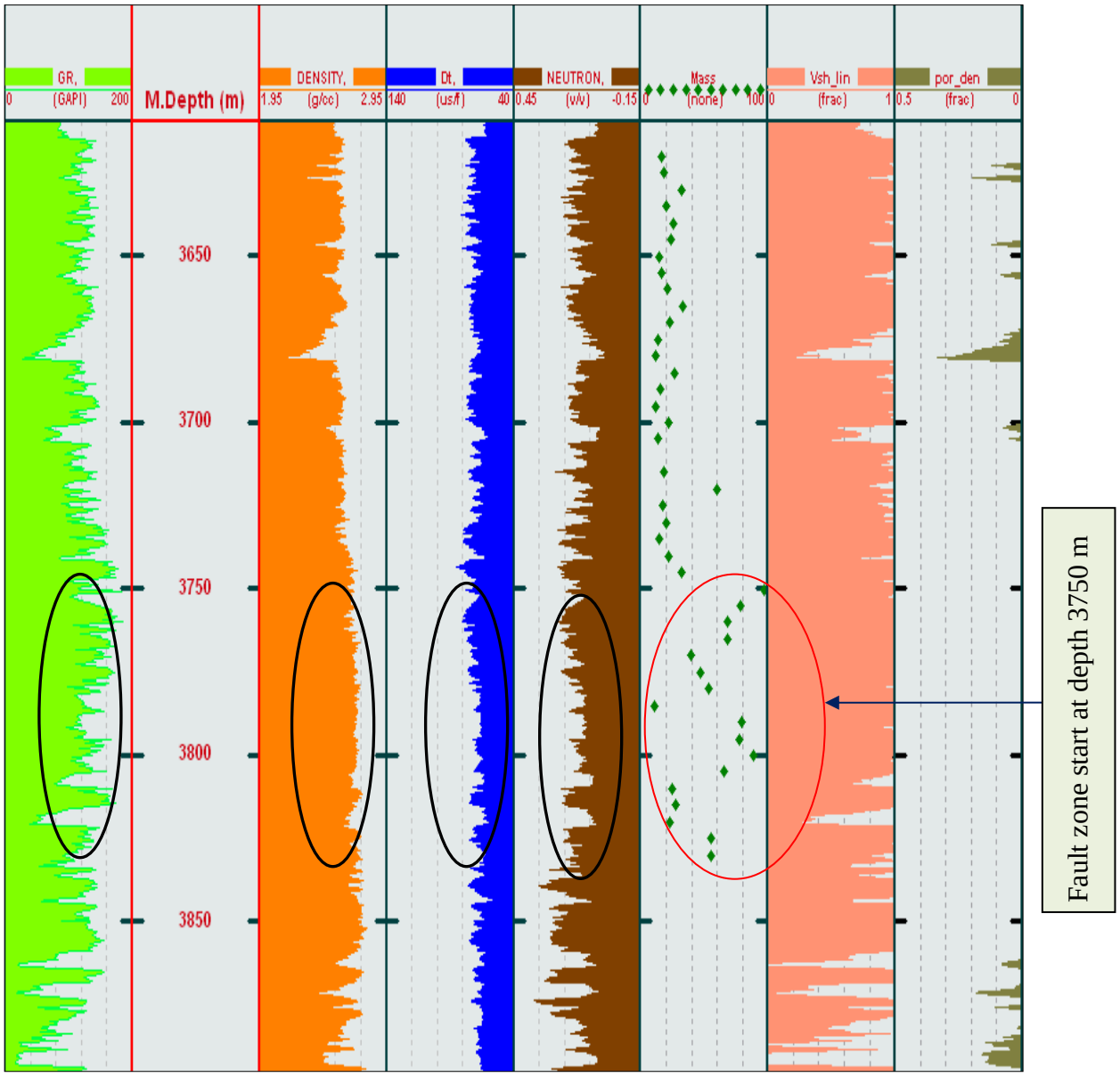

Figure 4-3: Comparison between the well logging and the magnetic susceptibility for identifying a fault zone in well A2.

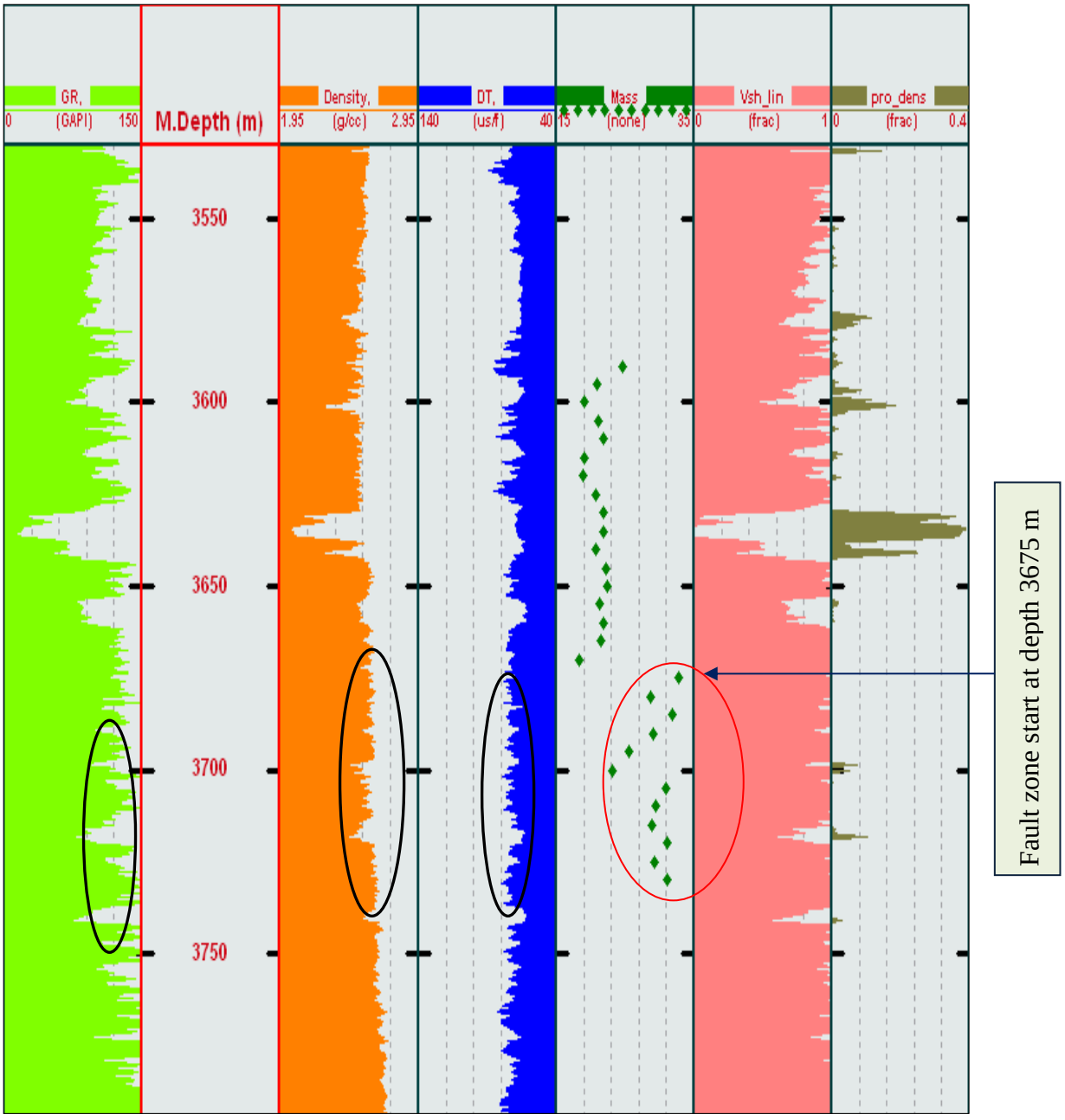

Figure 4-4: Comparison between the well logging and the magnetic susceptibility for identifying a fault zone in well A3.

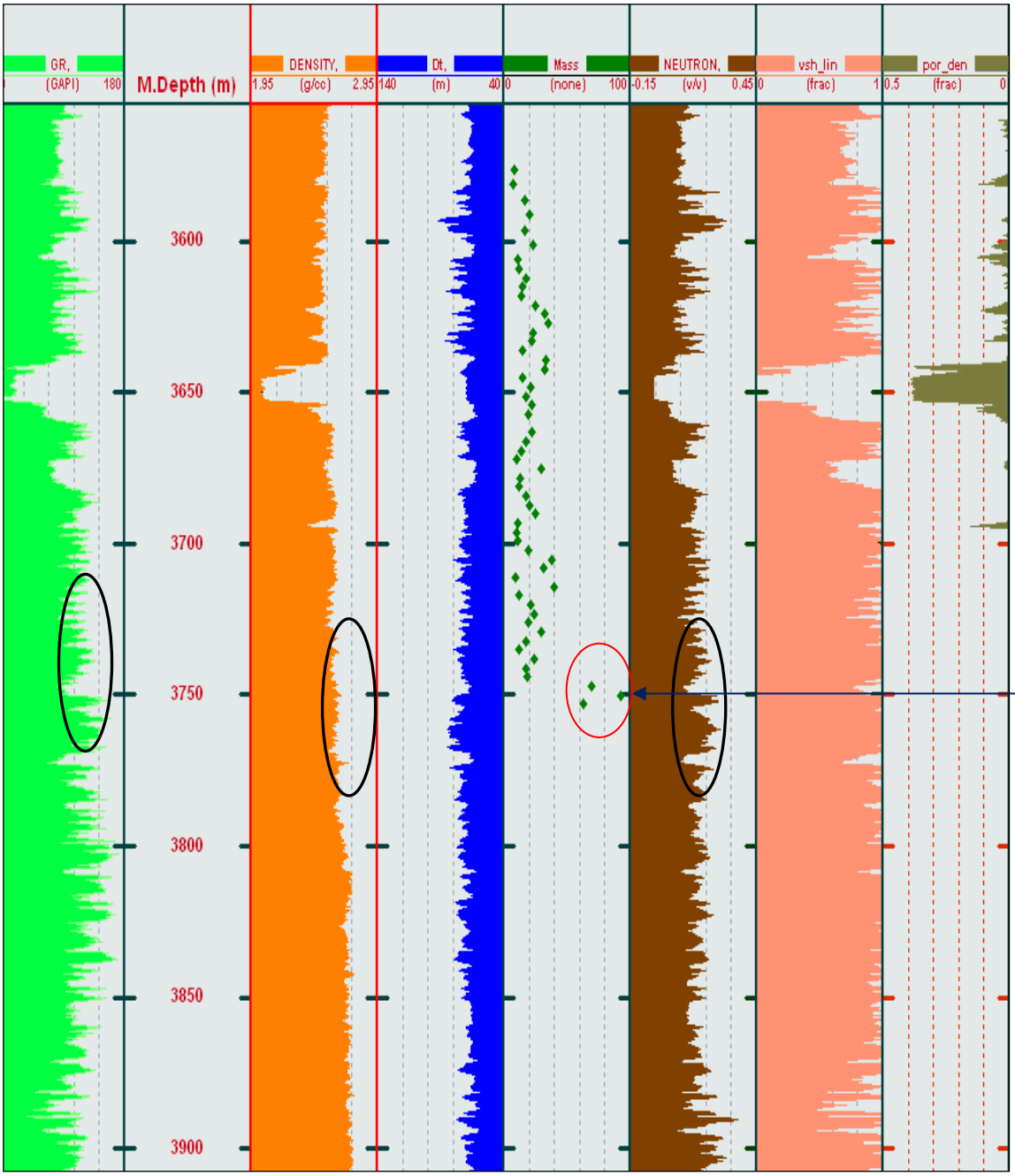

Figure 4-5: Comparison between the well logging and the magnetic susceptibility for identifying gas-water contact zone in well A1.

4.4.1 Histograms

Histograms of the log data have been used in the past to establish log data quality and to quickly visualize the log data distribution across the entire interval downhole. I therefore plotted histograms of the various log data for wells A1, A2 and A3. These are shown in Appendix A (Figures A1 to A14). It is interesting to note that the gamma ray, sonic (Dt), neutron, and density data have a similar distribution both above and at the fault zone. However, the mass magnetic susceptibility clearly gives a different distribution of the data when compared with the rest of the log data. Mean values, standard deviation and arithmetic mean of the gamma ray (GR), density, sonic, and mass magnetic susceptibility are listed in Appendix A in Tables A1 and A2 for Wells A2 and A3 respectively. The data in the tables clearly shows significant variations in the mass magnetic susceptibility data, whereas there is very little variation in the rest of the wireline log data at and above the fault zone, thereby indicating the potential usefulness of the mass magnetic susceptibility measurements on drill cuttings. Similar trends were seen in Well A1, where histograms from the conventional suite of log data are very similar above and below the gas water contact (GWC). However, the magnetic susceptibility histograms show a clear change at the fluid contacts.

4.4.2 Hysteresis loop

To confirm the validity of magnetic susceptibility data and results, the magnetic mineralogy of the drill cuttings above and at the fault zone was investigated. For this, magnetic hysteresis measurements were performed on representative drill cuttings using the VFTB (variable field translation balance) kit located in the Petrophysics laboratory at Heriot-Watt University. Magnetic hysteresis measurements (the basics are covered in **Chapter 2**) have the advantage of identifying the presence of diamagnetic, paramagnetic, ferromagnetic and antiferromagnetic minerals in the sample.

Two representative drill cutting samples, one from above the faults and the other from the fault zone, were selected for magnetic hysteresis measurements in each of the A2 and A3 wells. The samples above the faults for the two wells showed that they contain hematite mineral (evident from a large open kink at low applied fields and which extends to high applied fields) and that the hematite content is very similar. This is shown in Figures 4.6a and 4.6b. The difference in their slope at high fields is related to

the different amounts of clay content in these samples. On the other hand, the drill cuttings at the fault zone for the two wells showed the presence of magnetite (evident by a much bigger kink at low fields and which does not extend to high applied fields). This is shown in Figures 4.7a and 4.7b. In Figure 4.8, the combined magnetic hysteresis curves were shown for the two samples, above and at the fault zone respectively, for both wells A2 and A3. The blue curve showing the much higher magnetisation is at the fault zone, whereas the pink curve showing relatively lower magnetisation values is above the fault zone.

A similar result was seen for Well A1 in Figure 4.9, which shows magnetic hysteresis curves for the two samples, one at shallower depths in the gas zone and the other from the water zone. The shape of the curves for the two cutting samples reveals clear differences, which relate to the different mineral components the samples have. The sample at shallower depths in the gas zone shows the presence of hematite mineral. This is evident from the wide open hysteresis loop of the sample which saturates at relatively higher applied fields. On the other hand, the sample from the water zone, which saturates at lower fields shows a much bigger kink at low applied fields. This indicates the presence of a ferromagnetic mineral in the sample. The magnetic signatures are very similar to that of magnetite.

Magnetite is a ferrimagnetic mineral, and known as the most common iron oxide with chemical formula Fe_3O_4. "It is the most important magnetic mineral on Earth and occurs in the continental and oceanic crust as a primary or secondary mineral in igneous, sedimentary and low- and high-grade metamorphic rocks" (Petrovský, et al, 1998. Pp18).

Magnetite commonly forms at relatively high temperatures, although it also crystallizes at ambient temperatures in slightly reducing environments. In 1962, Lowenstam was the first to identify magnetite in the radula (tongue plate) teeth of chitons, showing that life had also devised mechanisms to synthesize magnetite by means of biochemical processes. According to Matthews (1976) and Zhang, Liu, and Su. (2010), the hematite present in the sedimentary rocks is transformed into magnetite in the presence of hydrogen sulphide. Therefore, it is possible that the presence of magnetite in the fault zones in Wells A2 and A3 could be due to high temperature hematite transformation.

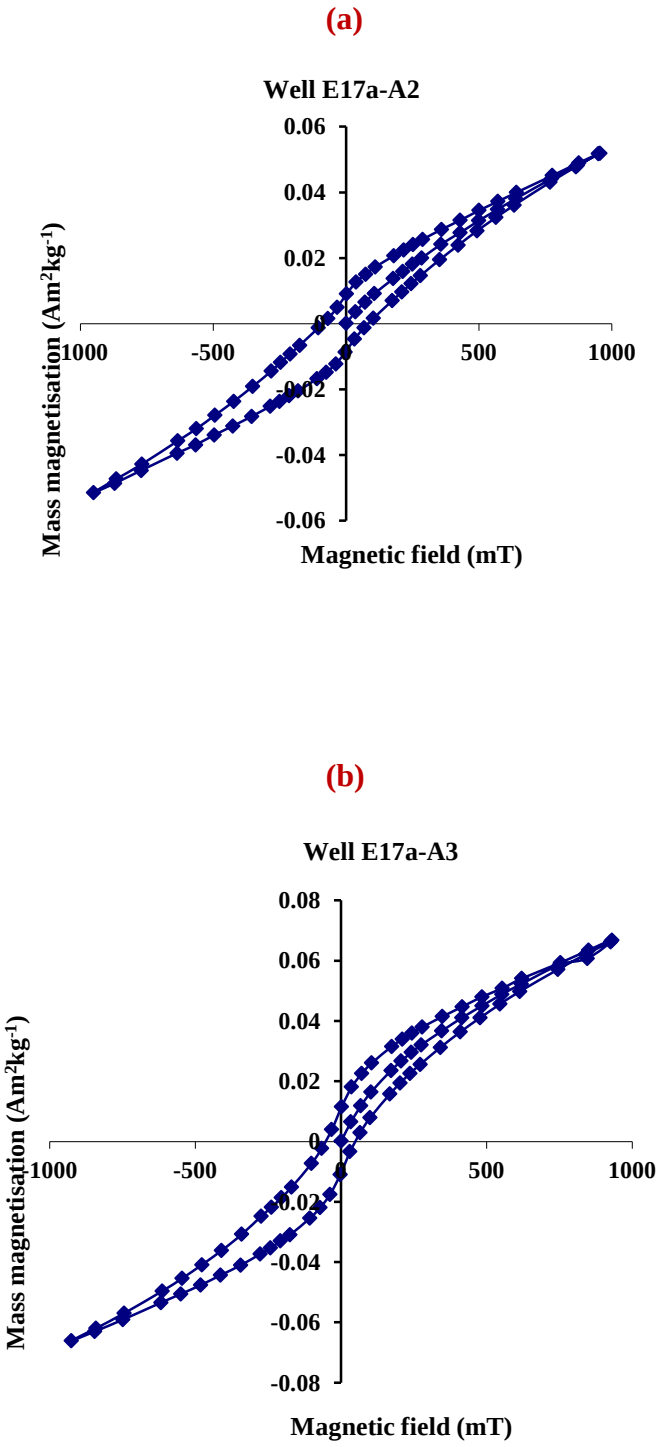

Figure 4-6: (a) The magnetic hysteresis curve for well A2 above the fault zone. (b) The magnetic hysteresis curve for well A3 above the fault zone.

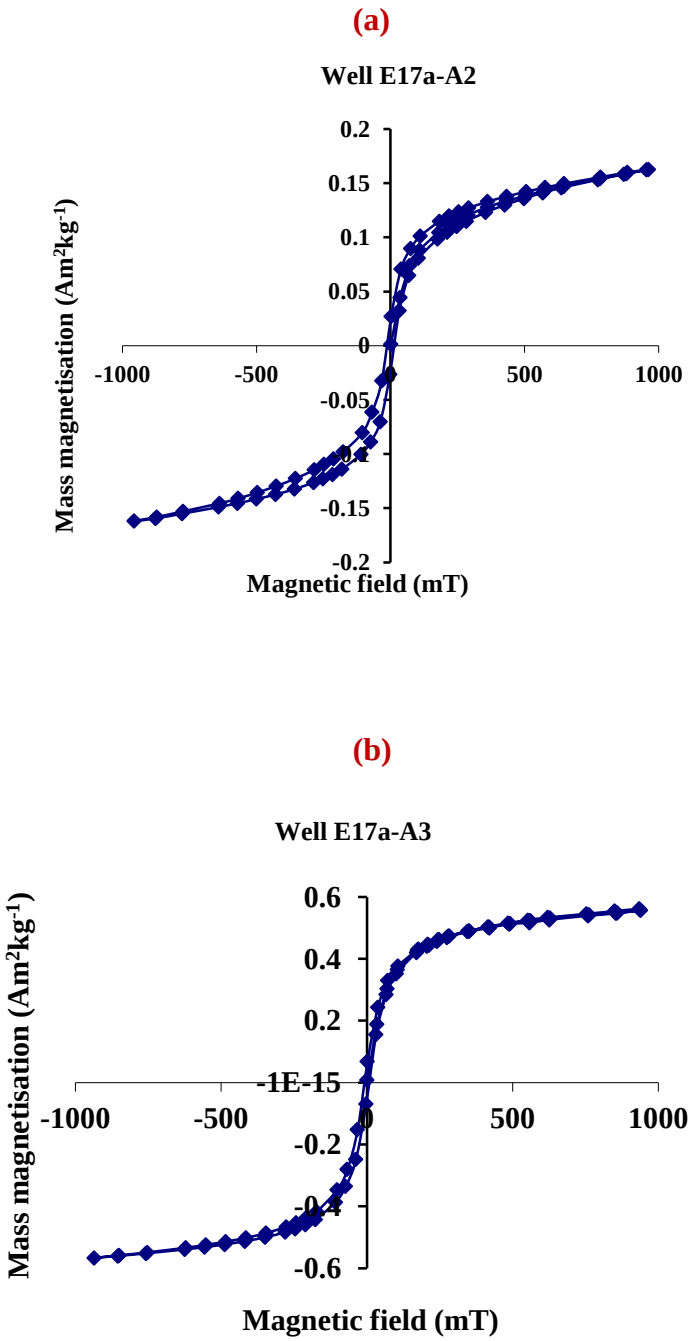

Figure 4-7: (a) The magnetic hysteresis curve for well A2 at the fault zone. (b) The Magnetic hysteresis curve for well A3 at the fault zone.

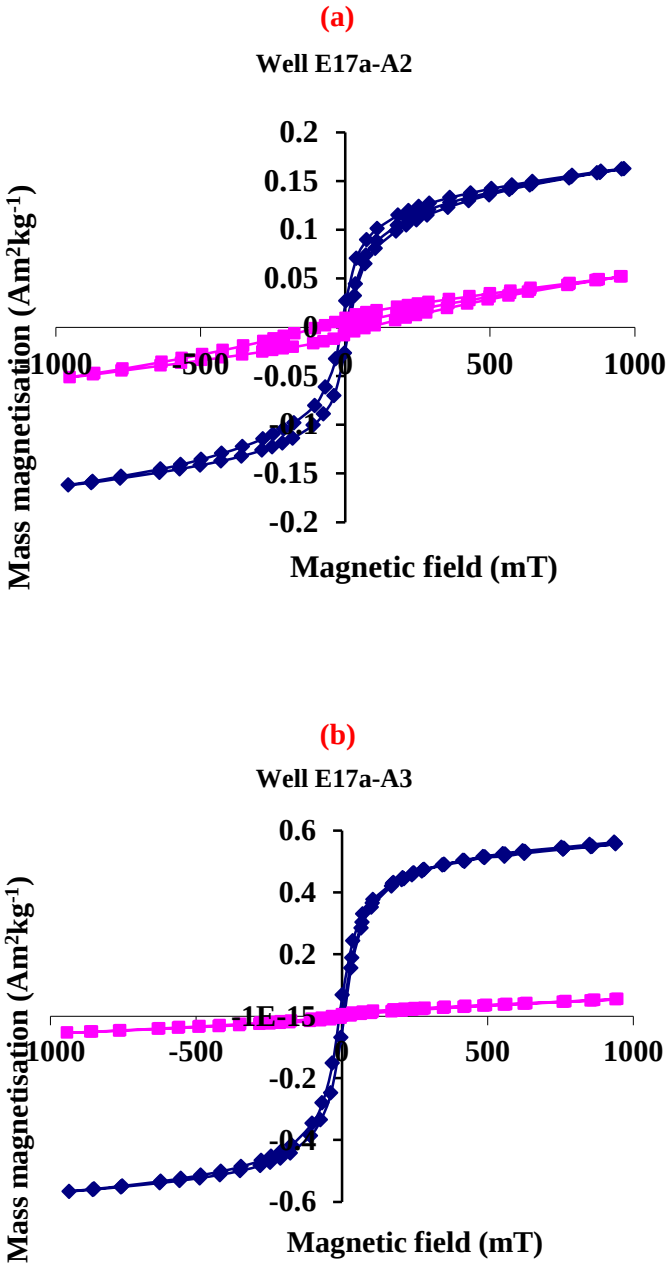

Figure 4-8: (a) For well A2, the hysteresis curves above and at the fault zone are shown in a combined plot for comparison purposes. The blue curve is at the fault zone whereas the pink curve is above the fault zone. (b) Similar curves are shown for well A3.

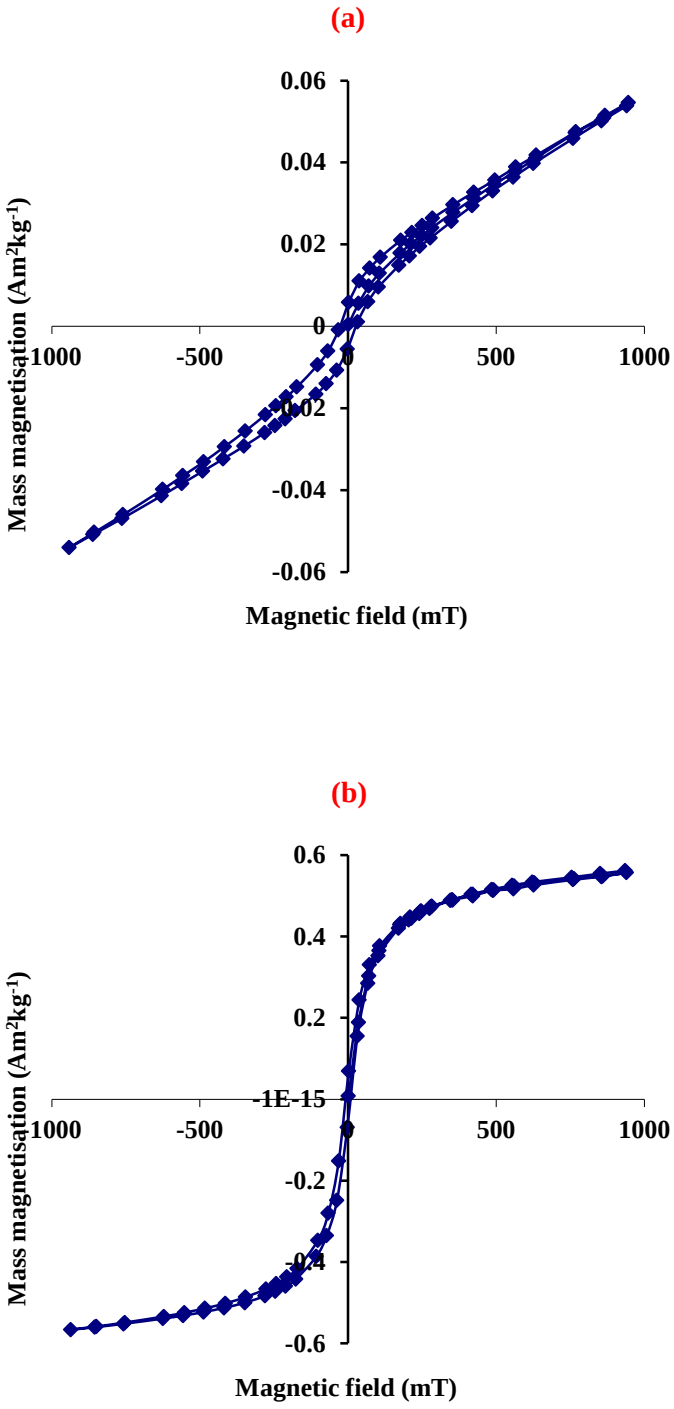

Figure 4-9: (a) The magnetic hysteresis curve of the sample for well A1 above the gas/water contact. (b) The magnetic hysteresis curve for well A1 at the gas/water contact.

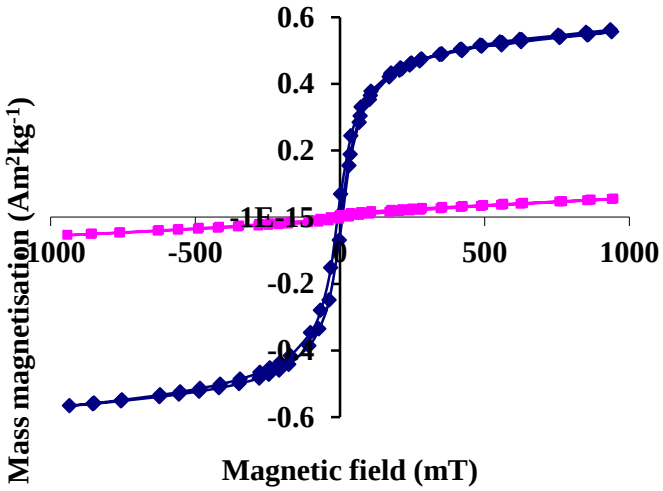

Figure 4-10: For well A1, the hysteresis curves above and below the GWC are shown in a combined plot for comparison purposes. The blue curve is below the GWC, whereas the pink curve is above the contact.

To further investigate the mineralogy of the drill cuttings and the reason for their higher magnetic response in the faulted interval, one usually visually inspects the cuttings to check for any abnormalities in their colour in the zone above the fault and at the fault. The visual observation revealed the presence of a reasonable number of black cuttings in the bags which belonged to the faulted interval, whereas the bags from above the fault zone contained mainly cuttings of the two colours consisting (red) brown and (white) grey. Therefore a collection of brown, white and black cuttings were collected and magnetic susceptibility measurements were performed on these individual cuttings. The Bartington MS2B meter used earlier does not have enough sensitivity for measuring the magnetic susceptibility of these mm-sized cuttings. Therefore Sherwood's MSB balance was used (the details of this kit are covered in **Chapter 2**) for measuring the magnetic susceptibility of these individual red, white and black cuttings.

In Figure 4.11, left, the mass magnetic susceptibility data with depth are plotted for the red and white cuttings of Well A3. The magnetic profiles of these cuttings show very little variation with depth and the trend is very consistent throughout the well. The red cuttings (likely to be hematite), however, show higher magnetic susceptibilities compared to the white cuttings (likely to be quartz). This is consistent with the fact that

the main matrix minerals like quartz or calcite are diamagnetic and show very small magnetic susceptibilities compared to antiferromagnetic minerals like hematite. Figure 4.11, right, shows the mass magnetic susceptibility profile with depth for black cuttings. These cuttings show significantly higher magnetic susceptibilities to those of the red and white cuttings. This reinforces our presumption for these black cuttings being magnetite (since in practice, magnetite mineral shows much higher magnetic susceptibilities compared to hematite).

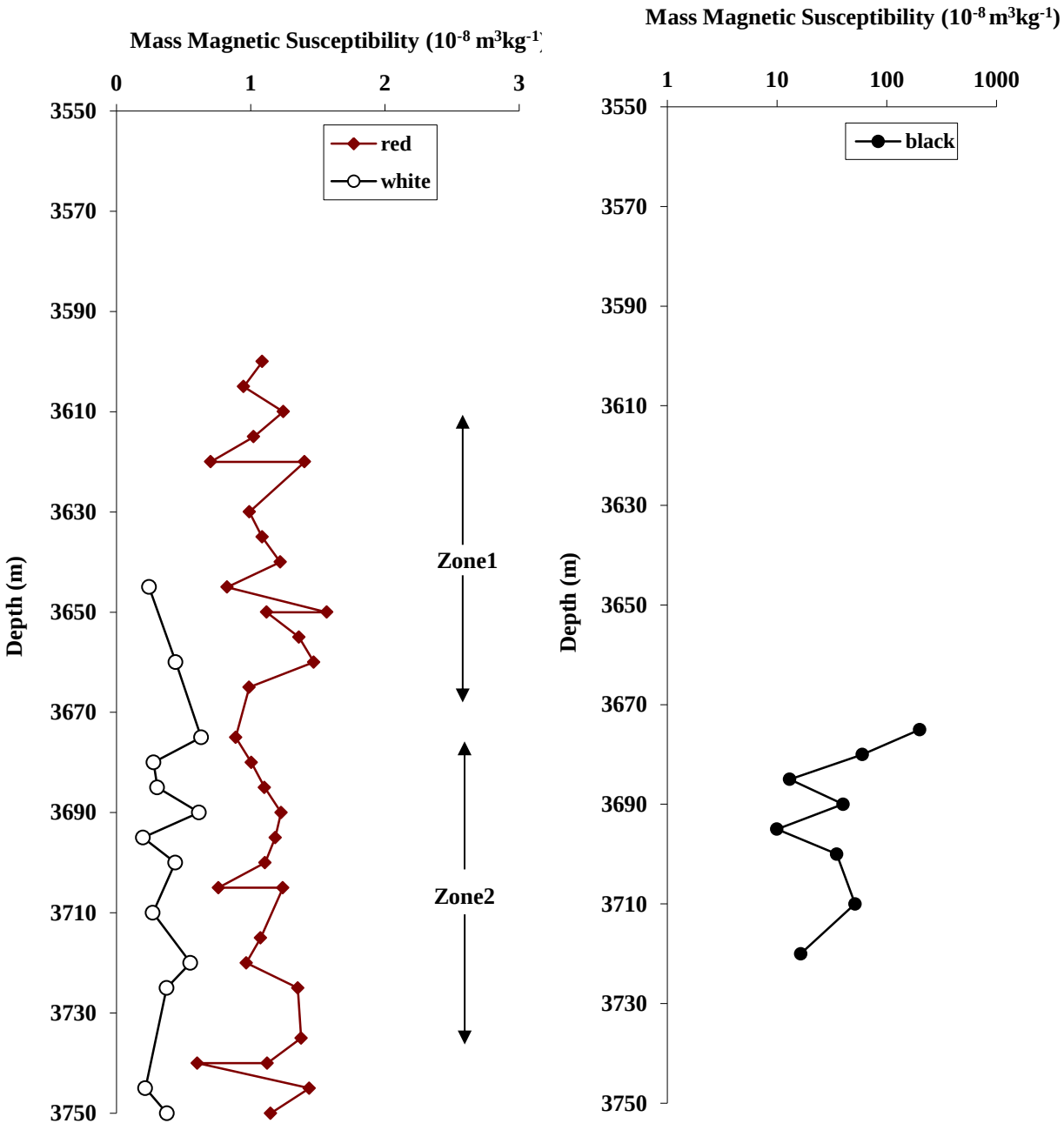

Figure 4-11: Left: mass magnetic susceptibility profiles of the red and white cuttings. Right: mass magnetic susceptibility profile of black cuttings.

4.4.3 Scanning Electron Microscopy (SEM)

Scanning Electron Microscopy (SEM) gives a huge range of information about the clays, the composition and morphology of the minerals which the clays contain and also provides information about the transformational clays and pedogenic mud aggregates. The scanning electron microscopy and energy dispersive X-ray analysis have been widely used to study sandstone reservoirs, since scanning electron microscopy (SEM) has a high resolution and energy dispersive X-ray analysis (EDAX's) can be used to identify mineral composition precisely through the analysis of chemical composition. These methods give more understanding about the effect of the clay mineralogy on the main petrophysical properties (porosity and permeability) and on other characteristics of the reservoir.

Scanning Electron Microscopy (SEM) and Energy Dispersive X-Ray Analysis (EDAX) studies were carried out in the laboratory of the Institute of Petroleum Engineering at Heriot-Watt University for both the black and red cuttings. Scanning electron microscopy (SEM) images made it possible to discriminate the different elements in the samples. The analysis of the results indicated that magnetite (Fe_3O_4) was the mineralogical phase responsible for the higher magnetic susceptibility values in the fault zone. Hematite (Fe_2O_3) was found in the cuttings above the fault zone.

Figure 4.13 shows the scanning electron microscopy (SEM) images of drill cuttings above the fault zone, which appear dark grey, suggesting the presence of hematite and the white stains is referred to the (Fe) mineral. The elemental analysis suggests the presence of Fe and the oxygen atomic percentage indicates the formation of iron oxides.

Figures 4.14a and 4.15a show the scanning electron microscopy (SEM) images of the drill cutting in the fault zone, showing a wide variety of grey and white shades. The whiter stains are usually characteristic of magnetite ($Fe_3O_{4)}$ and the dark grey is usually a mixture of other materials.

The results of the analysis of minerals present in the cutting above and at the fault zone are given in Table 4.2. From these results, it is confirmed that Fe ions are distributed in red cuttings less than in the black cuttings.

Figure 4-12: A typical Scanning Electron Microscopy instrument.

(a)

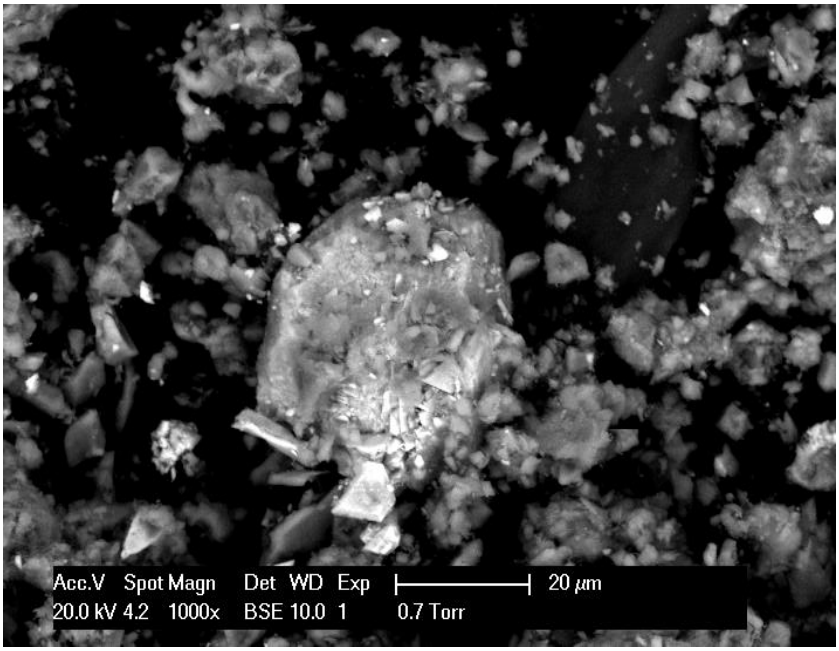

(b)

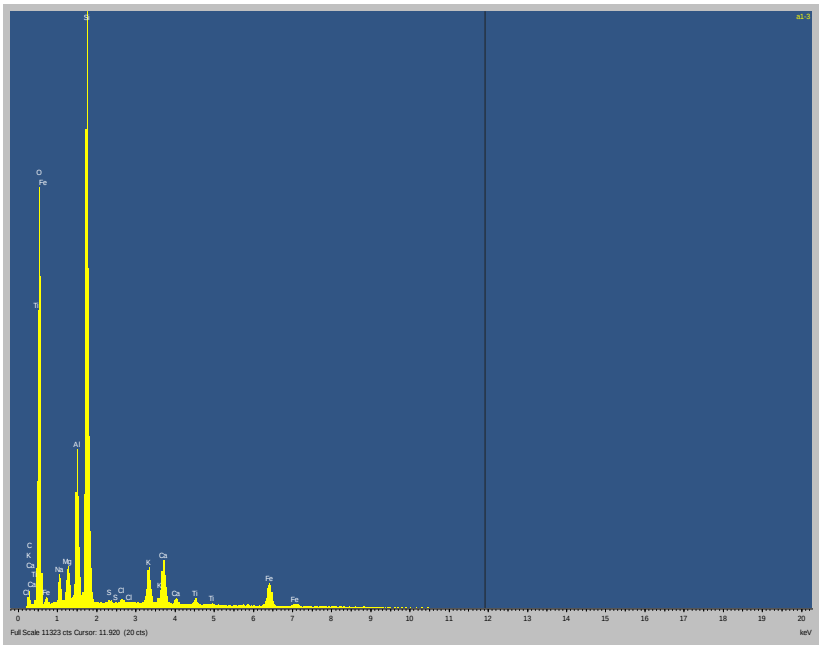

Figure 4-13: (a) The scanning electron microscopy (SEM) image of a red cutting (hematite appears dark-grey) for Well A2. (b) Energy dispersive x-ray analysis (EDAX) image of a red cutting for Well A2.

(a)

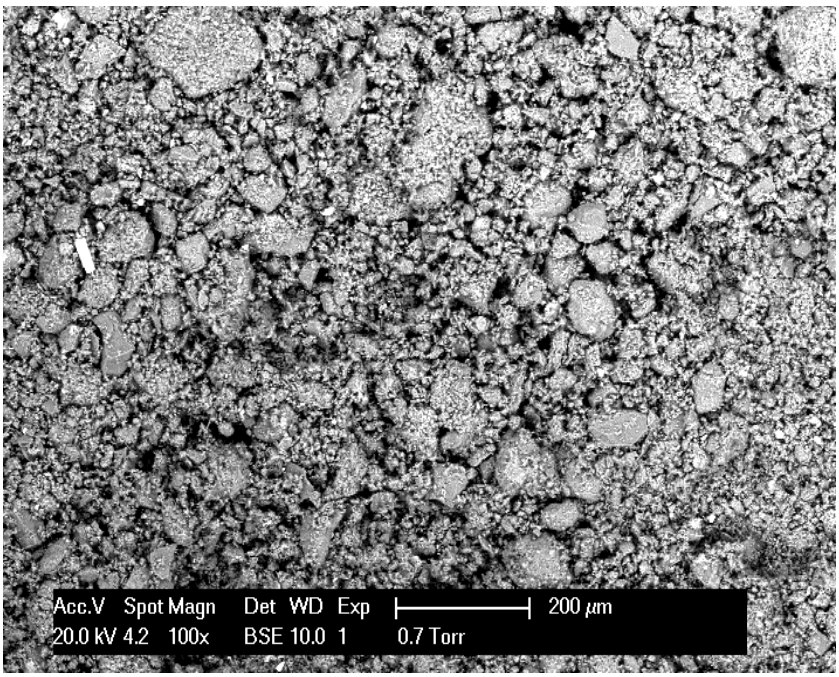

(b)

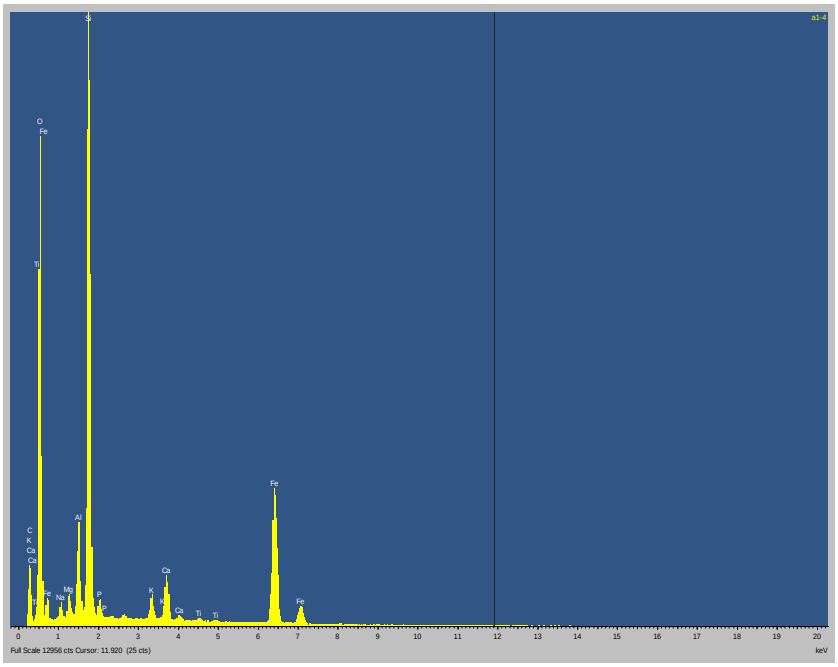

Figure 4-14: (a) The scanning electron microscopy (SEM) image of a black cutting for Well A2 (magnetite grains appear bright). (b) Energy dispersive x-ray analysis (EDAX) image of a black cutting for Well A2.

(a)

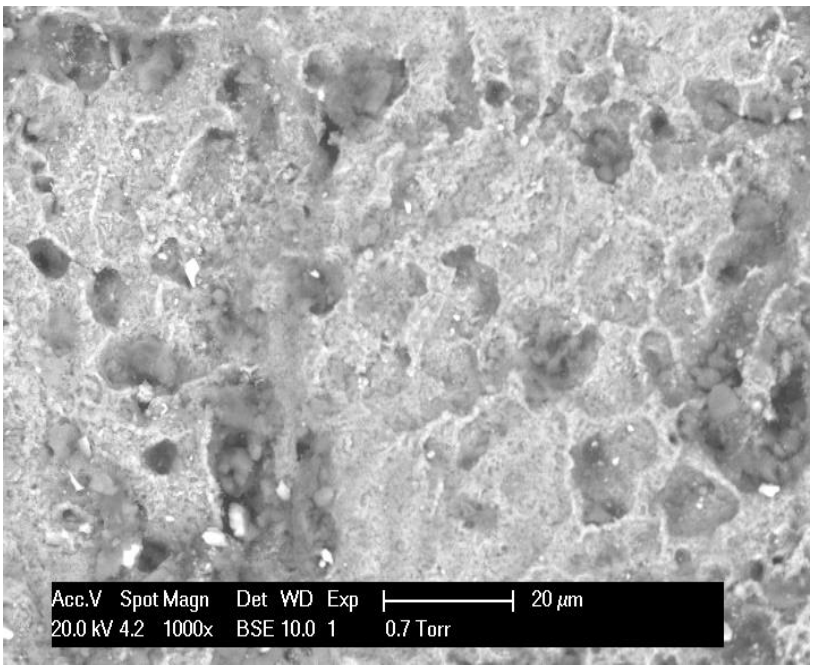

(b)

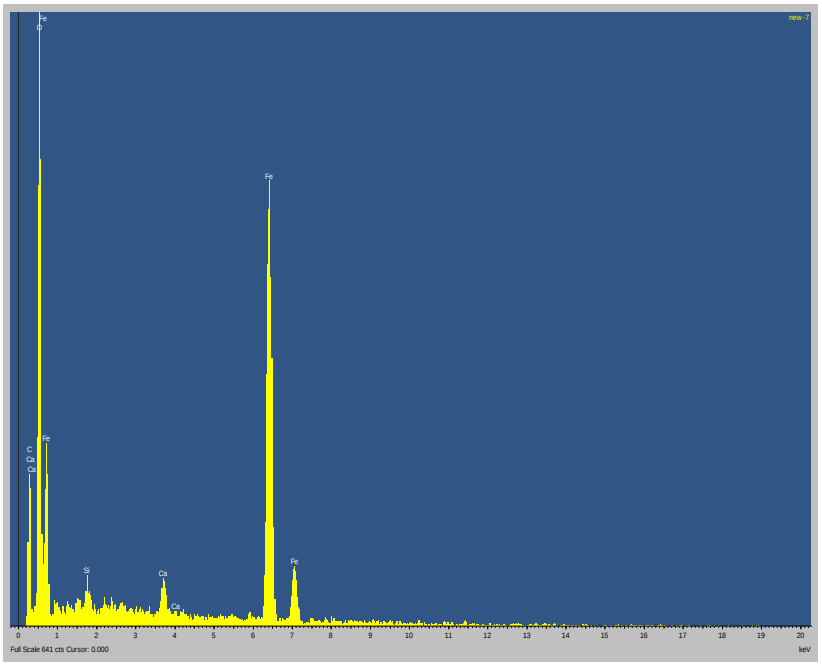

Figure 4-15: (a) The scanning electron microscopy (SEM) image of a black cutting for Well A3 (magnetite grains appear bright). (b) Energy dispersive x-ray analysis (EDAX) image of a black cutting for Well A3.

(a)

Element	Weight%	Atomic%
C	0	0
O	54.09	69.18
Na	1.85	1.62
Mg	1.65	1.33
Al	5.88	4.39
Si	26.25	17.3
Cl	0.21	0.12
K	1.27	1.17
Ca	1.04	1.53
Ti	0.59	0.25
Fe	7.17	3.11
Totals	100	100

(b)

Element	Weight%	Atomic%
C	13.74	26.63
O	35.62	51.84
Si	0.64	0.53
Ca	0.95	0.55
Fe	49.05	20.45
Totals	100	100

(c)

Element	Weight%	Atomic%
C	15.58	24.81
O	45.48	54.38
Na	0.7	0.58
Mg	0.7	0.55
Al	2.46	1.74
Si	15.76	10.74
P	0.7	0.43
K	0.86	0.42
Ca	1.84	0.88
Ti	0.2	0.08
Fe	15.71	5.38
Totals	100	100

Table 4-2: Summaries of the weight and atomic percentage of each element, (a) belonging to SEM 4.13a, (b) belonging to SEM 4.14 a), and (c) belonging to SEM 4.15a.

4.5 Conclusions

- Raw magnetic susceptibility measurements performed on drill cuttings show their potential use to detect faults and fluid contacts in sedimentary sequences. Such measurements can be performed at well site, thereby enabling companies to make important field developments decisions quickly. They can also be used onshore to help interpret data from other laboratory based core analysis techniques such as scanning electron microscopy (SEM) and energy dispersive X-ray analysis (EDAX).

- Histograms of the conventional wireline log data showed a very similar distribution above and below the fault zone, as well as in the gas water contact. However, histograms of magnetic susceptibility data showed clear differences for the various zones, showing the potential usefulness of the magnetic susceptibility data.

- Magnetic hysteresis measurements performed on drill cuttings above the fault zone indicated the presence of hematite mineral (evident by a large open kink at low applied fields and which extends to high applied fields). For drill cuttings in the fault zone, the magnetic hysteresis measurements showed the presence of magnetite (evident by a much bigger kink at low applied fields and which does not extend to high applied fields). This shows the potential usefulness of magnetic hysteresis measurements to help identify ferromagnetic and antiferromagnetic minerals in the drill cuttings and which in our particular case is related to the zones above and at the fault.

- For Well A1, the differences in the hysteresis measurements (which essentially relate to the differences in the magnetic mineralogy present in the samples of drill cuttings) related to the gas water contact. The samples of drill cuttings above the gas-water contact showed different hysteresis curves (representative of hematite) to those below the gas water contact (representative of magnetite). Such magnetic susceptibility measurements have therefore the potential to identify fluid contacts in certain reservoirs.

Chapter 5 Improved Reservoir Characterisation Using Novel Unconventional Crossplots between Magnetic Susceptibility and Downhole Wireline Log Data

5.1 Introduction

The first logging tools were created several years ago and since that time many companies have developed different tools to measure the different physical parameters in the formation. Wireline logs give most of the information about the properties of the formation in the borehole. These tools have the ability to transfer the data to the surface, and at the same time can store the data in downhole memory, which can be later downloaded at the surface to gain a lot of the information during the drilling. (Darling, 2005). Experts analyst can thus obtain a lot of information by interpreting the logs.

A huge number of crossplots are found in the literature which have utilized data from various wireline logging tools. These crossplots have a number of applications, including; 1) making environmental corrections to the downhole wireline data, 2) mineralogy identification, 3) porosity prediction and 4) fluid identification. In the work presented in this chapter, new crossplots were developed between the magnetic susceptibility of various rocks and clay minerals versus data from other key wireline logging tools. These new crossplots have their own importance and in some cases overcome the limitations from other conventional cross plots.

The following paragraphs give a brief introduction to the operating principle of and phenomena measured by various key wireline logging tools which have been used in this analysis and research to crossplot against the magnetic susceptibility data.

5.1.1 Gamma Ray Tool

The standard gamma ray tool is a passive tool which measures natural radioactivity from the formation material. The main radioactive minerals present in abundance in reservoir rocks are potassium, uranium, and thorium. The gamma ray tool measures the gamma rays emitted from these three radioactive minerals.

Certain versions of the National Gamma Ray Spectrometry (NGS) can also quantify the three radioactive minerals. These radioactive minerals are abundant in clays and. The gamma ray tool is therefore an important tool in quantifying the amount of clays and shale in the formation rocks as well as providing information about bed boundaries. The gamma ray response is measured in API units.

5.1.2 Neutron Tool

The neutron tool is the first tool using a radioactive source to detect one of the key petrophysical parameters, which is the porosity. The tool emits fast neutrons which collide with the hydrogen atoms in the formation. The detectors receive the energy deflected back. The more liquid there is in the formation means more the hydrogen atoms, which means a high porosity.

5.1.3 Density Tool

The first density tool was created by Lane-Wells Company the middle of 1950s (Labo, 1987). The modern density tool consists of a gamma-ray source and detector, mounted on a skid, which, means that the tool should be connected to the borehole wall. Gamma rays are emitted by the source and diffused through the formation. The number of diffused gamma rays reaching the detector at a fixed spacing from the source is counted. An increase in the counting rate by the detector indicates a decrease in bulk density in front of the skid. Conversely, a decrease in the counting rate indicates of the increasing in the bulk density (Alger, 1963).

5.1.4 Sonic Tool

The sonic tool measures the time it takes the wave to travel in the formation, the velocity of these waves depends on the kind of formation. (Glover 2013). The travel time or velocity is used to calibrate seismic data and to derive information on the porosity of a formation.

5.2 Objective and Scope of the Chapter

Magnetic susceptibility measurements have become one of the most important methods for investigating changes that have occurred in the lithology and the mineralogy, as these measurements are very quick and non-destructive, and different minerals have highly contrasting susceptibilities. Only limited information has reported in the literature over the years on measuring the magnetic susceptibility of sediments. Thus, little application of magnetic susceptibility to petrophysics has emerged, and no tools have been developed commercially. In this work new crossplots were developed between the magnetic susceptibility of various rocks and clay minerals versus data from other key wireline logging tools such as density, gamma ray and sonic tools. These crossplots show the potential usefulness of a downhole wireline magnetic susceptibility tool in that crossplotting data from such a tool with that from other wireline tools can be used to help in interpreting various formation petrophysical properties.

5.3 Crossplot between Mass Magnetic Susceptibility and Bulk Density

The relationship between formation bulk density with the density of the rock matrix ρma and fluid density ρ_f are related to each other by the following equation (Glover, 2013):

$$\rho_b = (1 - \phi)\, \rho_{ma} + \phi\, \rho_f \quad , \qquad (5.1)$$

Where:

ρ_b = the bulk density of the formation,

ρ_{ma} = the density of the rock matrix,

ρ_f = the density of the fluids occupying the porosity,

ϕ = the porosity of the rock.

The density of quartz, limestone and dolomite are 2.65 g/cm^3, 2.71 g/cm^3 and 2.87 g/cm^3 respectively. Porosity can range from 0% to in excess of 40% in majority of the reservoir rocks. Table 5.1 gives the matrix densities of some common minerals.

The volume magnetic susceptibility can be written as a linear contribution of the volume magnetic susceptibility of the rock matrix χ_v and the volume susceptibility of the fluid occupying the rock pore space χ_{vf}, with each present in proportion to $(1 - \phi)$ and ϕ, respectively:

$$\chi_{v} = (1 - \phi)\,\chi_{vma} + \phi\,\chi_{vf} \quad , \tag{5.2}$$

where:

χ_{vma} = Volume magnetic susceptibility of the rock matrix,

χ_{vf} = Volume magnetic susceptibility of the fluid occupying the porosity.

The mass magnetic susceptibility can be calculated if the bulk density and the volume magnetic susceptibility of the matrix are known. The following equation is used to calculate the mass magnetic susceptibility:

$$\chi_{m} = \frac{\chi_{v}}{\rho b} \quad , \tag{5.3}$$

where:

χ_m = Mass magnetic susceptibility,

χ_v = Volume magnetic susceptibility,

ρ_b = the bulk density of the formation.

Mineral	Bulk density (g/cm^3)	Volume Magnetic Susceptibility (10^{-5} SI)	Mass Magnetic Susceptibility ($10^{-8} m^3 kg^{-1}$)
Quartz	2.65	-1.643	-0.62
Calcite	2.71	-1.3008	-0.48
Dolomite	2.87	-3.444	-1.2
Fresh Water	1	-0.9	-0.9

Table 5-1: Density and mass magnetic susceptibility of the main matrix minerals.

The crossplot between mass magnetic susceptibility and bulk density is shown in Figure 5.1. Different reservoir matrix minerals have been plotted for their varying porosities. The void space has been assumed to be filled with water. As can be seen on the crossplot, different matrix minerals fall in different regions of the cross plot. This shows the first useful piece of information from this cross plot, as one can identify the type of matrix minerals in the reservoir rock. From Table 5.1, the mass magnetic susceptibility of dolomite is lower (more negative) than that of water. As the porosity in the dolomite matrix increases and more and more water fills the pores of the dolomite matrix, the overall mass magnetic susceptibility of the dolomite matrix increases (becomes more positive). On the other hand, mass magnetic susceptibility of both quartz and calcite is higher (less negative) than that of water. Therefore, as the porosity in these matrix minerals increases and more and more water fills the pores of the matrix, the overall mass magnetic susceptibility of these matrix minerals decreases.

Figure 5.2 shows the crossplot between volume magnetic susceptibility and bulk density. Such a crossplot would be particularly useful for a downhole magnetic susceptibility tool, where there will be bulk density information about the formation available. The bulk density information from the density tool would not be useful to convert volume magnetic susceptibility into mass magnetic susceptibility, due to different between the two tools in the depth of investigation and. If one plots the wireline volume magnetic susceptibility data versus the bulk density data, different matrix minerals would fall in different regions of the crossplot, therefore potentially helping to identify the type of matrix minerals present in the reservoir rock. From Table 5.1, it can be seen that the volume magnetic susceptibility of all three reservoir matrix minerals is lower (more negative) than that of water. As the porosity of the reservoir rock increases and more and more water fills the pores of the matrix, the overall volume magnetic susceptibility of the reservoir rock increases (becomes more positive).

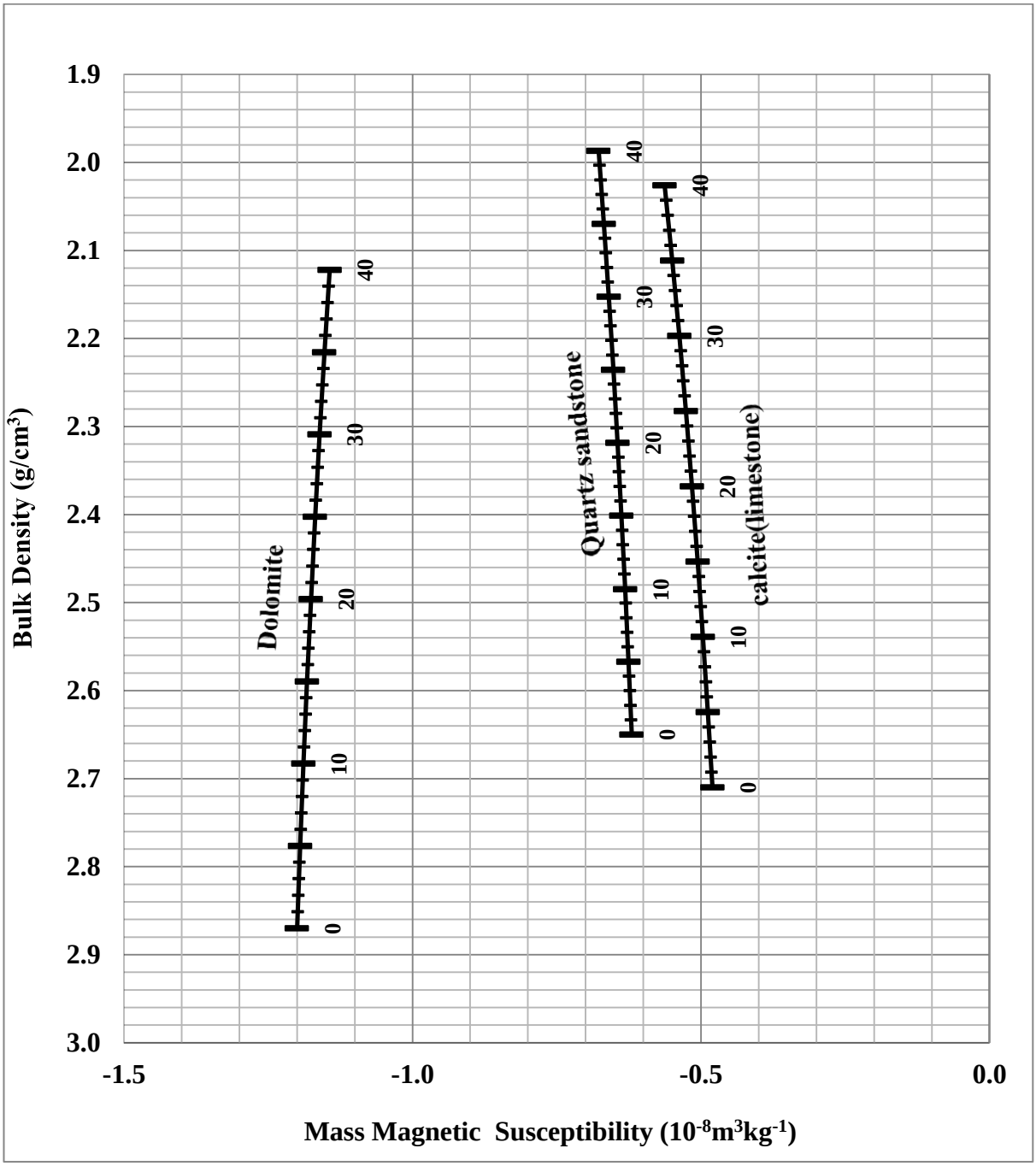

Figure 5-1: Mass magnetic susceptibility versus density crossplot, which can potentially be used for identifying and quantifying mineralogy and mixture porosity determination in simple mineral mixtures.

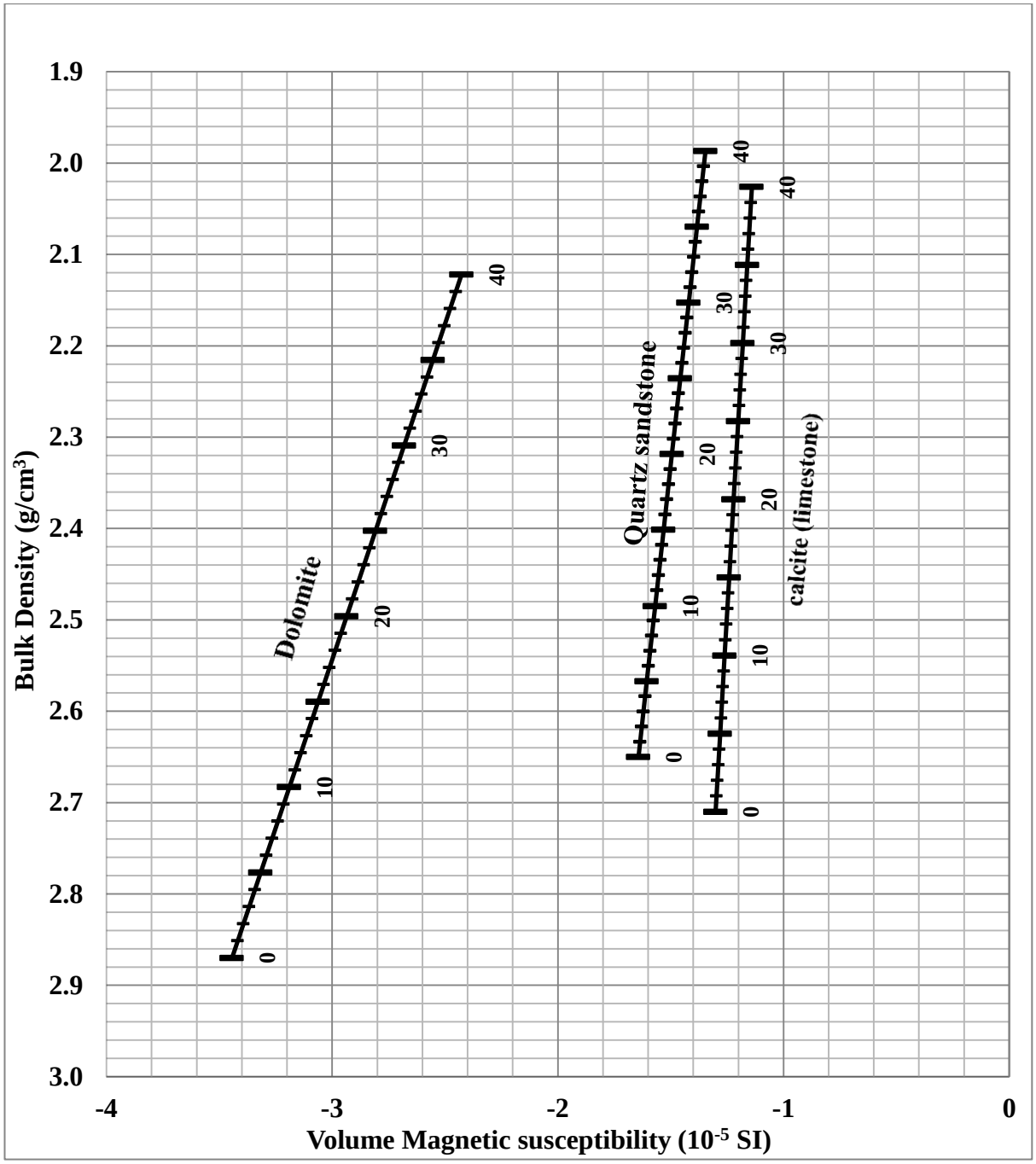

Figure 5-2: Volume magnetic susceptibility versus density crossplot**.**

The mass magnetic susceptibility versus density crossplot can also be used for quantifying minerals where matrix minerals are present as binary mixtures, for example a mixture of sandstone and limestone, or limestone with dolomite. An easy formula can be used to calculate the proportions of the two matrixes. In Figure 5.3, the point A lies between lines of sandstone and dolomite. The relative proportions of the two matrices can be calculated by connecting lines of equal porosities between the sandstone and dolomite matrix lines and then measuring the distances of point A from the sandstone and dolomite matrix lines. In the example shown in Figure 5.3, 'a' and 'b' are the distances of point A from the sandstone and dolomite lines. The percentages of quartz and dolomite can now be calculated using the formulas below.

Percentage of quartz

$$x = \frac{b}{a+b} \tag{5.4}$$

$$= \frac{3.7}{2+3.7} = 64.91\%$$

Percentage of dolomite

$$y = \frac{a}{a+b} \tag{5.5}$$

$$= \frac{2}{2+3.7} = 35.08\ \%$$

Therefore, point A corresponds to a volumetric proportion of about 65% quartz and 35% dolomite and the porosity of the mixture is around 21%. If the lithology were calcite and dolomite instead of quartz and dolomite, the lines for 'a' and 'b' would have been measured between calcite and dolomite lines. In that case, the porosity of the mixture would be around 23%; the mineral proportions would be 42% dolomite and 58% calcite. If the matrix consists of a mixture of three minerals rather than two, the crossplot cannot be used to further quantify the minerals any more. However, it would still provide information on the mixture porosity of the matrix, which would be around 22% for point A.

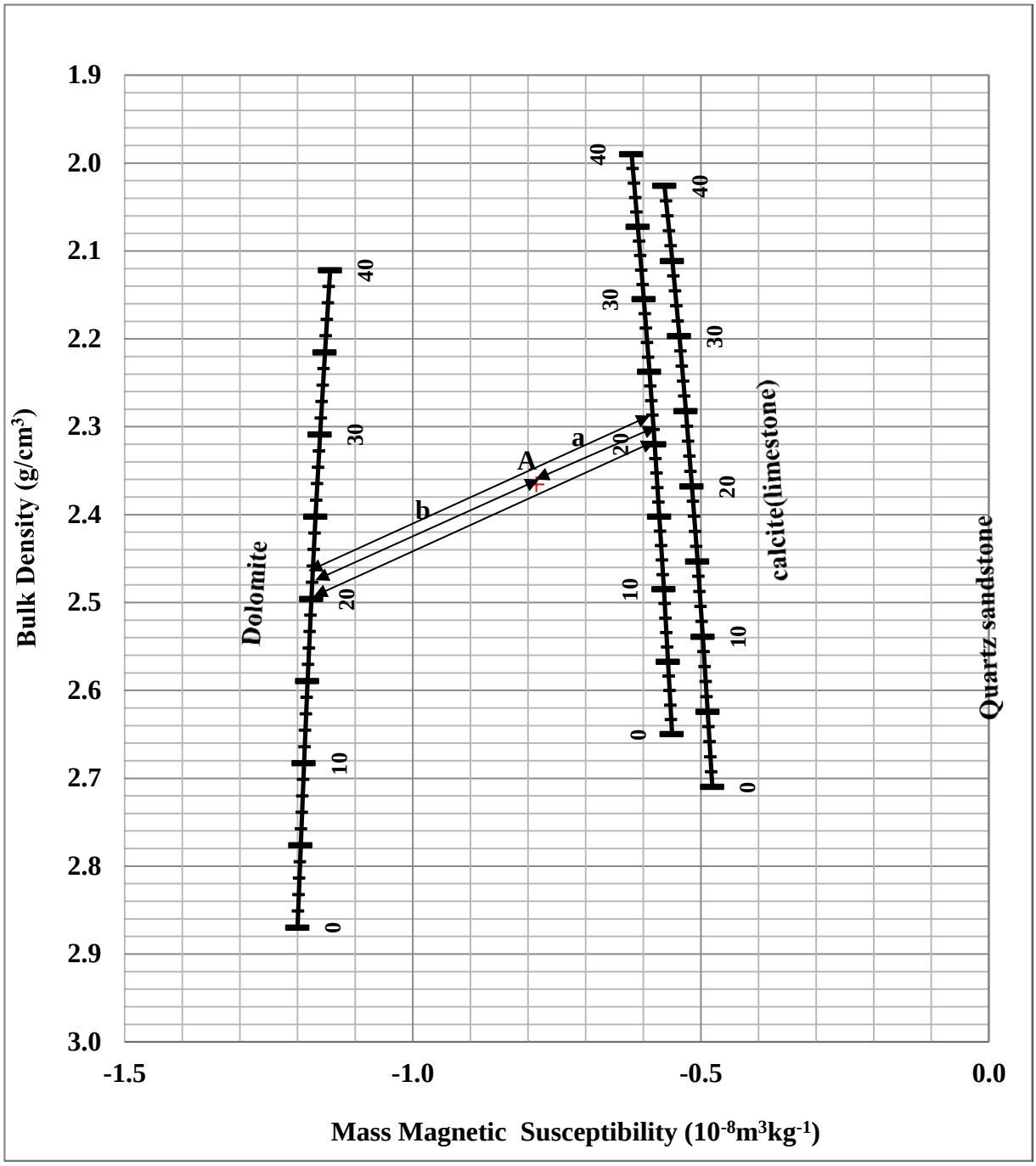

Figure 5-3: Determination of mixture porosity using magnetic susceptibility versus density crossplot.

Application of this technique is similar to those for other crossplots. The influence of invasion, the presence of shale, gas and the matrix mineralogy would have an effect on the location of data points. Further explanations will be made in the following sections.

5.3.1 Effect of Clays on Mass Magnetic Susceptibility versus Bulk Density Crossplot

The presence of clay minerals in a formation can generally cause an increase in the density reading (this is due to the relatively different bulk density of clays compared with matrix minerals). The majority of clays show a paramagnetic behaviour (only kaolinite has negative magnetic susceptibility), which would cause an increase in the magnetic susceptibility reading. Due to these effects, clays can easily be identified, if present, on the magnetic susceptibility versus bulk density crossplot (see Table 2.2 in **Chapter 2** for details on the mass magnetic susceptibility of various clay minerals).

In Figure 5.4, a template for quartz and illite mineral mixtures was created, the end points being 100% quartz and 100% illite. The lines in between the two end points show variations in the percentages of quartz and illite. The advantage of such a crossplot is that, by plotting the data, one can easily identify and quantify the percentage of illite clay in reservoir rock samples. Similar templates can be produced for other combinations of matrix and clay minerals. In Figure 5.4, the volume magnetic susceptibility was calculated using Equation 5.2, by changing the percentage of quartz and illite at various porosity values (ranging from 0-40%). The similar equation was used to calculate the bulk density of the individual mineral mixtures using theoretical bulk density values for illite and quartz. In order to determine mass specific magnetic susceptibility, the volume susceptibility values were divided by the bulk density for every porosity of the mixture.

The first line (100% Quartz) is approximately linear. The bulk density decreases with an increase in the porosity values. As the porosity increases, the pore space becomes filled with water. The mass magnetic susceptibility of quartz and water is not very different (-0.62 and -0.9 m^3kg^{-1} respectively). Therefore, there is no noticeable change in the slope of the 100% quartz line with varying porosity values. However, for the 100% illite line, the mass magnetic susceptibilities of illite and water are quite different (15 and -0.9 m^3kg^{-1} respectively). There is , therefore a noticeable change in the slope of the 100% illite line with varying porosity values.

Figure 5.5 shows the cross plot between mass magnetic susceptibility and bulk density, showing the variations in the mass magnetic susceptibility signal with a variation in the presence of illite clay (1-10%) in a quartz matrix. It is clear that such a crossplot is very sensitive in picking up small variations in clay in a quartz matrix. Another observation is that as more and more pores fill with clays, the points on the crossplot for magnetic susceptibility versus bulk density will move to the top right hand corner. This is due to the fact that an increase in clay causes an increase in magnetic susceptibility values and slightly increases in the bulk density values. Therefore, the location of the points would show if there are clays present in the reservoir matrix minerals.

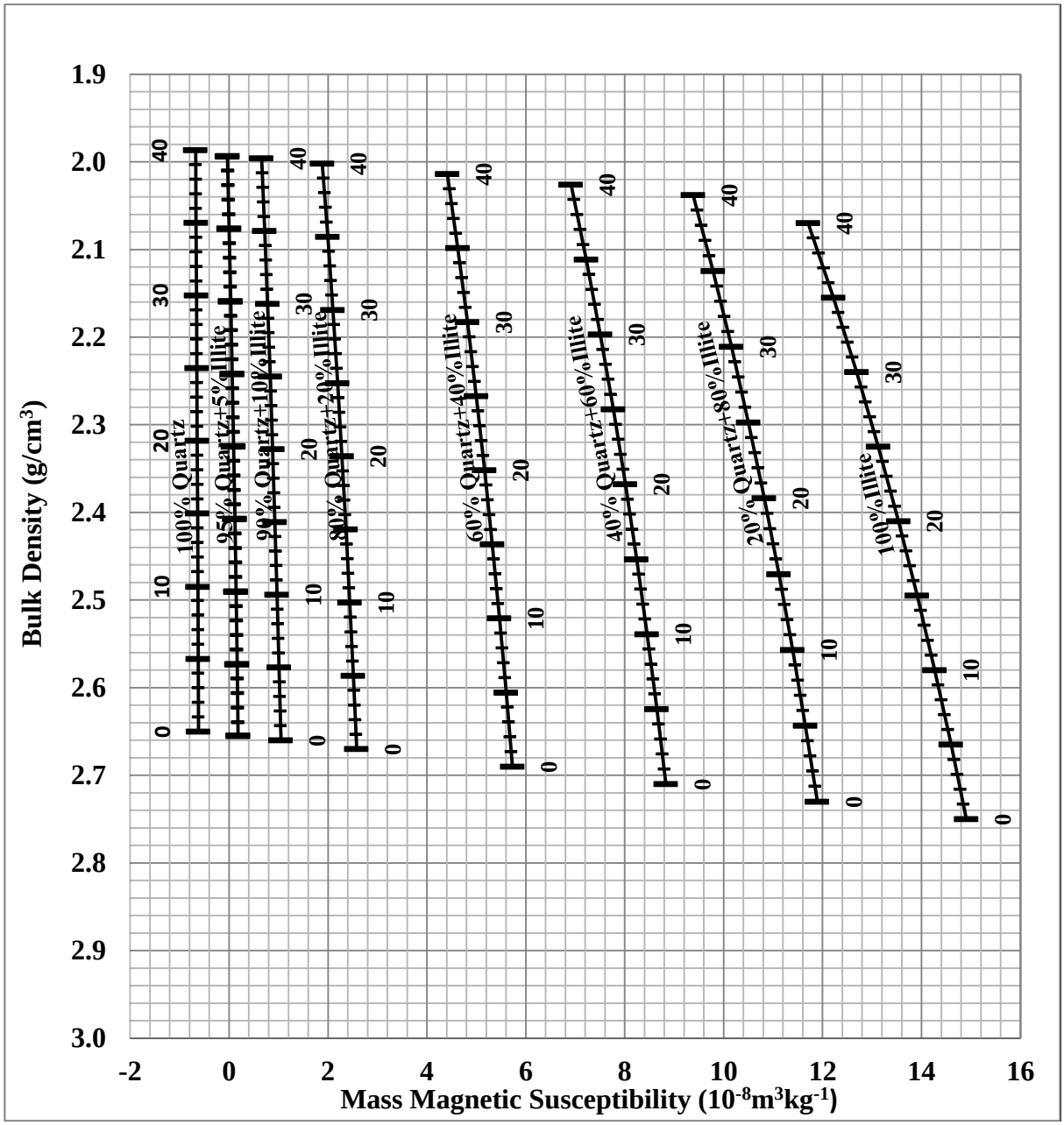

Figure 5-4: Crossplot between mass magnetic susceptibility and bulk density, showing the effect of the presence of illite clay in a quartz matrix.

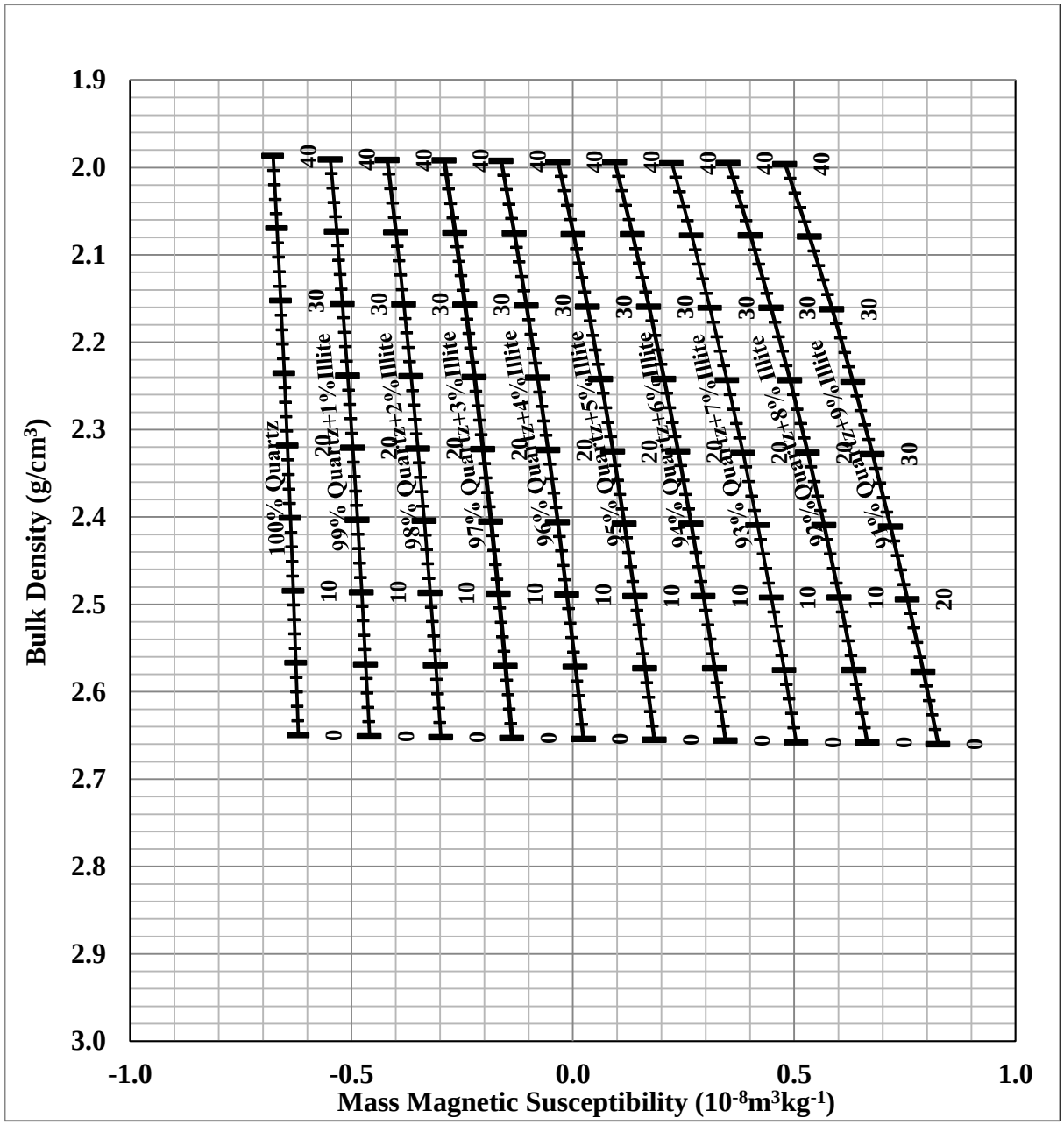

Figure 5-5: Crossplot between mass magnetic susceptibility and bulk density showing the effect of the presence of illite clay (1-10%) in a quartz matrix.

5.3.2 Effect of Gas on Mass Magnetic Susceptibility versus Bulk Density Crossplot

In previous crossplots, it was assumed that the pore volume is filled with water. Now the effect of gas in the pore space and its effect on the mass magnetic susceptibility versus bulk density crossplot will be shown. The effect of gas was added because of the large difference in the density response for gas compared with water. Figure 5.6 shows a crossplot between mass magnetic susceptibility and bulk density where gas is filling the pore spaces. We can see a separation of the two lines (the line where water is filling the pore spaces versus gas filling the pore spaces), with increasing porosity values (0 – 40%). This separation is mainly due to the density difference between gas and water. There was no significant change in mass magnetic susceptibility values as more and more gas fills the pores, due to increased porosity values. The bulk density reduces much more rapidly causing the values to move upwards on the crossplot.

Calculations have been made for both gas and fresh water and their effect on bulk density and mass magnetic susceptibility, using the following equation:

$$\rho_b = (1 - \phi)\,\rho_{ma} + \phi\,\rho_g \ , \qquad (5.6)$$

where:

ρ_b = the bulk density of the formation,

ρ_{ma} = the density of the rock matrix,

ρ_g = the density of the gas occupying the porosity,

ϕ = the porosity of the rock.

Figure 5.7 shows a crossplot between volume magnetic susceptibility and bulk density, where gas is filling the pore spaces. Again, we can see a separation of the two lines (the line where water is filling the pore spaces versus gas filling the pore spaces) with increasing porosity values (0 – 40%). For the crossplots in Figures 5.6 and 5.7, the volume magnetic susceptibility of air ($0.0029*10^{-5}$ SI) and the bulk density of methane (0.000089 g/cm^3) have been used. Although there can be subtle differences in the location of the points on these crossplots between water and gas filled pores, especially at lower porosity values, the information, combined with other crossplots, like neutron-density, can be used to confirm the presence of gas, for example.

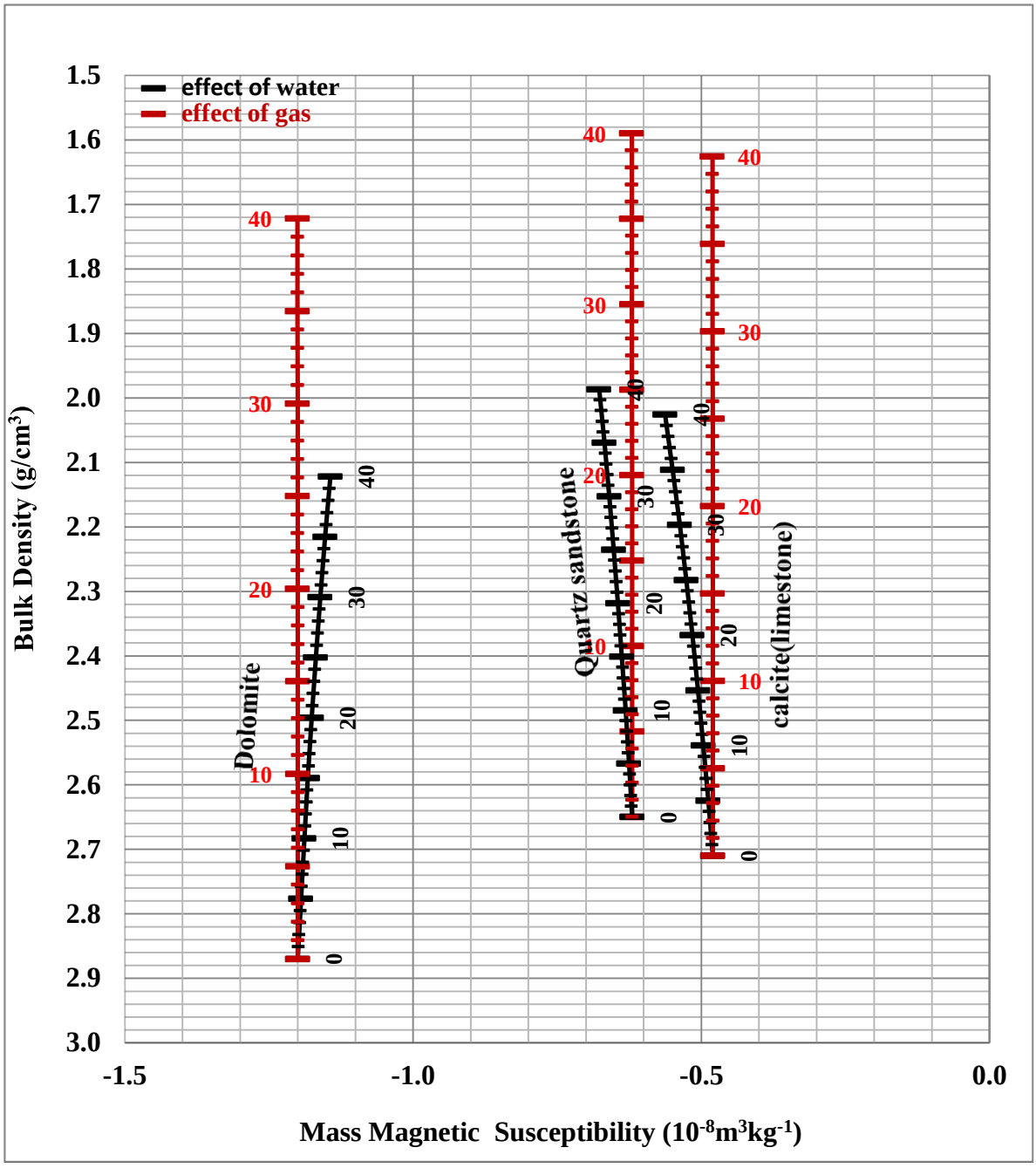

Figure 5-6: Crossplot of the effect of gas on mass magnetic susceptibility and bulk density

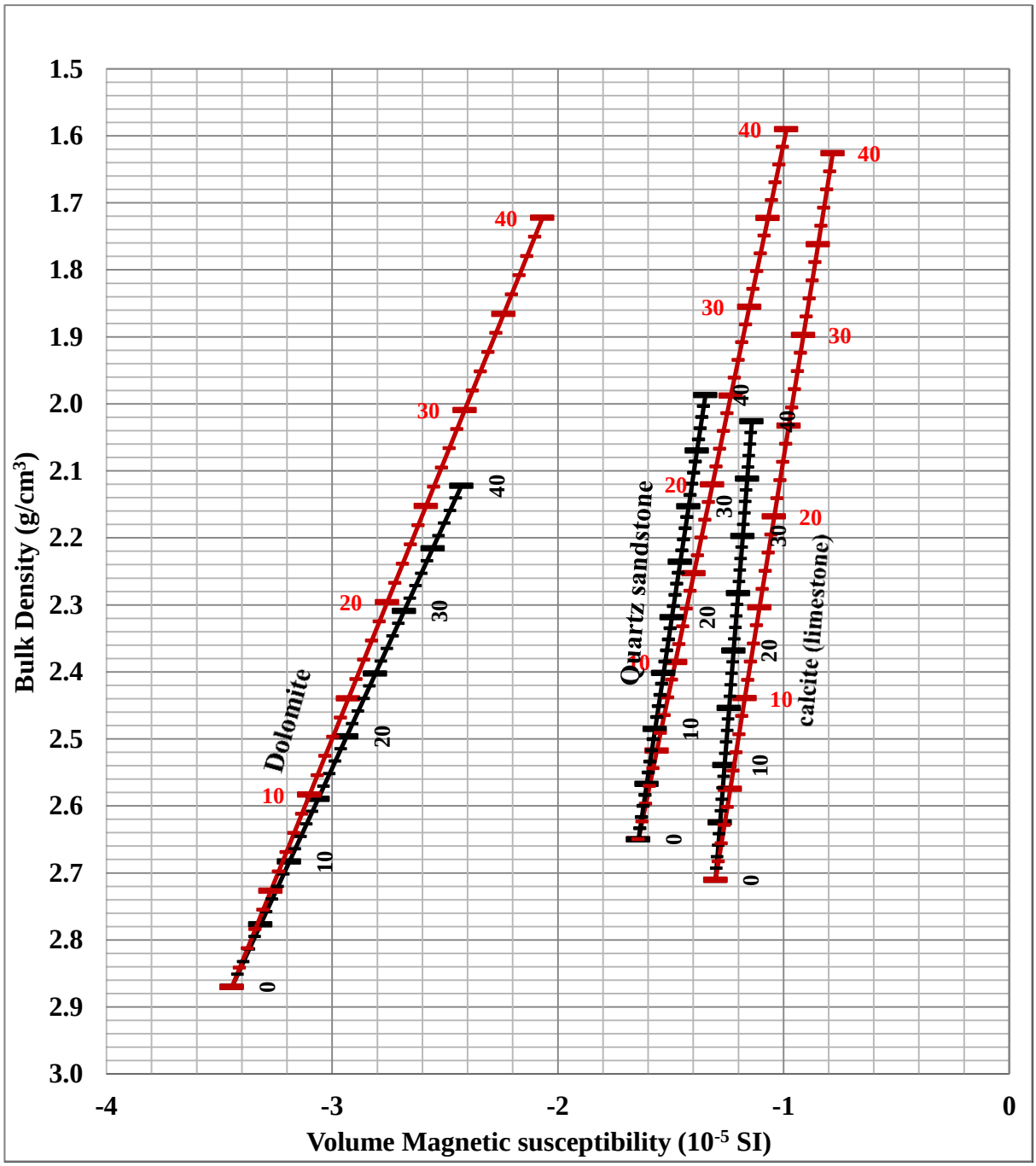

Figure 5-7: Crossplot of the effect of gas on volume magnetic susceptibility versus bulk density.

5.4 Experimental Data – Magnetic Susceptibility versus Density Crossplots

5.4.1 Case study one

In order to show the usefulness of the magnetic susceptibility and bulk density crossplots, the volume magnetic susceptibility was measured from a number of 1 inch diameter plug samples from a Middle Eastern reservoir which have collected from one of production well in libya . It was known that the main reservoir matrix of these sets of plug samples was dolomite. In the petrophysical laboratory at Heriot-Watt University, a subset of 15 samples was selected. The volume magnetic susceptibility was measured using a Bartington magnetic susceptibility MS2 meter. The bulk density of the samples was obtained by weighing them on a scale and then dividing the weight by the bulk volume of the samples. Volume magnetic susceptibility was converted into mass magnetic susceptibility by dividing the volume magnetic susceptibility by the bulk density of the sample. Figure 5.8 shows the mass magnetic susceptibility and bulk density data, plotted on the mass magnetic susceptibility versus bulk density crossplot. The data plotted on the crossplot shows a cloud of points around the dolomite line with porosities ranging between 15 to 23%. Once identified as a dolomite, the porosity for the points can be read directly off the dolomite line. Thus, the new crossplots can not only identify mineralogy but also help in the porosity prediction of the reservoir rock samples.

5.4.2 Case study two

For case study two, (PDC) drill cuttings from a tight gas reservoir rock in the German sector of the North Sea were used. Volume magnetic susceptibility of the drill cuttings was measured and subsequently the cuttings were weighed for their bulk density information. The volume susceptibility was subsequently converted into mass magnetic susceptibility before plotting it on the crossplot in Figure 5-9. The cuttings data appear in the upper right hand corner of the crossplot, indicating that the cuttings had some strongly magnetic minerals in them, which consequently pushed the points to the right hand side of the crossplot and well away from the lines for the main matrix minerals. Magnetic hysteresis measurements of the samples (covered in **Chapter 4**) revealed that these samples contained mainly hematite (with traces of magnetite), which caused their higher values of magnetic susceptibility. Hematite is acting as shale in this tight gas

reservoir and is the main cause for reduction in permeability values. The scatter of the data on the crossplot shows clearly that cuttings are not clean (as they are scattered

away from the matrix mineral lines). The fact that the data has plotted to the right of the matrix minerals indicates that the cuttings contain either clays or other magnetic minerals (hematite in this case). The bulk density of the cuttings was underestimated, due to void spaces between cuttings. This essentially caused a reduction in their bulk densities, thereby pushing the bulk density values towards lower end on the crossplot.

Another key observation was that the data were grouped in two subsets, according to their mass magnetic susceptibility values, i.e. between 18 - $23*10^{-8}$ m^3kg^{-1} and between 28 - $34*10^{-8}m^3kg^{-1}$. Further information from the operator revealed that the first set of data, with relatively lower values, belonged to the zone just above the fault while the latter, with relatively higher magnetic susceptibility values, corresponded to the fault zone itself. This was something which had not been seen in the past and shows some other potential uses of the crossplots developed in this chapter.

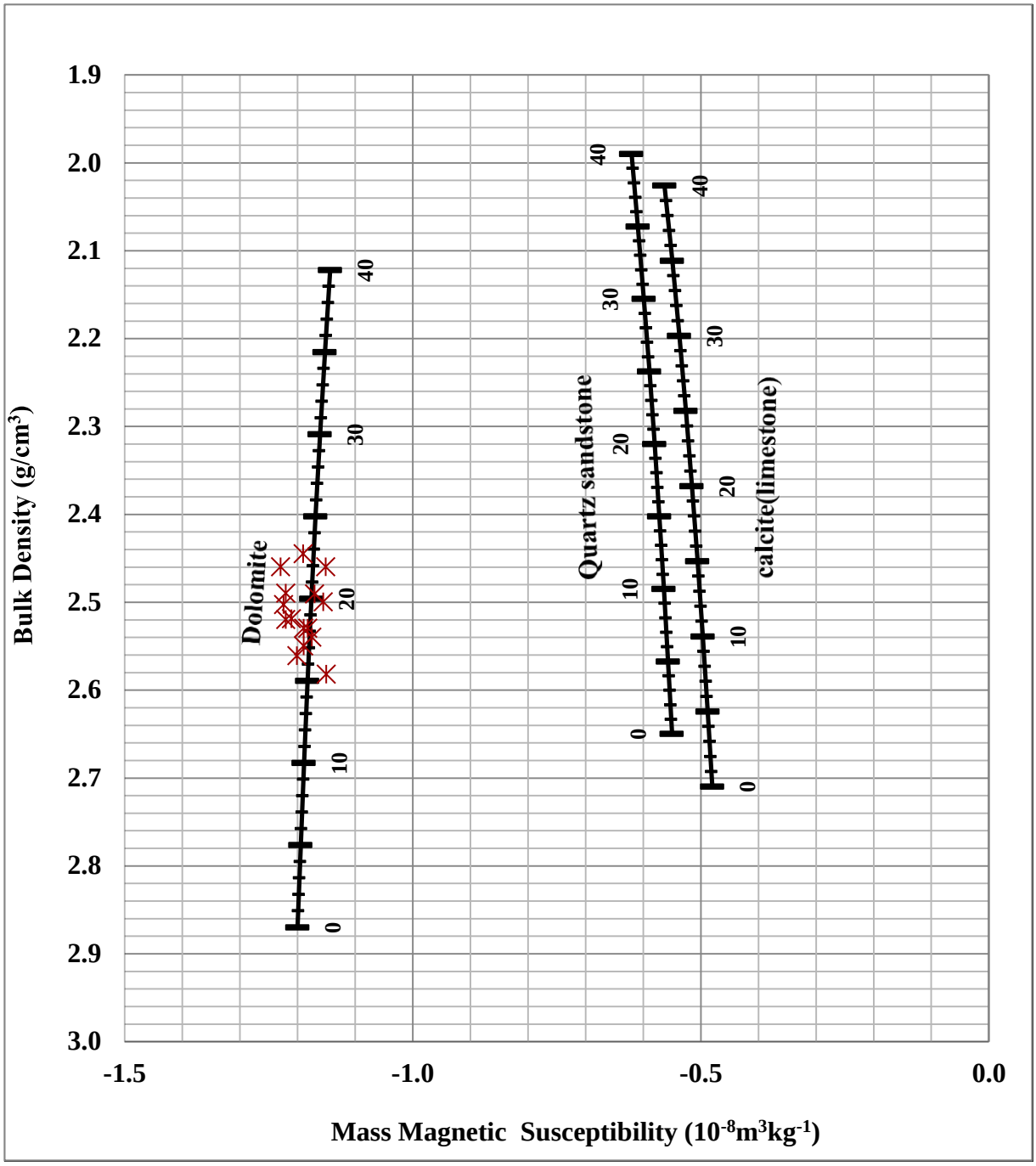

Figure 5-8: Using mass magnetic susceptibility versus density crossplot for identifying mineralogy

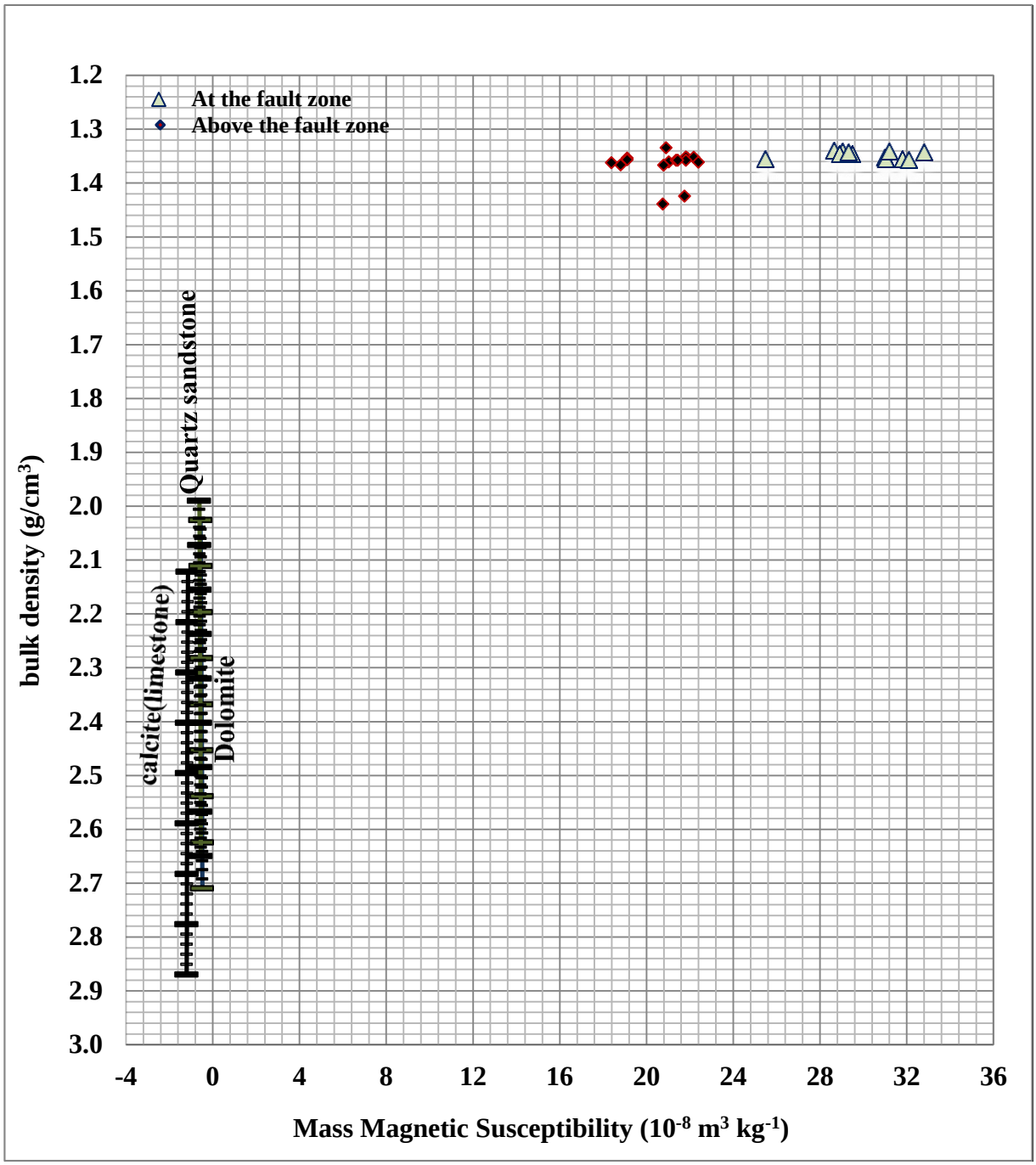

Figure 5-9: Crossplot of mass magnetic susceptibility and density for well A3, at the fault zone and above the fault zone.

5.4.3 Case study three

To further investigate the usefulness of the magnetic susceptibility versus bulk density crossplot, 363 plug samples were studied, which were provided by Shell from the UK North Sea. These samples belonged to a red sandstone and relatively tight gas reservoir. Figure 5.10 shows a crossplot between the permeability and bulk density of the plug samples. The majority of the permeability data lies between 0.1 – 1 mD, which shows that the reservoir is relatively tight. The bulk density values are rather high, with the majority of data lying between 3 – 3.5 g/ cm^3. The correlation coefficient of R^2=0.597 shows that the permeability is dependent on the bulk density of the samples. X-ray diffraction data from this reservoir were available, which confirmed the presence of abundant hematite in these samples, which also was the reason for them being red in colour. Due to the presence of hematite, this reservoir took my interest to check whether magnetic susceptibility measurements on this reservoir correlate with permeability, as has been shown in the work presented in previous chapters.

The volume magnetic susceptibility of the core plugs was therefore measured, which was subsequently converted into mass magnetic susceptibility by dividing the volume magnetic susceptibility by the bulk density of the plug samples. Figure 5.11 shows the mass magnetic susceptibility data of the plug samples, plotted on a density versus magnetic susceptibility crossplot. The mass magnetic susceptibility values for the majority of the core plugs lie between 1.3-3.5 $x10^{-8}m^3kg^{-1}$. It is clear that all the samples are located to the right and bottom side of the cross plot. This indicates that samples have magnetic minerals in them. The second observation from this crossplot is that the magnetic minerals are likely to be heavier than the three main matrix minerals (which are quartz, calcite and dolomite) shown on the cross plot. If there were no magnetic minerals in the samples, then the samples would have fallen in the region of the three lines corresponding to the main matrix minerals, either on a particular matrix line or in between the lines, if there was more than one matrix mineral- this has been discussed in the early part of this chapter.

Another key observation is that the mass magnetic susceptibility increases with an increase in the bulk density of the samples. The higher their bulk density, the higher the mass magnetic susceptibility of the samples, and the higher will be the presence of magnetic minerals in the samples.

The magnetic susceptibility of rocks increases going from acidic to basic rocks. In general, susceptibility depends on the magnetic mineral content in the rock, rather than being closely related to other rock physical properties. Thus, it is not possible to predict magnetic susceptibility from the lithologic rock type. However, in our study, magnetic susceptibility shows some degree of correlation with bulk density. When bulk density increases, magnetic susceptibility was seen to increase.

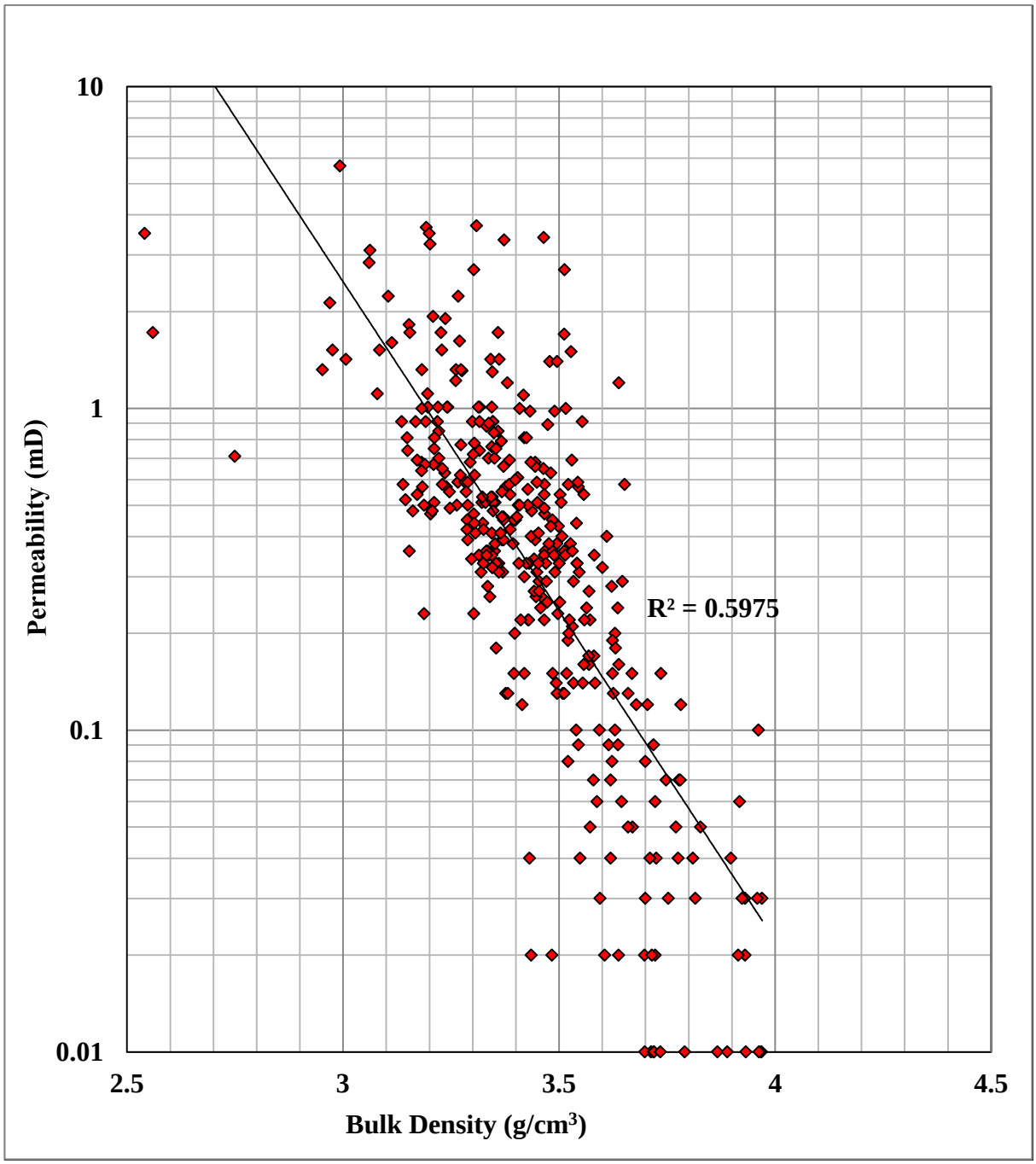

Figure 5-10: Bulk density versus permeability of the core plug samples**.**

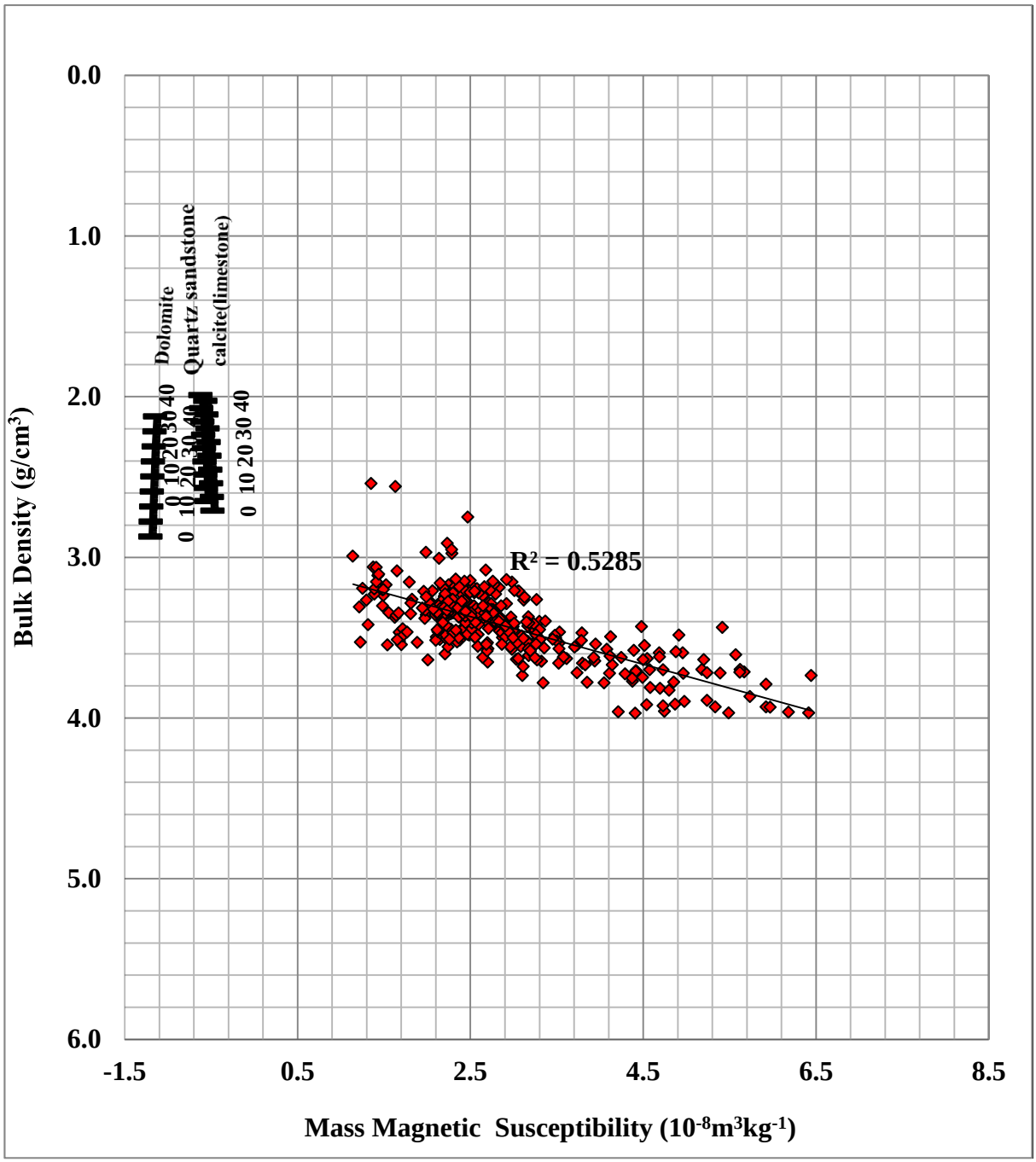

Figure 5-11: Crossplot between density and mass magnetic susceptibility of the core plug samples.

In Figure 5.12, samples with higher mass magnetic susceptibility and a higher bulk density are circled, indicated as sample 1, and a sample with lower mass magnetic susceptibility and lower bulk density is indicated as sample 2. This is to show to the reader how the colour of the samples changes with a change in mass magnetic susceptibility and bulk density values, which are essentially related to a variation of the hematite content. The effect of the hematite on the permeability has been discussed in great detail in **Chapter 3** of this thesis. Figure 5.13 shows photos of the two plugs, one with higher hematite content and the other with lower hematite content (sample 1 and sample 2 respectively).

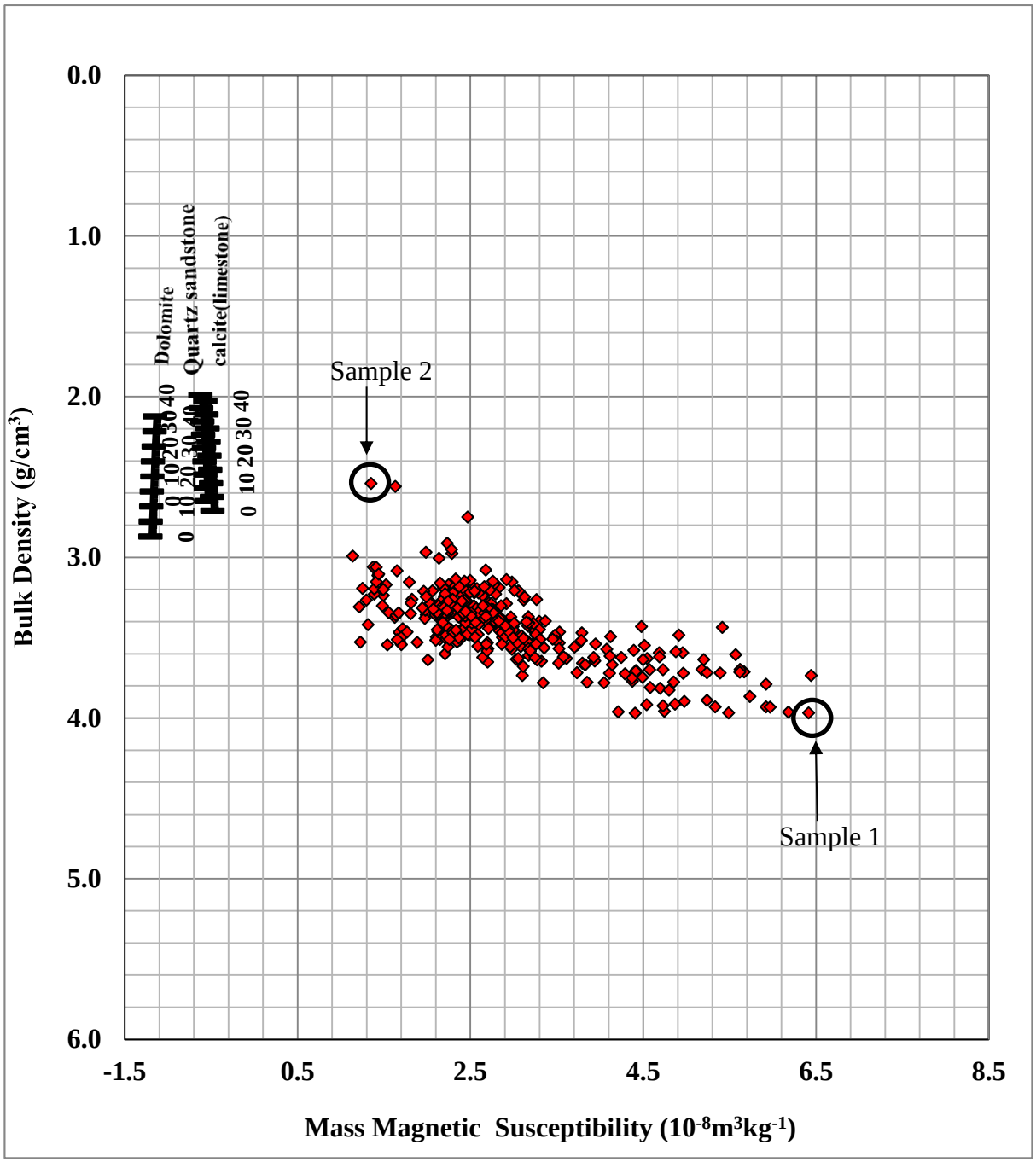

Figure 5-12: Sample with higher mass magnetic susceptibility and a higher bulk density indicated as sample (1); sample with lower mass magnetic susceptibility and lower bulk density indicated as sample (2).

Figure 5-13: Photos of the two plugs: sample 2 (plug A) has lower hematite content and sample 1 (plug B) has higher hematite content.

Figure 5.14 shows a crossplot of mass magnetic susceptibility versus permeability. There is a trend of high mass magnetic susceptibility corresponding to low permeability and vice versa. Mass magnetic susceptibility essentially exhibits a good correlation with permeability, with correlation coefficient R^2 =0.84. The mass magnetic susceptibility of the sample is primarily dependent on the hematite content, which is controlling permeability in this reservoir and other reservoirs shown throughout this thesis.

One of the advantages of magnetic susceptibility measurements on core plugs is that we can predict permeability on reservoir rock samples where there is no permeability data available. All we need is to have permeability measurements on a representative set of plug samples, which can be used for calibration for permeability predictions. Apart from core plugs, magnetic susceptibility measurements can also be used to predict permeability on slabbed sections of reservoir core in such tight gas reservoirs. Probe permeability measurements are rather qualitative on the slabbed core sections, as the acoustic pulse investigates only some of mm of the top section of the core. The magnetic susceptibility measurements carried out on the slabbed core can predict high resolution permeability by using regressions between magnetic susceptibility and permeability from the core plugs.

One of the future research studies would be to look at whether there exist generic trends between magnetic susceptibility and permeability (or between magnetic susceptibility and bulk density) in these relatively tight red sandstones. These generic trends can then be used to predict permeability and density from the magnetic susceptibility measurements, where there is no calibration data available.

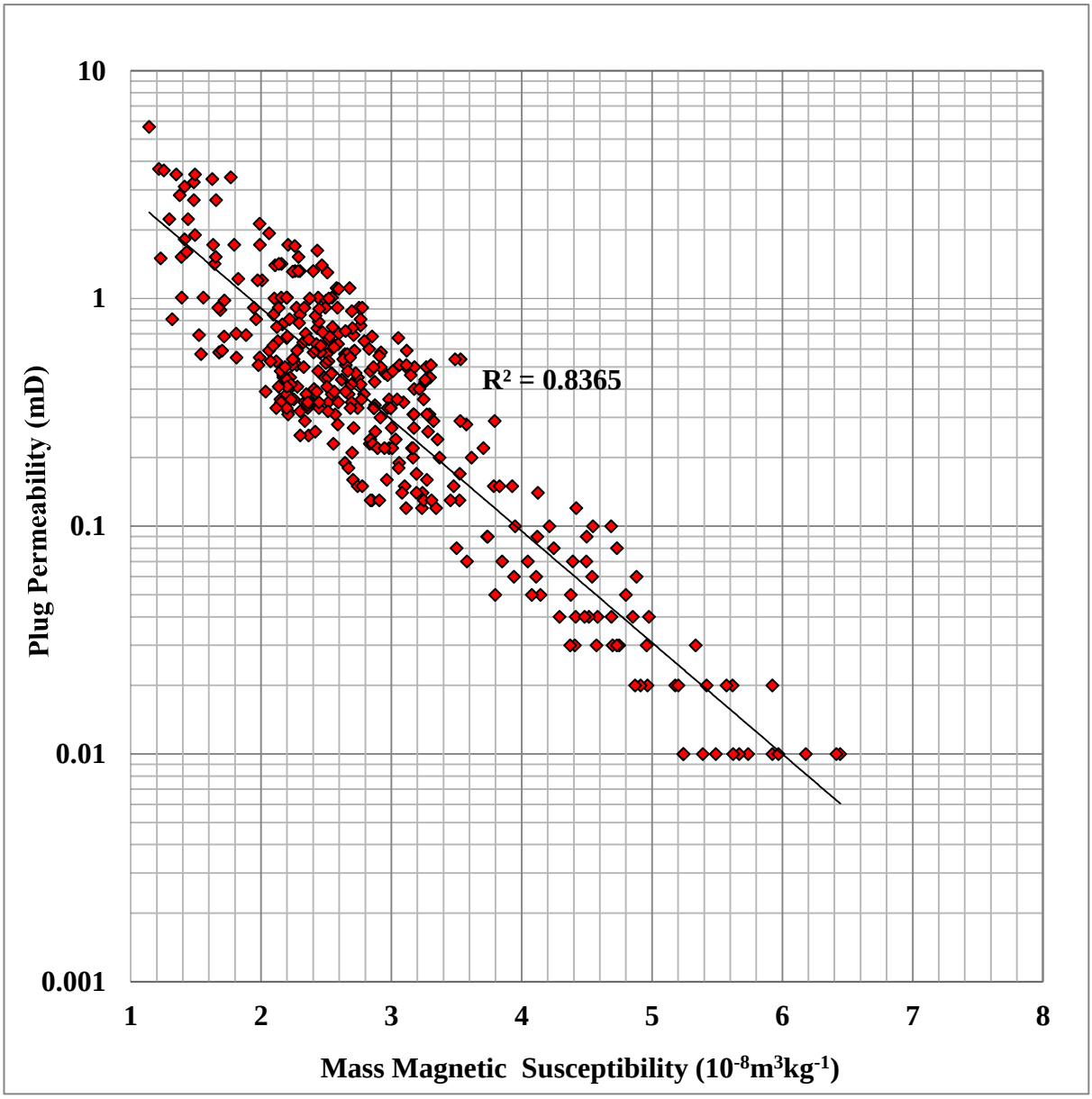

Figure 5-14: Crossplot between mass magnetic susceptibility and permeability of the core plug samples.

5.5 Crossplot between Mass magnetic susceptibility and transit time

In acoustic logging, the sound wave is traveling in the formation .The distance is measuring by calculating the time for sound wave to travel in the formation.(Ezekwe,2010). The μsec/ftis is unit of measuring the interval transit time Δt. The transit time is dependent on the porosity and the lithology of the formation. If the transit time of the formation is known, the porosity can be calculated by using the Wyllie time-average relationship. (Ezekwe, 2010).

$$\Delta t = (1 - \phi)\Delta t_{ma} + \phi \Delta t_f, \tag{5.7}$$

where

Δt_{ma}: matrix transit time,

Δ_{tf} : transit time of the fluid,

Φ : the porosity of the rock.

The interval transit time of various matrix minerals and water are given in Table 5.2. The transit time in dolomite matrix is 43.5 μsec/ft, 47.5 μsec/ft in limestone, and 54 μsec/ft in sandstone, and the interval transit time in fluid is 189 μsec/ft for fresh water.

Table 5.2 shows the transit time and magnetic susceptibility for common rocks and fluids.

Mineral	Volume Magnetic Susceptibility (10^{-5} SI)	Mass Magnetic Susceptibility ($10^{-8} m^3 kg^{-1}$)	Transit time μsec/ft
Quartz	-1.643	-0.62	54
Calcite	-1.3008	-0.48	47.5
Dolomite	-3.444	-1.2	43.5
Fresh Water	-0.9	-0.9	189

Table 5-2: Mass magnetic susceptibility and transit time for some common rocks and fluids.

The crossplot between mass magnetic susceptibility and transit time is shown in Figure 5.15, where different reservoir matrix minerals have been plotted for their varying porosities using Equation 5.7 and the data in Table 5.2. The void space has been assumed to be filled with water. As can be seen on the crossplot, different matrix minerals fall in different regions of the cross plot. This shows the usefulness of the crossplot in helping to identify the type of matrix minerals in the reservoir rock. Figure 5.16 shows the crossplot between volume magnetic susceptibility and transit. Such a crossplot would be particularly useful for a downhole magnetic susceptibility tool, where only the volume magnetic susceptibility information of the formation would be acquired. Once again, different matrix minerals fall in different regions of the crossplot, therefore potentially helping to identify the type of matrix minerals present in the reservoir rock.

As with the mass magnetic susceptibility versus density crossplot, the mass magnetic susceptibility versus transit time crossplot can likewise be used for quantifying minerals, if matrix minerals are present as binary mixtures: for example a mixture of sandstone and limestone, or limestone with dolomite. A simple formula like the one used earlier for the density versus mass magnetic susceptibility crossplot can be applied to calculate the relative proportions of the two matrix minerals.

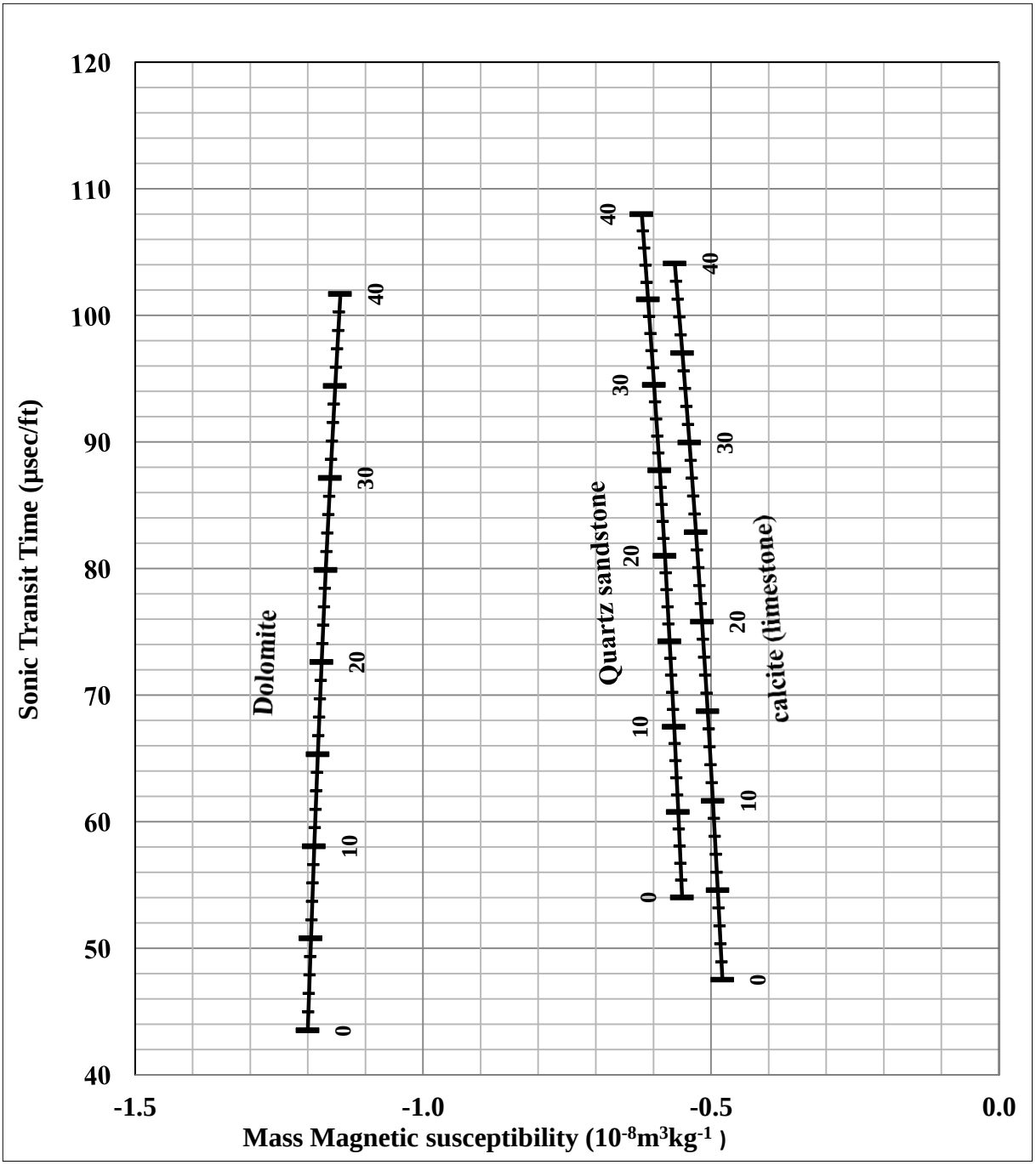

Figure 5-15: Mass magnetic susceptibility versus transit time crossplot, which can be potentially used for identifying lithology and mixture porosity determination in a simple mineral mixture.

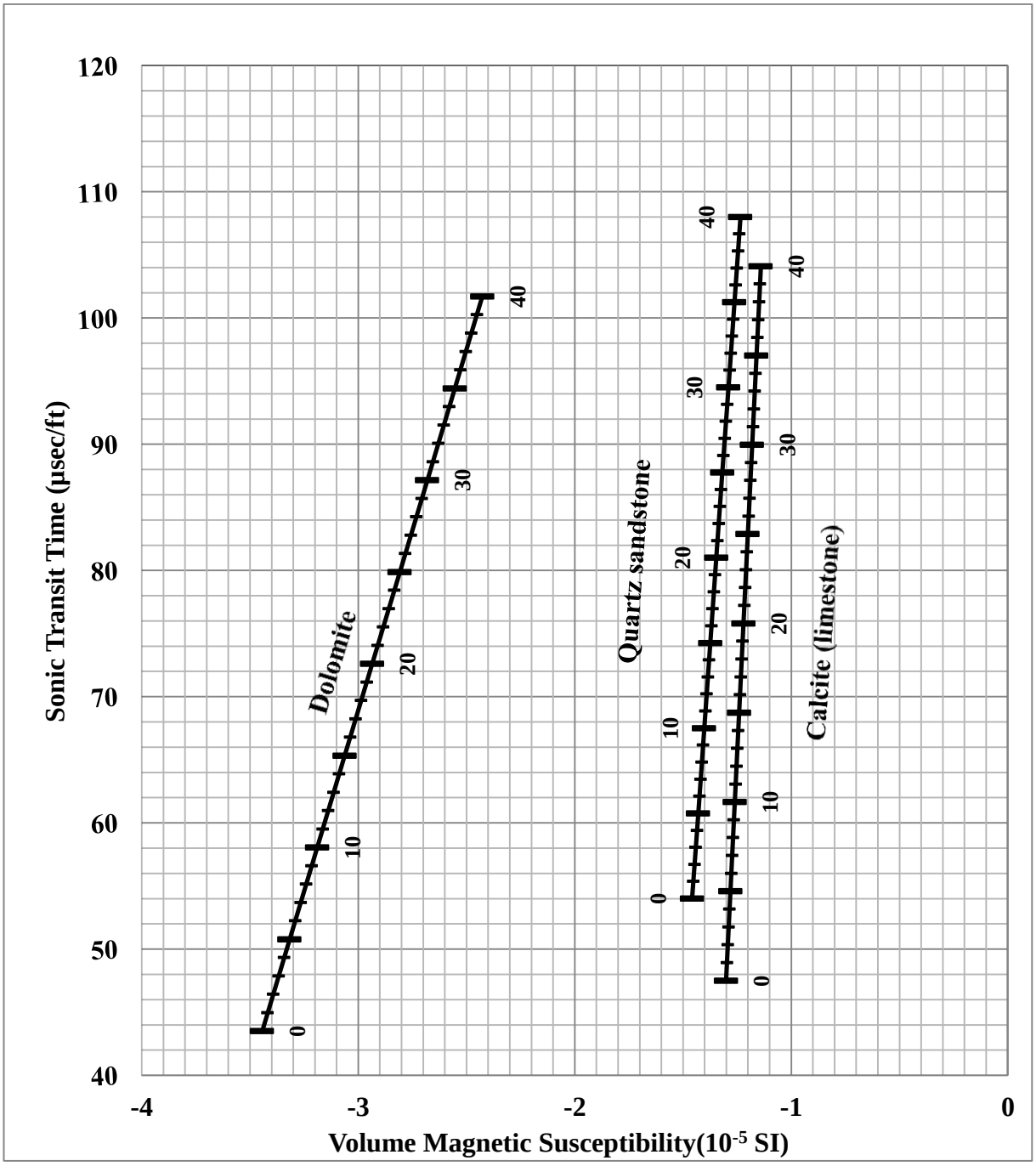

Figure 5-16: Volume magnetic susceptibility versus transit time cross plot.

5.6 Mass Magnetic Susceptibility versus Gamma Ray Cross Plot

The radiation in the rocks created by the gamma ray is due to the presence of the potassium and the isotopes radioactive of two elements of uranium and thorium (PetroWiki. 2013). An indication of the mineralogy and/or geochemistry can be obtained by knowing the concentrations of the three main radioactive elements, potassium, uranium and thorium in the formation (PetroWiki. 2013).

The spectral gamma ray log is a useful log: its usefulness benefits from its high resolution. It can be used to estimate volume and types of clay minerals. The clay minerals are primarily responsible for two sources of radioactivity, potassium, and thorium. Spectral gamma provides directly the amount of potassium and thorium present in the formation. Figure 5-17 shows a number of radioactive minerals as a function of their thorium and potassium contents. Therefore, in the standard cross plot of T versus K concentrations, various predefined windows are marked for these clay minerals. Low potassium (1%) and a moderate value of thorium (10 ppm) defines the montmorillonite area. Similarly, a higher value of potassium (4%) and a higher value of thorium (11ppm) define illite.

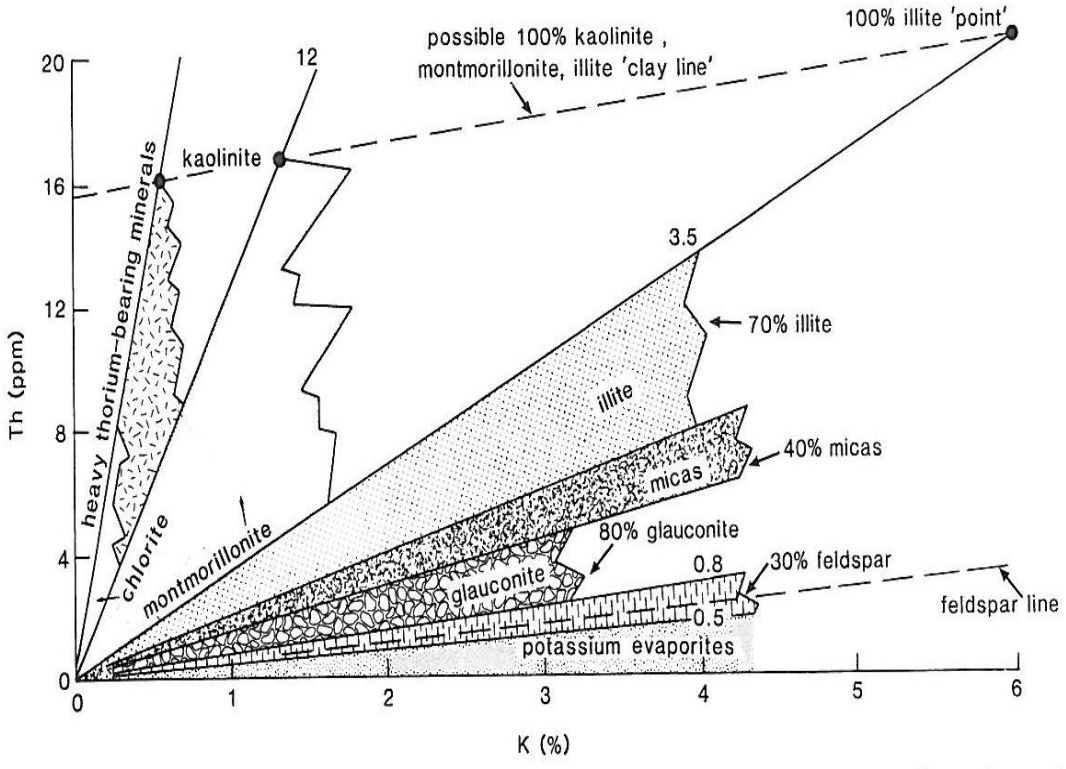

Figure 5-17: Thorium/potassium crossplot for mineral identification, using spectral gamma ray data. (Mohammadlou and Mork, 2012)

Another useful way of distinguishing between different clay minerals is by plotting thorium/potassium ratios versus mass magnetic susceptibility data of the different clay minerals. This is shown in Figure 5.18. Table 5.3 shows the thorium/potassium ratio and the mass magnetic susceptibility values of common clay minerals. The usefulness of this crossplot is that if we have samples containing illite and quartz, all of these samples would fall in the illite region. Likewise, for other clays, samples will fall in the respective clay region. A similar crossplot can be used between thorium/potassium ratios versus volume magnetic susceptibility. Such a crossplot can potentially identify various clay minerals by using log data from gamma rays verses volume magnetic susceptibility.

Minerals	Mass Magnetic Susceptibility ($10^{-8}m^3\ kg^{-1}$)	Th/K ratio
Illite	(15)	(2.6) – (2.9)
Smectite	(3.2)	(3.5) – (12)
Chlorite	(55.5)	(12) – (25)
Feldspar	(-0.49)	(0.3) – (0.6)
Kaolinite	(-2)	(12) – (25)
Biotite	(98)	(0.6) – (2)
Other Montmorillinite	(14)	(3.5) – (12)

Table 5-3: Thorium/potassium ratio and mass magnetic susceptibility values of common minerals.

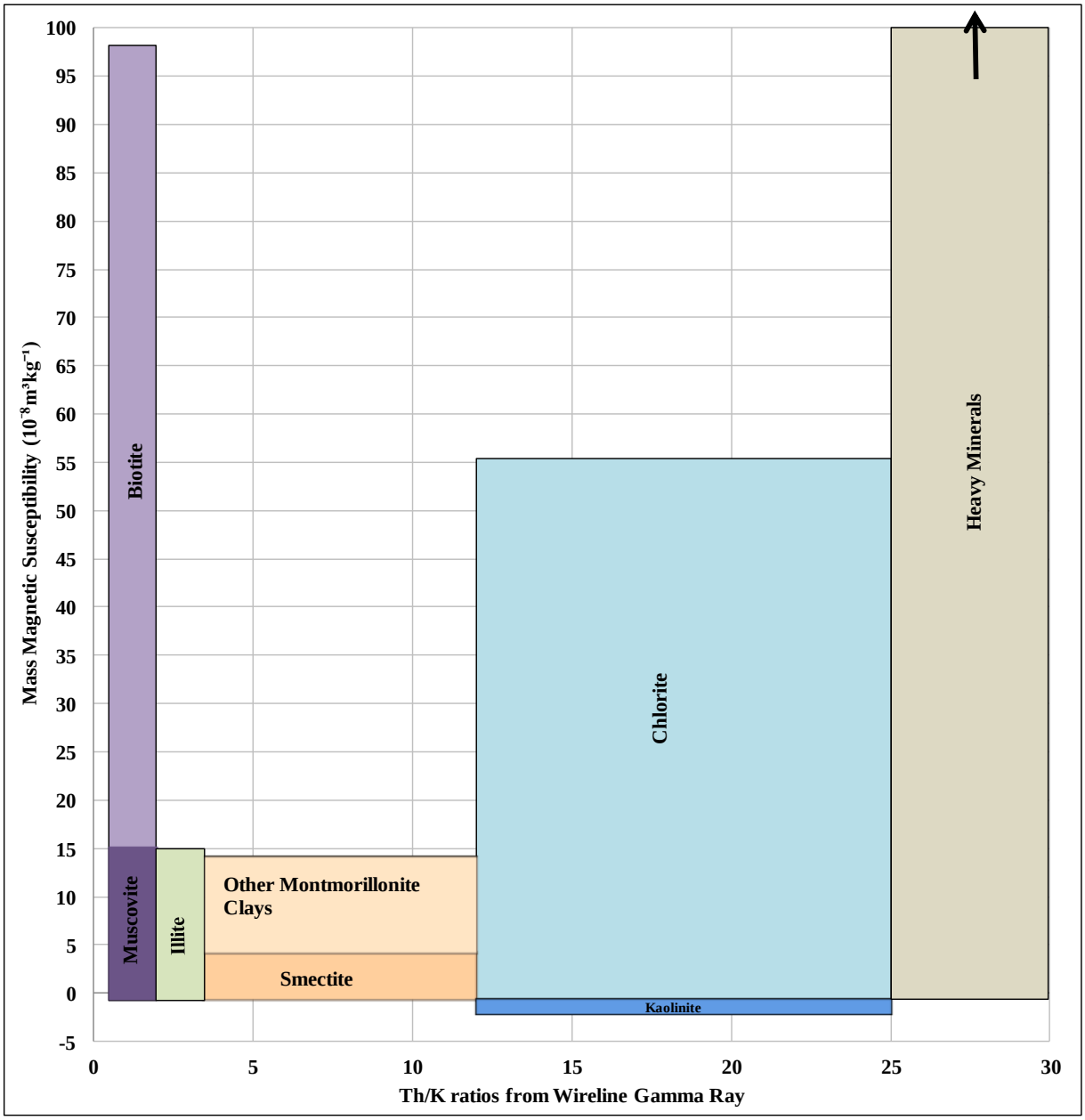

Figure 5-18: Thorium/potassium ratio and mass magnetic susceptibility values of common minerals.

5.7 Conclusions

- The mass magnetic susceptibility versus bulk density crossplot is very sensitive in picking up small variations in the amount of clay in a matrix mineral.

- In red sandstone reservoir samples, the higher the bulk density of the samples, the higher the mass magnetic susceptibility of the samples. This indicates higher hematite content in the samples, thereby resulting in a lower permeability. Magnetic susceptibility, therefore, shows good correlations and can be used in prediction of bulk density, hematite content and permeability, in these reservoirs.

- Magnetic susceptibility measurements can be used to predict permeability on core plugs and slabbed core, using calibration data on a representative set of plug samples.

- The mass magnetic susceptibility versus bulk density crossplot can be used for mineralogy determination, mineral quantification, and for mixture porosity, if more than one matrix mineral is present.

- The mass magnetic susceptibility versus transit time crossplot can be used for quantifying mixture porosity if more than one matrix mineral is present. Such a crossplot is less useful for mineralogy determination or in quantifying minerals, as the different matrix lines are quite close together.

- The crossplot between magnetic susceptibility (volume or mass) versus thorium /potassium ratios can be used to distinguish between different clay minerals.

Chapter 6

Conclusions and Future Recommendations

The main conclusions from this thesis can be summarized as follows:

6.1 Permeability Prediction using Novel Magnetic Techniques

- Magnetic susceptibility measurements undertaken on core samples from a relatively tight gas sandstone reservoir in the North Sea correlated well with permeability.

- Work presented in this thesis shows that samples with higher hematite content (1-3%) exhibited significantly lower permeabilities than samples with extremely low hematite content (less than 1%). In the samples with higher hematite content, thin section analysis revealed thin (approximately 10-15μm) rims of hematite cement surrounding quartz grains and blocking pore connections. This suggests that grain lining hematite cement is a major control on permeability in this reservoir.

- Magnetic hysteresis parameters plotted on a Day plot showed that permeability is independent of hematite particle size, for the samples in the reservoir studied. It therefore appears that the presence of the grain lining hematite cement rims (rather than the hematite particle size) is the main factor in reducing the permeability.

- Magnetic hysteresis measurements revealed the presence of hematite, paramagnetic clays, and a ferrimagnetic mineral (identified as magnetite from Curie temperature analysis) in the core samples. The measurements showed that all of the representative samples (with low and high hematite content) had a similar high field magnetic hysteresis slope, suggesting similar paramagnetic clay content. Samples with higher hematite content had lower permeability values. This further suggests that hematite cement is a major control on permeability in these samples.

- The magnetic results have important applications for the prediction of permeability in similar red samples in the North Sea. In addition, they may provide a direct link between permeability and the depositional system of hematite cement, thereby connecting the geology.

- The mass magnetic susceptibility versus bulk density cross plot is very sensitive in picking up small variations in the amount of clay in a matrix mineral.

- In red sandstone reservoir samples, the higher the bulk density of the samples, the higher the mass magnetic susceptibility of the samples. This indicates higher hematite content in the samples, resulting in a lower permeability. Magnetic susceptibility, therefore, shows good correlations and can be used in prediction of bulk density, hematite content and permeability in these reservoirs.

6.2 Detection of Faults and Fluid Contacts

- Raw magnetic susceptibility measurements performed on drill cuttings show their potential use to detect faults and fluid contacts in sedimentary sequences. Such measurements can be performed at well site, thereby enabling companies to make important field development decisions quickly. They can also be used onshore to help interpret data from other laboratory based core analysis techniques such as SEM and EDAX.

- Histograms of the conventional wireline log data showed a very similar distribution above and below the fault zone as well as in the gas water contact. However histograms of magnetic susceptibility data showed clear differences for the various zones, showing the potential usefulness of the magnetic susceptibility data.

- Magnetic hysteresis measurements performed on drill cuttings above the fault zone indicated the presence of hematite mineral (evident by a large open kink at low applied fields and which extends to high applied fields). For drill cuttings in the fault zone, the magnetic hysteresis measurements showed the presence of magnetite (evident by a much bigger kink at low applied fields and which does not extend to high applied fields). This shows the potential usefulness of magnetic hysteresis measurements to help identify ferromagnetic and antiferromagnetic minerals in the drill cuttings and which, in this particular case, is related to the zones above and at the fault.

- The differences in the hysteresis measurements (which essentially relate to the differences in the magnetic mineralogy present in the samples of drill cuttings)

related to the gas water contact. The samples of drill cuttings above the gas water contact showed different hysteresis curves (representative of hematite) to those below the gas water contact (representative of magnetite). Such magnetic susceptibility measurements have therefore the potential to identify fluid contacts in certain reservoirs.

6.3 Novel Crossplots

- Magnetic susceptibility measurements can be used to predict permeability on core plugs and slabbed core using calibration data on a representative set of plug samples.

- The mass magnetic susceptibility versus bulk density crossplot can be used for mineralogy determination, mineral quantification, and for mixture porosity, if more than one matrix mineral is present.

- The mass magnetic susceptibility versus transit time crossplot can be used for quantifying mixture porosity, if more than one matrix mineral is present. Such a crossplot is less useful for mineralogy determination or in quantifying minerals, as the different matrix lines are quite close together.

- The cross plot between magnetic susceptibility (volume or mass) versus thorium/potassium ratios can be used to distinguish between different clay minerals.

6.4 Future Recommendations

- In this work, magnetic susceptibility measurements have shown good correlation with permeability in a relatively tight gas sandstone reservoir in the North Sea. Hematite was coating the quartz grains and which was controlling permeability. It would be good to extend this study to other conventional and tight reservoirs to see if a similar correlation exists where other minerals (apart from hematite and typical permeability controlling clays) are controlling permeability.

- Extensive thin section analysis should be carried out to validate whether grain lining hematite is the key permeability controlling factor. Due to shortage of time, thin section analysis only performed on a handful of representative samples.

- These results show that all of the representative samples (with low and high hematite content) had a similar high field magnetic hysteresis slope, suggesting similar paramagnetic clay content in the samples. Further research is needed to establish the effect of these clays on permeability in these reservoir rock samples. Although hematite seems to exert major control, nevertheless, clays would have some impact too. The research in this thesis is unable to quantify this effect.

- In this work, the magnetic susceptibility measurements on drill cuttings seem to help in detection of the fault and gas/water contact in hydrocarbon bearing reservoir rocks. However, this is the first time the results of this kind were obtained. This application of magnetic susceptibility on drill cuttings needs to be analysed in more detail. For example, if the faults do not contain any magnetic minerals, how would the technique in this thesis help in the detection of faults? The same is true for fluid contacts.

- It was shown that magnetic susceptibility measurements can be used to predict permeability on core plugs and slabbed core using calibration data on a representative set of plug samples. This seems to be true if some sort of magnetic minerals are controlling permeability. How about if diamagnetic minerals like quartz overgrowth cements and siltstones are controlling permeability? The application of magnetic susceptibility on such reservoir rock samples needs careful study.

- Data from a variety of reservoir rocks carrying different mineralogies needs to be plotted on the various crossplots, in order to check the usefulness and effectiveness of the information acquired from the crossplots.

References

- Abd_Elmoula.I.A., Al-Hasani.S.A and Al-Jahwari.S.S. 2010.“Fluid Contact Determination in Tight Gas Reservoirs; Formation "B"Case Study”. Deep Gas Conference and Exhibition, 24-26 January, Manama, Bahrain, 179-180.

- Ahmed .M., Harb. M. . 2013. “Use of Accoustic Televiewer in Discontinuity Characterisation for Rock Slopes and Under Ground Excavations - A Case Study” Second International Conference on Engineering Geophysics.

- Alger, R. P., Raymer,L. L., Hoyle, W. R., and Tixier, M. P., 1963. “Formation Density Log Applications in Liquid Filled Holes”: *Journal of Petroleum Technology*, 15 (3), 321-332.

- Ali, A. and Potter, D. K. 2011a. Model Templates For Quantifying Permeability Controlling Paramagnetic Clay Minerals At In Situ Reservoir Temperatures: 2011 International Symposium of the Society of Core Analysts**,** Austin, Texas, USA, Paper SCA2011-47.

- Ali, A. and Potter, D. K. 2011b. “Thermomagnetic Analyses of the Permeability Controlling Minerals in Red and White Sandstones in Deep Tight Gas Reservoirs: Implications for Downhole Measurements”. *SPE Reservoir Evaluation and Engineering,* 14(5), 557-565.

- Ali, A. and Potter, D. K. 2012. Temperature Dependence of The Magnetic Properties Of Reservoir Rocks And Minerals and Implications For In Situ Borehole Predictions Of Petrophysical Parameters. Geophysics 77 (3): WA211-WA221.

- Ali, A., 2009. “System Modelling and Testing Of A Magnetic Susceptibility Device and Effect of Downhole In-Situ Temperatures on Magnetic Susceptibility.” PhD thesis, Heriot-Watt University, Institute of Petroleum Engineering, Edinburgh, UK.

- Alford, J., M. Blyth, E. Tollefsen, J. Crowe, J. Loreto, S. Mohammed, V. Pistre, and A. Rodriguez-Herrera, 2012, “Sonic logging while drilling — Shear answers, Oilfield Review”, 24, 4-15.

- Archie, G.E. 1950. "Introduction to Petrophysics of Reservoir Rocks". Bulletin of the American Association of Petroleum Engineering Geologists. 34 (5), 943-961.

- Argyle, K. S. and Dunlop, D. J., 1984. "Theoretical Domain Structure in Multidomain Magnetite Particles". Geophysical Research Letters. 11, 185-188.

- Argyle, K. S. and Dunlop, D. J., 1990. "Low-Temperature and High-Temperature Hysteresis of Small Multidomain Magnetites (215–540 nm)", J. Geophys. Res., 95(B5), 7069–7082.

- Assam, A., Basin, A., Nagar, G and Pradesh, A., 2004. "Detection of Structural Elements Using Borehole Imagery Techniques", 5th Conference and Exposition on Petroleum Geophysics, Hyderabad, India 135-139 pp.

- Bear. J, Fand.T and Marsily G., 1993, "Flow and Contaminant Transport in Fractured Rock". California, USA.

- Bagin, V. I., Ismail-zade, T. A., Malumyan, L. M., Pecherskiy, D. M., 1973. Magnetic studies of the sedimentary rocks of the productive formation in Azerbaijan. [Russian] [Magnitnye issledovaniya osadochnykh porod produktivnoy tolshchi Azerbaijana]. Proceedings of the IX conference: Problems of permanent geomagnetic field, magnetism of rocks and paleomagnetism. Part 2. Baku.

- Bagin, V. I., Malumyan, L. M., 1976. Iron-containing minerals in oil-impregnated sedimentary rocks from a producing rock mass of Azerbaidzhan. Translated from Russian by Georgia Moritz. Izvestiya Akademii Nauk SSSR. Fizika Zemli, 4, 273-277.

- Banerjee, S. K., 1971. "New Grain Size Limits For Palaeomagnetic Stability in Hematite". Nature, 232, 15-16.

- Barton, C., Zoback, M. D., and Burns,K, 1988. "In-Situ Stress Orientation and Magnitude at the Fenton Hill Geothermal Site, New Mexico, Determined from Wellbore Breakouts". Geophysical Research Letters, 5 (15), 467-470.

- Bijaksana.S., Zulaikah.S., and Hodych. J.P., 2009. "Magnetic Anisotropy and the Paleosecular Variation Record in Stalagmites from Njirak Cave, East Java: The Effect of Detrital Magnetite Emplaced in Small Cavities by Flooding Events" *Indonesian Journal of Physics*, 3 (20), 61-69.

- Brown, F., William and Jr., 1958. "Rigorous Approach to the Theory of Ferromagnetic Microstructure" *Journal of Applied Physics*, 29,470-471

- Bruno, M.S., and Nelson, R.B., 1991. "Microstructural Analysis of the Inelastic Behaviour of Sedimentary Rock", Mechanics of Materials, 2 (12), 95-118.

- Cassidy, J., 1981. "Techniques of Field Gamma-Ray Spectrometry" Mineralogical Magazine. 44, 391-398.

- Cavanough, G. L.,Holtham, P. N., 2001. Online measurement of magnetic susceptibility in titanium minerals processing.The AusIMM Proceedings 306 (2),1-6.

- Cavanough, G. L., Holtham, P. N., 2004. Rapid characterisation of magnetic separator feed stocks in titanium minerals processing. Physical Separation in Science and Engineering 13(3–4), Taylor & Francis, 141–152.

- Chevallier, R. and Mathieu, S., 1943. "Proprietes Magnetiques des Poudres d'hematite – Influence Des Dimensions Des Grains". Annales Phys. 18, 258-288.

- Cioppa, M. T., Al-Aasm, I. S., Symons, D. T. A., 2001. Paleomagnetic dating of diagenetic events in Paleozoic carbonate reservoirs of the Western Canada Sedimentary Basin. Conference of Rock the Foundation Convention, 18-22.

- Cogoini, M., 1998. "Determining the Origin of Soil Magnetic Susceptibility Anomalies in Hydrocarbon Environments". *AAPG Bulletin* 11, 2160-2161.

- Cogoini, M., 2001. "Investigation the Role of Microbial Versus Chemical Processes In magnetic Mineral Formation of Soils". The IRM Quarterly, 11 (12), 6-7.

- Collier. H, and Ridder. M., 1992. Utilization of the Borehole Televiewer in Fracture Analysis.

- Cooke-Yarborough, P., 1984. "A Review of Well Log Interpretation Techniques for Carbonate Reservoirs of South-East Asia". 5th Offshore South East Asia 21-24 February 1984, Singapore.

- Cooke, M. P., De Sa, A., 1981. A radio frequency method for the measurement of initial magnetic susceptibility, J. Phys. E: Sci. Instrum. 14 1192–1195.

- Costanzo-Alvarez, V., Aldana, M., Aristeguieta, O., Marcano, M. C., Aconcha, E., 2000. Study of magnetic contrasts in the Guafita oil field (South-Western Venezuela). Physics and Chemistry of the Earth, Part A-Solid Earth and Geodesy, 25 (5), 437-445.

- Crisan, O. and Crisan, A.D., 2011, "Phase transformation and Exchange bias Effects In Mechanically Alloyed Fe/Magnetite Powders". *Journal of Alloys and Compounds*, 23 (509), 6522–6527.

- Cornet, J. 2013 "Fracture detection and analysis from image log raw data". MSc thesis, Norwegian University of Science and Technology, Department of Petroleum Engineering and Applied Geophysics.

- Darling,T.,2005,"Well Logging and Formation Evaluation". Gulf Professional,USA.144 pp

- Day, R., Fuller, M. D. and Schmidt, V. A., 1977. "Hysteresis Properties of Titanomagnetites: Grain Size and Composition Dependence". Physics of the Earth and Planetary Interiors, 13, 260-267.

- Dearing, J. A., 1999. "Environmental magnetic susceptibility using the Bartington MS2 system".

- Dearing, J.A., Bird, P.M., Dann, R.J.L. and Benjamin, S.F., 1997. "Secondary Ferromagnetic Minerals in Welsh Soils: A Comparison of Mineral Magnetic Detection Methods and Implications For Mineral Formation". Geophysical Journal International, 130, 727-736.

- Dearing, J.A., Dann, R.J.L., Hay, K., Lees, J.A., Loveland, P.J., Maher, B.B. and O'Grady, K, 1996a. "Frequency-Dependent Susceptibility Measurements of Environmental Materials". Geophysical Journal International, 124, 228-240.

- Dearing, J.A., Hay, K. L., Baban, S.M. J., Huddleston, A.S., Wellington, K. M.H. and Loveland, P. J., 1996b. Magnetic susceptibility of soil: An evaluation of conflicting theories using a national data set. Geophysical Journal International, 127: 728-734.

- Dearing, J.A., Morton, R.I., Price, T.W. and Foster, I.D.L., 1986. "Tracing Movements of Topsoil by Magnetic Measurements: Two Case Studies". Physics of the Earth and Planetary Interiors, 42, 93-104.
- Deer, W.A., Howie, R.A., Zussman, J., 1992. "An Introduction to The Rock Forming Minerals", 2nd Ed. Longman Group UK Limited.

- DI, K., 2008. "Borehole Imaging (Borehole Imaging Technology)" [Online]. Available:http://petroleumcrudeoil.blogspot.co.uk/2008/11/borehole-imaging-borehole-imaging.html.

- Donovan, T. J., Forgey, R. L. and Roberts, A. A., 1979. "Aeromagnetic Detection of Diagenetic Magnetite over Oil Fields". AAPG Bulletin, 63, 245-248.

- Drobace, D., Maronic, Z., 1999. Multipurpose measuring device based on AC susceptometer, Fizika A (Zagreb) 8 165–172.

- Dunlop, D. J., 1973a. "Superparamagnetic and Single-Domain Threshold Sizes in Magnetite". *Journal of Geophysical Research*, 78, 1780-1793.

- Dunlop, D. J., 1973b. "Thermoremanent Magnetization in Submicroscopic Magnetite". *Journal of Geophysical Research*, 78, 7602-7613.

- Dunlop, D. J., 1981. "The Rock-Magnetism of Fine Particles". Physics of the Earth and Planetary Interiors 26, 1–26.

- Dunlop, D. J., 2002. "Theory and Application of the Day Plot (Mrs/Ms versus Hcr/Hc). Application to Data for Rocks, Sediments, and Soils". Journal of Geophysical Research, 107 (B3) doi: 10.1029/2001JB000486.

- Dunlop, D. J., 2002a. "Theory and Application Of The Day Plot (Mrs/Ms versus Hcr/Hc). 1. Theoretical Curves and Tests Using Titanomagnetite Data*". Journal of Geophysical Research*, 107 (B3), 4-1 – 4-22.

- Dunlop, D. J., 2002b. "Theory and Application Of The Day Plot (Mrs/Ms Versus Hcr/Hc). 2. Application to Data for Rocks, Sediments, and Soils". *Journal of Geophysical Research*, 107 (B3), 5-1 – 5-15.

- Dunlop, D. J., and Zdemir, O¨. (1997), Rock Magnetism, 573 pp., New York: Cambridge Univ. Press.

- Dunlop, D. J., and B. Carter-Stiglitz (2006), Day Plots of Mixtures of Superparamagnetic, Single-Domain, Pseudosingledomain, and Multidomain Magnetites, *J. Geophys. Res*., 111, B12S09, doi:10.1029/2006JB004499.

- Dunlop, D. J. and Bina, M. M., 1977. "The Coercive Force Spectrum of Magnetite at High Temperatures: Evidence for Thermal Activation below the Blocking Temperature". *Geophysical Journal of the Royal Astronomical Society*, 51, 121-147.

- Dunlop, D. J., Ozdemir, O., 1997. "Rock Magnetism: Fundamentals and Frontiers". Cambridge, Cambridge University Press, 573 pp.

- EPA, 2000, "Development Document for Final Effluent Limitations Guidelines and Standards for Synthetic-Based Drilling Fluids and other Non-Aqueous Drilling Fluids in the Oil and Gas Extraction Point Source Category," EPA-821-B-00-013, U.S.

- Evans, B., 2006. "Magnetic Characteristics of Carboniferous Continental Depositional Systems: Implications for the Recognition of Depositional Hiatuses" MSc Thesis, Polytechnic Institute and State University, Virginia, USA.

- Evans, M., and Heller.F ., 2003. "Environmental magnetism principles and applications of enviromagnetics". Academic Press Inc (USA). 299pp.

- Eventov, L., 1997. Application of magnetic methods in oil and gas exploration. The Leading Edge, 16 (5), 489-492.

- Eventov, L., 2000. The nature and interpretation of geophysical and geochemical anomalies over oil and gas fields. The Leading Edge, 19 (5), 488-490.

- Ezekwe, N., 2010. "Petroleum Reservoir Engineering Practice: Porosity of Reservoir Rocks". Prentice Hall. United State of America.pp5.

- Ferguson, T. D., 1979, "The Subsurface Alteration And Mineralization Of Permian Red Beds Overlying Several Oil Fields In Southern Oklahoma", Part II. *Oklahoma City Geological Society*", 29, 200–210.

- Filippycheva, L. G., Burakov, A. I., Bogdanovich, A. I., Belyaev, I. P., Gutner, A. B., 2001. Downhole magnetic stratigraphy in solving problems of correlation of heterofacial strata, sequence-stratigraphy for oil fields modelling, technology of operations, instrumentation [CD Rom]. EAGE 63th Conference and Technical Exhibition, Amsterdam, 11-15 June, 643 pp.

- Flaum, C., 1990. "Enhancing Geochemical Interpretation Using High Vertical Resolution Data". IEEE Transactions on Nuclear Science**,** 2 (37), 948-953.

- Foner, S. and McNiff E. J. Jr., 1968. "Very Low Frequency Integrating Vibrating Sample Magnetometer (VLFVSM) With High Differential Sensitivity in High Dc Fields", *Rev. Sci. Instrum.* 39, 171–179.

- Fukuma, K. and Torii, M.,1997,"Variable Shape of Magnetic Hysteresis Loops in the Chinese Loess-Paleosol Sequence".*Earth Planets Space,*50,1-9.

- Fuller, D., 1987."Classes of Magnetic Materials" [Online]. Available: http://www.irm.umn.edu/hg2m/hg2m_b/hg2m_b.html

- Gillen, K. P., Van der Voo, R., Thiessen, J. H., 1999. Late Cretaceous-early Tertiary remagnetization of the Devonian Swan Hills Formation recorded in carbonate cores from the Caroline gas field, Alberta, Canada. AAPG Bulletin, 83 (8), 1223-1235.

- Gleizes, G., Nedelec, A., and Bouchez, J., 1993, "Magnetic Susceptibility of the Mont-Louis Andorra Ilmentite-Type Granite (Pyrenees): A New Tool for the Petrographicb Characterization and regional mapping of Zoned Granite Plutons". *Journal of Geophysical Research*, 98, 4317-4331.

- Glover, P., (2013). "Petrophysics MSc Course Notes" Formation Density Log. Available:http://homepages.see.leeds.ac.uk/~earpwjg/PG_EN/CD%20Contents/GGL66565%20Petrophysics%20English/Chapter%2013.

- Gubbins, D, and Herrero-Bervera, E, 2007. "Encyclopedia of Geomagnetism and Paleomagnetism". Springer. UK.

- Hall, S. A., Evans, I., 1995. Paleomagnetic and magnetic properties of hydrocarbon reservoir from the Permian basin, southeastern New Mexico, USA. In: P. Turner and A. Turner, eds. Paleomagnetic application in hydrocarbon exploration and production. Geological Society Special Publication 98, London, 79-95.

- Hearst, J.R., Nelson, P.H. and Paillet, F.L., 2000. "Well Logging for Physical Properties". 2nd edition, New York, John Wiley and Sons, Ltd., 483 pp.

- Hill, R. W., 1982. "Advanced Student Experiments in Paramagnetism and Antiferromagnetism", *Eur. J. Phys*., 3, 75-79.

- Hill, R., 1963. "Elastic Properties of Reinforced Solids: Some Theoretical Principles", *J. Mech. Physics. Solids*, 11, 357-372.

- Hodych, J. and Bijaksana, S., 2002, "Plastically Deforming Clay-Rich Sediment to Help Measure the Average Remanence Anisotropy of Its Individual Magnetic Particles, and Correct for Paleomagnetic Inclination Shallowing". *Physics and chemistry of the earth*, 27, 1237-1279.

- Hrouda, F., 1973. "A Determination of the Symmetry of the Ferromagnetic Mineral Fabric in Rocks on The Basis of the Magnetic Susceptibility Anisotropy Measurements". *Gerl. Beitr. Geophys*., 82, 390-396.

- Hrouda, F., 1994. "A Technique for the Measurement of Thermal Changes of Magnetic Susceptibility of Weakly Magnetic Rocks by the CS-2 Apparatus and KLY- Kappabridge". *Geophys. J. Int.*, 118, 604-612.

- Hrouda, F., 2002." Low-Field Variation of Magnetic Susceptibility and Its Effect on the Anisotropy of Magnetic Susceptibility of Rocks". *Geophys. J. Int.*,150, 1-9.

- Hrouda, F., 2003. "Indices for Numerical Characterization of the Alteration Processes of Magnetic Minerals Taking Place during Investigation of Temperature Variation of Magnetic Susceptibility". *Stud. Geophys. Geod.*, 47, 847-861.

- http://geology.about.com/library/bl/blnutshell_fault-type.htm

- http://science.jrank.org/pages/4083/Magnetism-Types.

- http://science.jrank.org/pages/4083/Magnetism-Types-magnetism.html

- http://science.jrank.org/pages/4083/Magnetism-Types-magnetism.html">Magnetism - Types of Magnetism

- Hunt, C. P., Moskowitz, B. M., Banerjee, S. K, 1995. Rock physics and phase relations: a handbook of physical constants. AGU Reference Shelf 3. Magnetic Properties of Rocks and Minerals, 189-204.

- Ivakhnenko, O. P. 2006. "Magnetic Analysis of Petroleum Reservoir Fluids, Matrix Mineral Assemblages and Fluid-Rock Interactions". Ph.D. thesis, Heriot-Watt University, Edinburgh, UK.
- Ivakhnenko, O. P. and Potter, D. K. 2008. "The Use of Magnetic Hysteresis and Remanence Measurements for Rapidly and Non-Destructively Characterizing Reservoir Rocks and Fluids". *Petrophysics* 49 (1): 47-56.

- Ivakhnenko, O.P. and Potter, D.K., 2004, Magnetic Susceptibility of Petroleum Reservoir Fluids". *Physics and Chemistry of the Earth*, 29 (2004), pp. 899-907.

- Ivakhnenko, O.P. and Potter, D.K., 2006. The Use of Magnetic Hysteresis and Remanence Measurements in Rapidly and Non-destructively Characterising Reservoir Rocks and Fluids". Society of Core Analysts Held In Trondheim, Norway 12-16.

- Ivakhnenko, O.P. and Potter, D.K., 2008. "The Use of Magnetic Hysteresis and Remanence Measurements for Rapidly and Non-Destructively Characterizing Reservoir Rocks and Fluids". *Journal of Petrophysics*, 49 (1), 47-56.

- Jiang, S., 2012. "Clay Minerals from the Perspective of Oil and Gas Exploration" China. Advances in Petroleum Exploration and Development, 2, (2), 1-11.

- Kailas, S., 2008. Matrial Siience: Chapter16. Magnetic properties.pp1-2.

- Keller, G.V., 1981. Exploration for Geothermal Energy. In: Fitch, A.A. (Ed.),Developments in Geophysical Exploration. Methods – 2. Applied Science Pub., pp. 107-150.

- Killeen, P.G. 1997. "Borehole Geophysics Exploring the Third Dimension", Fourth Decennial International Conference on Mineral Exploration" *edited by* A.G. Gubins, Ottawa, Ontario, Canada 31-42.

- Kittel, C., 1949. "Physical Theory of Ferromagnetic Domains". *Reviews of Modern Physics*, 21 (4), 541–583.

- Kirkland,K., 2007. "Electricity and Magnetism". New York . pp19.

- Kittel, C., 1996. "Introduction to Solid State Physics", 7th edition, John Wiley.

- Klimentos, T.,Farghaly, A. and Qleibo, M.,2003. "Finding Faults with Shear-Wave Anisotropy".44th *Annual logging symposium*, 22-25 June 2003.

- Labo, J., 1987. "A Practical Introduction to Borehole Geophysics: An Overview of Wireline Well Logging Principles for Geophysicists" Society of Exploration Geophysicists.330pp.

- Leroy, and J.W. Raese, editors, 1977, "Subsurface Geology", Colorado School of Mines, Golden, 941 pp.

- Li, B., Al-Awadi, M., Perrin, C., Al-Khabbaz, M., Al-Ashwak, S., and Al-Qadeeri, B, 2009 ,"Fracture and Sub-Seismic Fault Characterization for Tight Carbonates in Challenging Oil-Based Mud Environment – Case study From North Kuwait Jurassic Reservoirs".

- Lin, W., Yeh, E., Hung, J., Haimson, B. and Hirono, T.,2010, "Localized rotation of Principal Stress around faults and Fractures determined from Borehole Breakouts in Hole B of the Taiwan Chelungpu-Fault Drilling Project (TCDP)", *Tectonophysics, 482,82-90.*
- Liu, Q. S. and Liu, S. G., 1999. "Magnetic and Mineralogical Characteristics of Reservoir Rocks in the Yakela Oil Field, Northern Tarim Basin and Their Implications for Magnetic Detection of Oil and Gas Accumulations". *Chinese Science Bulletin,* 44 (2), 174-177.

- Liu, Q. S., Xu, W. K., Deing, S. F., Wang, X. F., 1996. "A Study for Relationship between Hydrocarbon Migration and Soil Magnetism above Oil and Gas Fields in China". *Acta Geophysica Sinica*, 39 (6), 804-812.

- Liu, Q., Banerjee, S. K., Jackson, M. J., Zhu, R., Pan, Y., 2002. "Effects of Low Temperature Oxidation on Natural Remanent Magnetization of Chinese Loess". *Chinese Science Bulletin*, 47 (24), 2100-2105.

- Loi, D,. Mazzoni. S,. Gigliotti. M,. Baio. C,. Borghi, M,. Baldini.D,. Italiano, F., and Cantini, S., 2011. "Unlocking Thin Beds Potential: Gas Identification Through Downhole Fluid Analysis" Canadian Unconventional Resources Conference. Alberta, Canada, 148967, 29-30.

- Lu, G,. McCabe C, Henry, D. J. and Schedl, A. 1994. "Origin of Hematite Carrying A Late Paleozoic Remagnetization in A Quartz Sandstone Bed From the Silurian Rose Hill Formation", Virginia, USA. *Earth and Planetary Science Letters 126*: 235-246.

- Lupini, J.F., Skinner, A.E., and Vaughan, P.R., 1981. "The Drained Residual Strength of Cohesive Soils". *Geotechnique,* 213, 31-181.

- Martın-Hernandez, F., and . Ferre. E. C., 2007, "Separation of paramagnetic and ferrimagnetic anisotropies: A review, J. Geophys. Res"., 112, B03105, doi:10.1029/2006JB004340.

- Matthews, A., 1976. "Magnetite Formation by the Reduction of Hematite with Iron under Hydrothermal Conditions". American Mineralogist, 61, 927-932.

- McBride, E.F., 1989. "Quartz Cement in sandstones: a review", *Earth science reviews,* 26, 69-112.

- Mohammadlou. M. and Mørk. M. B., 2012. "How Log Interpreter Uses SEM Data for Clay Volume Calculation, Scanning Electron Microscopy".

- Monier-Williams, M.E., Davis, R.K., Paillet, F.L. Turpening, R.M., Sol S.J.Y. and Schneider, G.W., 2009. "Review of Borehole Based Geophysical Site Evaluation Tools and Techniques". Golder Associates, University of Arkansas and Michigan Technical University.

- Morrow, C., Radney, B., and Byerlee, J., 1992. "Fault Mechanics and Transport Properties of Rocks". Academic Press, San Diego.523.

- Moll, W.F, 2001, "Baseline studies of the clay minerals society source clays: Geological origin. Clays and Clay Minerals". 49, 374–380.

- Moskowitz, B. M., 1991, Hitchhiker's Guide to Magnetism, Environmental Magnetism Workshop, pp. 1–38, Minneapolis, The Institute for Rock Magnetism and the Global Paleorecords Research Training Group.

- Nagata, T., 1940. *Bull. Earthquake Res. Inst*., vol. 18, p. l02.

- Neff, T.M., 1987. "Biological Effects of Drilling Fluids, Drill Cutting and Produce Waters". Pages 469-480. In: D.F. Boesh and N.N. Rabalais, Eds., Long- Term effects of offshore oil and gas development. London, Elsevier Applied Science Publishers.

- Nelson, P.H. 1994, "Permeability- Porosity Relationships in Sedimentary Rocks". *The log analyst*, 35 (3): (38-61).

- Pabortsava. K., Purse .A., Wagner. H., and Thomsen. L., 2011, "The Influence of Drill Cuttings on Physical Characteristics of Phytodetritus". *Marine Pollution Bulletin*, 62, (10), 2170-2180.

- Perez, A, L. D'Onofrio, M. Bosch, and E. Zapata., 2011. "Association between magnetic susceptibilities and hydrocarbon deposits in the Barinas-Apure Basin, Venezuela". Journal of Geophysics, 76, 35-41.

- Petrovský, E., Kapicka, A., Jordanova, N., Knab., and M,Hoffmann V.,1998. "Low-field magnetic susceptibility: a proxy method of estimating increased pollution of different environmental systems". Environmental Geology.

- Petrowiki., 2013. "Gamma ray logs" .SPE. Available: http://petrowiki.org/Gamma_ray_logs.

- Philip. H. and Nelson. 1993. "Magnetic Susceptibility Logs from Sedimentary and Volcanic Environments". SPWLA 34th Annual Logging Symposium, 13-16 June 1993, Calgary, Alberta .

- Pitman, E.D. and Larese, R.E., 1991. "Impaction of lithic Sands: Experimental Results and Application" American association of Petroleum Geologist Bulletin, 75 1270-1299.

- Potter, D. K and Ivakhnenko, O. P., 2008. "Clay Types - Sensitive Quantification and Anisotropy in Synthetic and Natural Reservoir Samples Using Low- and High-Field Magnetic Susceptibility for Improved Petrophysical Appraisals". *Petrophysics* 49 (1): 57-66.

- Potter, D. K. 2007. "Magnetic Susceptibility as a Rapid, Non-Destructive Technique for Improved Petrophysical Parameter Prediction". *Petrophysics* 48 (3): 191-201.

- Potter, D. K., Ali, A, Imhmed, S., and Schleifer, N., 2011b. "Quantifying the Effects of Core Cleaning, Core Flooding and Fines Migration Using Sensitive Magnetic Techniques: Implications for Permeability Determination and Formation Damage". *Petrophysics* 52 (6): 444-451.

- Potter, D. K., Ali, A. and Ivakhnenko, O. P., 2009. "Quantifying the Relative Roles of Illite and Hematite on Permeability in Red and White Sandstones Using Low and High Field Magnetic Susceptibility". 2009 International Symposium of the Society of Core Analysts, Noordwijk aan Zee, The Netherlands, Paper SCA2009-11.

- Potter, D. K., Corbett, P. W. M., Barclay, S. A. and Haszeldine, R. S., 2004. "Quantification of Illite Content in Sedimentary Rocks Using Magnetic Susceptibility A Rapid Complement or Alternative to X-Ray Diffraction". *Journal of Sedimentary Research, Research Methods Papers Section* 74 (5): 730-735.

- Potter, D.K., Al-Ghamdi, T.M., and Ivakhnenko, O.P., 2011a. "Sensitive Carbonate Reservoir Rock Characterization from Magnetic Hysteresis Curves and Correlation with Petrophysical Properties". *Petrophysics,* 52 (1): 50-57.

- Raith, M., Raase. Reinhardt. P.,2012. "Guide To Thin Section Microscopy". 2th edition. ppii.

- Ramanujan, R., 2009. "Magnetic Particles for Biomedical Applications". Biomedical Materials, Springer Science+Business Media, LLC.

- Rao, R., 2012. "Electromagnetic waves and transmission lines" PHI learning privet ltd. New Delhi.

- Robin, P., Bordas le Floch, N., Roure, F., Frizon, de Lamotte, D., 2000. Magnetic fabric analysis and deformation in sandstone reservoir. Geophysical Research Abstracts, Vol. 2.

- Saffer, D.M. and Marone, C., 2003. "Comparison of Smectite- and Illite-Rich Gouge Frictional Properties: Application to The Updip Limit of the Seismogenic Zone Along Subduction Megathrusts". *Earth Planet. Sci. Lett*., 215:219–235.

- Schlumberger, 1995. "DSI—Dipole Sonic Imager*:* Houston. Schlumberger Wireline and Testing". SMP-5128.

- Schlumberger, 2004b: "FMI Fullbore Formation Microimager". Schlumberger, report, August, pp 2.

- Shipboard Scientific,1998, "Introduction, in Proceedings of the Ocean Drilling Program 174B Initial Reports", edited by K. Becker and M. J. Malone, pp. 3-9, Ocean Drilling Program, College Station, Texas (Ocean Drilling Program), doi:10.2973/odp.proc.ir.174b.101.1998.

- Siddiqui, S. Khamees.A.A., Sadler, R , Hughes, G.W., 2003. "A Density-Based Imaging Technique to Supplement FMI Images for Sedimentary Facies Modeling." International Symposium of the Society of Core Analysts**,** Austin, Dhahran, KSA, Saudi Aramco. Paper SCA203-58.

- Siemianowski, S. 2010. "Approaches to Studying Smectic Layer Elasticity and Field Induced Deformations" .PhD Thesis, Manchester University, School of Physics and Astronomy, Manchester, UK.

- Siswantoro, M.P., Indra, T.B. and Prasetyo, I.A., 1999. "The Application of Modular Formation Dynamics Tester -MDT with a Dual Packer Module in Difficult Conditions in Indonesia" *SPE Reservoir Evaluation and Engineering*., 6, 76-79.

- Smith. R.C. and Zrostlik, R., 1999. "Inverse Compensation for Ferromagnetic Hysteresis," Proc. 38th IEEE Conf. Dec. and Control, Phoenix, AZ, pp. 2875-2880.

- Spies, B.R., Frischknecht F.C., 1992. Electromagnetic sounding. In: Nabighiam, M.N. (Ed.) Electromagnetic methods in applied geophysics, vol. 2. SEG, pp. 285-426.

- Sulovsky, P., 2002, "Mineralogy and Chemistry of Conventional and Fluidised Bed Coal Ashes". *Czech Geological Survey*, 1 (77), 1–11.

- Sutherland, L., 2010 "Suspended Solids Esem Analysis and Interpretation from Production Wells: A-02a".

- Stradling, A, 1991. Mathematical models of dry high-intensity magnetic separators, PhD thesis in Department of Mineral and Metallurgical Engineering, University of Queensland, Brisbane.

- Tarling, D. H., Hrouda, F., 1993. The magnetic anisotropy of rocks. Chapman and Hall, London, 217 pp.

- Thompson, R. and Oldfield, F., 1986. "Environmental Magnetism". London: Allen and Unwin.

- Thomson, A. 1978. "Petrography and diagenesis of the Houston Sandstone Reservoirs at Bassfield, Jefferson Davis County, Mississippi". *Transactions, Gulf Coast Association of Geological Societies*,28,651-664.

- Todd, A.C., Tweedie. J. 1978 "Total rock characterisation of North Sea sandstones with particular reference to interstitial clays". Europec, London, paper 93.

- Tauxe, L., 2005: Lectures in Paleomagnetism, Draft version, 1-2 – 1-5.

- Tauxe, L., 2008: Lectures in Paleomagnetism, Draft version, 6-1 – 6-15.

- Tucker, M.E., 1981, Sedimentary Petrology: an Introduction: Oxford, United Kingdom, Blackwell Science Ltd.

- Weiss,P a., G. Foex, 1926. Le Magnétisme. Paris: Armand Colin,), p.162f.

- Williams. J., Johnson.C, 2000. "Borehole-Wall Imaging with Acoustic and Optical Televiewers for Fractured-Bedrock Aquifer Investigations". Seventh International Symposium on Borehole Geophysics for Minerals, Geotechnical, and Groundwater Applications; Houston, Texas. p. 43-53.

- Wilson, M.D., Pittman,E.D., 1977 Authigenic Clays in Sandstone: Recognition and Influence on Reservoir Properties and Paleoenvironmental analysis: *J.Sedment.Petrology*, 47,3-31.

- Wilson,M ., 1994. "Reservoir Quality Assessment and Prediction in Clastic Rocks". pp62-65.

- Worden, R. H., Morad.S., 2003. "Clay Mineral Cements in Sandstones". 34th edition, Wiley-Blackwell Ltd. pp 30.

- Yang, A., 1992. "A Geostatistical Well Correlation Method that Can Identify Faults" International Meeting on Petroleum Engineering, Beijing, China, 24-27 March1992. 3-10pp.

- Zhang. C,. Liu. Q,. Huang. B, and Y, Su., 2010. "Magnetic Enhancement Upon Heating of Environmentally Polluted Samples Containing Haematite and Iron" Palaeomagnetism and Geochronology Laboratory of the State Key Laboratory of Lithospheric Evolution, Institute of Geology and Geophysics, Chinese Academy of Sciences.

Appendix A

Histograms Well A2

(a)

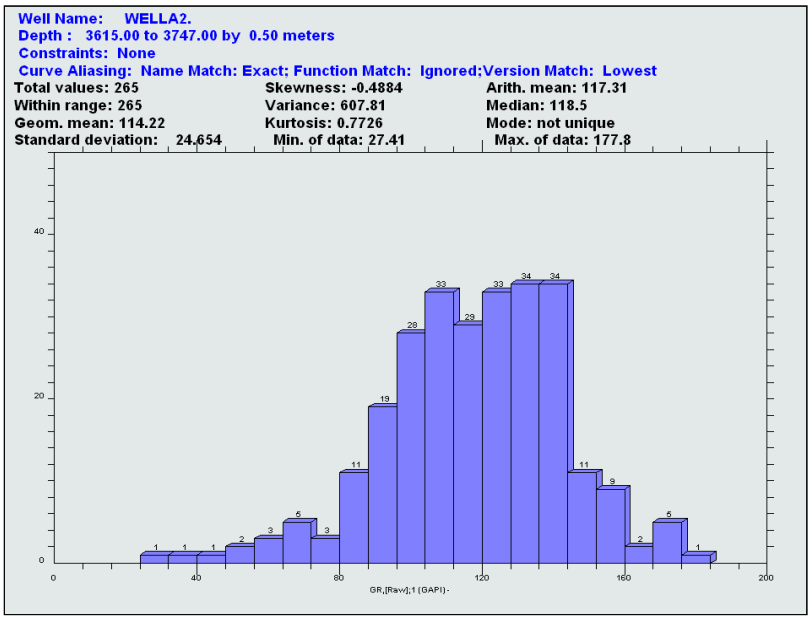

(b)

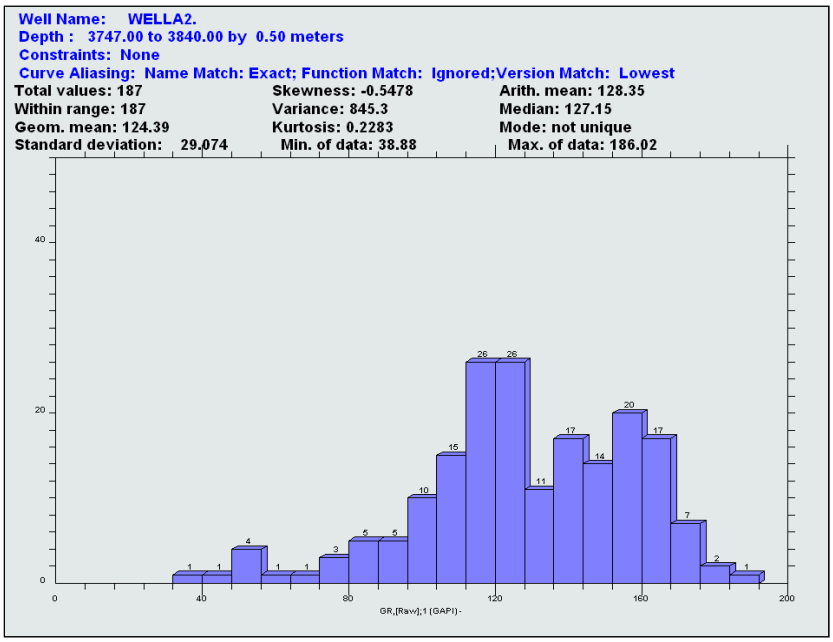

Figure A 1: (a) The histogram of GR above the fault zone. (b) The histogram of GR at the fault zone.

(a)

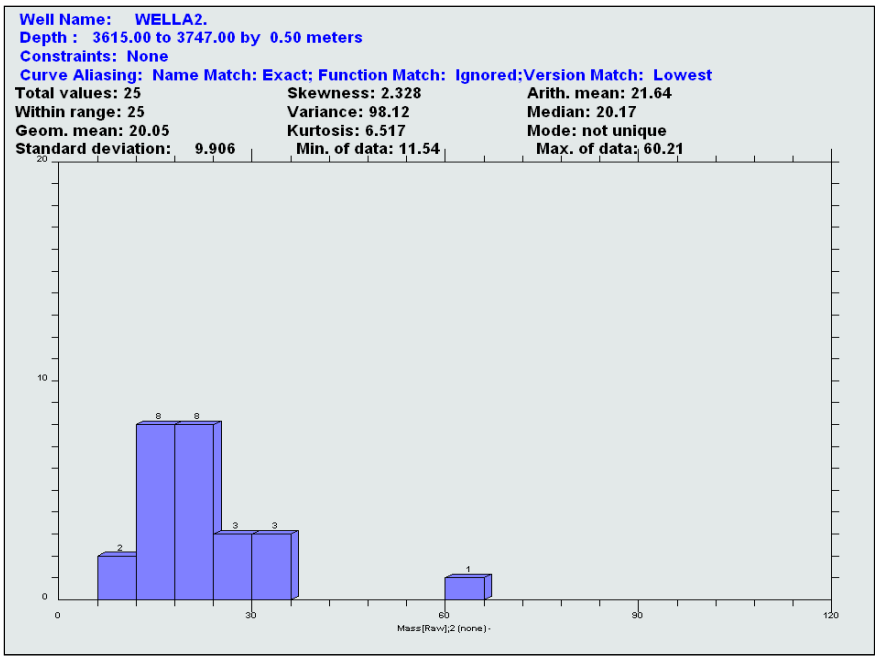

(b)

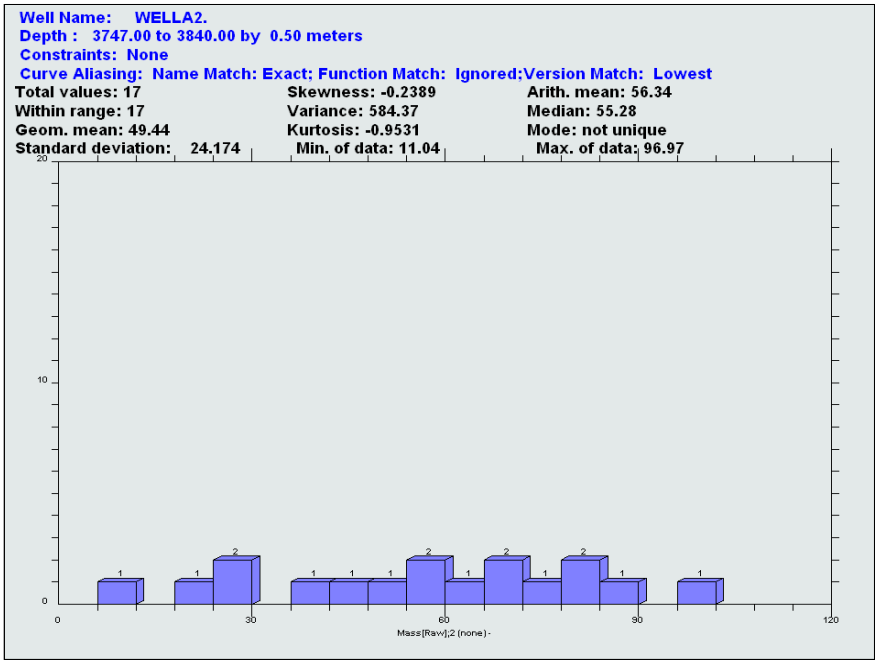

Figure A 2: (a).The histogram of mass magnetic susceptibility above the fault zone. (b) The histogram of mass magnetic susceptibility at the fault zone.

(a)

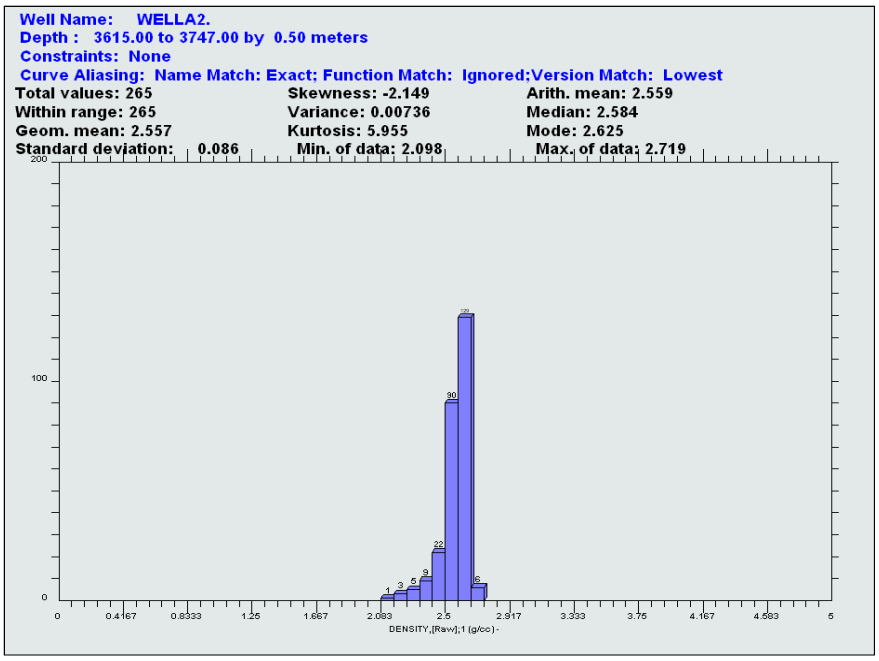

(b)

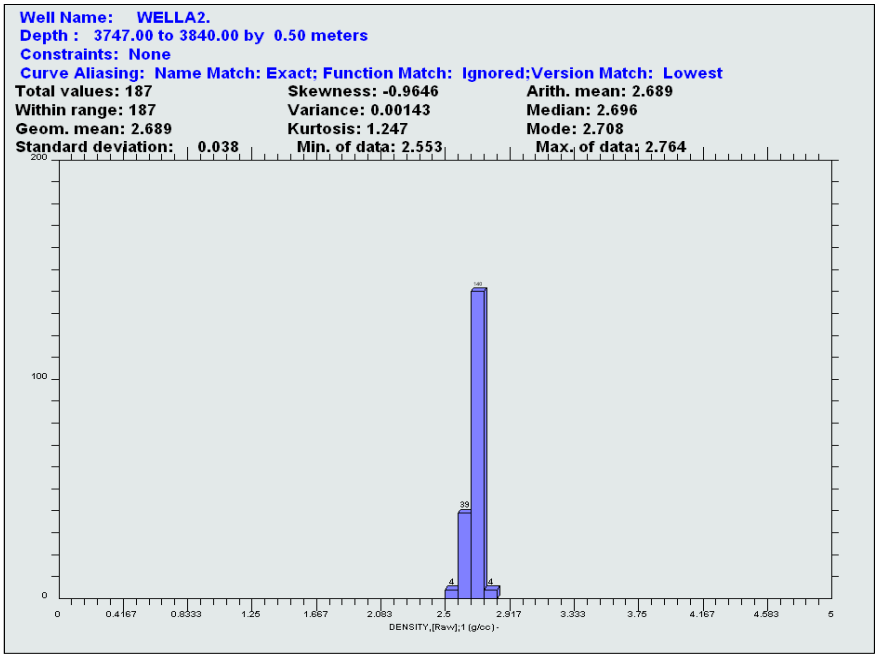

Figure A 3: (a) The histogram of density above the fault zone. (b) Shows the histogram of density at the fault zone.

(a)

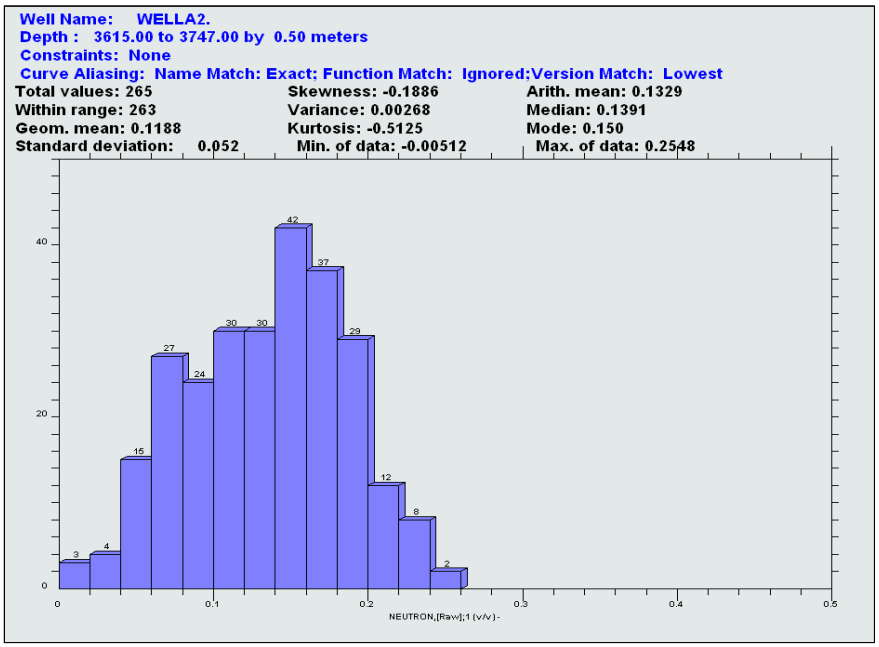

(b)

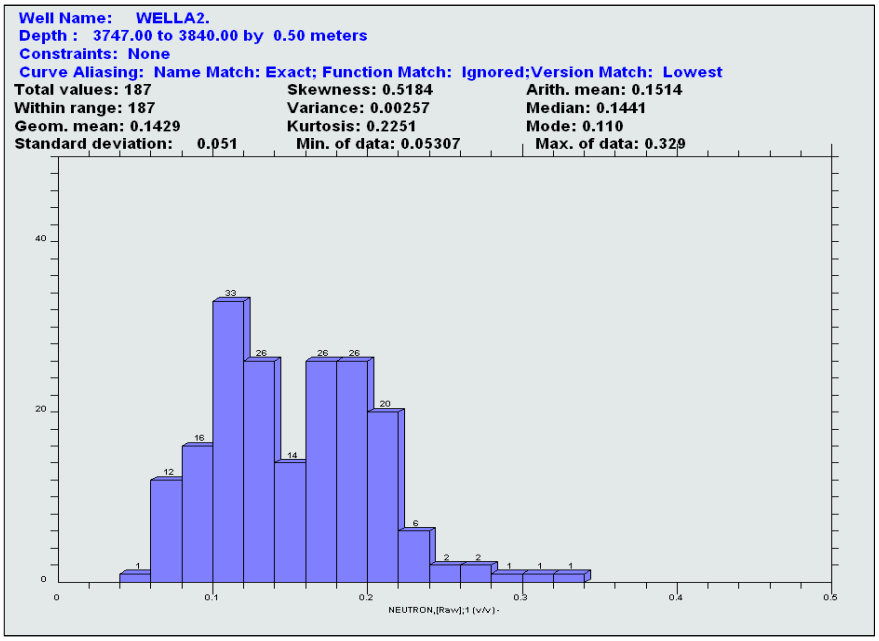

Figure A 4: (a) The histogram of neutron above the fault zone. (b) The histogram of neutron at the fault zone.

(a)

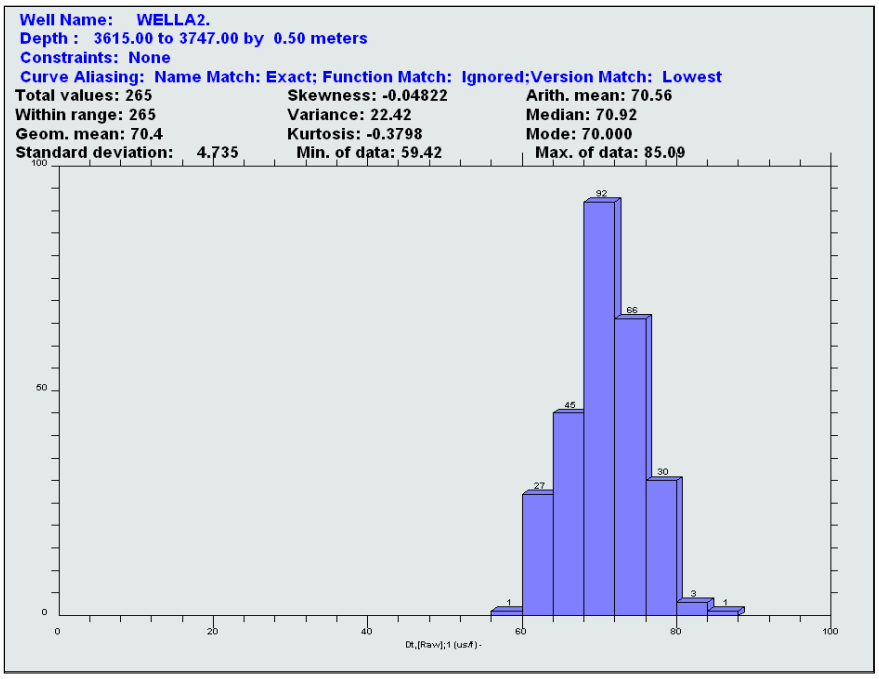

(b)

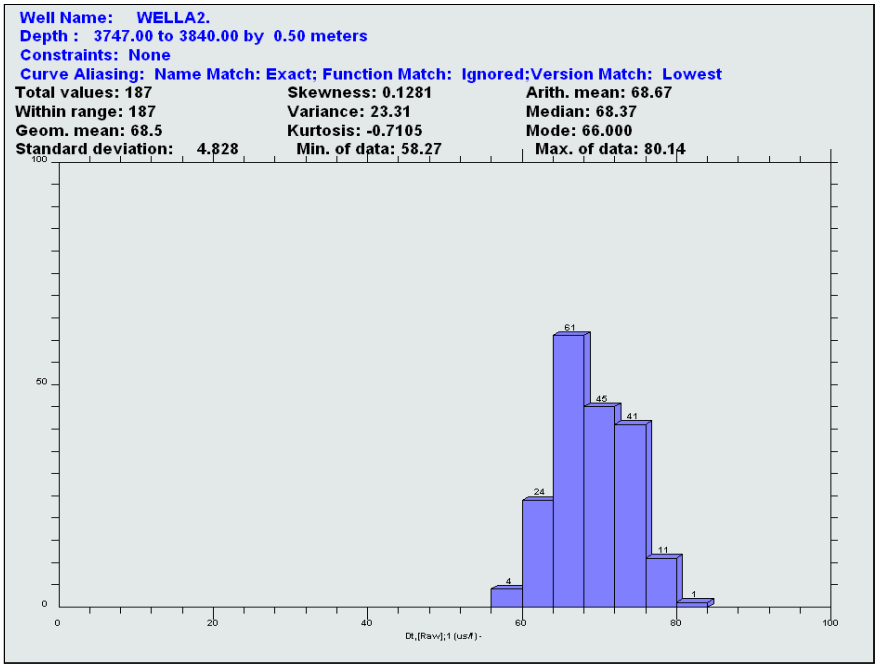

Figure A 5: (a) The histogram of Dt above fault zone. (b) The histogram of Dt at the fault zone.

(a)

Wireline/Lab Tools	No of samples	Geom. mean	Standard deviation	Arith. mean
Gamma Ray (GR)	256	114.22	24.654	117.31
Sonic travel time (DT)	265	70.4	4.735	70.56
Density	265	2.557	0.086	2.559
Mass Magnetic Susceptibility	25	20.05	9.906	21.64
Neutron	265	0.1188	0.052	0.1329

(b)

logs Tool	No of samples	Geom. mean	Standard deviation	Arith. mean
Gamma Ray (GR)	187	124.39	29.074	128.35
Sonic travel time (Dt)	187	68.5	4.828	68.67
Density	187	2.689	0.038	2.689
Mass Magnetic Susceptibility	17	49.44	24.174	56.34
Neutron	187	0.1429	0.051	0.1514

Table A 1: Well A2, (a) Summary of the geometric mean, standard deviation and arithmetic mean of the wireline logs above the fault zone, (b) at the fault zone**.**

Histograms Well A3

(a)

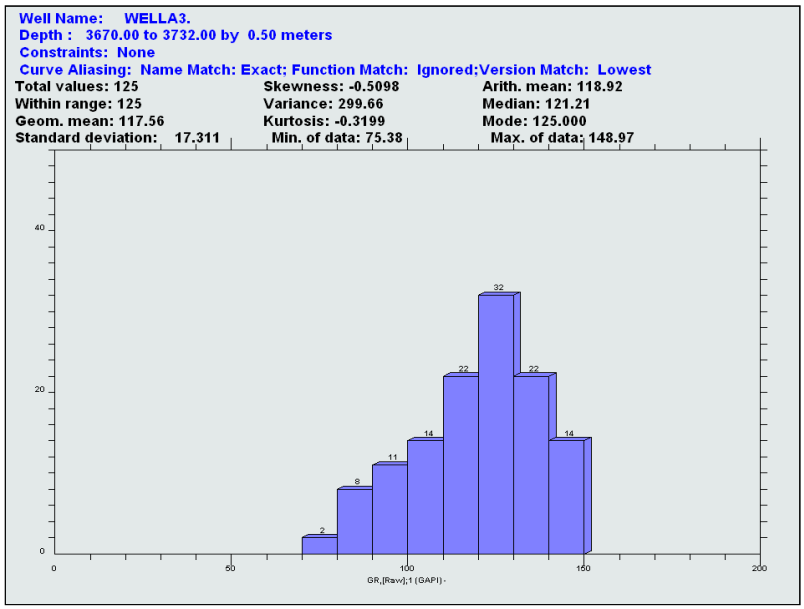

(b)

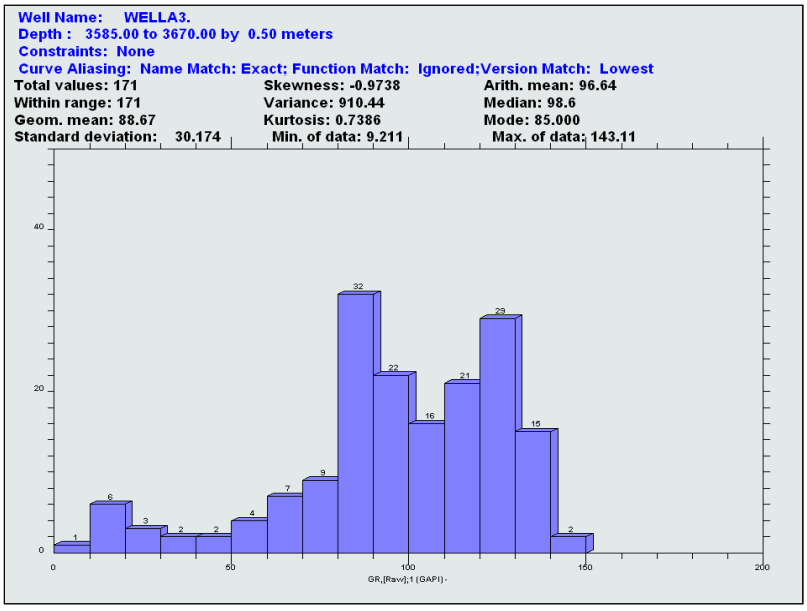

Figure A 6: (a) The Histogram of GR above the fault zone. (b) The histogram of GR at the fault zone.

(a)

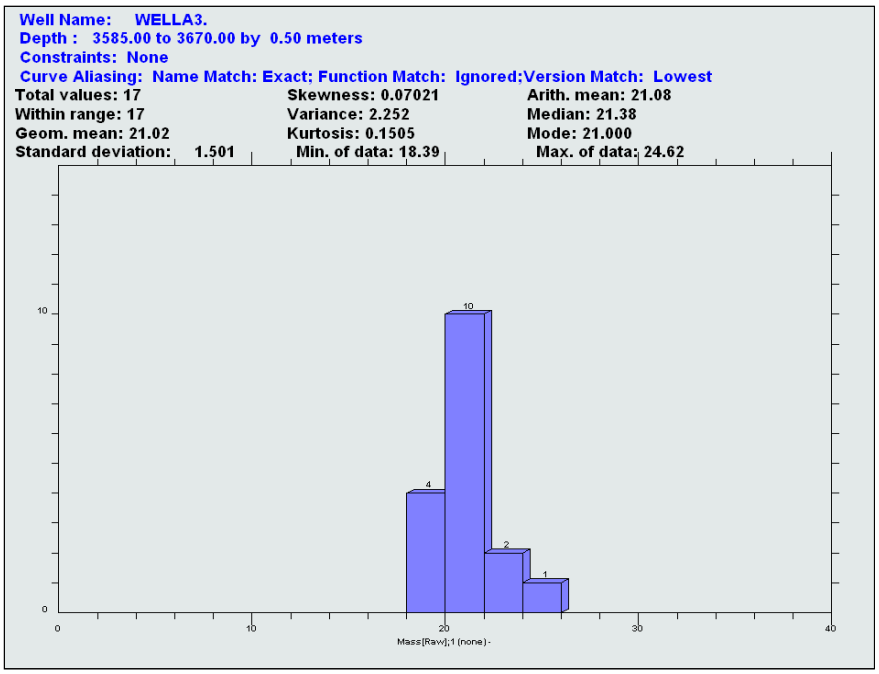

(b)

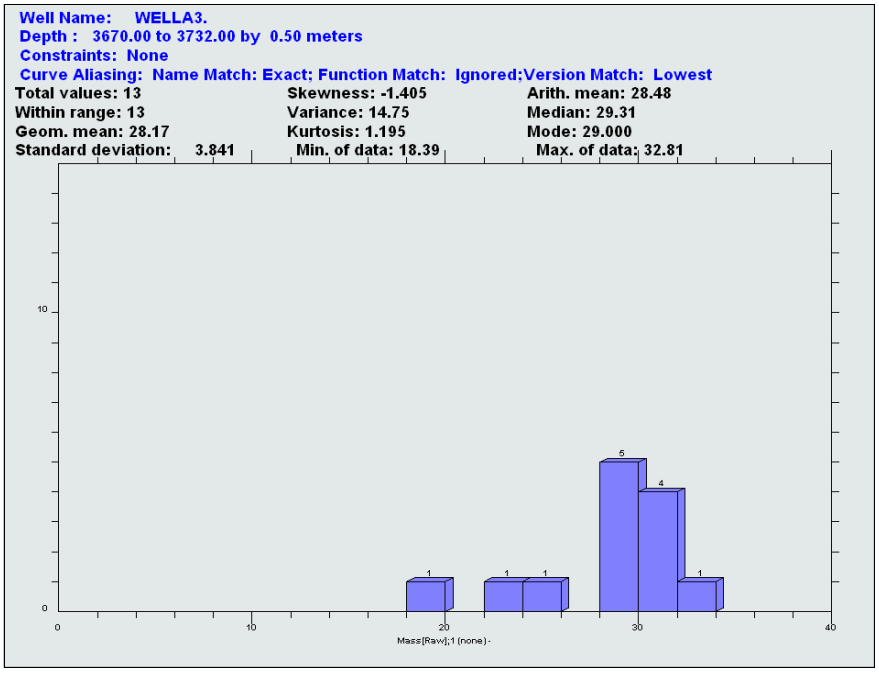

Figure A 7: (a) The histogram of mass magnetic susceptibility above the fault zone. (b) The histogram of mass magnetic susceptibility at the fault zone.

(a)

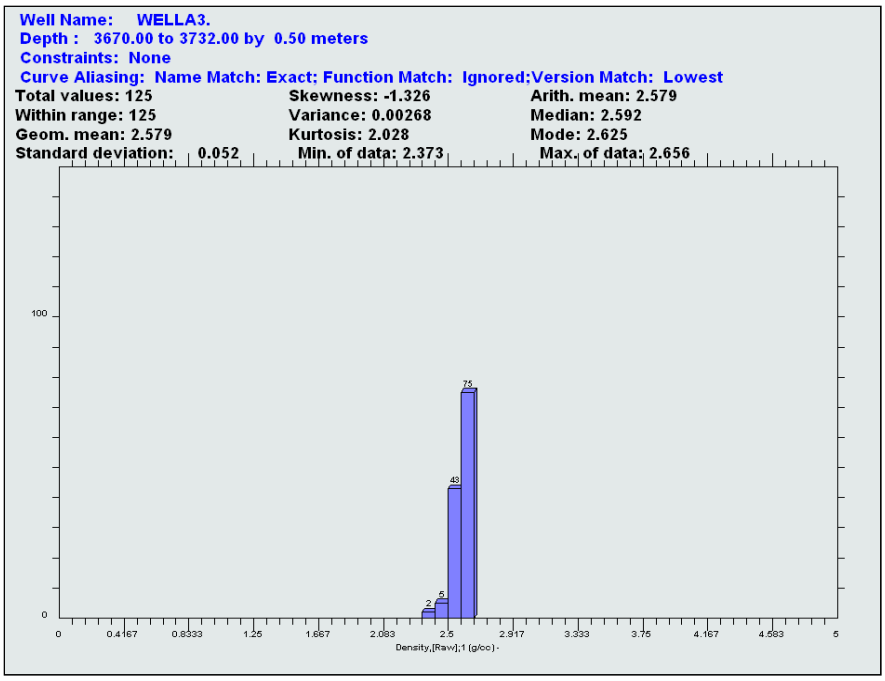

(b)

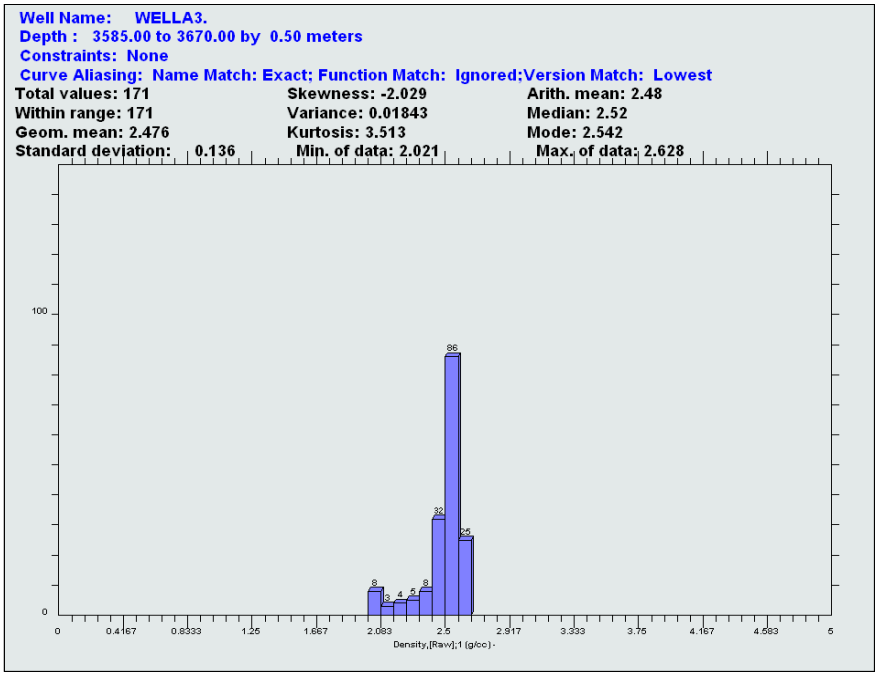

Figure A 8:(a) The histogram of density above the fault zone. (b) The histogram of density at the fault zone.

(a)

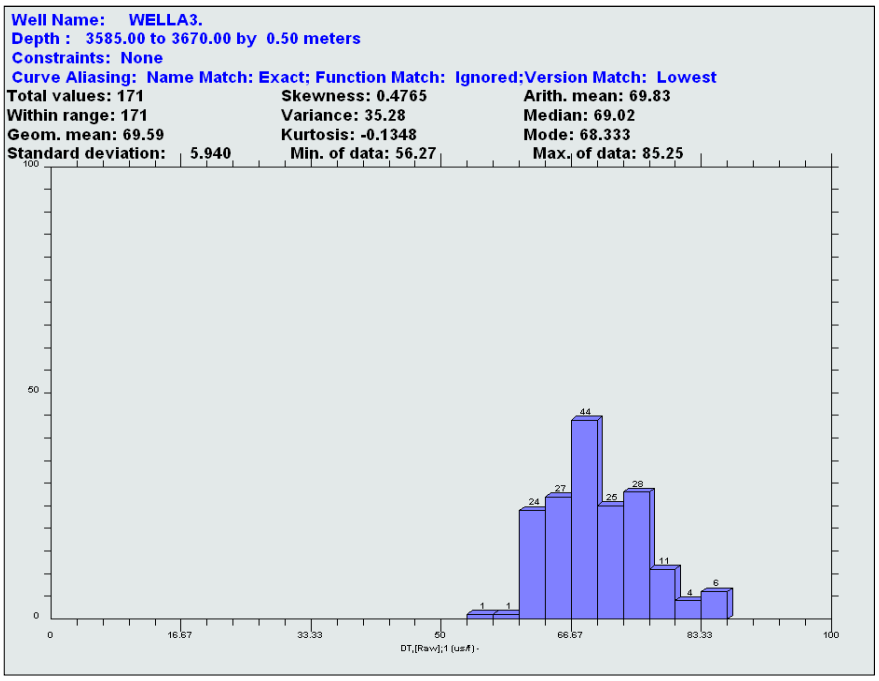

(b)

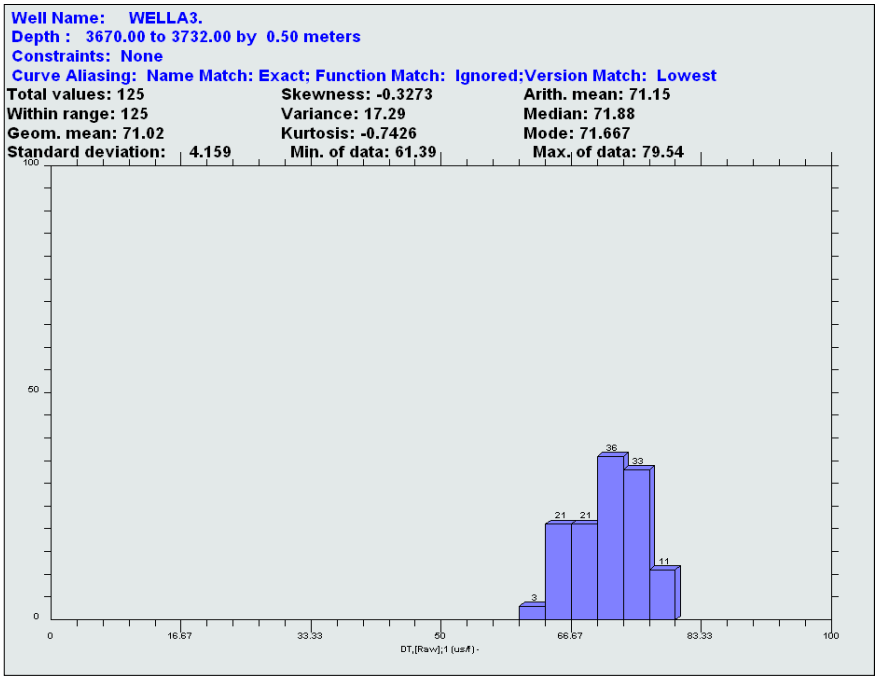

Figure A 9: (a) The histogram of Dt above the fault zone. (b) The histogram of Dt at the fault zone.

(a)

Log Tool	No of samples	Geom. mean	Standard deviation	Arith. mean
Gamma Ray (GR)	171	88.67	30.174	96.64
Sonic travel time (Dt)	171	69.59	5.940	69.83
Density	171	2.476	0.136	2.48
Mass Magnetic Susceptibility	17	21.02	1.501	21.08

(b)

Log Tool	No of samples	Geom. mean	Standard deviation	Arith. mean
Gamma Ray (GR)	125	117.56	17.311	118.92
Sonic travel time (Dt)	125	71.02	4.159	71.15
Density	125	2.579	0.052	2.579
Mass Magnetic Susceptibility	13	28.17	3.841	28.48

Table A 2: Well A3, (a) Summary of the geometric mean, standard deviation and arithmetic mean of the wireline logs above the fault zone; (b) at the fault zone**.**

Histograms Well A1

(a)

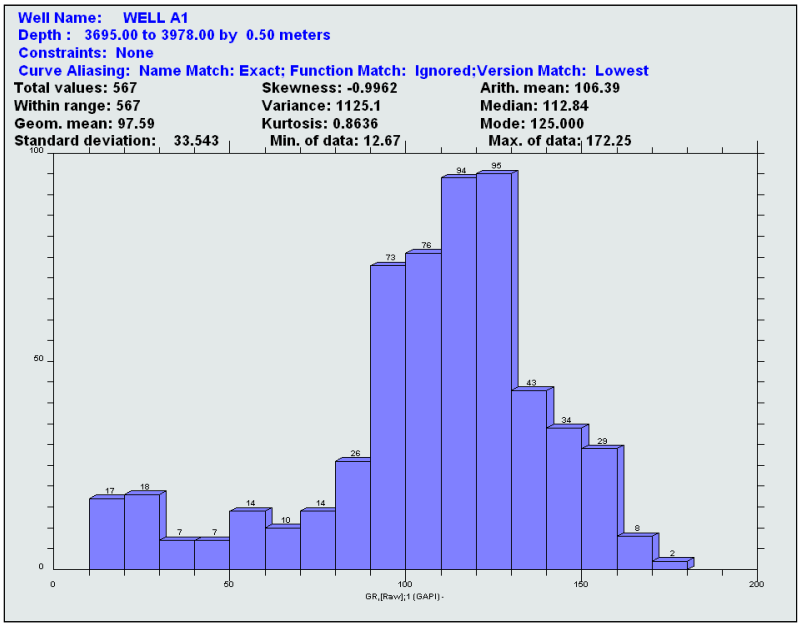

(b)

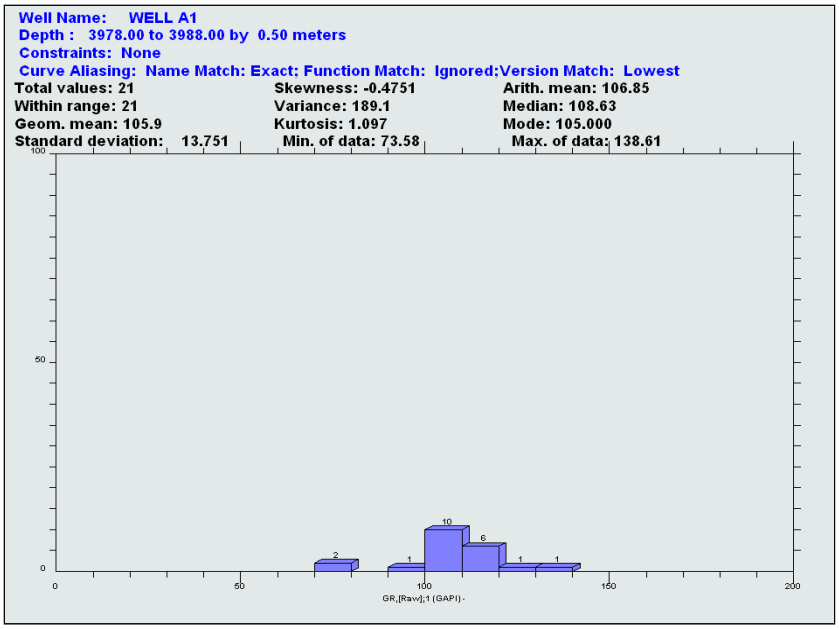

Figure A 10: (a) The histogram of GR above the gas/water contact. (b) The histogram of GR at gas/water contact.

(a)

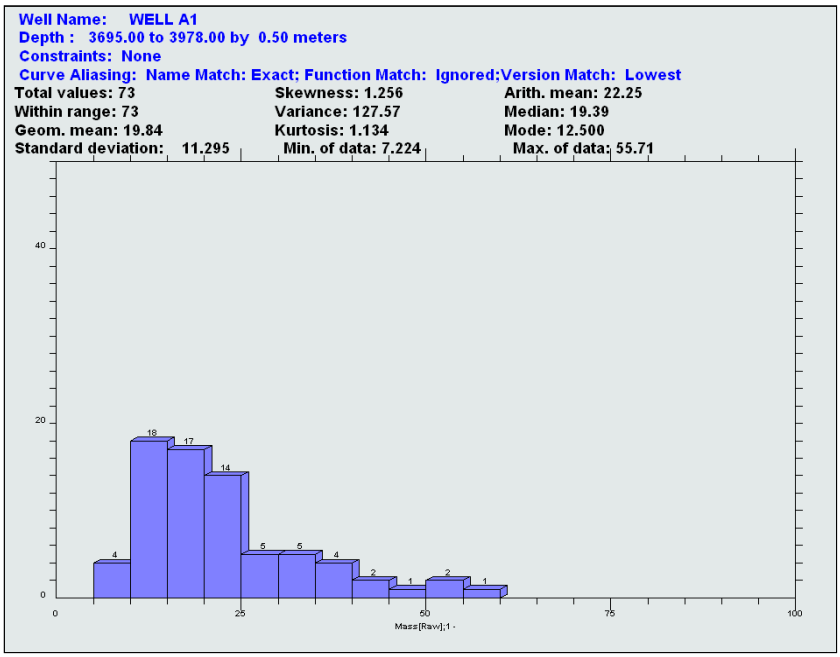

(b)

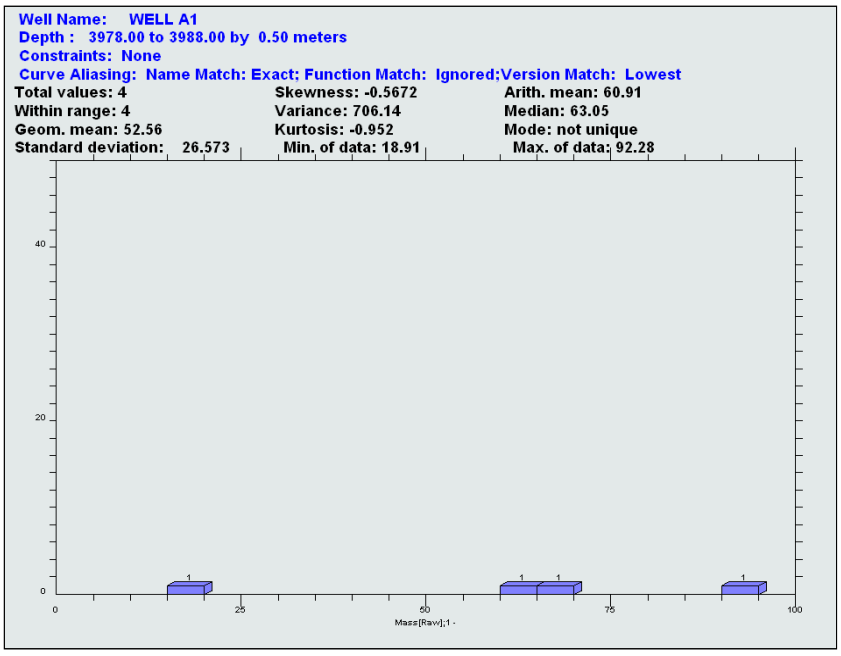

Figure A 11: (a) The histogram of mass magnetic susceptibility above the gas/water contact. (b) The histogram of mass magnetic susceptibility at gas/water contact.

(a)

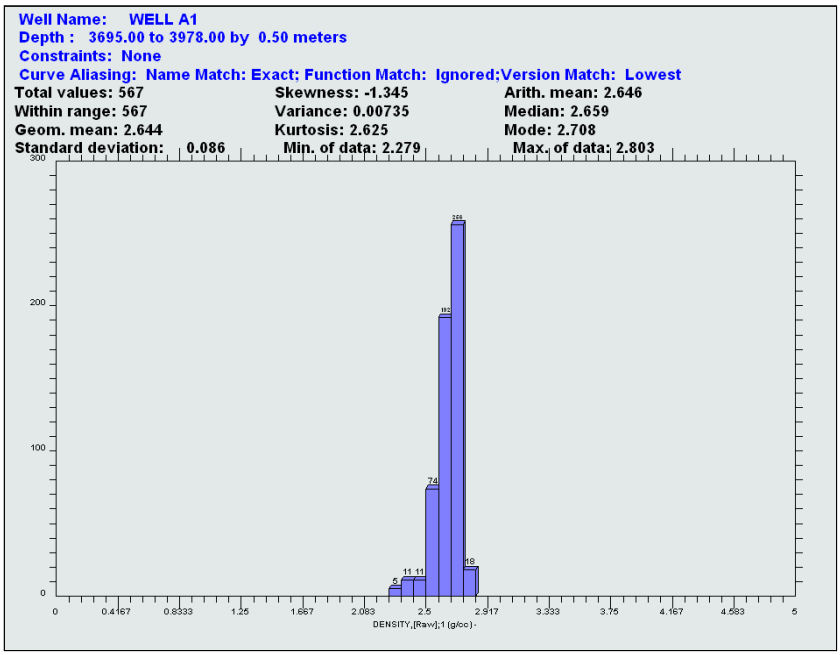

(b)

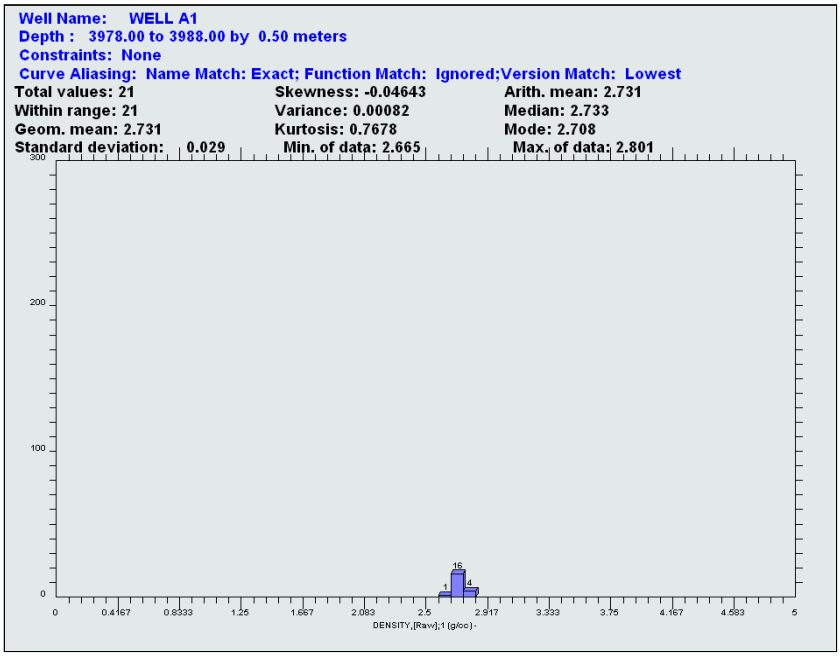

Figure A 12: (a) The histogram of density above the gas/Water contact. (b) The histogram of density at the gas/water contact.

(a)

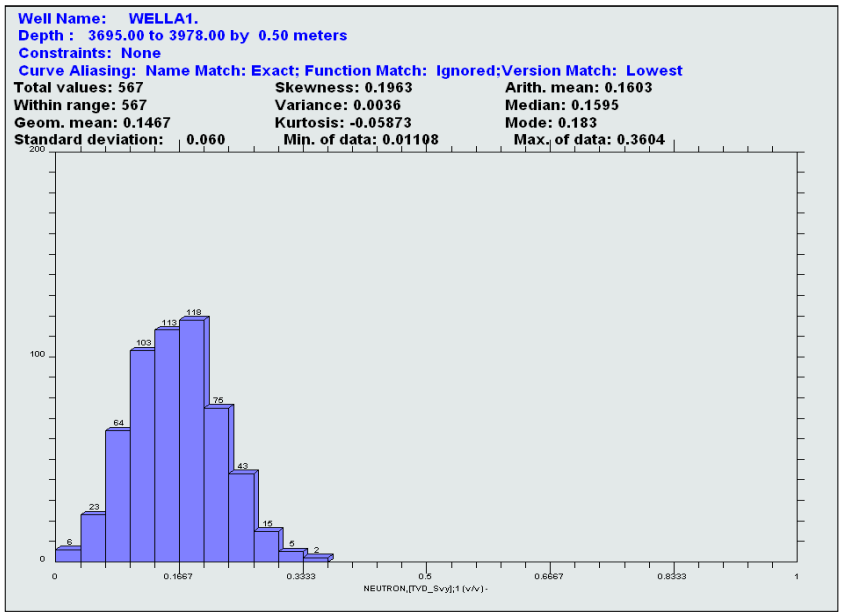

(b)

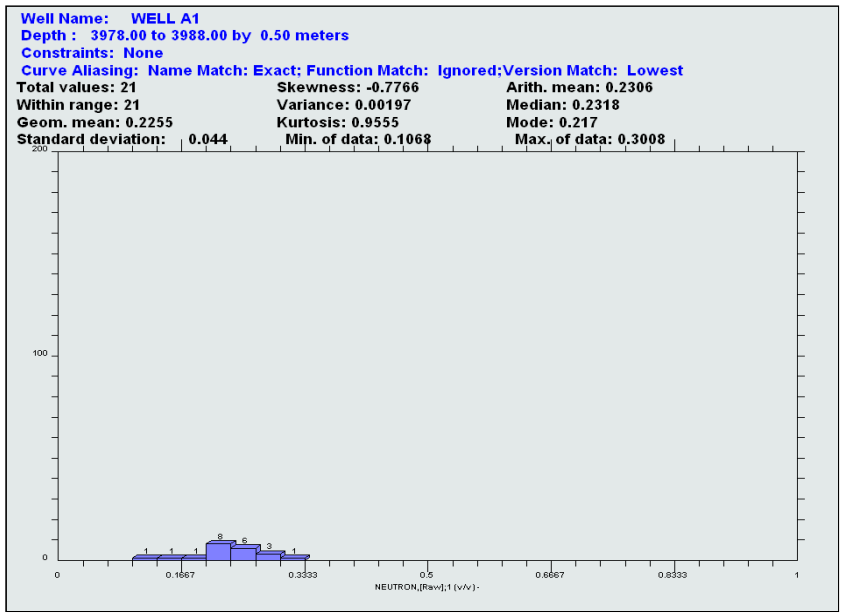

Figure A 13: (a) The histogram of neutron above the gas/water contact. (b) The histogram of neutron at the gas/water contact.

(a)

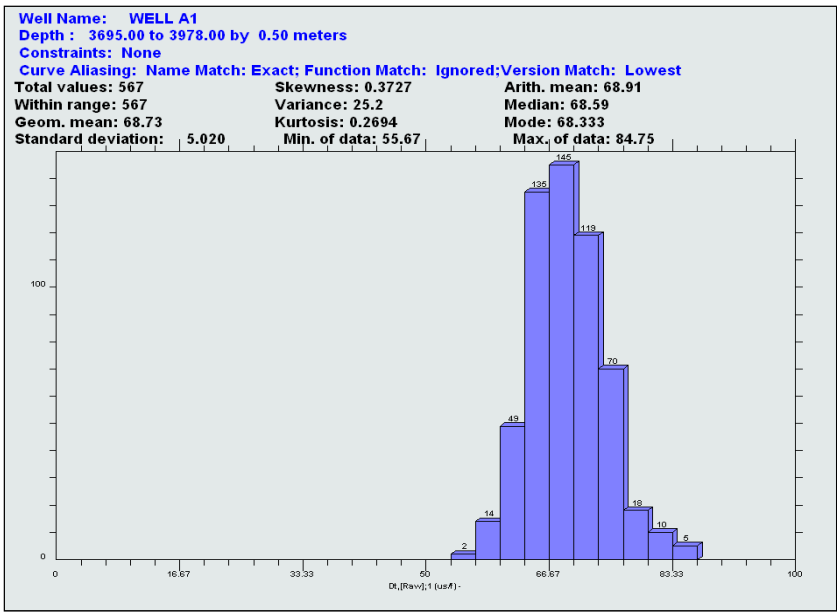

(b)

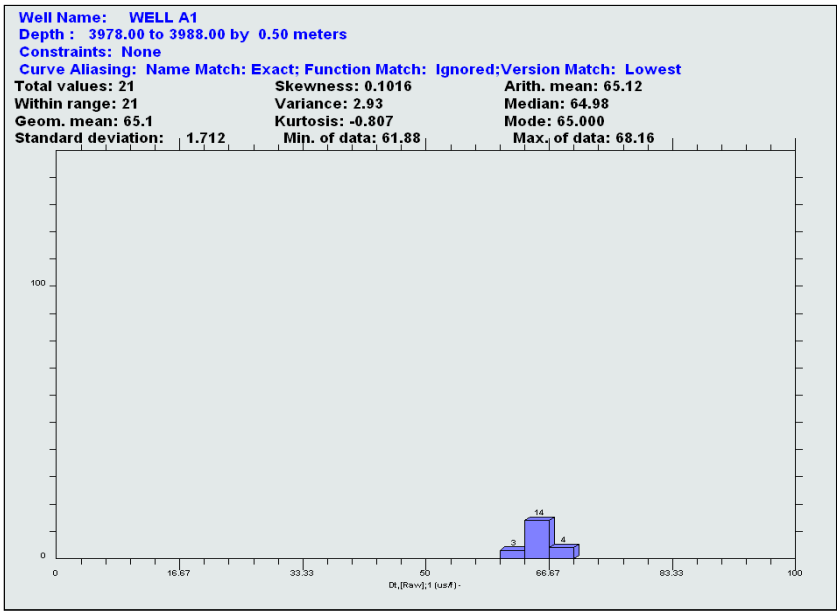

Figure A 14:(a) The histogram of Dt above the gas/water contact. (b) The histogram of Dt at gas/water contact.

(a)

log Tool	No of samples	Geom. mean	Standard deviation	Arith .mean
Gamma Ray (GR)	567	97.59	33.543	106.39
Acoustic (DT)	567	68.73	5.020	68.91
Density	567	2.644	0.086	2.646
Mass Magnetic Susceptibility	73	19.84	11.295	22.25
Neutron	567	0.1467	0.060	0.1603

(b)

log Tool	No of samples	Geom. mean	Standard deviation	Arith. mean
Gamma Ray (GR)	21	105.9	13.751	106.85
Acoustic (DT)	21	65.1	1.712	65.12
Density	21	2.731	0.029	2.731
Mass Magnetic Susceptibility	4	52.56	26.573	60.91
Neutron	21	0.2255	0.044	0.2306

Table A 3: (a) Summaries of the geometric mean, standard deviation and arithmetic mean of the five well logs above the gas/water contact. (b) Summaries of the geometry mean standard deviation and arithmetic mean of the four well logs at and below the gas/water contact.

No. of measurements per bag of drill cuttings	Depth 3595 (m) MMS ($10^{-8}m^3Kg^{-1}$)	Depth 3600 (m) MMS ($10^{-8}m^3Kg^{-1}$)	Depth 3605 (m) MMS ($10^{-8}m^3Kg^{-1}$)	Depth 3610 (m) MMS ($10^{-8}m^3Kg^{-1}$)	Depth 3615 (m) MMS ($10^{-8}m^3Kg^{-1}$)	Depth 3620 (m) MMS ($10^{-8}m^3Kg^{-1}$)	Depth 3625 (m) MMS ($10^{-8}m^3Kg^{-1}$)
1	20.12515125	14.83486239	21.19883467	18.18687815	15.30743802	19.67096307	16.40779412
2	21.0422928	18.11576763	23.0667147	19.23303965	17.71731191	19.88696925	18.33226744
3	20.36401799	17.88716814	22.19645756	20.3	15.04741507	19.7137881	19.87511381
4	20.67513812	18.2918552	20.74911504	19.56340553	16.37168012	19.30390567	20.4624
5	19.89020501	18.2918552	21.66873199	20.09289941	16.25243991	17.05846154	20.49220685
6	19.62202247	19.54359712	21.38574578	20.53333333	16.55385757	17.26078577	20.70331126
7	21.39023622	19.86004549	20.53333333	21.60801782	16.97142857	17.65283843	22.9839196
8	21.17065463	18.54357798	20.50714286	20.34403471	18.98217391	19.7568	23.47258065
9	22.54531371	18.47348378	19.87242136	20.27074928	18.35895197	19.0650655	23.42106803
10	22.25229358	20.09289941	21.26077429	20.56710526	18.52070485	19.48751793	22.72796486
11	23.13442623	19.07696629	20.59721816	22.54640523	18.49354839	18.98217391	22.05
12	21.25633803	19.47114187	20.91881041	18.63013294	20.68808824	19.30390567	21.12191582
13	21.46460177	19.21892883	21.35436537	21.17065463	19.36097561	18.92363091	20.62741935
14	21.52810651	18.92731214	23.48980191	20.36401799	20.2125	18.9	19.36097561
15	20.09289941	19.50513775	21.19883467	23.48980191	20.25771812	19.96002939	20.70331126
16	21.15473684	18.52410501	21.33115997	24.63539955	19.8	20.934375	19.64251627
17	21.30746706	20.2879761	19.43278932	24.00044978	19.7137881	20.36401799	20.73382461
18	20.77976366	20.72128146	21.37004405	22.67815924	19.60733533	21.19883467	21.2297593
19	20.27074928	18.50711665	21.2297593	23.6984456	20.47729258	22.24571006	19.21892883
20	20.42526316	20.76880734	21.82597968	25.51239669	19.50513775	21.7	19.38963731
21	21.2297593	20.55208181	20.74911504	24.73197378	20.34403471	0.177562225	20.2879761
22	19.51165049	19.45959885	19.84338934	25.85284974	20.56442089	20.37929482	19.77117904
23	20.87225519	19.06666667	21.06078148	24.8405267	20.90326895	18.37232338	21.04397906
24	20.16581986	19.97470588	20.94996277	22.52898876	20.58	20.22703091	22.25548387
25	20.18446602	19.9507997	20.31832461	22.201373	21.29188003	19.27549669	21.77856626
26	21.63755396		19.09285714		21.20256217	20.27074928	20.93956835
27	20.61230769		20.87225519		20.01886514	19.46166419	23.01696621
28	20.70331126				20.49220685	17.5	20.43267974
29	20.90326895				19.97470588		
30					19.82890511		
Avg. MMS Value	**20.90731277**	**19.11790955**	**21.03980444**	**21.90324155**	**19.11335452**	**18.82263908**	**20.80297549**

No. of measurements per bag of drill cuttings	Depth 3630 (m) MMS ($10^{-8}m^3Kg^{-1}$)	Depth 3635 (m) MMS ($10^{-8}m^3Kg^{-1}$)	Depth 3640 (m) MMS ($10^{-8}m^3Kg^{-1}$)	Depth 3645 (m) MMS ($10^{-8}m^3Kg^{-1}$)	Depth 3650 (m) MMS ($10^{-8}m^3Kg^{-1}$)	Depth 3655 (m) MMS ($10^{-8}m^3Kg^{-1}$)	Depth 3660 (m) MMS ($10^{-8}m^3Kg^{-1}$)
1	23.42106803	21.14877384	21.72596221	22.51370558	22.42818792	18.46647145	20.49220685
2	24.7139738	21.87906977	21.79434783	24.09074492	19.10678337	20.81655172	20.74911504
3	25.38313953	21.771669	20.87175573	23.5589404	20.48687783	21.46132723	22.27866667
4	23.13442623	20.19847328	22.42058824	23.75118694	20.89447236	22.47847534	21.84183007
5	23.62739726	21.45235378	23.62951289	23.71445004	23.2848	22.92939439	21.35436537
6	22.74461538	23.78284066	24.30563674	24.61701493	20.77976366	19.65672938	22.36148699
7	25.25466377	20.91529903	23.87974684	24.11315789	23.91082898	20.77976366	22.2863706
8	22.87163498	22.5787024	21.29382716	21.49630724	23.62739726	21.24525547	21.52810651
9	24.48908686	22.21832061	20.36808957	21.88951965	22.13112583	19.78557902	23.90347826
10	22.90647372	22.95532359	20.2125	24.02534596	22.74461538	21.34734446	22.59669421
11	22.21285081	22.43629993	20.14480911	24.23663891	23.40394737	22.25548387	21.49630724
12	23.87516779	21.75336323	19.64790503	24.0779562	23.66341463	23.64593796	21.62199856
13	21.37004405	22.72292406	19.86004549	24.29180577	23.54161765	19.78557902	19.7137881
14	23.43124528	22.98731707	19.17391304	23.66341463	23.8516269	21.1372549	21.7
15	23.03145401	22.97130919	20.15831099	23.93817126	23.1	21.71566787	21.83495874
16	19.82890511	21.59198813	20.00412371	20.22755026	22.05	20.93956835	19.59267016
17	19.44721604	21.84827586	19.6529372	23.5589404	23.08334535	19.77117904	22.48110065
18	20.96974063	21.22526464	19.74626866	19.98940397	23.15010846	21.4804428	23.13442623
19	22.91247232	21.42179487	19.8653897	19.00972424	22.61209031	23.54161765	23.26787791
20	20.04841328	21.28535032	20.08695652	21.05973054	22.67815924	21.4804428	21.70469799
21	19.02352941	20.91529903	20.56961131	19.74244186	22.33553957	20.33353293	22.69901887
22	19.09285714	21.16551724	20.12863071	23.53783169	21.85770349	22.9839196	24.23717855
23	19.41838399	19.85402456	20.70331126	20.39459459	21.90546249	21.24525547	23.53783169
24	21.18340611	21.71076923	20.26698113	18.90944528	22.98031088	20.90326895	23.25098039
25	20.82590674	21.60364372	19.92197125	19.15353075	23.26787791	21.59309286	21.43298969
26	17.28641425	21.70616949	20.35384615	21.43298969	22.59563319	22.72796486	20.43267974
27	18.26589428	21.66531752	19.70294118	18.98058691	22.08237885	21.33870968	21.30746706
28	20.09289941			21.15473684	20.64255319		19.51551724
29							20.7185567
30							22.82823529
							20.7185567
Avg. MMS Value	**21.82172664**	**21.76909089**	**20.75888591**	**22.18320955**	**22.40654189**	**21.32762262**	**21.82642445**

No. of measurements per bag of drill cuttings	Depth 3665 (m) MMS ($10^{-8}m^3Kg^{-1}$)	Depth 3670 (m) MMS ($10^{-8}m^3Kg^{-1}$)	Depth 3675 (m) MMS ($10^{-8}m^3Kg^{-1}$))	Depth 3680 (m) MMS ($10^{-8}m^3Kg^{-1}$)	Depth 3685 (m) MMS ($10^{-8}m^3Kg^{-1}$)	Depth 3690 (m) MMS ($10^{-8}m^3Kg^{-1}$)	Depth 3695 (m) MMS ($10^{-8}m^3Kg^{-1}$)
1	22.4	18.71305638	30.42932166	26.16428571	32.14518072	25.94888559	25.4386016
2	21.96946676	18.83883495	33.63165034	27.11283988	32.85259366	33.38169839	23.71445004
3	21.82597968	19.33239852	34.80538117	28.26511289	35.5124451	32.59985391	22.69473684
4	19.2471712	17.58883249	36.01336303	28.11129272	33.03419689	26.37167382	23.03145401
5	18.38571429	17.7610984	35.12671977	30.22659574	34.16698459	32.16940467	22.41147541
6	23.1	16.8	31.70106383	28.83978659	35.74421053	30.9168437	20.01176471
7	19.34447853	17.80837004	34.20810203	28.34769905	32.52857143	22.01664145	20.1674833
8	23.15010846	17.29925706	31.22649701	28.95011477	34.98842975	23.1	21.34734446
9	19.13469686	17.52528902	34.11692308	30.29673203	34.18245877	34.31106095	21.65313175
10	21.168	17.80837004	31.0464	28.30052356	34.10575916	13.32147239	27.18232759
11	21.60646552	17.55065123	34.46666667	27.38169336	33.30854638	13.51171662	26.78466258
12	21.25060423	18.39912473	31.43505155	28.25825243	30.43196415	23.68146453	26.6416476
13	21.73711725	19.17672035	32.22066421	30.72061856	31.18246896	24.4215103	27.18232759
14	21.34734446	18.98217391	29.6924254	29.11327832	33.47922358	34.36277317	26.85185725
15	20.53708029	19.16269203	31.99279141	29.51178707	33.52742981	31.89116143	26.61920578
16	20.40991736	18.98217391			33.11503268	24.97108251	25.57003012
17	19.61415162	19.74244186			33.47973568	25.47571116	25.21819495
18	20.52210066	19.60733533			27.82460377	26.67698987	26.20195049
19	19.60733533				24.34722433	31.47728911	27.3
20	21.60801782				28.68292683	24.87692308	29.05639153
21	22.25548387				25.34629898	34.32476534	28.90588235
22	22.01771596				29.06966292	21.33115997	27.8628866
23	21.75336323				30.40714286	24.93333333	27.49840116
24	23.03145401				29.83045388	32.10220588	27.30933333
25	23.89298507					25.29662577	28.04877687
26	24.62815385					31.67699317	27.80146951
27	23.76570605					34.23378378	25.62523844
28						32.77702703	
Avg. MMS Value	**21.45594861**	**18.39326779**	**32.80753474**	**28.64004085**	**31.80389773**	**29.043**	**25.48633429**

No. of measurements per bag of drill cuttings	Depth 3700 (m) MMS ($10^{-8}m^3Kg^{-1}$)	Depth 3705 (m) MMS ($10^{-8}m^3Kg^{-1}$)	Depth 3710 (m) MMS ($10^{-8}m^3Kg^{-1}$)	Depth 3715 (m) MMS ($10^{-8}m^3Kg^{-1}$)	Depth 3720 (m) MMS ($10^{-8}m^3Kg^{-1}$)	Depth 3725 (m) MMS ($10^{-8}m^3Kg^{-1}$)	Depth 3730 (m) MMS ($10^{-8}m^3Kg^{-1}$)
1	22.13112583	31.36576047	28.16255443	25.30956522	32.73467337	24.32654867	35.29309577
2	20.88775056	33.99240876	27.57486911	30.70715901	31.48573585	26.25998537	35.74797347
3	21.42863671	33.10771513	29.95346386	31.0345773	31.66824926	25.92137405	33.25995624
4	23.08334535	32.24653179	29.61366279	29.52782609	33.06700508	27.74085779	36.41891892
5	21.88951965	32.14948454	30.20364465	29.57486989	31.63695652	28.22940276	33.82744807
6	23.31871814	31.752	30.59189189	29.48717569	33.13229399	29.62442748	32.8397351
7	22.26217617	32.24229607	30.43196415	30.82329803	32.31658219	28.53529412	35.33139111
8	23.31871814	31.89116143	25.53157895	27.59215988	30.71136691	27.9723824	33.48082822
9	22.4973913	31.50464945	29.4	28.06958457	31.040625	28.75212766	32.60567588
10	22.51370558	31.79771341	28.49339207	30.74325718	30.13934911	29.17894737	34.85748503
11	22.41617329	31.41460843	24.45882353	29.88595041	30.7659292	29.57486989	32.19690265
12	23.43821376	33.17553191	25.92137405	30.54070278	32.55704698	30.31875	34.4195122
13	24.255	30.51836138	29.44461305	30.29620818	31.55121951	28.10137581	34.22484663
14	24.56202532	30.07261993	32.24446086	29.75183246	30.31875	28.75212766	32.36345178
15	22.39478779	29.90580645	29.35552194	28.63801296	30.27474601	28.47088036	33.40508982
16	23.68091716	28.028	31.59792746	29.0044843	31.93782004	28.32170659	26.78466258
17	23.4489426	27.84561934	27.08861132	28.64059041	31.99279141	29.29175258	31.7251711
18	23.59148936	29.21032258	29.33495575	24.48233598	29.61366279	28.84568528	32.52857143
19	22.87870302	28.875	29.42174556	29.04790419	31.43828184	30.9255745	34.15685393
20	24.10888554	31.10564885	29.02617801	30.24958175	31.92360515	31.45821665	33.50652341
21	23.31871814	27.72	30.29673203	23.54161765	30.95634518	33.09100145	27.9039823
22	22.28743719	29.91806167	31.80983607		29.37774413	32.12582781	28.86661829
23	23.6984456	30.11707317	28.96119403		30.85695266	33.35515695	26.22162162
24	23.30174672	33.21150765	29.04790419		30.66094808	30.9115134	24.67225131
25	23.20043478	31.89116143	30.56307692		27.67944404	32.58687023	24.63539955
26	23.48441755	32.761934	31.82142857		28.21610738		25.92962138
27	24.76486486	28.93959732	30.95634518		30.45803982		25.88185976
28	23.5589404		32.19366516		30.38823529		30.51836138
29	23.26787791		31.91447368		31.02383721		27.00923077
30	24.21938326						25.18076336
Avg. MMS Value	**23.10694972**	**30.99113241**	**29.49709963**	**28.90231876**	**31.03187393**	**29.30690627**	**31.19312677**

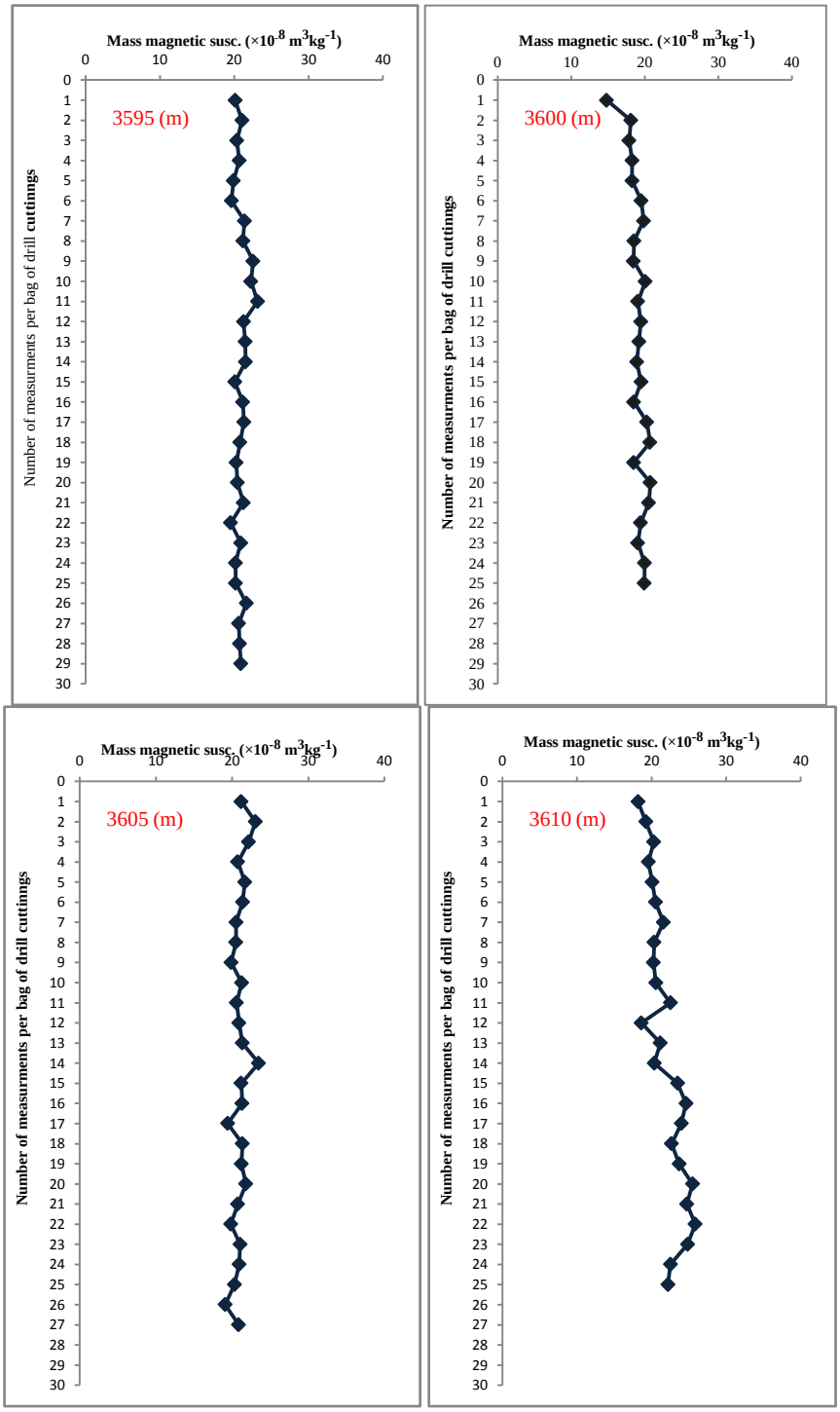
Mass magnetic susc. (×10-8 m3kg-1)
Number of measurments per bag of drill cuttings
3595 (m)
3600 (m)
3605 (m)
3610 (m)

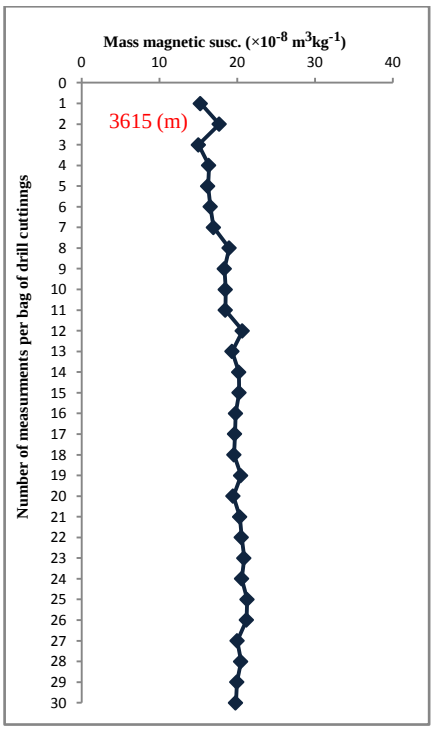
Mass magnetic susc. (×10-8 m3kg-1)
0 10 20 30 40
3615 (m)
Number of measurments per bag of drill cuttinngs
0 1 2 3 4 5 6 7 8 9 10 11 12 13 14 15 16 17 18 19 20 21 22 23 24 25 26 27 28 29 30

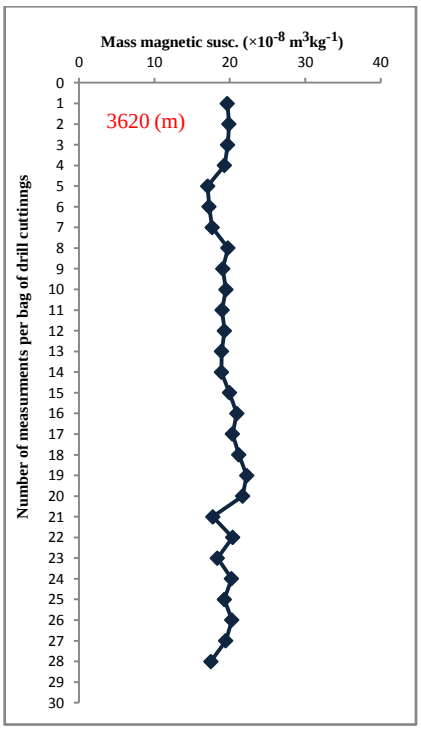
Mass magnetic susc. (×10-8 m3kg-1)
0 10 20 30 40
3620 (m)
Number of measurments per bag of drill cuttinngs
0 1 2 3 4 5 6 7 8 9 10 11 12 13 14 15 16 17 18 19 20 21 22 23 24 25 26 27 28 29 30

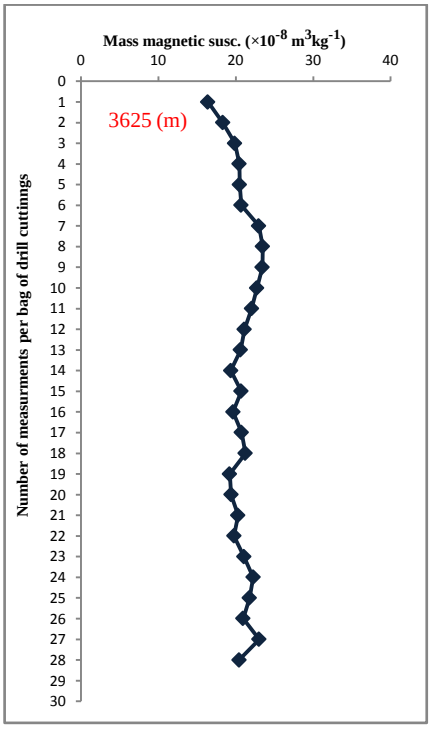
Mass magnetic susc. (×10-8 m3kg-1)
0 10 20 30 40
3625 (m)
Number of measurments per bag of drill cuttinngs
0 1 2 3 4 5 6 7 8 9 10 11 12 13 14 15 16 17 18 19 20 21 22 23 24 25 26 27 28 29 30

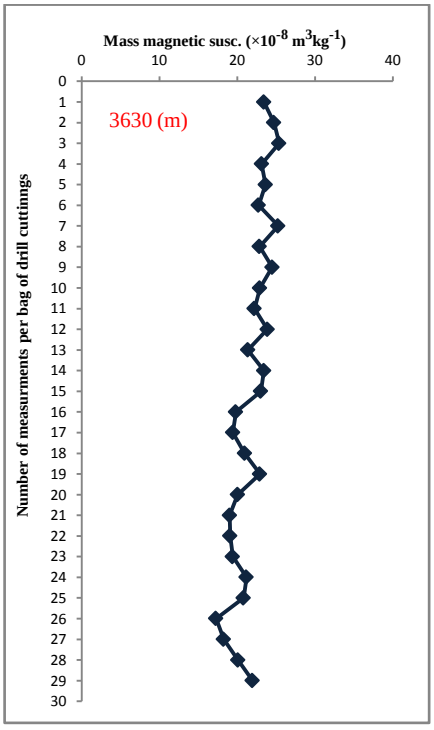
Mass magnetic susc. (×10-8 m3kg-1)
0 10 20 30 40
3630 (m)
Number of measurments per bag of drill cuttinngs
0 1 2 3 4 5 6 7 8 9 10 11 12 13 14 15 16 17 18 19 20 21 22 23 24 25 26 27 28 29 30

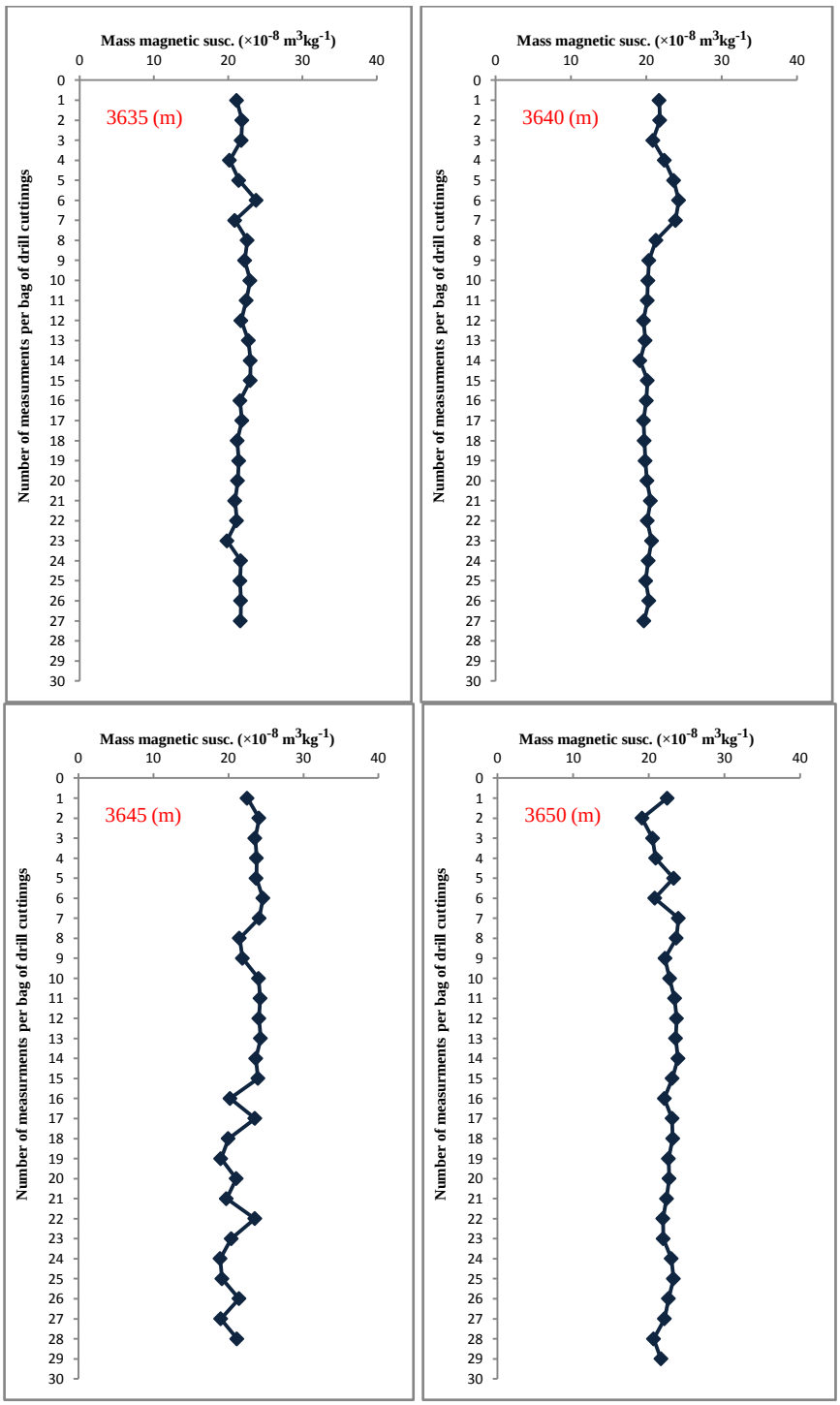
Mass magnetic susc. (×10-8 m3kg-1)
0 10 20 30 40
Number of measurments per bag of drill cuttings
3635 (m)
Mass magnetic susc. (×10-8 m3kg-1)
0 10 20 30 40
Number of measurments per bag of drill cuttings
3640 (m)
Mass magnetic susc. (×10-8 m3kg-1)
0 10 20 30 40
Number of measurments per bag of drill cuttings
3645 (m)
Mass magnetic susc. (×10-8 m3kg-1)
0 10 20 30 40
Number of measurments per bag of drill cuttings
3650 (m)

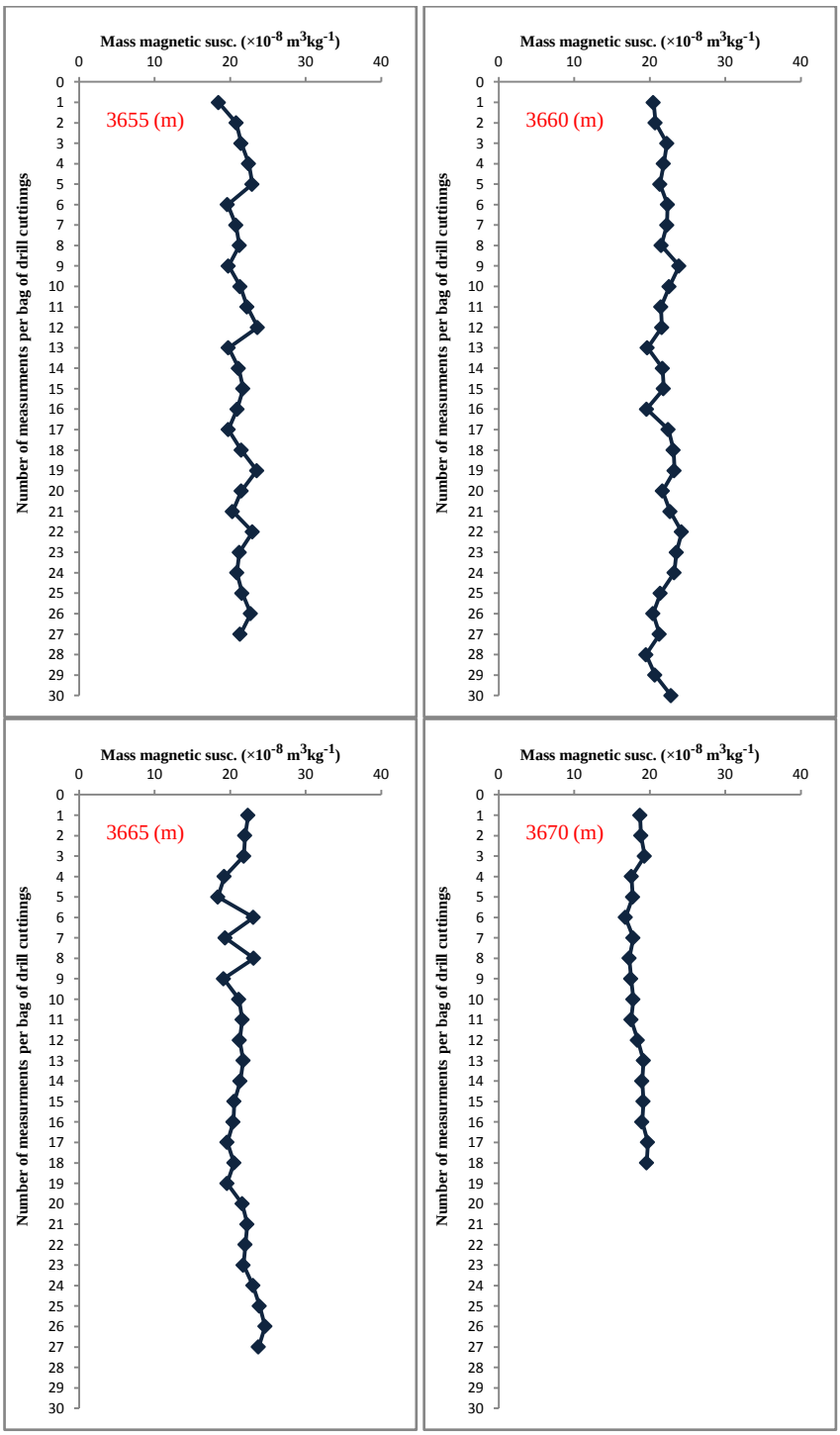
Mass magnetic susc. (×10-8 m3kg-1)
0
10
20
30
40
Number of measurments per bag of drill cuttings
3655 (m)
3660 (m)
3665 (m)
3670 (m)

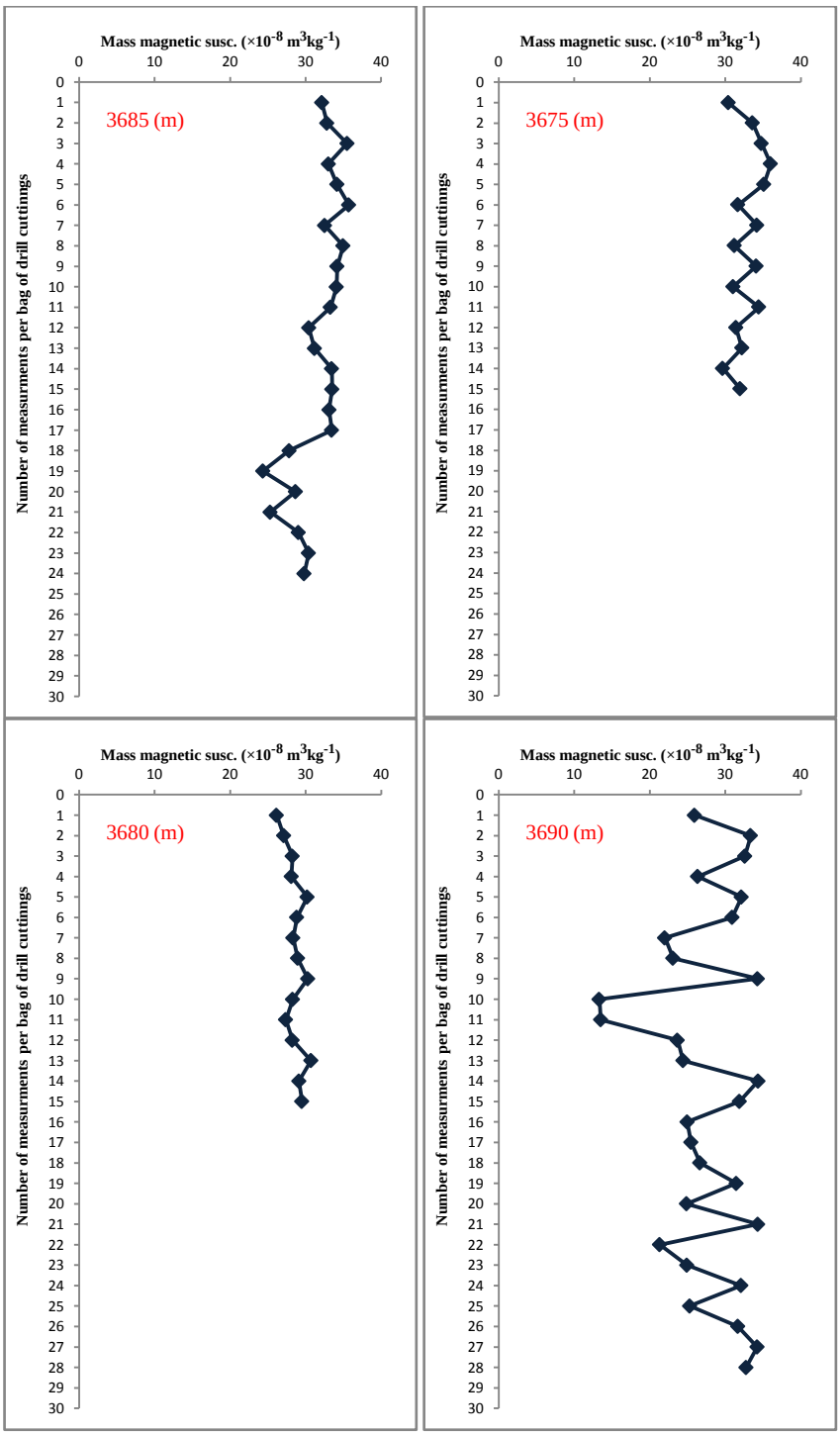
Mass magnetic susc. (×10-8 m3kg-1)
0 10 20 30 40
Number of measurments per bag of drill cuttings
3685 (m)
Mass magnetic susc. (×10-8 m3kg-1)
0 10 20 30 40
Number of measurments per bag of drill cuttings
3675 (m)
Mass magnetic susc. (×10-8 m3kg-1)
0 10 20 30 40
Number of measurments per bag of drill cuttings
3680 (m)
Mass magnetic susc. (×10-8 m3kg-1)
0 10 20 30 40
Number of measurments per bag of drill cuttings
3690 (m)

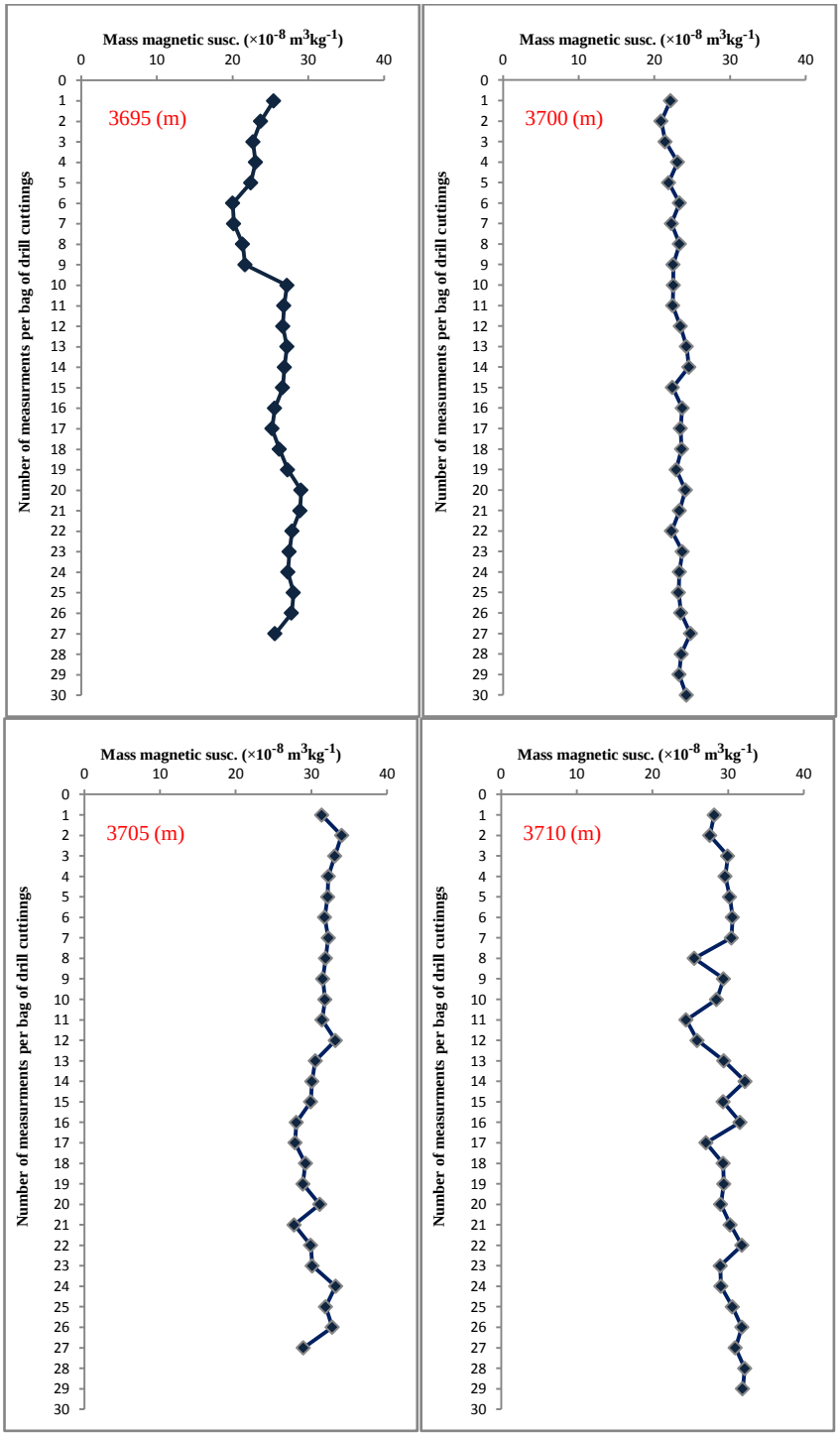
Mass magnetic susc. (×10-8 m3kg-1)
0 10 20 30 40
Number of measurments per bag of drill cuttings
3695 (m)
Mass magnetic susc. (×10-8 m3kg-1)
0 10 20 30 40
Number of measurments per bag of drill cuttings
3700 (m)
Mass magnetic susc. (×10-8 m3kg-1)
0 10 20 30 40
Number of measurments per bag of drill cuttings
3705 (m)
Mass magnetic susc. (×10-8 m3kg-1)
0 10 20 30 40
Number of measurments per bag of drill cuttings
3710 (m)

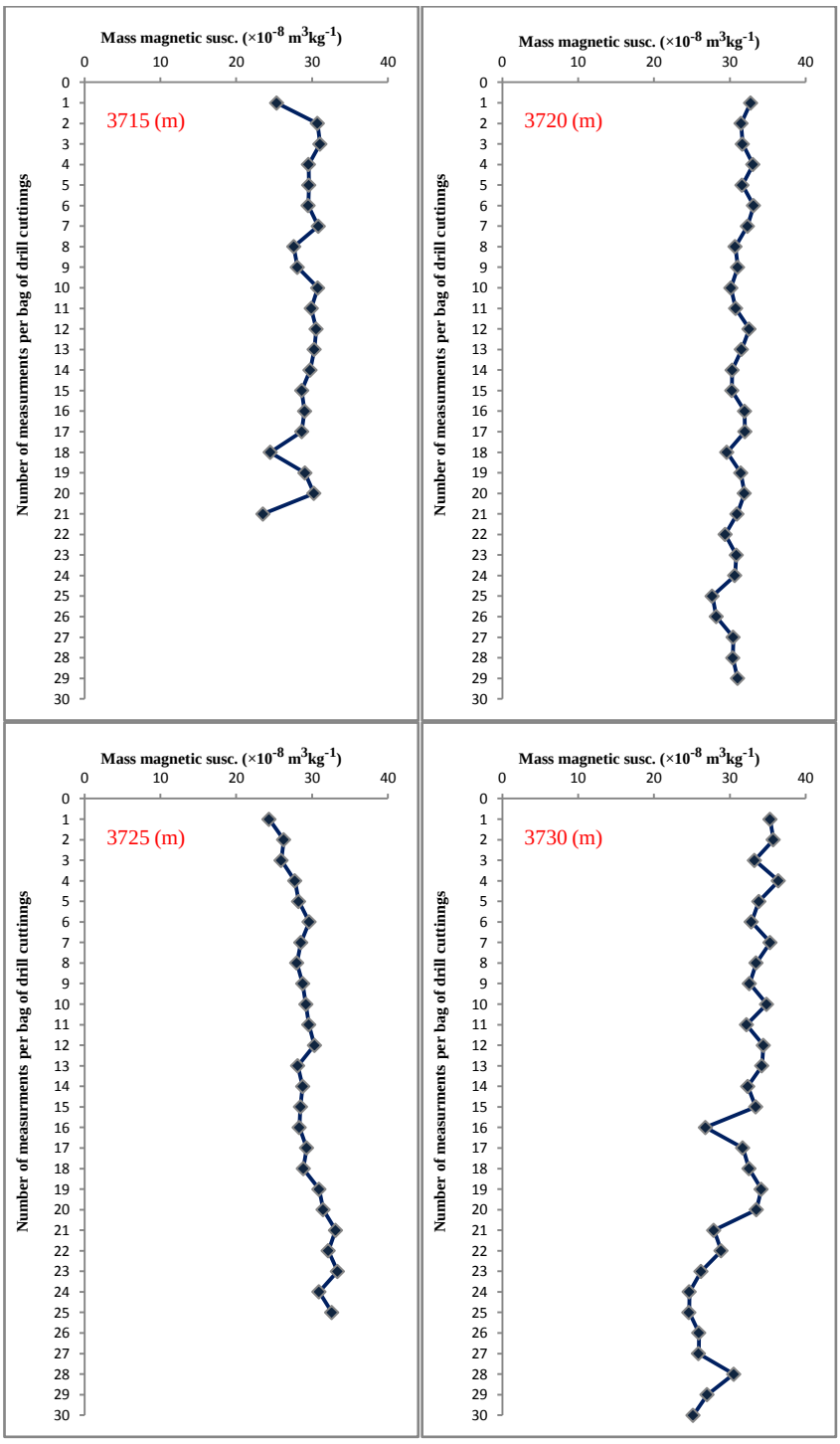
Mass magnetic susc. (×10-8 m3kg-1)
0
10
20
30
40
Number of measurments per bag of drill cuttings
3715 (m)
3720 (m)
3725 (m)
3730 (m)

Depth (m)	Mass magnetic susceptibility Well A2
3620	16.54
3625	18.6
3630	31.85
3635	20.17
3640	25.28
3645	24.14
3650	14.4
3655	16.15
3660	21.37
3665	33.08
3670	22.58
3675	13.27
3680	11.54
3685	26.39
3690	15.45
3695	11.86
3700	21.54
3705	13.07
3715	18.07
3720	60.21
3725	17.11
3730	20.17
3735	14.78
3740	21.57
3745	31.9
3750	96.97
3755	78.5
3760	67.95
3765	68.03
3770	39.25
3775	47.08
3780	53.73
3785	11.04
3790	78.95
3795	77.62
3800	88.53
3805	65.63
3810	24.93
3815	26.97
3820	22.5
3825	55.28
3830	54.82

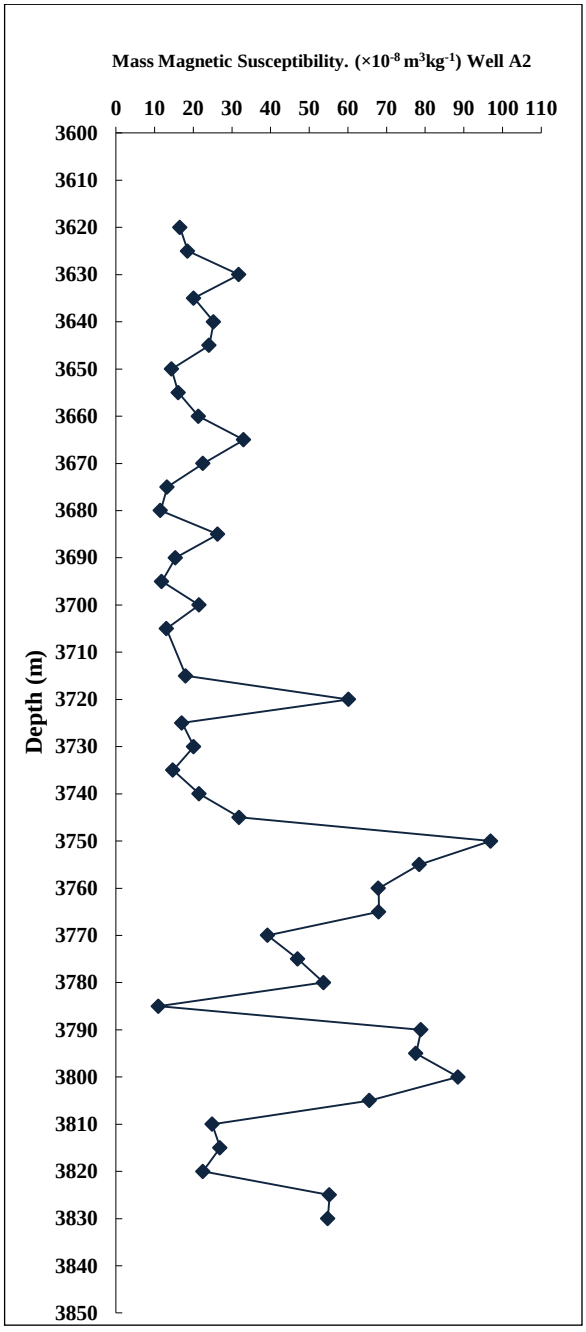

Depth (m)	Mass magnetic susceptibility Well A3
3595	20.907
3600	19.118
3605	21.04
3610	21.903
3615	19.113
3620	18.82
3625	20.803
3630	21.822
3635	21.769
3640	20.759
3645	22.183
3650	22.407
3655	21.38
3660	21.826
3665	21.456
3670	18.393
3675	32.808
3680	28.64
3685	31.804
3690	29.043
3695	25.49
3700	23.107
3705	30.991
3710	29.497
3715	28.902
3720	31.032
3725	29.307
3730	31.193

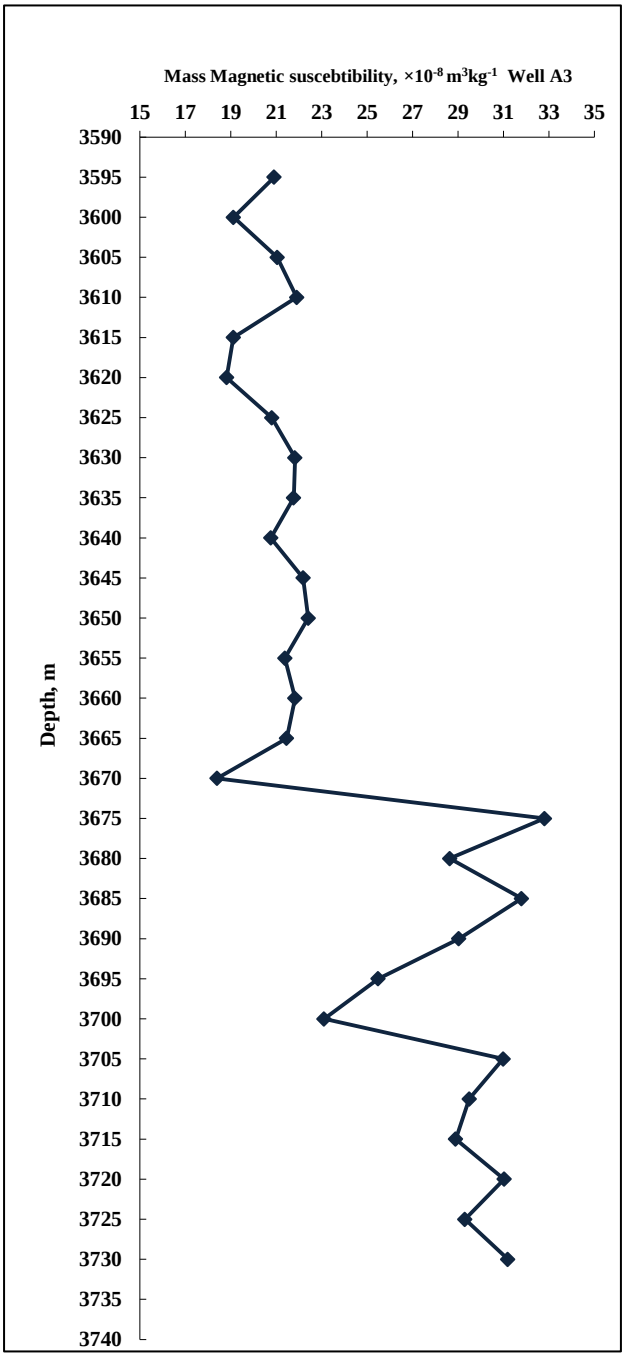

Depth (m)	Mass magnetic susceptibility Well A1
3576	8.763
3581	7.224
3586	16.76
3591	20.36
3596	16.76
3601	23.49
3606	11.28
3609	12.36
3612	17.43
3615	15.14
3618	13.61
3621	25.35
3624	32.39
3627	35.16
3630	23.05
3633	22.16
3636	15.18
3639	32.93
3642	32.36
3645	14.42
3648	21.62
3651	17.79
3654	22.52
3657	19.26
3663	22.38
3666	17.78
3669	13.84
3672	10.25
3675	30.04
3678	13
3681	11.71
3684	17.66
3687	20.02
3690	24.69
3693	11.17
3696	10.63
3699	10.78
3702	19.39
3705	37.7
3708	31.6
3711	9.475
3714	39.5
3717	11.71
3720	21.2
3723	24.04
3726	19.11
3729	29.68
3732	17.23
3735	11.76
3738	24.03
3741	17.26
3744	18.91
3747	69.39
3750	92.28
3753	63.05

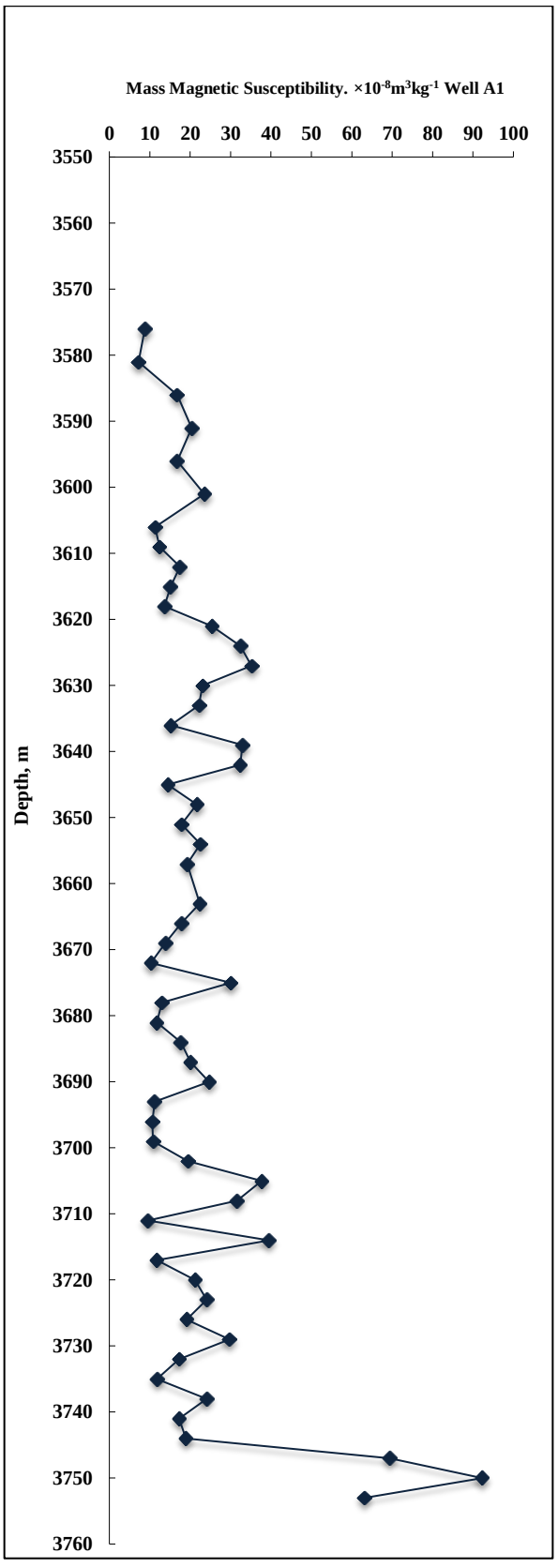

Appendix B

Data used in the X-plot between Magnetic Susceptibility (Mass & Volume) versus Bulk Density

Porosity (%)	Bulk Density of Quartz (g/cm3)	Volume Magnetic Susceptibility of Quartz (10^{-5} SI units)	Mass Magnetic Susceptibility of Quartz ($10^{-8} m^3 Kg^{-1}$)
0	2.650	-1.643	-0.620
0.01	2.634	-1.636	-0.621
0.02	2.617	-1.628	-0.622
0.03	2.601	-1.621	-0.623
0.04	2.584	-1.613	-0.624
0.05	2.568	-1.606	-0.625
0.06	2.551	-1.598	-0.627
0.07	2.535	-1.591	-0.628
0.08	2.518	-1.584	-0.629
0.09	2.502	-1.576	-0.630
0.1	2.485	-1.569	-0.631
0.11	2.469	-1.561	-0.632
0.12	2.452	-1.554	-0.634
0.13	2.436	-1.546	-0.635
0.14	2.419	-1.539	-0.636
0.15	2.4025	-1.532	-0.637
0.16	2.386	-1.524	-0.639
0.17	2.370	-1.517	-0.640
0.18	2.353	-1.509	-0.641
0.19	2.337	-1.502	-0.643
0.2	2.32	-1.494	-0.644
0.21	2.304	-1.487	-0.646
0.22	2.287	-1.480	-0.647
0.23	2.271	-1.472	-0.648
0.24	2.254	-1.465	-0.650
0.25	2.2375	-1.457	-0.651
0.26	2.221	-1.450	-0.653
0.27	2.205	-1.442	-0.654
0.28	2.188	-1.435	-0.656
0.29	2.172	-1.428	-0.657
0.3	2.155	-1.420	-0.659
0.31	2.139	-1.413	-0.661
0.32	2.122	-1.405	-0.662
0.33	2.106	-1.398	-0.664
0.34	2.089	-1.390	-0.666
0.35	2.0725	-1.383	-0.667
0.36	2.056	-1.376	-0.669
0.37	2.040	-1.368	-0.671
0.38	2.023	-1.361	-0.673
0.39	2.007	-1.353	-0.674
0.4	1.99	-1.346	-0.676

Porosity (%)	Bulk Density of Calcite (g/cm3)	Volume Magnetic Susceptibility of Calcite (10^{-5} SI units)	Mass Magnetic Susceptibility of Calcite ($10^{-8} m^3 Kg^{-1}$)
0	2.71	-1.301	-0.480
0.01	2.693	-1.297	-0.482
0.02	2.676	-1.293	-0.483
0.03	2.659	-1.289	-0.485
0.04	2.642	-1.285	-0.486
0.05	2.6245	-1.281	-0.488
0.06	2.607	-1.277	-0.490
0.07	2.590	-1.273	-0.491
0.08	2.573	-1.269	-0.493
0.09	2.556	-1.265	-0.495
0.1	2.539	-1.26072	-0.497
0.11	2.522	-1.257	-0.498
0.12	2.505	-1.253	-0.500
0.13	2.488	-1.249	-0.502
0.14	2.471	-1.245	-0.504
0.15	2.4535	-1.24068	-0.506
0.16	2.436	-1.237	-0.508
0.17	2.419	-1.233	-0.510
0.18	2.402	-1.229	-0.511
0.19	2.385	-1.225	-0.513
0.2	2.368	-1.22064	-0.515
0.21	2.351	-1.217	-0.518
0.22	2.334	-1.213	-0.520
0.23	2.317	-1.209	-0.522
0.24	2.300	-1.205	-0.524
0.25	2.2825	-1.2006	-0.526
0.26	2.265	-1.197	-0.528
0.27	2.248	-1.193	-0.530
0.28	2.231	-1.189	-0.533
0.29	2.214	-1.185	-0.535
0.3	2.197	-1.18056	-0.537
0.31	2.180	-1.177	-0.540
0.32	2.163	-1.173	-0.542
0.33	2.146	-1.169	-0.545
0.34	2.129	-1.165	-0.547
0.35	2.1115	-1.161	-0.550
0.36	2.094	-1.157	-0.552
0.37	2.077	-1.153	-0.555
0.38	2.060	-1.148	-0.557
0.39	2.043	-1.144	-0.560
0.4	2.026	-1.14048	-0.563

Porosity (%)	Bulk Density of Dolomite (g/cm3)	Volume Magnetic Susceptibility of Dolomite (10^{-5} SI units)	Mass Magnetic Susceptibility of Dolomite ($10^{-8} m^3 Kg^{-1}$)
0	2.870	-3.444	-1.2000
0.01	2.851	-3.419	-1.1989
0.02	2.833	-3.393	-1.1979
0.03	2.814	-3.368	-1.1968
0.04	2.795	-3.342	-1.1957
0.05	2.777	-3.317	-1.1946
0.06	2.758	-3.291	-1.1935
0.07	2.739	-3.266	-1.1923
0.08	2.720	-3.240	-1.1912
0.09	2.702	-3.215	-1.1900
0.1	2.683	-3.190	-1.1888
0.11	2.664	-3.164	-1.1876
0.12	2.646	-3.139	-1.1864
0.13	2.627	-3.113	-1.1852
0.14	2.608	-3.088	-1.1839
0.15	2.590	-3.062	-1.1826
0.16	2.571	-3.037	-1.1813
0.17	2.552	-3.012	-1.1800
0.18	2.533	-2.986	-1.1787
0.19	2.515	-2.961	-1.1773
0.2	2.496	-2.935	-1.1760
0.21	2.477	-2.910	-1.1746
0.22	2.459	-2.884	-1.1732
0.23	2.440	-2.859	-1.1717
0.24	2.421	-2.833	-1.1703
0.25	2.403	-2.808	-1.1688
0.26	2.384	-2.783	-1.1673
0.27	2.365	-2.757	-1.1658
0.28	2.346	-2.732	-1.1642
0.29	2.328	-2.706	-1.1626
0.3	2.309	-2.681	-1.1610
0.31	2.290	-2.655	-1.1594
0.32	2.272	-2.630	-1.1577
0.33	2.253	-2.604	-1.1561
0.34	2.234	-2.579	-1.1543
0.35	2.216	-2.554	-1.1526
0.36	2.197	-2.528	-1.1508
0.37	2.178	-2.503	-1.1490
0.38	2.159	-2.477	-1.1472
0.39	2.141	-2.452	-1.1453
0.4	2.122	-2.426	-1.1434

Data used in the X-plot between Magnetic Susceptibility (Mass &Volume) versus Transit Time

Porosity (%)	Sonic Transit Time (sec/ft)	Volume Magnetic Susceptibility of Quartz (10^{-5} SI units)	Mass Magnetic Susceptibility of Quartz ($10^{-8} m^3 Kg^{-1}$)
0	54.000	-1.643	-0.620
0.01	55.350	-1.636	-0.621
0.02	56.700	-1.628	-0.622
0.03	58.050	-1.621	-0.623
0.04	59.400	-1.613	-0.624
0.05	60.750	-1.606	-0.625
0.06	62.100	-1.598	-0.627
0.07	63.450	-1.591	-0.628
0.08	64.800	-1.584	-0.629
0.09	66.150	-1.576	-0.630
0.1	67.500	-1.569	-0.631
0.11	68.850	-1.561	-0.632
0.12	70.200	-1.554	-0.634
0.13	71.550	-1.546	-0.635
0.14	72.900	-1.539	-0.636
0.15	74.250	-1.532	-0.637
0.16	75.600	-1.524	-0.639
0.17	76.950	-1.517	-0.640
0.18	78.300	-1.509	-0.641
0.19	79.650	-1.502	-0.643
0.2	81.000	-1.494	-0.644
0.21	82.350	-1.487	-0.646
0.22	83.700	-1.480	-0.647
0.23	85.050	-1.472	-0.648
0.24	86.400	-1.465	-0.650
0.25	87.750	-1.457	-0.651
0.26	89.100	-1.450	-0.653
0.27	90.450	-1.442	-0.654
0.28	91.800	-1.435	-0.656
0.29	93.150	-1.428	-0.657
0.3	94.500	-1.420	-0.659
0.31	95.850	-1.413	-0.661
0.32	97.200	-1.405	-0.662
0.33	98.550	-1.398	-0.664
0.34	99.900	-1.390	-0.666
0.35	101.250	-1.383	-0.667
0.36	102.600	-1.376	-0.669
0.37	103.950	-1.368	-0.671
0.38	105.300	-1.361	-0.673
0.39	106.650	-1.353	-0.674
0.4	108.000	-1.346	-0.676

Porosity (%)	Sonic Transit Time (sec/ft)	Volume Magnetic Susceptibility of Calcite (10^{-5} SI units)	Mass Magnetic Susceptibility of Calcite ($10^{-8} m^3 Kg^{-1}$)
0	47.500	-1.301	-0.480
0.01	48.915	-1.297	-0.482
0.02	50.330	-1.293	-0.483
0.03	51.745	-1.289	-0.485
0.04	53.160	-1.285	-0.486
0.05	54.575	-1.281	-0.488
0.06	55.990	-1.277	-0.490
0.07	57.405	-1.273	-0.491
0.08	58.820	-1.269	-0.493
0.09	60.235	-1.265	-0.495
0.11	63.065	-1.257	-0.498
0.12	64.480	-1.253	-0.500
0.13	65.895	-1.249	-0.502
0.14	67.310	-1.245	-0.504
0.15	68.725	-1.241	-0.506
0.16	70.140	-1.237	-0.508
0.17	71.555	-1.233	-0.510
0.18	72.970	-1.229	-0.511
0.19	74.385	-1.225	-0.513
0.2	75.800	-1.221	-0.515
0.21	77.215	-1.217	-0.518
0.22	78.630	-1.213	-0.520
0.23	80.045	-1.209	-0.522
0.24	81.460	-1.205	-0.524
0.25	82.875	-1.201	-0.526
0.26	84.290	-1.197	-0.528
0.27	85.705	-1.193	-0.530
0.28	87.120	-1.189	-0.533
0.29	88.535	-1.185	-0.535
0.3	89.950	-1.181	-0.537
0.31	91.365	-1.177	-0.540
0.32	92.780	-1.173	-0.542
0.33	94.195	-1.169	-0.545
0.34	95.610	-1.165	-0.547
0.35	97.025	-1.161	-0.550
0.36	98.440	-1.157	-0.552
0.37	99.855	-1.153	-0.555
0.38	101.270	-1.148	-0.557
0.39	102.685	-1.144	-0.560
0.4	104.100	-1.140	-0.563

Porosity (%)	Sonic Transit Time (sec/ft)	Volume Magnetic Susceptibility of Dolomite (10^{-5} SI units)	Mass Magnetic Susceptibility of Dolomite ($10^{-8} m^3 Kg^{-1}$)
0	43.500	-3.444	-1.2000
0.01	44.955	-3.419	-1.1989
0.02	46.410	-3.393	-1.1979
0.03	47.865	-3.368	-1.1968
0.04	49.320	-3.342	-1.1957
0.05	50.775	-3.317	-1.1946
0.06	52.230	-3.291	-1.1935
0.07	53.685	-3.266	-1.1923
0.08	55.140	-3.240	-1.1912
0.09	56.595	-3.215	-1.1900
0.1	58.050	-3.190	-1.1888
0.11	59.505	-3.164	-1.1876
0.12	60.960	-3.139	-1.1864
0.13	62.415	-3.113	-1.1852
0.14	63.870	-3.088	-1.1839
0.15	65.325	-3.062	-1.1826
0.16	66.780	-3.037	-1.1813
0.17	68.235	-3.012	-1.1800
0.18	69.690	-2.986	-1.1787
0.19	71.145	-2.961	-1.1773
0.2	72.600	-2.935	-1.1760
0.21	74.055	-2.910	-1.1746
0.22	75.510	-2.884	-1.1732
0.23	76.965	-2.859	-1.1717
0.24	78.420	-2.833	-1.1703
0.25	79.875	-2.808	-1.1688
0.26	81.330	-2.783	-1.1673
0.27	82.785	-2.757	-1.1658
0.28	84.240	-2.732	-1.1642
0.29	85.695	-2.706	-1.1626
0.3	87.150	-2.681	-1.1610
0.31	88.605	-2.655	-1.1594
0.32	90.060	-2.630	-1.1577
0.33	91.515	-2.604	-1.1561
0.34	92.970	-2.579	-1.1543
0.35	94.425	-2.554	-1.1526
0.36	95.880	-2.528	-1.1508
0.37	97.335	-2.503	-1.1490
0.38	98.790	-2.477	-1.1472
0.39	100.245	-2.452	-1.1453
0.4	101.700	-2.426	-1.1434

Effect of Illite Clay on Mass Magnetic Susceptibility and Bulk Density

Porosity (%)	Bulk Density of 100% Quartz (g/cm3)	Volume Magnetic Susceptibility of Quartz (10^{-5} SI units)	Mass Magnetic Susceptibility of Quartz ($10^{-8} m^3 Kg^{-1}$)
0	2.650	-1.643	-0.620
0.01	2.634	-1.636	-0.621
0.02	2.617	-1.628	-0.622
0.03	2.601	-1.621	-0.623
0.04	2.584	-1.613	-0.624
0.05	2.568	-1.606	-0.625
0.06	2.551	-1.598	-0.627
0.07	2.535	-1.591	-0.628
0.08	2.518	-1.584	-0.629
0.09	2.502	-1.576	-0.630
0.1	2.485	-1.569	-0.631
0.11	2.469	-1.561	-0.632
0.12	2.452	-1.554	-0.634
0.13	2.436	-1.546	-0.635
0.14	2.419	-1.539	-0.636
0.15	2.4025	-1.532	-0.637
0.16	2.386	-1.524	-0.639
0.17	2.370	-1.517	-0.640
0.18	2.353	-1.509	-0.641
0.19	2.337	-1.502	-0.643
0.2	2.32	-1.494	-0.644
0.21	2.304	-1.487	-0.646
0.22	2.287	-1.480	-0.647
0.23	2.271	-1.472	-0.648
0.24	2.254	-1.465	-0.650
0.25	2.2375	-1.457	-0.651
0.26	2.221	-1.450	-0.653
0.27	2.205	-1.442	-0.654
0.28	2.188	-1.435	-0.656
0.29	2.172	-1.428	-0.657
0.3	2.155	-1.420	-0.659
0.31	2.139	-1.413	-0.661
0.32	2.122	-1.405	-0.662
0.33	2.106	-1.398	-0.664
0.34	2.089	-1.390	-0.666
0.35	2.0725	-1.383	-0.667
0.36	2.056	-1.376	-0.669
0.37	2.040	-1.368	-0.671
0.38	2.023	-1.361	-0.673
0.39	2.007	-1.353	-0.674
0.4	1.99	-1.346	-0.676

Porosity (%)	Bulk Density of 95% Quartz+ 5% Illite (g/cm3)	Volume Magnetic Susceptibility of 95% Quartz+ 5% Illite (10^{-5} SI units)	Mass Magnetic Susceptibility of 95% Quartz + 5% ($10^{-8} m^3 Kg^{-1}$)
0	2.655	0.4892	0.1842
0.01	2.63944	0.4753	0.1801
0.02	2.62288	0.4614	0.1759
0.03	2.60632	0.4475	0.1717
0.04	2.58976	0.4336	0.1674
0.05	2.5732	0.4197	0.1631
0.06	2.55664	0.4058	0.1587
0.07	2.54008	0.3919	0.1543
0.08	2.52352	0.3780	0.1498
0.09	2.50696	0.3641	0.1452
0.1	2.4904	0.3502	0.1406
0.11	2.47384	0.3363	0.1360
0.12	2.45728	0.3225	0.1312
0.13	2.44072	0.3086	0.1264
0.14	2.42416	0.2947	0.1216
0.15	2.4076	0.2808	0.1166
0.16	2.39104	0.2669	0.1116
0.17	2.37448	0.2530	0.1065
0.18	2.35792	0.2391	0.1014
0.19	2.34136	0.2252	0.0962
0.2	2.3248	0.2113	0.0909
0.21	2.30824	0.1974	0.0855
0.22	2.29168	0.1835	0.0801
0.23	2.27512	0.1696	0.0746
0.24	2.25856	0.1558	0.0690
0.25	2.242	0.1419	0.0633
0.26	2.22544	0.1280	0.0575
0.27	2.20888	0.1141	0.0516
0.28	2.19232	0.1002	0.0457
0.29	2.17576	0.0863	0.0397
0.3	2.1592	0.0724	0.0335
0.31	2.14264	0.0585	0.0273
0.32	2.12608	0.0446	0.0210
0.33	2.10952	0.0307	0.0146
0.34	2.09296	0.0168	0.0080
0.35	2.0764	0.0029	0.0014
0.36	2.05984	-0.0109	-0.0053
0.37	2.04328	-0.0248	-0.0122
0.38	2.02672	-0.0387	-0.0191
0.39	2.01016	-0.0526	-0.0262
0.4	1.9936	-0.0665	-0.0334

Porosity (%)	Bulk Density of 90% Quartz+10% Illite (g/cm3)	Volume Magnetic Susceptibility of 90% Quartz+10% Illite (10^{-5} SI units)	Mass Magnetic Susceptibility of 90% Quartz+10% Illite ($10^{-8}m^3Kg^{-1}$)
0	2.66	2.78825	1.0482
0.01	2.6434	2.7513675	1.0408
0.02	2.6268	2.714485	1.0334
0.03	2.6102	2.6776025	1.0258
0.04	2.5936	2.64072	1.0182
0.05	2.577	2.6038375	1.0104
0.06	2.5604	2.566955	1.0026
0.07	2.5438	2.5300725	0.9946
0.08	2.5272	2.49319	0.9865
0.09	2.5106	2.4563075	0.9784
0.1	2.494	2.419425	0.9701
0.11	2.4774	2.3825425	0.9617
0.12	2.4608	2.34566	0.9532
0.13	2.4442	2.3087775	0.9446
0.14	2.4276	2.271895	0.9359
0.15	2.411	2.2350125	0.9270
0.16	2.3944	2.19813	0.9180
0.17	2.3778	2.1612475	0.9089
0.18	2.3612	2.124365	0.8997
0.19	2.3446	2.0874825	0.8903
0.2	2.328	2.0506	0.8808
0.21	2.3114	2.0137175	0.8712
0.22	2.2948	1.976835	0.8614
0.23	2.2782	1.9399525	0.8515
0.24	2.2616	1.90307	0.8415
0.25	2.245	1.8661875	0.8313
0.26	2.2284	1.829305	0.8209
0.27	2.2118	1.7924225	0.8104
0.28	2.1952	1.75554	0.7997
0.29	2.1786	1.7186575	0.7889
0.3	2.162	1.681775	0.7779
0.31	2.1454	1.6448925	0.7667
0.32	2.1288	1.60801	0.7554
0.33	2.1122	1.5711275	0.7438
0.34	2.0956	1.534245	0.7321
0.35	2.079	1.4973625	0.7202
0.36	2.0624	1.46048	0.7081
0.37	2.0458	1.4235975	0.6959
0.38	2.0292	1.386715	0.6834
0.39	2.0126	1.3498325	0.6707
0.4	1.996	1.31295	0.6578

Porosity (%)	Bulk Density of 80% Quartz+20% Illite (g/cm3)	Volume Magnetic Susceptibility of 80% Quartz+20% Illite (10^{-5} SI units)	Mass Magnetic Susceptibility of 80% Quartz+20% Illite ($10^{-8}m^3Kg^{-1}$)
0	2.67	6.8856	2.578876
0.01	2.6533	6.807744	2.565765
0.02	2.6366	6.729888	2.552487
0.03	2.6199	6.652032	2.53904
0.04	2.6032	6.574176	2.525421
0.05	2.5865	6.49632	2.511626
0.06	2.5698	6.418464	2.497651
0.07	2.5531	6.340608	2.483494
0.08	2.5364	6.262752	2.46915
0.09	2.5197	6.184896	2.454616
0.1	2.503	6.10704	2.439888
0.11	2.4863	6.029184	2.424962
0.12	2.4696	5.951328	2.409835
0.13	2.4529	5.873472	2.394501
0.14	2.4362	5.795616	2.378957
0.15	2.4195	5.71776	2.363199
0.16	2.4028	5.639904	2.347222
0.17	2.3861	5.562048	2.33102
0.18	2.3694	5.484192	2.314591
0.19	2.3527	5.406336	2.297928
0.2	2.336	5.32848	2.281027
0.21	2.3193	5.250624	2.263883
0.22	2.3026	5.172768	2.24649
0.23	2.2859	5.094912	2.228843
0.24	2.2692	5.017056	2.210936
0.25	2.2525	4.9392	2.192764
0.26	2.2358	4.861344	2.17432
0.27	2.2191	4.783488	2.155598
0.28	2.2024	4.705632	2.136593
0.29	2.1857	4.627776	2.117297
0.3	2.169	4.54992	2.097704
0.31	2.1523	4.472064	2.077807
0.32	2.1356	4.394208	2.057599
0.33	2.1189	4.316352	2.037072
0.34	2.1022	4.238496	2.016219
0.35	2.0855	4.16064	1.995032
0.36	2.0688	4.082784	1.973503
0.37	2.0521	4.004928	1.951624
0.38	2.0354	3.927072	1.929386
0.39	2.0187	3.849216	1.90678
0.4	2.002	3.77136	1.883796

Porosity (%)	Bulk Density of 60% Quartz+40% Illite (g/cm3)	Volume Magnetic Susceptibility of 60% Quartz+40% Illite (10^{-5} SI units)	Mass Magnetic Susceptibility of 60% Quartz+40% Illite ($10^{-8} m^3 Kg^{-1}$)
0	2.69	15.4142	5.7302
0.01	2.6731	15.2511	5.7054
0.02	2.6562	15.0879	5.6803
0.03	2.6393	14.9248	5.6548
0.04	2.6224	14.7616	5.6291
0.05	2.6055	14.5985	5.6030
0.06	2.5886	14.4353	5.5765
0.07	2.5717	14.2722	5.5497
0.08	2.5548	14.1091	5.5226
0.09	2.5379	13.9459	5.4951
0.1	2.521	13.7828	5.4672
0.11	2.5041	13.6196	5.4389
0.12	2.4872	13.4565	5.4103
0.13	2.4703	13.2934	5.3813
0.14	2.4534	13.1302	5.3518
0.15	2.4365	12.9671	5.3220
0.16	2.4196	12.8039	5.2918
0.17	2.4027	12.6408	5.2611
0.18	2.3858	12.4776	5.2300
0.19	2.3689	12.3145	5.1984
0.2	2.352	12.1514	5.1664
0.21	2.3351	11.9882	5.1339
0.22	2.3182	11.8251	5.1010
0.23	2.3013	11.6619	5.0675
0.24	2.2844	11.4988	5.0336
0.25	2.2675	11.3357	4.9992
0.26	2.2506	11.1725	4.9642
0.27	2.2337	11.0094	4.9288
0.28	2.2168	10.8462	4.8927
0.29	2.1999	10.6831	4.8562
0.3	2.183	10.5199	4.8190
0.31	2.1661	10.3568	4.7813
0.32	2.1492	10.1937	4.7430
0.33	2.1323	10.0305	4.7041
0.34	2.1154	9.8674	4.6645
0.35	2.0985	9.7042	4.6244
0.36	2.0816	9.5411	4.5835
0.37	2.0647	9.3779	4.5420
0.38	2.0478	9.2148	4.4999
0.39	2.0309	9.0517	4.4570
0.4	2.014	8.8885	4.4134

Porosity (%)	Bulk Density of 40% Quartz+60% Illite (g/cm3)	Volume Magnetic Susceptibility of 40% Quartz+60% Illite (10^{-5} SI units)	Mass Magnetic Susceptibility of 40% Quartz+60% Illite ($10^{-8}m^3Kg^{-1}$)
0	2.7100	23.9428	8.8350
0.01	2.6929	23.6944	8.7988
0.02	2.6758	23.4459	8.7622
0.03	2.6587	23.1975	8.7251
0.04	2.6416	22.9491	8.6876
0.05	2.6245	22.7007	8.6495
0.06	2.6074	22.4522	8.6110
0.07	2.5903	22.2038	8.5719
0.08	2.5732	21.9554	8.5323
0.09	2.5561	21.7069	8.4922
0.1	2.5390	21.4585	8.4516
0.11	2.5219	21.2101	8.4104
0.12	2.5048	20.9617	8.3686
0.13	2.4877	20.7132	8.3263
0.14	2.4706	20.4648	8.2833
0.15	2.4535	20.2164	8.2398
0.16	2.4364	19.9680	8.1957
0.17	2.4193	19.7195	8.1509
0.18	2.4022	19.4711	8.1055
0.19	2.3851	19.2227	8.0595
0.2	2.3680	18.9742	8.0128
0.21	2.3509	18.7258	7.9654
0.22	2.3338	18.4774	7.9173
0.23	2.3167	18.2290	7.8685
0.24	2.2996	17.9805	7.8190
0.25	2.2825	17.7321	7.7687
0.26	2.2654	17.4837	7.7177
0.27	2.2483	17.2352	7.6659
0.28	2.2312	16.9868	7.6133
0.29	2.2141	16.7384	7.5599
0.3	2.1970	16.4900	7.5057
0.31	2.1799	16.2415	7.4506
0.32	2.1628	15.9931	7.3946
0.33	2.1457	15.7447	7.3378
0.34	2.1286	15.4962	7.2800
0.35	2.1115	15.2478	7.2213
0.36	2.0944	14.9994	7.1617
0.37	2.0773	14.7510	7.1010
0.38	2.0602	14.5025	7.0394
0.39	2.0431	14.2541	6.9767
0.4	2.0260	14.0057	6.9130

Porosity (%)	Bulk Density of 20% Quartz+80% Illite (g/cm3)	Volume Magnetic Susceptibility of 20% Quartz+80% Illite (10^{-5} SI units)	Mass Magnetic Susceptibility of 20% Quartz+80% Illite ($10^{-8} m^3 Kg^{-1}$)
0	2.7300	32.4714	11.8943
0.01	2.7127	32.1377	11.8471
0.02	2.6954	31.8040	11.7994
0.03	2.6781	31.4703	11.7510
0.04	2.6608	31.1365	11.7019
0.05	2.6435	30.8028	11.6523
0.06	2.6262	30.4691	11.6020
0.07	2.6089	30.1354	11.5510
0.08	2.5916	29.8017	11.4993
0.09	2.5743	29.4680	11.4470
0.1	2.5570	29.1343	11.3939
0.11	2.5397	28.8005	11.3401
0.12	2.5224	28.4668	11.2856
0.13	2.5051	28.1331	11.2303
0.14	2.4878	27.7994	11.1743
0.15	2.4705	27.4657	11.1175
0.16	2.4532	27.1320	11.0598
0.17	2.4359	26.7983	11.0014
0.18	2.4186	26.4645	10.9421
0.19	2.4013	26.1308	10.8820
0.2	2.3840	25.7971	10.8209
0.21	2.3667	25.4634	10.7590
0.22	2.3494	25.1297	10.6962
0.23	2.3321	24.7960	10.6325
0.24	2.3148	24.4623	10.5678
0.25	2.2975	24.1286	10.5021
0.26	2.2802	23.7948	10.4354
0.27	2.2629	23.4611	10.3677
0.28	2.2456	23.1274	10.2990
0.29	2.2283	22.7937	10.2292
0.3	2.2110	22.4600	10.1583
0.31	2.1937	22.1263	10.0863
0.32	2.1764	21.7926	10.0131
0.33	2.1591	21.4588	9.9388
0.34	2.1418	21.1251	9.8633
0.35	2.1245	20.7914	9.7865
0.36	2.1072	20.4577	9.7085
0.37	2.0899	20.1240	9.6292
0.38	2.0726	19.7903	9.5485
0.39	2.0553	19.4566	9.4665
0.4	2.0380	19.1228	9.3831

Porosity (%)	Bulk Density Of 100% Illite (g/cm3)	Volume Magnetic Susceptibility Of 100% Illite (10^{-5} SI units)	Mass Magnetic Susceptibility Of 100% Illite ($10^{-8} m^3 Kg^{-1}$)
0	2.75	41	14.9091
0.01	2.733	40.581	14.8485
0.02	2.716	40.162	14.7872
0.03	2.699	39.743	14.7251
0.04	2.682	39.324	14.6622
0.05	2.665	38.905	14.5985
0.06	2.648	38.486	14.5340
0.07	2.631	38.067	14.4686
0.08	2.614	37.648	14.4024
0.09	2.597	37.229	14.3354
0.1	2.58	36.81	14.2674
0.11	2.563	36.391	14.1986
0.12	2.546	35.972	14.1288
0.13	2.529	35.553	14.0581
0.14	2.512	35.134	13.9865
0.15	2.495	34.715	13.9138
0.16	2.478	34.296	13.8402
0.17	2.461	33.877	13.7655
0.18	2.444	33.458	13.6899
0.19	2.427	33.039	13.6131
0.2	2.41	32.62	13.5353
0.21	2.393	32.201	13.4563
0.22	2.376	31.782	13.3763
0.23	2.359	31.363	13.2950
0.24	2.342	30.944	13.2126
0.25	2.325	30.525	13.1290
0.26	2.308	30.106	13.0442
0.27	2.291	29.687	12.9581
0.28	2.274	29.268	12.8707
0.29	2.257	28.849	12.7820
0.3	2.24	28.43	12.6920
0.31	2.223	28.011	12.6005
0.32	2.206	27.592	12.5077
0.33	2.189	27.173	12.4134
0.34	2.172	26.754	12.3177
0.35	2.155	26.335	12.2204
0.36	2.138	25.916	12.1216
0.37	2.121	25.497	12.0212
0.38	2.104	25.078	11.9192
0.39	2.087	24.659	11.8155
0.4	2.07	24.24	11.7101

Effect of Small Increases of Illite present in Quartz Matrix on Mass Magnetic Susceptibility and Bulk Density.

Porosity (%)	Bulk Density Of 100% Quartz (g/cm3)	Volume Magnetic Susceptibility Of 100% Quartz (10^{-5} SI units)	Mass Magnetic Susceptibility Of 100% Quartz ($10^{-8} m^3 Kg^{-1}$)
0	2.650	-1.643	-0.620
0.01	2.634	-1.636	-0.621
0.02	2.617	-1.628	-0.622
0.03	2.601	-1.621	-0.623
0.04	2.584	-1.613	-0.624
0.05	2.568	-1.606	-0.625
0.06	2.551	-1.598	-0.627
0.07	2.535	-1.591	-0.628
0.08	2.518	-1.584	-0.629
0.09	2.502	-1.576	-0.630
0.1	2.485	-1.569	-0.631
0.11	2.469	-1.561	-0.632
0.12	2.452	-1.554	-0.634
0.13	2.436	-1.546	-0.635
0.14	2.419	-1.539	-0.636
0.15	2.4025	-1.532	-0.637
0.16	2.386	-1.524	-0.639
0.17	2.370	-1.517	-0.640
0.18	2.353	-1.509	-0.641
0.19	2.337	-1.502	-0.643
0.2	2.32	-1.494	-0.644
0.21	2.304	-1.487	-0.646
0.22	2.287	-1.480	-0.647
0.23	2.271	-1.472	-0.648
0.24	2.254	-1.465	-0.650
0.25	2.2375	-1.457	-0.651
0.26	2.221	-1.450	-0.653
0.27	2.205	-1.442	-0.654
0.28	2.188	-1.435	-0.656
0.29	2.172	-1.428	-0.657
0.3	2.155	-1.420	-0.659
0.31	2.139	-1.413	-0.661
0.32	2.122	-1.405	-0.662
0.33	2.106	-1.398	-0.664
0.34	2.089	-1.390	-0.666
0.35	2.0725	-1.383	-0.667
0.36	2.056	-1.376	-0.669
0.37	2.040	-1.368	-0.671
0.38	2.023	-1.361	-0.673
0.39	2.007	-1.353	-0.674
0.4	1.99	-1.346	-0.676

Porosity (%)	Bulk Density Of 99% Quartz+1% Illite (g/cm3)	Volume Magnetic Susceptibility Of 99% Quartz+1% Illite (10^{-5} SI units)	Mass Magnetic Susceptibility Of 99% Quartz+1% Illite ($10^{-8}m^3Kg^{-1}$)
0	2.65100	-2.6213	-0.9888
0.01	2.63449	-2.6041	-0.9885
0.02	2.61798	-2.5869	-0.9881
0.03	2.60147	-2.5697	-0.9878
0.04	2.58496	-2.5524	-0.9874
0.05	2.56845	-2.5352	-0.9871
0.06	2.55194	-2.5180	-0.9867
0.07	2.53543	-2.5008	-0.9863
0.08	2.51892	-2.4836	-0.9860
0.09	2.50241	-2.4664	-0.9856
0.1	2.48590	-2.4492	-0.9852
0.11	2.46939	-2.4320	-0.9848
0.12	2.45288	-2.4147	-0.9845
0.13	2.43637	-2.3975	-0.9841
0.14	2.41986	-2.3803	-0.9837
0.15	2.40335	-2.3631	-0.9833
0.16	2.38684	-2.3459	-0.9828
0.17	2.37033	-2.3287	-0.9824
0.18	2.35382	-2.3115	-0.9820
0.19	2.33731	-2.2943	-0.9816
0.2	2.32080	-2.2770	-0.9811
0.21	2.30429	-2.2598	-0.9807
0.22	2.28778	-2.2426	-0.9803
0.23	2.27127	-2.2254	-0.9798
0.24	2.25476	-2.2082	-0.9793
0.25	2.23825	-2.1910	-0.9789
0.26	2.22174	-2.1738	-0.9784
0.27	2.20523	-2.1565	-0.9779
0.28	2.18872	-2.1393	-0.9774
0.29	2.17221	-2.1221	-0.9769
0.3	2.15570	-2.1049	-0.9764
0.31	2.13919	-2.0877	-0.9759
0.32	2.12268	-2.0705	-0.9754
0.33	2.10617	-2.0533	-0.9749
0.34	2.08966	-2.0361	-0.9743
0.35	2.07315	-2.0188	-0.9738
0.36	2.05664	-2.0016	-0.9733
0.37	2.04013	-1.9844	-0.9727
0.38	2.02362	-1.9672	-0.9721
0.39	2.00711	-1.9500	-0.9715
0.4	1.99060	-1.9328	-0.9710

Porosity (%)	Bulk Density Of 98% Quartz+2% Illite (g/cm3)	Volume Magnetic Susceptibility Of 98% Quartz+2% Illite (10^{-5} SI units)	Mass Magnetic Susceptibility Of 98% Quartz+2% Illite ($10^{-8}m^3Kg^{-1}$)
0	2.6520	-0.7900	-0.2979
0.01	2.6355	-0.7911	-0.30
0.02	2.6190	-0.7922	-0.30
0.03	2.6024	-0.7933	-0.30
0.04	2.5859	-0.7944	-0.31
0.05	2.5694	-0.7955	-0.3096
0.06	2.5529	-0.7966	-0.31
0.07	2.5364	-0.7977	-0.31
0.08	2.5198	-0.7988	-0.32
0.09	2.5033	-0.7999	-0.32
0.1	2.4868	-0.8010	-0.3221
0.11	2.4703	-0.8021	-0.32
0.12	2.4538	-0.8032	-0.33
0.13	2.4372	-0.8043	-0.33
0.14	2.4207	-0.8054	-0.33
0.15	2.4042	-0.8065	-0.3355
0.16	2.3877	-0.8076	-0.34
0.17	2.3712	-0.8087	-0.34
0.18	2.3546	-0.8098	-0.34
0.19	2.3381	-0.8109	-0.35
0.2	2.3216	-0.8120	-0.3498
0.21	2.3051	-0.8131	-0.35
0.22	2.2886	-0.8142	-0.36
0.23	2.2720	-0.8153	-0.36
0.24	2.2555	-0.8164	-0.36
0.25	2.2390	-0.8175	-0.3651
0.26	2.2225	-0.8186	-0.37
0.27	2.2060	-0.8197	-0.37
0.28	2.1894	-0.8208	-0.37
0.29	2.1729	-0.8219	-0.38
0.3	2.1564	-0.8230	-0.3817
0.31	2.1399	-0.8241	-0.39
0.32	2.1234	-0.8252	-0.39
0.33	2.1068	-0.8263	-0.39
0.34	2.0903	-0.8274	-0.40
0.35	2.0738	-0.8285	-0.3995
0.36	2.0573	-0.8296	-0.40
0.37	2.0408	-0.8307	-0.41
0.38	2.0242	-0.8318	-0.41
0.39	2.0077	-0.8329	-0.41
0.4	1.9912	-0.8340	-0.4188

Porosity (%)	Bulk Density Of 97% Quartz+3% Illite (g/cm3)	Volume Magnetic Susceptibility Of 97% Quartz+3% Illite (10^{-5} SI units)	Mass Magnetic Susceptibility Of 97% Quartz+3% Illite ($10^{-8} m^3 Kg^{-1}$)
0	2.653	-0.3640	-0.1372
0.01	2.63647	-0.3694	-0.1401
0.02	2.61994	-0.3747	-0.1430
0.03	2.60341	-0.3801	-0.1460
0.04	2.58688	-0.3854	-0.1490
0.05	2.57035	-0.3908	-0.1520
0.06	2.55382	-0.3962	-0.1551
0.07	2.53729	-0.4015	-0.1582
0.08	2.52076	-0.4069	-0.1614
0.09	2.50423	-0.4122	-0.1646
0.1	2.4877	-0.4176	-0.1679
0.11	2.47117	-0.4230	-0.1712
0.12	2.45464	-0.4283	-0.1745
0.13	2.43811	-0.4337	-0.1779
0.14	2.42158	-0.4390	-0.1813
0.15	2.40505	-0.4444	-0.1848
0.16	2.38852	-0.4498	-0.1883
0.17	2.37199	-0.4551	-0.1919
0.18	2.35546	-0.4605	-0.1955
0.19	2.33893	-0.4658	-0.1992
0.2	2.3224	-0.4712	-0.2029
0.21	2.30587	-0.4766	-0.2067
0.22	2.28934	-0.4819	-0.2105
0.23	2.27281	-0.4873	-0.2144
0.24	2.25628	-0.4926	-0.2183
0.25	2.23975	-0.4980	-0.2223
0.26	2.22322	-0.5034	-0.2264
0.27	2.20669	-0.5087	-0.2305
0.28	2.19016	-0.5141	-0.2347
0.29	2.17363	-0.5194	-0.2390
0.3	2.1571	-0.5248	-0.2433
0.31	2.14057	-0.5302	-0.2477
0.32	2.12404	-0.5355	-0.2521
0.33	2.10751	-0.5409	-0.2566
0.34	2.09098	-0.5462	-0.2612
0.35	2.07445	-0.5516	-0.2659
0.36	2.05792	-0.5570	-0.2706
0.37	2.04139	-0.5623	-0.2755
0.38	2.02486	-0.5677	-0.2804
0.39	2.00833	-0.5730	-0.2853
0.4	1.9918	-0.5784	-0.2904

Porosity (%)	Bulk Density Of 96% Quartz+4% Illite (g/cm3)	Volume Magnetic Susceptibility Of 96% Quartz+4% Illite (10^{-5} SI units)	Mass Magnetic Susceptibility Of 96% Quartz+4% Illite ($10^{-8} m^3 Kg^{-1}$)
0	2.654	0.0630	0.0237
0.01	2.63746	0.0534	0.0202
0.02	2.62092	0.0437	0.0167
0.03	2.60438	0.0341	0.0131
0.04	2.58784	0.0245	0.0095
0.05	2.5713	0.0149	0.0058
0.06	2.55476	0.0052	0.0020
0.07	2.53822	-0.0044	-0.0017
0.08	2.52168	-0.0140	-0.0056
0.09	2.50514	-0.0237	-0.0094
0.1	2.4886	-0.0333	-0.0134
0.11	2.47206	-0.0429	-0.0174
0.12	2.45552	-0.0526	-0.0214
0.13	2.43898	-0.0622	-0.0255
0.14	2.42244	-0.0718	-0.0296
0.15	2.4059	-0.0815	-0.0339
0.16	2.38936	-0.0911	-0.0381
0.17	2.37282	-0.1007	-0.0424
0.18	2.35628	-0.1103	-0.0468
0.19	2.33974	-0.1200	-0.0513
0.2	2.3232	-0.1296	-0.0558
0.21	2.30666	-0.1392	-0.0604
0.22	2.29012	-0.1489	-0.0650
0.23	2.27358	-0.1585	-0.0697
0.24	2.25704	-0.1681	-0.0745
0.25	2.2405	-0.1778	-0.0793
0.26	2.22396	-0.1874	-0.0843
0.27	2.20742	-0.1970	-0.0892
0.28	2.19088	-0.2066	-0.0943
0.29	2.17434	-0.2163	-0.0995
0.3	2.1578	-0.2259	-0.1047
0.31	2.14126	-0.2355	-0.1100
0.32	2.12472	-0.2452	-0.1154
0.33	2.10818	-0.2548	-0.1209
0.34	2.09164	-0.2644	-0.1264
0.35	2.0751	-0.2741	-0.1321
0.36	2.05856	-0.2837	-0.1378
0.37	2.04202	-0.2933	-0.1436
0.38	2.02548	-0.3029	-0.1496
0.39	2.00894	-0.3126	-0.1556
0.4	1.9924	-0.3222	-0.1617

Porosity (%)	Bulk Density Of 95% Quartz+5% Illite (g/cm3)	Volume Magnetic Susceptibility Of 95% Quartz+5% Illite (10^{-5} SI units)	Mass Magnetic Susceptibility Of 95% Quartz+5% Illite ($10^{-8} m^3 Kg^{-1}$)
0	2.655	0.4892	0.1842
0.01	2.63944	0.4753	0.1801
0.02	2.62288	0.4614	0.1759
0.03	2.60632	0.4475	0.1717
0.04	2.58976	0.4336	0.1674
0.05	2.5732	0.4197	0.1631
0.06	2.55664	0.4058	0.1587
0.07	2.54008	0.3919	0.1543
0.08	2.52352	0.3780	0.1498
0.09	2.50696	0.3641	0.1452
0.1	2.4904	0.3502	0.1406
0.11	2.47384	0.3363	0.1360
0.12	2.45728	0.3225	0.1312
0.13	2.44072	0.3086	0.1264
0.14	2.42416	0.2947	0.1216
0.15	2.4076	0.2808	0.1166
0.16	2.39104	0.2669	0.1116
0.17	2.37448	0.2530	0.1065
0.18	2.35792	0.2391	0.1014
0.19	2.34136	0.2252	0.0962
0.2	2.3248	0.2113	0.0909
0.21	2.30824	0.1974	0.0855
0.22	2.29168	0.1835	0.0801
0.23	2.27512	0.1696	0.0746
0.24	2.25856	0.1558	0.0690
0.25	2.242	0.1419	0.0633
0.26	2.22544	0.1280	0.0575
0.27	2.20888	0.1141	0.0516
0.28	2.19232	0.1002	0.0457
0.29	2.17576	0.0863	0.0397
0.3	2.1592	0.0724	0.0335
0.31	2.14264	0.0585	0.0273
0.32	2.12608	0.0446	0.0210
0.33	2.10952	0.0307	0.0146
0.34	2.09296	0.0168	0.0080
0.35	2.0764	0.0029	0.0014
0.36	2.05984	-0.0109	-0.0053
0.37	2.04328	-0.0248	-0.0122
0.38	2.02672	-0.0387	-0.0191
0.39	2.01016	-0.0526	-0.0262
0.4	1.9936	-0.0665	-0.0334

Porosity (%)	Bulk Density Of 94% Quartz+6% Illite (g/cm3)	Volume Magnetic Susceptibility Of 94% Quartz+6% Illite (10^{-5} SI units)	Mass Magnetic Susceptibility Of 94% Quartz+6% Illite ($10^{-8} m^3 Kg^{-1}$)
0	2.656	0.9160	0.3449
0.01	2.63944	0.8978	0.3402
0.02	2.62288	0.8797	0.3354
0.03	2.60632	0.8615	0.3306
0.04	2.58976	0.8434	0.3257
0.05	2.5732	0.8252	0.3207
0.06	2.55664	0.8070	0.3157
0.07	2.54008	0.7889	0.3106
0.08	2.52352	0.7707	0.3054
0.09	2.50696	0.7526	0.3002
0.1	2.4904	0.7344	0.2949
0.11	2.47384	0.7162	0.2895
0.12	2.45728	0.6981	0.2841
0.13	2.44072	0.6799	0.2786
0.14	2.42416	0.6618	0.2730
0.15	2.4076	0.6436	0.2673
0.16	2.39104	0.6254	0.2616
0.17	2.37448	0.6073	0.2558
0.18	2.35792	0.5891	0.2498
0.19	2.34136	0.5710	0.2439
0.2	2.3248	0.5528	0.2378
0.21	2.30824	0.5346	0.2316
0.22	2.29168	0.5165	0.2254
0.23	2.27512	0.4983	0.2190
0.24	2.25856	0.4802	0.2126
0.25	2.242	0.4620	0.2061
0.26	2.22544	0.4438	0.1994
0.27	2.20888	0.4257	0.1927
0.28	2.19232	0.4075	0.1859
0.29	2.17576	0.3894	0.1790
0.3	2.1592	0.3712	0.1719
0.31	2.14264	0.3530	0.1648
0.32	2.12608	0.3349	0.1575
0.33	2.10952	0.3167	0.1501
0.34	2.09296	0.2986	0.1426
0.35	2.0764	0.2804	0.1350
0.36	2.05984	0.2622	0.1273
0.37	2.04328	0.2441	0.1195
0.38	2.02672	0.2259	0.1115
0.39	2.01016	0.2078	0.1034
0.4	1.9936	0.1896	0.0951

Appendix B

Porosity (%)	Bulk Density Of 93% Quartz+7% Illite (g/cm3)	Volume Magnetic Susceptibility Of 93% Quartz+7% Illite (10^{-5} SI units)	Mass Magnetic Susceptibility Of 93% Quartz+7% Illite ($10^{-8} m^3 Kg^{-1}$)
0	2.658	1.3420	0.5049
0.01	2.64142	1.3196	0.4996
0.02	2.62484	1.2972	0.4942
0.03	2.60826	1.2747	0.4887
0.04	2.59168	1.2523	0.4832
0.05	2.5751	1.2299	0.4776
0.06	2.55852	1.2075	0.4719
0.07	2.54194	1.1851	0.4662
0.08	2.52536	1.1626	0.4604
0.09	2.50878	1.1402	0.4545
0.1	2.4922	1.1178	0.4485
0.11	2.47562	1.0954	0.4425
0.12	2.45904	1.0730	0.4363
0.13	2.44246	1.0505	0.4301
0.14	2.42588	1.0281	0.4238
0.15	2.4093	1.0057	0.4174
0.16	2.39272	0.9833	0.4109
0.17	2.37614	0.9609	0.4044
0.18	2.35956	0.9384	0.3977
0.19	2.34298	0.9160	0.3910
0.2	2.3264	0.8936	0.3841
0.21	2.30982	0.8712	0.3772
0.22	2.29324	0.8488	0.3701
0.23	2.27666	0.8263	0.3630
0.24	2.26008	0.8039	0.3557
0.25	2.2435	0.7815	0.3483
0.26	2.22692	0.7591	0.3409
0.27	2.21034	0.7367	0.3333
0.28	2.19376	0.7142	0.3256
0.29	2.17718	0.6918	0.3178
0.3	2.1606	0.6694	0.3098
0.31	2.14402	0.6470	0.3018
0.32	2.12744	0.6246	0.2936
0.33	2.11086	0.6021	0.2853
0.34	2.09428	0.5797	0.2768
0.35	2.0777	0.5573	0.2682
0.36	2.06112	0.5349	0.2595
0.37	2.04454	0.5125	0.2506
0.38	2.02796	0.4900	0.2416
0.39	2.01138	0.4676	0.2325
0.4	1.9948	0.4452	0.2232

Appendix B

Porosity (%)	Bulk Density Of 92% Quartz+8% Illite (g/cm3)	Volume Magnetic Susceptibility Of 92% Quartz+8% Illite (10^{-5} SI units)	Mass Magnetic Susceptibility Of 92% Quartz+8% Illite ($10^{-8} m^3 Kg^{-1}$)
0	2.658	1.7680	0.6652
0.01	2.64142	1.7413	0.6592
0.02	2.62484	1.7146	0.6532
0.03	2.60826	1.6880	0.6472
0.04	2.59168	1.6613	0.6410
0.05	2.5751	1.6346	0.6348
0.06	2.55852	1.6079	0.6285
0.07	2.54194	1.5812	0.6221
0.08	2.52536	1.5546	0.6156
0.09	2.50878	1.5279	0.6090
0.1	2.4922	1.5012	0.6024
0.11	2.47562	1.4745	0.5956
0.12	2.45904	1.4478	0.5888
0.13	2.44246	1.4212	0.5819
0.14	2.42588	1.3945	0.5748
0.15	2.4093	1.3678	0.5677
0.16	2.39272	1.3411	0.5605
0.17	2.37614	1.3144	0.5532
0.18	2.35956	1.2878	0.5458
0.19	2.34298	1.2611	0.5382
0.2	2.3264	1.2344	0.5306
0.21	2.30982	1.2077	0.5229
0.22	2.29324	1.1810	0.5150
0.23	2.27666	1.1544	0.5070
0.24	2.26008	1.1277	0.4990
0.25	2.2435	1.1010	0.4908
0.26	2.22692	1.0743	0.4824
0.27	2.21034	1.0476	0.4740
0.28	2.19376	1.0210	0.4654
0.29	2.17718	0.9943	0.4567
0.3	2.1606	0.9676	0.4478
0.31	2.14402	0.9409	0.4389
0.32	2.12744	0.9142	0.4297
0.33	2.11086	0.8876	0.4205
0.34	2.09428	0.8609	0.4111
0.35	2.0777	0.8342	0.4015
0.36	2.06112	0.8075	0.3918
0.37	2.04454	0.7808	0.3819
0.38	2.02796	0.7542	0.3719
0.39	2.01138	0.7275	0.3617
0.4	1.9948	0.7008	0.3513

Porosity (%)	Bulk Density Of 91% Quartz+9% Illite (g/cm3)	Volume Magnetic Susceptibility Of 91% Quartz+9% Illite (10^{-5} SI units)	Mass Magnetic Susceptibility Of 91% Quartz+9% Illite ($10^{-8}m^3Kg^{-1}$)
Porosity (%)	Bulk Density Of Quartz (g/cm3)	Volume Magnetic Susceptibility Of Quartz (10^{-5} SI units)	Mass Magnetic Susceptibility Of Quartz ($10^{-8}m^3Kg^{-1}$)
0	2.650	-1.643	-0.620
0.01	2.624	-1.627	-0.620
0.02	2.597	-1.610	-0.620
0.03	2.571	-1.594	-0.620
0.04	2.544	-1.577	-0.620
0.05	2.518	-1.561	-0.620
0.06	2.491	-1.545	-0.620
0.07	2.465	-1.528	-0.620
0.08	2.438	-1.512	-0.620
0.09	2.412	-1.495	-0.620
0.1	2.385	-1.479	-0.620
0.11	2.359	-1.463	-0.620
0.12	2.332	-1.446	-0.620
0.13	2.306	-1.430	-0.620
0.14	2.279	-1.413	-0.620
0.15	2.253	-1.397	-0.620
0.16	2.226	-1.381	-0.620
0.17	2.200	-1.364	-0.620
0.18	2.173	-1.348	-0.620
0.19	2.147	-1.331	-0.620
0.2	2.120	-1.315	-0.620
0.21	2.094	-1.298	-0.620
0.22	2.067	-1.282	-0.620
0.23	2.041	-1.266	-0.620
0.24	2.014	-1.249	-0.620
0.25	1.988	-1.233	-0.620
0.26	1.961	-1.217	-0.620
0.27	1.935	-1.200	-0.620
0.28	1.908	-1.184	-0.620
0.29	1.882	-1.167	-0.620
0.3	1.855	-1.151	-0.620
0.31	1.829	-1.135	-0.620
0.32	1.802	-1.118	-0.621
0.33	1.776	-1.102	-0.621
0.34	1.749	-1.085	-0.621
0.35	1.723	-1.069	-0.621
0.36	1.696	-1.053	-0.621
0.37	1.670	-1.036	-0.621
0.38	1.643	-1.020	-0.621
0.39	1.617	-1.003	-0.621
0.4	1.590	-0.987	-0.621

Effect of Gas on Mass Magnetic Susceptibility versus Bulk Density

Porosity (%)	Bulk Density Of Dolomite (g/cm3)	Volume Magnetic Susceptibility Of Dolomite (10^{-5} SI units)	Mass Magnetic Susceptibility Of Dolomite ($10^{-8} m^3 Kg^{-1}$)
0	2.870	-3.444	-1.200
0.01	2.841	-3.410	-1.200
0.02	2.813	-3.375	-1.200
0.03	2.784	-3.341	-1.200
0.04	2.755	-3.306	-1.200
0.05	2.727	-3.272	-1.200
0.06	2.698	-3.238	-1.200
0.07	2.669	-3.203	-1.200
0.08	2.640	-3.169	-1.200
0.09	2.612	-3.134	-1.200
0.1	2.583	-3.100	-1.200
0.11	2.554	-3.065	-1.200
0.12	2.526	-3.031	-1.200
0.13	2.497	-2.997	-1.200
0.14	2.468	-2.962	-1.200
0.15	2.440	-2.928	-1.200
0.16	2.411	-2.893	-1.200
0.17	2.382	-2.859	-1.200
0.18	2.353	-2.825	-1.200
0.19	2.325	-2.790	-1.200
0.2	2.296	-2.756	-1.200
0.21	2.267	-2.721	-1.200
0.22	2.239	-2.687	-1.200
0.23	2.210	-2.653	-1.200
0.24	2.181	-2.618	-1.200
0.25	2.153	-2.584	-1.200
0.26	2.124	-2.549	-1.200
0.27	2.095	-2.515	-1.200
0.28	2.066	-2.480	-1.200
0.29	2.038	-2.446	-1.200
0.3	2.009	-2.412	-1.200
0.31	1.980	-2.377	-1.200
0.32	1.952	-2.343	-1.200
0.33	1.923	-2.308	-1.200
0.34	1.894	-2.274	-1.201
0.35	1.866	-2.240	-1.201
0.36	1.837	-2.205	-1.201
0.37	1.808	-2.171	-1.201
0.38	1.779	-2.136	-1.201
0.39	1.751	-2.102	-1.201
0.4	1.722	-2.068	-1.201

Porosity (%)	Bulk Density Of Calcite (g/cm3)	Volume Magnetic Susceptibility Of Calcite (10^{-5} SI units)	Mass Magnetic Susceptibility Of Calcite ($10^{-8} m^3 Kg^{-1}$)
0	2.710	-1.301	-0.480
0.01	2.683	-1.288	-0.480
0.02	2.656	-1.275	-0.480
0.03	2.629	-1.262	-0.480
0.04	2.602	-1.249	-0.480
0.05	2.575	-1.236	-0.480
0.06	2.547	-1.223	-0.480
0.07	2.520	-1.210	-0.480
0.08	2.493	-1.197	-0.480
0.09	2.466	-1.184	-0.480
0.1	2.439	-1.171	-0.480
0.11	2.412	-1.158	-0.480
0.12	2.385	-1.145	-0.480
0.13	2.358	-1.132	-0.480
0.14	2.331	-1.119	-0.480
0.15	2.304	-1.106	-0.480
0.16	2.276	-1.093	-0.480
0.17	2.249	-1.080	-0.480
0.18	2.222	-1.067	-0.480
0.19	2.195	-1.054	-0.480
0.2	2.168	-1.041	-0.480
0.21	2.141	-1.028	-0.480
0.22	2.114	-1.015	-0.480
0.23	2.087	-1.002	-0.480
0.24	2.060	-0.989	-0.480
0.25	2.033	-0.976	-0.480
0.26	2.005	-0.963	-0.480
0.27	1.978	-0.950	-0.480
0.28	1.951	-0.937	-0.480
0.29	1.924	-0.924	-0.480
0.3	1.897	-0.911	-0.480
0.31	1.870	-0.898	-0.480
0.32	1.843	-0.885	-0.480
0.33	1.816	-0.872	-0.481
0.34	1.789	-0.860	-0.481
0.35	1.762	-0.847	-0.481
0.36	1.734	-0.834	-0.481
0.37	1.707	-0.821	-0.481
0.38	1.680	-0.808	-0.481
0.39	1.653	-0.795	-0.481
0.4	1.626	-0.782	-0.481